MSS-008

7th Mss 8th ~9th 門

5

METEOROID POPULATIONS AND ORBITS

Z. CEPLECHA

Statistical studies of the photographic data on atmospheric trajectories and orbits of meteors (from 10^{-4} g to hundreds of tons) point to 5 groups of bodies with different structure and composition. The following classification is proposed: Fireball group I ≡ exceptional cases of so-called "asteroidal" bodies among Super-Schmidt (SS) and small-camera (SC) meteors ≡ ordinary chondrites. Fireball group II ≡ group A among SS and SC = carbonaceous chondrites. Group B among SS and SC ≡ dense cometary materials with small perihelion distances (not distinguishable among fireballs). Fireball group IIIa ≡ group C among SS and SC ≡ regular cometary material. Fireball group IIIB ≡ group D (above C) of SS and SC ≡ Draconid-shower type of cometary material. Statistics of the orbits for separate groups is considered and characteristic orbits are given.

I want to speak about different populations of meteoroids in the mass range from 10^{-4} to 10^{8} g and about their relations to the other bodies of the solar system. All we know about them have to be derived from their atmospheric trajectories. Only during this extremely short interval of their lifetime, these meteoroids are accessible for observations. The collision of the meteoroid with the atmosphere gives rise to a luminous trajectory of a duration of a few tenth to some ten seconds for these masses. The meteoroid penetrating into the atmosphere with initial velocity somewhere from 72 to 11 km/s is first heated up to the point, where a severe ablation and evaporation begins. This heating goes up exponentially approximately following the uprise of the air density. After the ablation starts, the gas close to the body is mainly composed of hot meteoroid vapors emitting the light, which can be observed on the Earth's surface. Thus we do not actually observe the meteoroid itself, but some luminous volume surrounding and following it.

We usually denote the height, where we begin to observe the light of a meteor, as its beginning height. After all the mass is ablated or the velocity slowed down to few kilometers per second, the meteor phenomenon is terminated and we denote the corresponding height as the terminal or the end height.

If we would have two meteoroids of the same initial velocity, mass and the same angle of incidence, then any observed difference in the beginning height and the terminal height should be associated with the difference in the meteoroid structure and composition. Even if the situation is complicated by different initial velocity, mass and angle of incidence, still the study of meteor beginning and terminal heights is a good and rather simple mean for distinguishing among meteoroid populations of different composition and structure. At the same time the initial velocity as a vector (the direction opposite to the

velocity vector is usually denoted as meteor radiant by meteor astronomers) and the known position of the Earth in its orbit give us all we need to compute the meteoroid orbit. We can then compare statistics of orbits with statistics of beginning and terminal heights, which results in orbital characteristics and orbital differences among meteoroid populations (groups).

To do so, we need good and precise observations of the meteor phenomenon. Moreover we need homogeneous material for statistical purposes. The photographic data obtained from at least two stations separated by several tens of kilometers (or even few hundreds of kilometers for fireballs) are the best possibility. Such observations give us data on heights of individual points of the meteor trajectory, velocities, decelerations and light intensities. The meteoroid mass is determined from the integrated light intensity. In principle three different types of cameras used for recording meteors resulted in three statistical sets of data. These sets have already been used separately to study meteoroid populations. This review is an attempt to intercompare all the results and to propose a classification of meteoroid populations valid for the entire mass-range.

The oldest results were obtained using classical small-cameras. The Harvard double-station program initiated by Fred L. Whipple in 1936 (Whipple 1938, 1954; Jacchia *et al.* 1965) gave the first results on small-camera meteors usable for statistical purposes. In this review I complemented this observational material of the small-camera meteors by observations from Dushanbe, Odessa and Ondrejov; altogether 364 sporadic meteors were used. (See Ceplecha 1965, p. 47 to 51 for details). The small-camera meteors have typical masses from 10^{-1} to 10^{3} g.

Thanks to the endeavor of F. L. Whipple, photographic data on smaller meteoroids became available, after the project of Baker Super-Schmidt cameras had been accomplished by the Harvard Observatory (Jacchia and Whipple 1956). The precisely reduced orbits of 413 faint photographic meteors with longer trajectories proved to be highly selective in favor of the classical cometary population. Thus I use here the more complete material of 2529 meteors photographed by Super-Schmidt cameras and reduced and published by McCrosky and Posen (1961). (See Ceplecha (1967) page 35 to 47 for details). This material proved to be homogeneous and very good for statistical purposes. The Super-Schmidt meteors have a typical mass-range from 10^{-3} to 10 g.

The third observational material available only recently is that on fireballs. Fred L. Whipple was again with it as the director of the Smithsonian Astrophysical Observatory, when the effort of R. E. McCrosky resulted in operating the Prairie Network for fireballs. (McCrosky and Posen 1968). A recent study of populations among fireballs were based on data of 232 events photographed by the Prairie Network during 7 years. (Ceplecha and McCrosky 1976). The typical mass-range for fireballs is from 10^{2} to 10^{6} g.

Different meteoroid populations were first recognized independently by Jacchia (1958) and Ceplecha (1958). The differences in beginning heights proved to be the most important tool for recognition of different meteoroid populations among Super-Schmidt and small-camera meteors, when and if the right dependence on velocity was considered. (Ceplecha 1967, 1968; Cook 1973). Two main discrete levels of meteor beginning heights separated by 10 km difference has been found. The lower level was denoted A, the higher was denoted C. The C-group of meteoroids was recognized to contain two populations of orbits: one with ecliptically concentrated short-period orbits was denoted C_1 and the other with random orbital inclinations of long-period orbits was denoted C_2. The classical meteor showers with known parent comets are of the type C_1 and C_2; thus the cometary origin of meteoroids of the whole C-group is quite certain.

The question of meteoroid bulk densities for separate groups proved to be more complicated. The A-group was recognized to contain meteoroids of about 3 times greater bulk densities than the C-group. The problem with calibration

TABLE I

SURVEY OF METEOROID POPULATIONS AMONG PHOTOGRAPHIC METEORS. RELATIONSHIP OF METEOR GROUPS FOUND IN DIFFERENT PHOTOGRAPHIC DATA

Observational Material	Super-Schmidt Cameras				Small-Camera meteors					PN-fireballs					properties of the meteoroid material		
typical mass-range	10^{-3} to 10 g				10^{-1} to 10^{3} g					d) 10^{2} to 10^{6} g							
group	% obs.	characteristic orbit a	e	i	group	% obs.	characteristic orbit a	e	i	group	% obs. a)	characteristic orbit a	e	i	ρ g/cm^3	log σ s^2/cm^2	assumed composition
"asteroidal" meteors	< 1	2.4 c)	.64 c)	15° c)	"asteroidal" meteors	5	2.5 b)	.64 b)	10° b)	I	32	2.4	.68	6°	3.7	-11.5	ordinary chondrites
A	54	2.3	.61	1°	A	37	2.5	.64	4°	II	37	2.3	.61	5°	2.1	-11.3	carbonaceous chondrites
B	6	2.4	.92	5°	B	7	2.5	.90	6°	--	--	--	--	--	1.0	-11.1	dense cometary material
C_1	9	2.2	.80	6°	C_1	16	2.5	.80	5°	IIIA	9	2.4	.82	4°	0.6	-10.9	regular cometary material
C_2	31	∞	.99	random	C_2	30	∞	.99	random	IIIAi f)	9	∞	.99	random	0.6	-10.9	regular cometary material
D (above C)	< 1	3.3 e)	.70 e)	25° e)	D (above C)	5	3.1 b)	.77 b)	10° b)	IIIB	13	3.0	.70	13°	0.2	-10.7	soft cometary material of Draconid type

Data in the Table are based on photographic observations of ~2600 sporadic meteors; the percentage number does not contain major classical showers; the values of the maxima of statistical distributions of a, e, and i are given, if not stated otherwise.

ρ is the bulk density of meteoroid; σ is the ablation coefficient.

a) rough estimates from the numbers of computed trajectories (42, 37, 6, 6, 9% respectively) assuming twice big reduction preference of group I over the group III.
b) median from 12 cases. c) only two meteors recognized as asteroidal (No 7946 and 19816); their average elements are given.
d) the biggest bodies photographed within fireball networks so far have the mass of the order of 10^8 g.
e) Draconid shower orbit. (2 Super-Schmidt members of the stream).
f) all high-inclined near-parabolic orbits.

MSS-008

of these relative values by bodies of "known" composition was the reason of overestimated densities by Ceplecha (1967, 1968). The problem of the velocity dependence of meteor beginning heights and calibration problems was the reason of underestimated densities by Verniani (1965, 1967) and Jacchia *et al.* (1965). The calibration through the data on fireball populations with knowing the actual bodies in case of the Pribram and the Lost City meteorites, gave the values of densities intermediate to both the extreme results. The A-group contains bodies with average bulk densities of about 2.1 g/cm^3, while the C-group contains bodies with average densities of 0.6 g/cm^3 (Table I).

Two additional smaller groups were found among Super-Schmidt and small-camera meteors. The intermediate group B has typical orbits with small perihelion distances and aphelion close to Jupiter. There seems to be not a direct cometary association to meteoroids of this group, but the Geminid shower is a typical member of the B-group, and as far as Geminids are assumed to be cometary in origin, the whole group B should be associated with comets. According to Cook (1973) the B-group meteoroids should be associated with less dense cores of smaller cometary nuclei that have lost their surfaces and are too small to have been observed. The bulk density of meteoroids of this group should be close to 1 g/cm^3.

The other smaller group was referred to as a group "above C" accounting for very high beginning heights. The Draconid meteor shower is a typical member of this group. I will denote this group as D-group. It contains extremely soft meteoroids with the lowest known densities from all types of solid cometary material coming to the Earth (0.2 g/cm^3).

Very few meteoroids among Super-Schmidt and small-camera meteors penetrated deep into the atmosphere and indicated thus stronger structure and density than those of the A-group. These meteors were called by some authors "asteroidal," which is not a good name presuming the origin. The average bulk density of these bodies is 3.7 g/cm^3 in the density scale used in this review (Table I).

Except bulk density, another parameter characterizing the composition and structure of the meteor body is the ablation coefficient $\sigma = \Lambda / (2\Gamma\xi)$, where Λ is the heat-transfer coefficient, Γ the drag coefficient and ξ the energy necessary for ablation of 1 g of the meteoroid material. The ablation coefficient is a quantitative measure how readily the meteoroid ablates. Knowing the mass and velocity, the ablation coefficient can be determined from the photographic observations of meteors. The A-group of meteoroids contains bodies with ablation coefficient 3 times smaller than the C-group. Thus the meteoroids of the C-group are more readily ablated and even a big initial mass cannot penetrate deep into the atmosphere.

The attempt to study the fireballs the same way as the fainter meteors using the beginning heights proved to be useless. But different penetrating abilities were found to be a good criterion for distinguishing among different fireball populations. Thus the end heights turned out to be the most important for recognition of fireball populations. The main difference of this approach is an additional mass dependence of the used criteria. Also the problem of significant terminal mass was encountered, which had been negligible for fainter meteors.

Four groups of different composition and structure were found among fireballs (Ceplecha and McCrosky 1976) and were denoted by Roman numerals eventually with a letter suffix. Group I is of the greatest density and contains Příbram (Ceplecha 1961) and Lost City (McCrosky *et al.* 1971) meteorites, the only two meteorite falls photographed. Thus the average bulk density of fireballs of group I was assumed 3.7 g/cm^3 using data of these two meteorites as safe calibration values. Group I is evidently connected with ordinary chondrites.

The meteoroids of the group II have a somewhat lower density of 2.1 g/cm^3

and they are very likely belonging to carbonaceous chondrites. Except for the reasons given in favor of this identification in the paper by Ceplecha and McCrosky (1976), there is a brand-new evidence from spectral records of the Kamyk fireball obtained at the Ondrejov Observatory in March 1976. (This fireball was photographed from 11 stations of the European Network for fireballs; Ceplecha *et al.* 1977). This fireball penetrated to 32 km and was a sure member of the group II; the extremely good spectral (15 Å/mm) contain more than 500 features in the visible region and show relatively strong emissions of the CN molecule demonstrating the abundance of carbon.

Fireballs of the groups IIIA and IIIAi have densities of 0.6 g/cm^3 and have direct evidence of cometary origin through showers. The group IIIA contains orbits of short period and ecliptic concentration and the group IIIAi contains long-period randomly-inclined orbits. A very good spectrum of a fireball of the group IIIAi was published (Ceplecha 1971) and relatively strong emissions of CN were found. Thus also low density cometary material in long-period orbits does contain carbon.

The fireballs of the group IIIB have densities of 0.2 g/cm^3 and they contain fireballs of the Draconid meteor shower. This is a very distinct group and contains relatively quite a number of fireballs.

The interrelations of all the groups is presented in Table I. Altogether 6 populations are present with 5 different compositions among the meteoroids in the considered mass-range. The average bulk density and ablation coefficients are given for each group and a probable composition and structure is proposed.

↑ 8th

↓ 9th

9th → The identification of the fireball group I and the so-called "asteroidal" meteors with the ordinary chondrites is mainly based on the two photographed meteorite falls: Příbram and Lost City. The identification of the group IIIB and of the group D with the Draconid shower is based on observed members of this shower in all three observational materials. The C-group meteors and the IIIA group meteors are easily identified as regular cometary material through showers with known parent comets. The identification of the A group with the group II and with the carbonaceous chondrites comes out then quite naturally and moreover it is supported by the spectral evidence already mentioned.

Table I contains "characteristic" orbits for each of the groups. To avoid any misunderstanding I strongly stress that these values are mostly maxima of broad irregular statistical distributions (sometimes medians as marked in Table I). It is not possible to separate all these populations using only the orbital elements.

There is not much difference in semimajor axes for ordinary chondrites, carbonaceous chondrites and cometary material with ecliptic concentrations; all values are from 2.2 to 2.5 A.U. The Draconid-shower type of material has longer semimajor axes of slightly more than 3 A.U. The cometary material with randomly inclined orbits has of course very large semimajor axes, which is symbolicly denoted by $= \infty$ in Table I.

The orbital distinction among groups is mostly in eccentricities: ordinary and carbonaceous chondrites have the orbits with the smallest eccentricity, 0.6. The Draconid type of material has somewhat higher eccentricities, 0.7, the regular cometary material with ecliptic concentration even higher, 0.8, followed by the dense cometary material of the B-group, 0.9, and by the cometary material with randomly inclined orbits with eccentricity approaching 1.

There is a very little difference in characteristic orbits of ordinary chondrites and of carbonaceous chondrites. But the statistical distribution of the semimajor axes is strikingly different (Fig. 1). The number of observed orbits of ordinary chondrites increases almost linearly with their semimajor axes starting with a = 1 A.U. and then suddenly drops forming a cut-off at 2.7 A.U. The decrease is 7 times steeper than the increase! The carbonaceous chondrites have a symmetrical distribution with maximum at 2.3 A.U. and still

enough orbits with a = 3 A.U. A small second maximum in the distribution of semimajor axes for carbonaceous chondrites near 1.2 A.U. (quite missing for the regular chondrites) may indicate a secondary Earth's or Moon's component.

The Příbram meteorite has the orbit very close to the maxima of distribution for ordinary chondrites, while the Lost City meteorite is on ascending parts of the distributions of a and e. Especially eccentricity of the Lost City orbit is much lower than is the average. The orbit of Pribram is more typical for the ordinary chondrites than that of the Lost City.

Because the so-called "asteroidal" meteors are very rare among faint meteors, the distributions of the orbital elements of the group-I fireballs are actually the first hint at statistics of the orbits of ordinary chondrites from photographic records. The fireball-group-I data can be considered as representative of ordinary chondrites. The orbital data for any detailed study should be taken from the original paper (Ceplecha and McCrosky 1976).

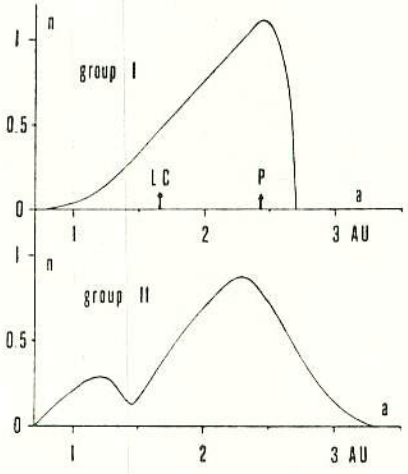

Figure 1. Distribution of semimajor axes, a, of group I fireballs (ordinary chondrites) and group II fireballs (carbonaceous chondrites). The scale of the relative number of fireballs, n, is chosen so that the integral number of all cases is equal 1. LC is the Lost City meteorite, P is the Pribram meteorite.

The inclinations for all groups except C_2 and IIIAi show an ecliptical concentration, but the maxima of distributions are not at 0^o exactly. They are usually between 0^o and 10^o. This may be due to planetary collisions and perturbations as already pointed out by McCrosky and Posen (1961). The only higher inclination than 10^o at the maximum of distribution is that of the Draconid type group.

The parent bodies of the softest Draconid type material are short period comets, one of them being the Giacobini-Zinner belonging to the Draconid meteor shower. Meteoroids of this type are very rare among the observed faint bodies and are growing in number toward the big masses forming 13% of the observed fireballs.

The parent bodies of the C_1 and IIIA group are short-period comets again; most of the classical meteor showers are of this type and a lot of direct well-established cometary associations is available. This group forms 9% of all Super-Schmidt meteors; it increases to maximum of 16% from the small-camera meteors and again becomes less significant with 9% from the fireballs. Also

the classical meteor showers are the most distinct and numerous among the small-camera meteors.

The parent bodies of the C_2 and IIIAi group are long-period comets; showers as *e.g.* Perseids with association to comet Swift-Tuttle 1862 III are within this group and one can hardly doubt the cometary origin of it. The Super-Schmidt and small-camera meteors contain 30% of this long-period cometary component, which decreases to 9% for fireballs.

The parent bodies of the B-group have to be of the same nature as the parent body of the Geminid meteor shower. The cometary origin is highly probable. The B-group forms 6 and 7% of all faint meteors and was not separated among fireballs.

The A-group and the group II belonging to carbonaceous chondrites are the most numerous among all the studied masses. They form 54% of all observed Super-Schmidt meteors, 37% of the small-camera meteors and 32% of the fireballs. Cook (1973) prefers the cometary origin of this group ascribing it to the core of a cometary nucleus. A strong support to this view is the one existing association of a meteor shower of type A with a known comet: τ Herculids (Lindblad 1971) with the comet Schwassman-Wachmann 3. Its eventual observation in 1979 return may cast some more light on the problem. The scarcity of ordinary chondrites among smaller meteoroids in contrast to the abundance of carbonaceous chondrites points to different origin. The differences in the distribution of semimajor axes (Fig. 1) support this view. The cometary origin for carbonaceous chondrites seems to be a strong possibility. If carbonaceous chondrites are not cometary, they should at least be connected with different type of objects than the ordinary chondrites.

The parent bodies of the ordinary chondrites are mostly believed to be asteroidal bodies (Anders 1971). The difficulties with this view from the point of Earth crossing orbits are discussed in many papers of this Colloquium.

The importance of the carbonaceous chondrites among all sizes of the studied meteoroids is evident. This is well demonstrated by the ratio of cometary to asteroidal meteoroids. If we assume that carbonaceous chondrites are of cometary origin, then the observed ratio of the bodies with cometary to the bodies with asteroidal origin is > 100 for meteoroids of 10^{-1} g, 20 for 10 g, and 2 for 10^4 g. If we assume that the carbonaceous chondrites are of asteroidal origin, the picture is strikingly different. The observed ratio of cometary to asteroidal bodies is then 0.8 for 10^{-1} g, 1.4 for 10 g, and 0.4 for 10^4 g.

The total mass range, in which the meteoroid populations were studied in this review, is from 10^{-3} to 10^6 g for almost all the available photographic meteors. Few extreme cases of low and very big masses outside this mass range that has been photographed can be classified in the same population groups presented here. Adding these extreme wings of the distribution, we can assume the total mass-range of meteoroid studied to be from 10^{-4} g to hundreds of tons. It is interesting that one of the biggest initial masses on photographic records belongs to the Draconid type (Ceplecha 1976).

At the end I want to mention a paradox in connection with the fireballs and meteorite falls. If somehow we could organize all the incoming meteoroids to be of the same mass, velocity and angle of incidence but having different composition and structure as given in Table I, then the meteorite fall of an ordinary chondrite will be preceded by the *faintest* meteor phenomenon from all the 5 different compositional groups. If we would observe the brightest possible fireball, we may be sure it belongs to the soft Draconid type of material. This material is ablated high in the atmosphere. On the other hand, the faint fireball belonging to the meteorite fall of an ordinary chondrite, would have very long trajectory penetrating very deep into the atmosphere , while the Draconid type would have only very short trajectory ending very high. Thus, an

observation of a very bright fireball does not necessarily mean a meteorite fall. The dependence of the brightness on the mass in real situation works partly against the paradox and makes the picture quite complicated. Thus decisions if to search or not to search for meteorites after a bright fireball passage, should be done rather on the basis of criteria, which takes into account the end height, the mass (or brightness) and the velocity with the angle of incidence (Ceplecha and McCrosky 1976).

REFERENCES

Anders, E. 1971, in *Physical Studies of Minor Planets*, (ed. T. Gehrels, NASA, Washington), p. 429.

Babadzanov, P. B., Kramer, E. N. 1963, *Ionosphere and Meteors 12*, Publ. House Acad. Sci. USSR, Moscow.

Ceplecha, Z. 1958, *Bull. Astron. Inst. Czech.*, *9*, 154.

Ceplecha, Z. 1961, *Bull. Astron. Inst. Czech.*, *12*, 21.

Ceplecha, Z. 1967, *Smithson. Contr. Astrophys.*, *11*, 35.

Ceplecha, Z. 1968, *Smithson. Astrophys. Obs. Spec. Rep. 279*.

Ceplecha, Z. 1971, *Bull. Astron. Inst. Czech.*, *22*, 219.

Ceplecha, Z. 1976, in, *Lecture Notes in Physics 48*, (ed. H. Elsässer, H. Fechtig, Springer Verlag, Heidelberg), 385.

Ceplecha, Z., Bocek, J., Jezkova, M. 1977, *Bull. Astron. Inst. Czech.*, *28*, in preparation.

Ceplecha, Z., McCrosky, R. E. 1976, *Center for Astrophys.*, Prepr. Ser. 442.

Cook, A. F. 1973, *Smithson. Contr. Astrophys.*, No. 14.

Jacchia, L. G. 1958, *Smithson. Contr. Astrophys.*, *2*, 181.

Jacchia, L. G., Kopal, Z., and Millman, P. M. 1950, *Astrophys. J.*, *111*, 104.

Jacchia, L. G., Verniani, F., and Beiggs, R. E. 1965, Smithson. Astrophys. Obs. Spec. Rep. 175.

Jacchia, L. G., Whipple, F. L. 1956, in *Vistas in Astron. 2*, (ed. A. Beer, London), p. 982.

Jacchia, L. G., Whipple, F. L. 1961, *Smithson. Contr. Astrophys.*, *4*, 97.

Kresák, L. 1970, *Bull. Astron. Inst. Czech.*, *21*, 1.

Lindblad, B. A. 1971, Smithson. Contr. Astrophys., No. 12.

Marsden, B. G. 1972, *Catalogue of Cometary Orbits*, Smithson. Astrophys. Obs., Cambridge.

McCrosky, R. E. 1968, Smithson. Astrophys. Obs. Spec. Rep., 280.

McCrosky, R. E. 1968, in *Physics and Dynamics of Meteors*, (eds. L. Kresak, P. M. Millman; D. Reidel Publ. Comp., Dordrecht), p. 265.

McCrosky, R. E. 1971, in *Physical Studies of Minor Planets*, (ed. T. Gehrels, NASA, Washington), p. 395.

McCrosky, R. E., Posen, A. 1961, *Smithson. Contr. Astrophys.*, *4*, 15.

McCrosky, R. E. 1968, Smithson. Astrophys. Obs. Spec. Rep., 273.

McCrosky, R. E., Posen, A., Swartz, G., and Shao, C. -Y. 1971, *J. Geophys. Res.*, *76*, 4090.

Vanysek, V. 1971, in *Physical Studies of Minor Planets*, (ed. T. Gehrels, NASA Washington), p. 465.

Verniani, F. 1965, *Smithson. Contr. Astrophys.*, *8*, 141.

Verniani, F. 1967, *Smithson. Contr. Astrophys.*, *10*, 181.

Wetherill, G. W. 1971, in *Physical Studies of Minor Planets*, (ed. T. Gehrels, NASA, Washington), p. 447.

Whipple, F. L. 1938, *Proc. of the Amer. Philos. Soc.*, 79, 499.

Whipple, F. L. 1954, *Astron. J.*, *59*, 201.

MSS-008

DISCUSSION

CHAPMAN: Is it understood what physical process or processes could yield the different size distributions for "asteroidal meteors" and types A/II implied by your table? I would have thought that rapid collisional fragmentation processes would have made the population indices of most small particle populations similar, whatever the sources of the particles.

CEPLECHA: For a long time we know from our observations that faint photographic meteors almost lack the "asteroidal" type of objects which appeared among fireballs as the group I quite well populated. I am an observationalist and I have no real explanation for this.

WHIPPLE: If small chondrites originated with the meteorites (exposure to space) they would have been destroyed by collisions in the typical exposure ages of the meteorites, ~10^6 yr or more. The life times of the interplanetary particles is ~10^4 yr and destruction is mostly by collisions.

CEPLECHA: If one searches for some division between two grossly different origins, then just the absence of the group I bodies in smaller mass-ranges puts the division between the groups I and II.

HUGHES: Verniani found that the density of meteoroids varied as a function of mass (ρ = 3.5 g cm^{-3} for $m < 10^{-5}$ g; ρ = 0.8 g cm^{-3} for $10^{-5} < m < 10^{-1}$ g; ρ = 0.3 g cm^{-3} for $m > 10^{-1}$ g). How do your results change this conclusion? Why was Verniani mistaken?

CEPLECHA: I have no idea about densities of the radar meteors ($< 10^{-5}$ gr); I spoke only about the photographic meteors. Verniani's values are only average values, when all well distinguishable groups are dealt with together. This and the problem with calibration are the reasons that Verniani's densities are smaller. I have the opportunity, now, to calibrate the density scale by Příbram and Lost City meteorite densities and to deal with separate groups. To speak about "average" density of all meteoroids in a given mass-range gives not much sense to me. You can compute such a value from the percentage of the groups and from their densities.

MILLMAN: In regard to the mean densities of meteoroids given by Verniani, which are found on the basis of meteor physical theory, I feel that they show the correct relative change as we move from 1 g objects to those in the 10^{-4} to 10^{-6} g range. However, conclusions of Brownlee and his coworkers, in their study of extraterrestrial micrometeorites, suggest that the absolute densities of Verniani should be increased somewhat. One must also distinguish between whether a density is quoted as a bulk density at a conglomerate or as a density of one of the grains forming this conglomerate.

KRESAK: Your table indicates a conspicuous deficiency of long-period cometary material in the Prairie-Network data. However, these data are biased by a selection of meteors with a minimum duration of about 1 second required for their timing. Would there still remain a considerable disproportion after applying the due correction?

CEPLECHA: I already applied a correction which enhanced 6% of computed orbits into 9%. If there is some more correction necessary, I am not sure, but you will never obtain 30% like for fainter meteoroids.

ARNOLD: I wish to remind the group that carbonaceous chondrites are by defini-

39. Current Evolution of Meteoroids

J. S. DOHNANYI
Bellcomm, Inc.
Washington, D.C.

The observed mass distribution of meteoroids at 1 AU from the Sun is briefly reviewed in a survey that ranges over the bulk of the mass spectrum from micrometeoroids to meteorite parent objects. The evolution of meteoroids under the influence of collisions, planetary perturbations, the Poynting-Robertson effect and radiation pressure is then discussed.

Most micrometeoroids are expelled from the solar system by radiation pressure shortly after their production as secondary ejecta during impact by larger objects or as dust ejected by comets. Particles that survive will eventually be swept out by the Poynting-Robertson effect.

Meteoroids in the radio and photographic ranges are destroyed in collisions faster than they can be replaced by the production of secondary fragments during collisions between larger objects. The source of new particles needed to maintain the population of these meteoroids in a stationary distribution may be material expelled by comets.

The survival of large objects is limited by gravitational scattering during close planetary encounters and by collisions as well, if they spend sufficient time in the asteroid belt. The observed radiation-exposure ages of chondrites are shown to be consistent with this model.

THE DISTRIBUTION OF THE MASSES of meteoroids is governed by several processes (Whipple, 1967). Large numbers of new objects are injected into the solar system by comets. Many small objects are removed by the Poynting-Robertson effect (Robertson, 1937; Wyatt and Whipple, 1950); particles are destroyed by interparticle collisions and their shattering into fragments creates new particles (Whipple, 1967; Dohnanyi, 1967). The influence of these collisions on the distribution of meteoroid masses has recently been discussed by Dohnanyi (1970; to be referred to as D-I in this paper), who showed that the distribution of meteoroids in the photographic range and of fainter ones is not likely to be stationary unless many of the particles, destroyed by collisions, are replaced by new ones given off by comets; the influence of radiation pressure on the size distribution of such cometary debris was also stressed (D-I).

The orbital elements of meteoroids undergo frequent and random changes caused by planetary perturbations (Öpik, 1951; Arnold, 1965). The influence of this process on the radiation exposure age distribution of meteorites has recently been discussed by Wetherill (1967) and Wetherill and Williams (1968). This age distribution was found to be sensitive to the survival times of meteorite-producing objects with respect to catastrophic collisions and to the rate at which these objects can "diffuse" through the solar system as a result of random gravitational perturbations caused by close planetary encounters (Öpik, 1966).

In this paper we shall discuss some aspects of the current evolution of the mass distribution of meteoroids; orbits will only be considered to the extent that they may influence the mass distribution. This will be shown to lead to a self-consistent description of the dominating processes controlling the mass distribution of meteoroids with masses ranging from micrometeoroids to meteorite-producing objects having masses of tens of tons.

OBSERVATIONAL EVIDENCE

This section is a discussion of the observed distribution of sporadic meteoroids ranging in size from micrometeoroids to large objects.

The flux $n(m)\ dm$ of meteoroids having a mass in the range m to dm incident on a unit area per 2π sr per unit time will be taken as:

$$n(m)\ dm = am^{-\alpha}\ dm \qquad (1)$$

where a and α are constants in different mass ranges; α is known as the population index.

Figure 1 is a plot of the cumulative flux $N(m)$ of meteoroids into Earth's atmosphere per meter^2 per sec per 2π steradians having a mass of m kg or greater.

$$N(m) = \int_m^{M_\infty} n(M)\ dM \qquad (2)$$

where M_∞ is the mass of the largest object included among meteoroids. Near the small mass limit of the distribution, I used the results of the Pioneer 8 and 9 data obtained by Berg and Gerloff (1970), multiplied by two to correct for the Earth's focusing effect. These authors have found an indication of a "cutoff" in the population of meteoroids, at a mass of about 5×10^{-15} kg, which sets the effective upper limit to the flux of penetrating particles, as seen in figure 1.

The points labelled Explorer XXIII and Pegasus are the influx rates measured by these satellites, and are based on calibrations by Naumann (1968) and Naumann et al. (1969). The penetration sensors aboard Explorer XXIII and Pegasus were calibrated in the laboratory by firing particles at meteoric velocities into sensors similar to those actually flown. Since many of these particles were accelerated gas dynamically, a fraction of their

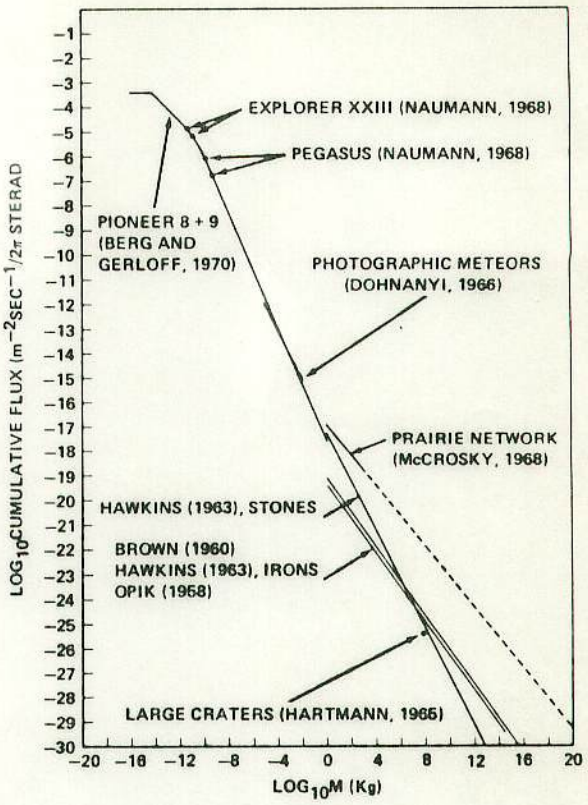

FIGURE 1.—Cumulative flux ($m^{-2}\ s^{-1}/2\pi$ sr) of meteoroids into Earth's atmosphere having a mass of m (kg) or greater.

masses may have ablated during the acceleration, so that the indicated flux is likely an upper limit. Some micrometeoroids may, however, be fluffy and of low density (Soberman, 1971) and would be less penetrating than were the laboratory particles of equal mass, so that the indicated flux may also be a lower limit. The nominal flux is, however, in agreement with the penetration flux measured by the Ariel II satellite (Jennison et al., 1967). Since it is difficult to estimate precisely the uncertainties involved, an order of magnitude approximation may be the most accurate estimate that can be attained at the present time.

Data from visual, radar and photographic observations as well as zodiacal light studies have been considered before (Whipple, 1967; Dohnanyi, 1965). A best estimate to fit these data has been obtained in D-I; it has the form of equation (1) with

$\alpha = 1.5$, for micrometeoroids, $m \leq 10^{-10}$ kg

$\alpha = 13/6$, for larger meteoroids but smaller than meteorite producing objects, $10^{-10}\ \text{kg} \leq m < 1\ \text{kg}$ (3)

This simple model gives a good fit to the data, as can be seen from the appropriate portions of the curve in figure 1. Numerical flux values are given in table 1.

Mass distributions obtained from satellite microphone measurements have been discussed by Kerridge (1970) and McDonnell (1971); because of calibration difficulties, many of these data are difficult to interpret. In those cases where calibration difficulties have likely been overcome, the results are comparable to the penetration data (Kerridge, 1970).

Mass fluxes of micrometeoroids estimated from particle collection experiments on board rockets and satellites are subject to uncertainties arising from contamination and identification difficulties (see Fechtig et al., 1968; Dohnanyi, 1971a, for an annotated bibliography) and will not be employed in this study. Many of these particles are comparable to or smaller than the wavelength of light; a discussion of the interaction of such small particles with the solar radiation field requires a discussion of interference effects and is beyond the scope of this paper.

The influx rate of meteorite-producing objects has been estimated variously by Brown (1960), Hawkins (1963), and Öpik (1958); their estimates are plotted in figure 1. These data are based on the mass distribution of recovered meteorites and their estimated rates of fall. Hartmann's (1965) estimate of the flux rate of large crater-producing objects is also indicated.

Precise photographic observation of fireballs from the Prairie Network Project led McCrosky (1968b) to obtain as the cumulative flux (in MKS units) for these objects:

$$N(m) = 10^{-16.96}\, m^{-0.62} \qquad 1 \leq m \leq 10^{4}\ \text{kg} \quad (4)$$

As can be seen from figure 1, this flux is about an order of magnitude higher than that of Hawkins' (1963) stones and about two orders of magnitude higher than the other earlier estimates. Extrapolation (dashed line in fig. 1) of the Prairie Network data leads to an even greater difference. Uncertainties in the photometric masses of these objects are not believed to span this discrepancy

TABLE 1.—*Differential Flux of Meteoroids* $n(m) = am^{-\alpha}$ *for Different Mass Ranges*[a]

Mass range	a, $m^{-2}\ s^{-1}\ kg^{\alpha-1}/2\pi$ sr	α
$m < 5\times10^{-15}$ kg		<3/2
$5\times10^{-15}\ \text{kg} \leq m \leq 10^{-10}$ kg	1.4×10^{-11}	3/2
$10^{-10}\ \text{kg} \leq m < 1$ kg	3×10^{-18}	13/6

[a] See equation (1) in text.

(McCrosky and Ceplecha, 1970); low density, fragile objects whose fragments do not survive atmospheric entry are believed responsible for the higher flux of fireballs than had been estimated earlier for meteorite producing objects.

INFLUENCE OF COLLISIONS

Meteoroids frequently undergo mutual collisions. Since these collisions are inelastic, the target particles may either lose a small portion of their mass (erosive collisions) or be completely broken up (catastrophic collisions). The net result is a change in the meteoroid distribution.

The equation that expresses the dependence of the population on collisions can be written as

$$\frac{\partial f(m,t)}{\partial t}\,dm = \frac{\partial f(m,t)}{\partial t}\,dm\,|_{\text{erosion}} + \frac{\partial f(m,t)}{\partial t}\,dm\,|_{\text{catastrophic collisions}} + \frac{\partial f(m,t)}{\partial t}\,dm\,|_{\text{creation by fragmentation}} \qquad (5)$$

where $f(mt)\,dm$ is the particle number density function, i.e., the number of particles per unit volume of space in the mass range m to $m+dm$. The number density $f(m,t)\,dm$ is perpetually altered by erosive and catastrophic collisions and the creation of fragments in the mass range m to $m+dm$ by the crushing of larger objects during inelastic collisions.

It has been shown (Dohnanyi, 1969 and D-I) that, for a distribution with a population index $\alpha = 13/6$ the contribution of particle creation, expressed by the last term in equation (5), is

16th MSS

流星の密度（Meteor Density）

小笠原 雅弘
M. Ogasawara

Abstract

Meteor Density is the most important parameter of its physical structures and origin.

I computed the density(ρm) of 12 meteors selected from K.P.M.(Kanto-Photographic-Meteor) Network precisely-reduced data. There are two groups in these meteors. High density group (ρm 2.1-3.7g/cm^3) meteors may originate from Apollo-Amor asteroids. Meteor streams are associated with the comets. It is confirmed that they are all belong to the low density group (ρm<1g/cm^3).

And I surmarize the quantative analysis of meteor photograps, which can be done by using the integrated luminosity (photometric mass) or by a study of the deceleration of the meteoroid (dynamic mass).

軌道が正確に計算されている隕石．（3ケだけ）

{ トリノ・チェコ ― プリムラム
　米 ― ロスト・シティ
　カナダ ― イニス・フリー

そこで落下は確認されていないが．隕石らしき写真からの軌道が重要性をもつ

1．はじめに

一般に流星は彗星を起源としている．しかし，地上に落下してくる隕石は軌道を調べたところ Apollo－Amor Asteroids 起源と考えられている．落下が精密に観測されて軌道が求められた隕石は未だ三例にすぎない．日々数多く観測される流星のなかに隕石状の物質が混じっていないだろうか．隕石状物質が流星に含まれているならば，軌道を求めることによってより明確に隕石の起源をさぐることはできないだろうか．

彗星を起源とするものと，小惑星を起源とする流星があると考えた時，その差を最も良くきわだたせるものは密度の違いであろう．彗星に起源をもつなら，密度は 1g/cm^3 以下になるが，小惑星に起源をもつとするなら隕石からの類推によって 2.1～3.7g/cm^3 の密度になるだろう．関東写真流星連絡会（KPM）のネットワークによって，1972～1980年に観測されたデータから流星の密度とその軌道分布を調べてみた．あわせて密度の定量的算出法もまとめてみる．

2．流星の発光点と消滅点高度分布

Fig.－1 は，流星の発光点－消滅点高度を，速度を横軸にとってまとめたものである．速度が速くなるほど，発光点，消滅点ともに高くなる傾向がはっきりとあらわれている．

KPM－7501，7722（関東写真流星連絡会の No.）の2つの流星の消滅点が40km台と

住所：〒182　調布市　布田　2－9－1　清風堂ビル 406 号

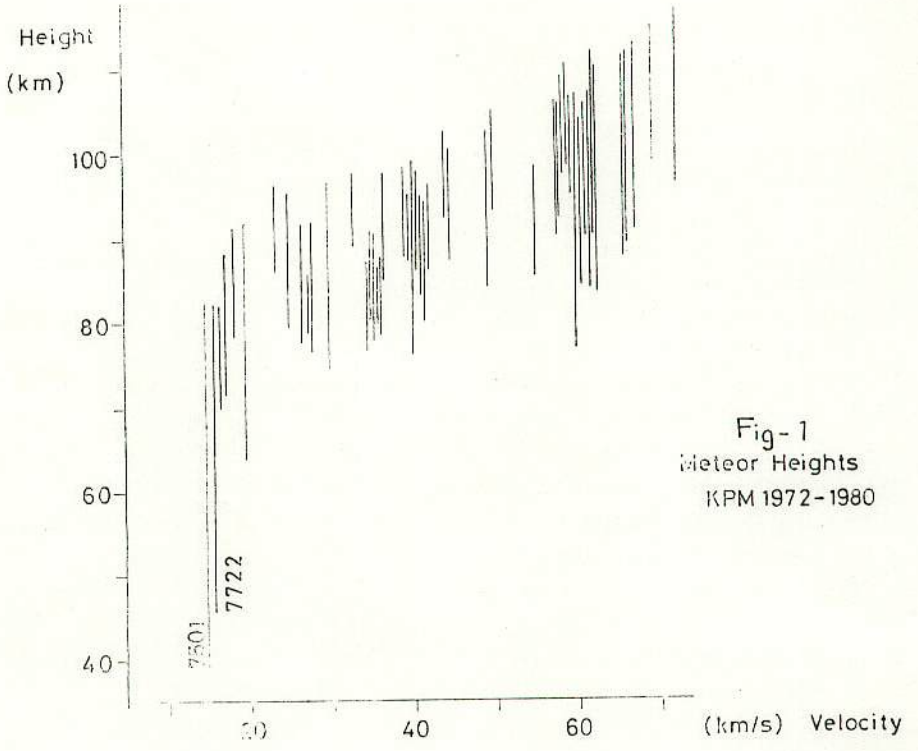

Fig-1
Meteor Heights
KPM 1972-1980

他のものに比べて大変低いのが注目される。このことからこの2つの流星は相当こわれにくい性質をもっていると考えられる。普通の流星物質が、ガサガサした低密度の物質であるのに対して、この二例はコンパクトにまとまった比較的硬い岩石状の高密度物質でできていると推定される。

Ceplecha (1967) などは、発光点高度に着目して流星を分類、定性的に密度を求めている。しかし流星の発光点は、それを撮るカメラや観測地からの距離、空の状態によって大きく変わってくるので確定的なデータとはいえない。

そこで定量的に密度を算出するために、二種類の定量的解析を行ない、それを比較して一致点を見い出す方法を用いた。以下に具体的解析法をまとめる。

3. 測光質量と力学質量

流星の質量を計算する2つの方法がある。流星体が空気の抵抗を受けて減速する様子から求められるDynamic mass (力学的質量) と、流星の持っている運動エネルギーのうちどれだけが光に変わるかをもとにしたPhotometric mass (測光質量) である。

Dynamic mass (Md) は(1)式で与えられる。

$$M_d \dot{V} = -C_D F \rho V^2 \quad \cdots\cdots (1)$$

C_D : Drag Coefficient　空気抵抗係数：0.5（流星のとき仮定）

F : Cross Section of the meteorite, ρ : Atmospheric density

ただし断面積 F は

$$F = A (M_d/\rho_m)^{2/3} \quad \cdots\cdots (2)$$

A : Shape factor, ρ_m : Meteoric density　普：1.2

したがって

$$M_d^{1/3} = -C_D \cdot A \cdot \rho_m^{-2/3} \rho V^2 / \dot{V} \quad \cdots\cdots (3)$$

となる．計算では大気密度は U.S. Standard Atmosphere (1962) の値を用い，A は球形として 1.2 なる値を使った．C_D は，観測されるような明るい流星ではその前面に Compress された大気のキャップができて $C_D \sim 0.5$ 位になるとされているので $C_D = 0.5$ を用いた．

Photometric mass (M_p) は次のようにして求める．ある単位時間に流星体から気化した質量 $-\dot{M}_p$ は，$-\frac{1}{2}\dot{M}_p V^2$ の運動エネルギーを持っている．光のエネルギー I は，

$$I = -\frac{\tau}{2} \dot{M}_p V^2 \quad \cdots\cdots (4)$$

τ : luminous efficiency

であらわされる．

ゆえに $\dot{M}_p = -\frac{2}{\tau} \cdot \frac{I}{V^2}$ となり，回転シャッターで切断された Segments を各々写真測光を行ない，数値分析してゆく．(5)式によって M_p を求めることができる．

$$M_p = -\frac{2}{\tau} \int_0^{t_{end}} \frac{I(t)}{(V(t))^2} dt \quad \cdots\cdots (5)$$

luminous efficiency については いろいろな人の研究があるが，ここでは Verniani (1964) による $\tau = 1 \times 10^{-19} \cdot V \quad \cdots\cdots (6)$ (c.g.s. unit) を用いた．

4. 密度による分類

このようにして求められた M_d（実線）と M_p（点線）を Fig-2 にまとめる．M_d は，ρ_m を 0.1～3.7 g/cm³ のフリーパラメーターとして変化させてみた．

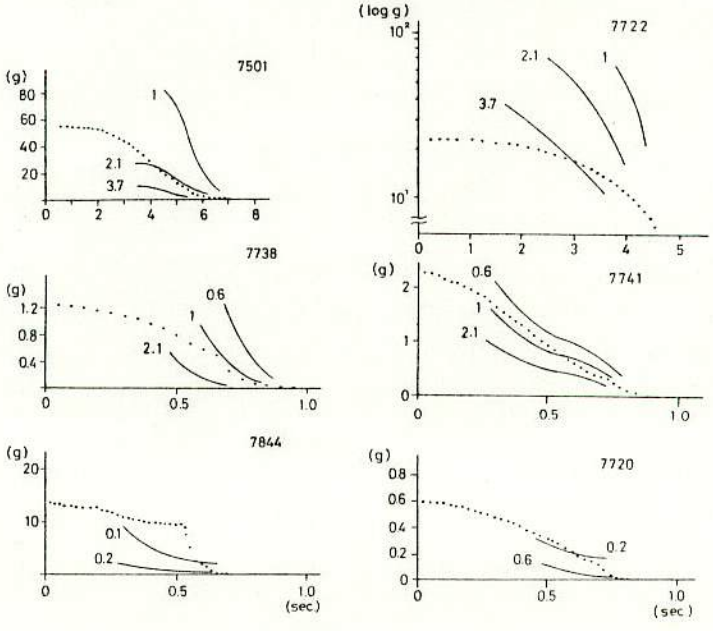

Fig.-2
M_d と M_p の比較
（6例）

両者の一致するところがその流星体の密度をあらわす。流星によって相当密度の違っていることがわかる。

KPM 7501, 7722など ρ_m 2.1～3.7g/cm³ のものを High density group、7738以下の ρ_m < 1g/cm³ のものを Low density group と分類することができる。

つぎに流星の密度と軌道の関係を調べてみる。Fig-3は、Kresak (1967) が提唱している a/e Diagram に、Apollo - Amor Asteroids と、密度の調べられた流星を図示したものである。

5. 考察とまとめ

流星における密度の差は何を意味するのだろうか。High density group は、その密度がC, O-Chondrite と一致している。また Apollo-Amor Asteroid は反射スペクトルが得られた例は少ないが、Amor type のうち (433) Eros は H 5-6, (1685) Toro は L 5-6 の O-Chondrite であることが知られている。他の多くも O-Chondrite 状であることがわかっている。一方、1978 SB, などは C-Chondrite 状ではないかという観測がある。このような点を考慮すると、High density group の流星は、Apollo-Amor を Origin とする Chondrite 状物体といって間違いはないであろう。

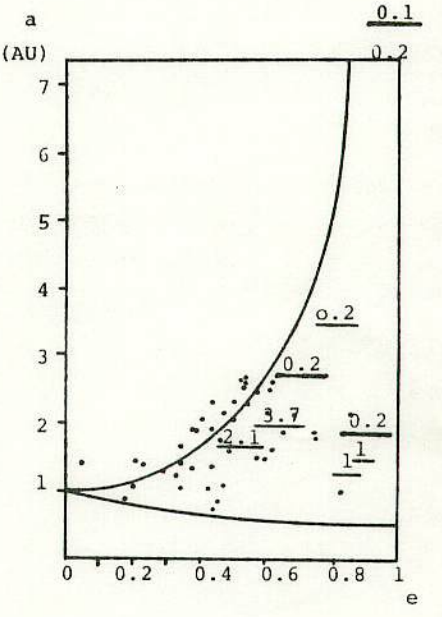

Fig.3 Meteoric Density a/e Diagram

一方、Low density group に属するのは、Stream を成すもので、これらの Origin は Comet である。a の違いによって密度が大分変わっている。KPM 7738, 7741 は Geminids に属している。この Stream の流星は、ρ_m ～1g/cm³ と割り合い大きい。他は 0.2g/cm³ 以下と極端に小さな値が求められた。

Brownlee etal. (1973) らが、U-2 による Flight や Balloon で採集した Cosmic Dust の写真を見ると、多孔質で Low density な粒子が混じっているようである。Comet の核から放出された後、H_2O, CO_2, ice が蒸発してこのように多孔質な物質をつくりあげたのだろう。

Low density group に属する流星の密度の多くが 1g/cm³ をしたまわるのは、ここで求められた density が bulk density であり、多孔質の物質ではそれを構成する物質の density は大きくとも、bulk density は相当に小さなものになる効果が働くためであろう。とすると、a の違いによって密度の差を生じるというのは porous の度合いを反映しているのだろうか。

Acknowledgement

この研究をまとめるにあたり、東大地震研の長沢 工氏より多大の助言をいただいた。流星の測定や軌道計算の面で、KPM（関東写真流星連絡会）の落合孝志、寺田充、木村直人、富田哲行氏、日本大学文理学部物理学教室、日本大学天文学研究会、東京理科大学天文部の方々をはじめとする多くの人々に協力をいただいた。

ここに感謝の意を表します。

References

- Z. Ceplecha (1967) Smithson. Contr. Astrophys. 11, 35
- F. Verniani (1964) SAO Special Report No. 145
- F. Verniani (1967) Smithson. Contr. Astrophys. 10, 181
- L. Kresak (1967) Meteor Orbits and Dust NASA SP-135 SCA Vol. 11 p 9-34
- D. Brownlee etal. (1973) Evolutionary and Physical Properties of Meteoroids NASA SP-319 p 291-295

Discussion

田村 真一：Dynamic mass の estimation には入射角が考慮されているのか。
小笠原　：軌道計算をする過程で入射角は計算されている。
古在 由秀：Atmospheric density の estimate もその過程で考慮されていると考えられる。
向井 正　：Obs. velocity と real velocity との間の誤差は。
小笠原　：それも軌道計算の過程で Obs. velocity を real velocity に直して計算している。
長谷川 一郎：photometric mass の観測誤差はどれくらいか。またそれが dynamic mass から推定した密度にどの程度影響するか。
小笠原　：mag. の測定誤差が ±0.2 mag. 程度であるので、photometric mass の誤差は 10 ～ 20% になる。dynamic mass は ρ_m の 2 乗で変わるので Mp の 20% 誤差 はほとんど影響はない。

16th用 14th MSS

20. Cosmic Dust in the Atmosphere and in the Interplanetary Space at 1 AU Today and in the Early Solar System

P210 表紙だけ

H. Fechtig
Max-Planck-Institut für Kernphysik
Heidelberg, Germany

富田
(武蔵高)

where

N/F = cumulative number of craters on the equilibrium curve
$\Phi(m)$ = cumulative flux of the corresponding meteoroids.

For 0.3 mm diameter craters (observable on small lunar surface samples) the mean crater lifetime is approximately 10^7 yr. For 1-m diameter craters the lifetime is 10^8 to 10^9 yr which is consistent with cosmic-ray-exposure age determinations for the Apollo 12 soil of 350 million yr (Kirsten, Steinbrunn, and Zähringer, 1971).

The latest progress has been gained by scanning smooth-crater glass linings of sample No. 12063.106, glass-coated sample No. 12024.8.1, and a glass ellipsoid from sample No. 14257 (Fechtig, Mehl, Neukum, and Schneider, 1972). It was possible to discover and count craters down to about 0.3μ diameters with a $D^{-0.8}$ size distribution. The crater number density for craters $\geq 1\mu$ diameter is found to be 10^3 craters per cm^2. The conversion into fluxes according to Neukum and Dietzel (1971) results in a $m^{-0.6}$ distribution down to 0.15μ diameter particles (fig. 7).

The overall meteoroid flux distribution as derived from the distribution of lunar craters is shown in the flux diagram of figure 8. The general slope in the mass distribution is -1 according to equation (7). The distribution shows a depletion at about 30μ-diameter particle size. There, the slope changes to -0.6 down to meteoroid masses of about 10^{-15} g. These submicron-sized craters are considered as an important observation concerning the existence of submicron-sized solid

P215

THE PRESENT METEOROID FLUX

Figure 9 shows the flux of cosmic dust cumulatively plotted as a function of mass. The results are discussed in four groups:

(a) Results from lunar crater distributions
(b) Results obtained in interplanetary deep space (including zodiacal light measurements)
(c) Spacecraft results (between Earth and Moon and from Lunar Orbiter)
(d) Results from dust collectors and detectors in the atmosphere (rocket- and balloon-borne experiments).

Lunar Craters

The general mass distribution derived from lunar-crater statistics have been discussed in the previous section. The results are labeled "MOON" in figure 9. The slope for larger particles ($>30\mu$ diameter) is -1, for smaller particles ($<30\mu$ diameter), -0.6.

Interplanetary Deep Space

アレクサンダーらは

Measurements were reported by Alexander et al. (1971) from the Mariner IV dust experiment and by Berg and Gerloff (1971) from the Pioneer 8 and 9 experiments. Leinert (1971) has calculated fluxes from earlier zodiacal-light measurements by Elsässer (1958), Ingham (1961) and Weinberg (1964).

From the Pioneer dust experiment a cutoff was

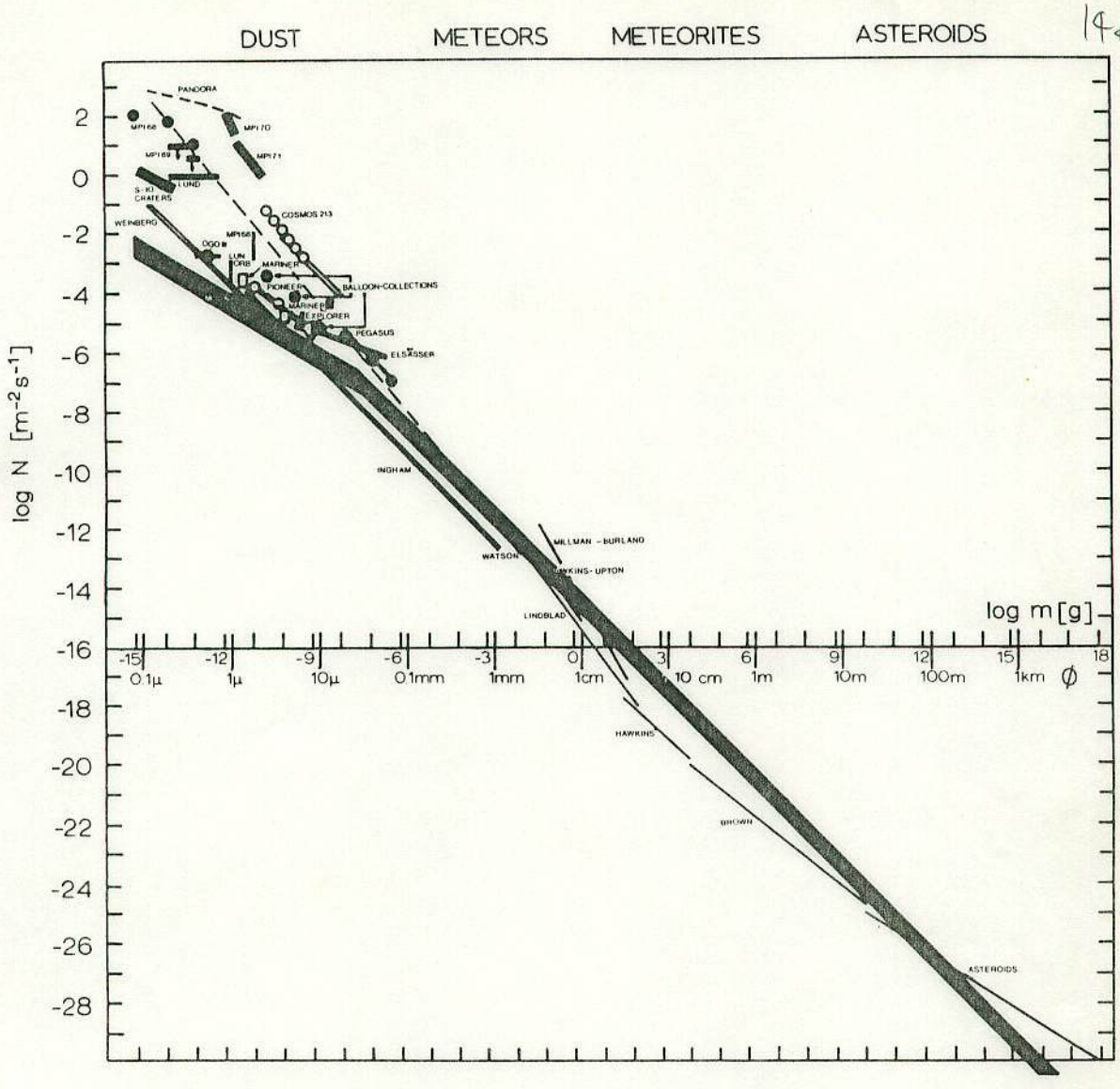

FIGURE 8.—Cumulative meteoroid fluxes as a function of mass.

reported (Berg and Gerloff, 1971; Gerloff and Berg, 1971) at about 10^{-11} g and interpreted with orbit elements according to Dohnanyi (1969). Generally, the *in situ* results and the indirect measurements of the zodiacal light are very similar. The cutoff from the zodiacal-light measurements is a question of interpretation.

A comparison of these results with the results from lunar-crater statistics leads one to question the Pioneer detection cutoff of particles at 10^{-11} g. On the contrary, submicron-sized lunar craters have been found, thus indicating the existence of submicron-sized particles in the interplanetary space. Two possible explanations of this apparent discrepancy are as follows:

(a) If a variable particle-size cutoff exists because of chemical composition, the smallest particles are nonmetallics (silicates, quartz). The general lack of metals for the smallest particles influences heavily the ion production of the impact detectors used in the Pioneer mission as discussed in a previous section of this paper.

(b) The Pioneer dust experiment with a quasi-circular orbit around the Sun cannot detect

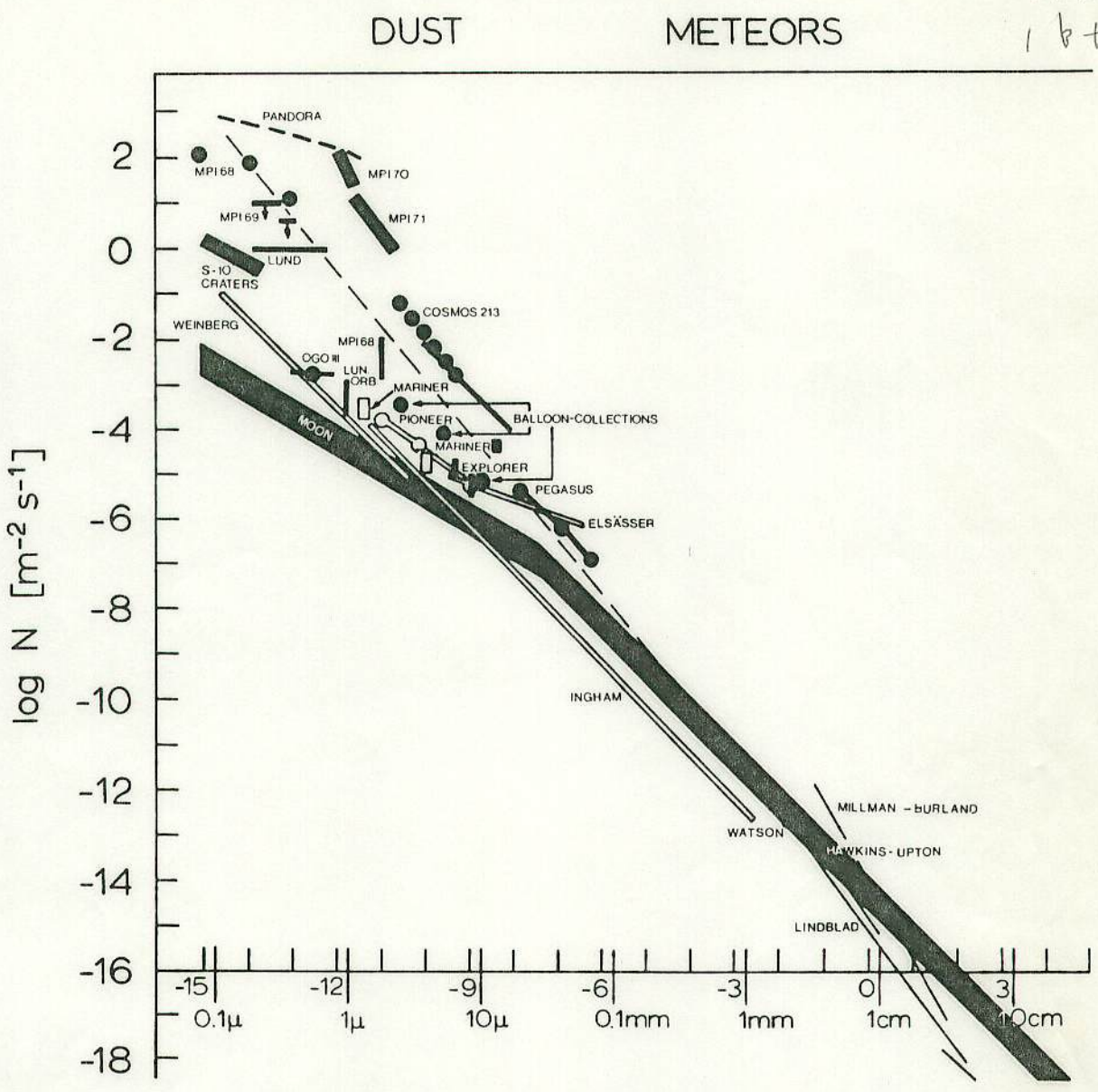

FIGURE 9.—Cumulative cosmic dust fluxes as a function of mass.

circularly orbiting particles, since the relative velocity is not high enough for small particles to penetrate the thin foil in front of the detector and produce enough ions to be recorded. (The lowest relative velocity must exceed 0.7 km/s to be detected.)

Spacecraft Results

Higher fluxes have been measured by Earth and Moon satellites. Using different techniques, results were reported from the following experiments: capacitive detectors on Pegasus (Anon., 1966, 1967), penetration-experiment on Explorer XXIII (Naumann, 1966), microphones on Cosmos 213 (Nazarova and Rybakov, 1971), ionization detector on OGO III (Alexander, Arthur, and Bohn, 1971), ionization detector on Lunar Orbiter 35 (Alexander et al., 1971), and the S 10- S 12-craters (Hemenway et al., 1968). Two possible explanations for these higher near-Earth fluxes are:

(a) Temporarily higher influxes of lunar debris are produced both by impacts of meteor streams and sporadic dust particles on the lunar surface. This origin was discussed by Alexander et al. (1971). Gault et al. (1963) and Colombo et al. (1966) have also discussed this problem.

(b) Fireballs that might be of low-density material (Dubin, 1971) form disintegrated products.

Atmospheric Dust

The highest flux numbers are reported from experiments in the atmosphere using rocket and balloon-borne dust collectors and detectors. Based on the Pandora and the balloon-top collections by Hemenway et al. (1971), the balloon collections of Brownlee et al. (1971), the MPI 68, 69, 70 collections (Auer et al., 1970; Fechtig and Feuerstein, 1970; Fechtig, Feuerstein, and Rauser, 1971), the LUSTER 68 flight through a NLC display (Farlow et al., 1970), and the detector results of "Lund" (Lindblad et al., 1970), MPI 70, 71 (Fechtig, Feuerstein, and Rauser, 1971; Rauser and Fechtig, 1972), one can state the following items:

(a) No cutoff down to masses of about 10^{-15} g could be found.

(b) Easily fragile particles are evident and support Jacchia's (1955) and Verniani's (1969) observations of low-density material.

(c) Large variations probably due to meteor shower activities and Noctilucent Cloud displays are observed for the fluxes.

(d) Still not sufficiently known is the influence of the upper atmosphere on the dynamics of small particles. In 1970 we (Rauser and Fechtig, 1972) measured a velocity profile of micron-sized particles between 70 and 110 km altitude.

The measured velocities are lower than expected at 110 km altitude which suggests that the particles are of a fluffy low-density material. However, the measured velocities are about 2 orders of magnitudes higher than expected (Kornblum, 1969) at 70 to 80 km altitudes. The existence of a temperature minimum at about 85 km altitude leads one to expect a diameter and/or density increase of particles by absorption of condensable material like water or CO_2. This mechanism might also explain the Noctilucent Clouds. A layering effect can be calculated from the detailed data.

Finally, total influx rates can be calculated from the flux curve. One calculates a total daily influx of interplanetary material on the Earth of about 25 tons. This number is consistent with investigations by Keays et al. (1970). These authors have investigated lunar samples for meteoritic components. Although the investigations were carried out in a completely different scientific field, the results show an agreement.

SUMMARY

This paper contains a description of techniques used in recent experiments to detect and analyze cosmic dust and micrometeorites. Furthermore, the results both from the study of lunar crater statistics and from *in situ* measurements have been reviewed.

Ionization detectors and controlled collectors represent important progress in the techniques used in the research field of cosmic dust.

The results from lunar crater statistics show an agreement with the results obtained from *in situ* measurements in interplanetary space and derived from zodiacal-light measurements. The near-Earth results show an enhancement in the flux numbers. This can be caused either by secondary lunar debris or by disintegration of low-density fireballs in the outer atmosphere.

For future experiments *in situ* measurements are needed in interplanetary space. The question of the chemical composition of particles is important with respect to the origin of cosmic dust.

17th MSS 流星会議資料

流星物質の空間密度について

81' 流星会議

二見広志 小林秀行
寺田充

最近、流星の光度と質量の関係についての議論が盛んになるにあたり、この関係を利用して、流星の計数観測の目的の1つである流星物質の空間密度を質量をもって表わしたらどうだろうかと思いつき、その解析方法をまとめたので発表することにする。

1. 流星の光度と質量の関係

流星の光度と質量の関係は、通常、写真観測により対地速度の変化と光度から求める。しかし、この方法は速度変化がよく観測されるような大流星でなければ使えず0～4等程度の流星ではこの方法で質量を求めることは不可能である。そこで今回は、流星の単体モデルを用い、数値シミュレーションによって質量と光度の関係を求めてみた。

ここで、流星物質の密度は0.3g/cm³とし、等級は最大等級を用い、光度は絶対等級を算出し、これを用いる。

絶対等級	質量
−3	1.90 g
−2	0.80
−1	0.33
0	0.13
1	0.055
2	0.023
3	0.010
4	0.005
5	0.002

単体モデルについては、次の連立微分方程式を数値的に解いた。

$$\frac{dV}{dt} = -\Gamma A m^{-\frac{1}{3}} \rho_m^{-\frac{2}{3}} \rho_a V^2$$

$$\frac{dm}{dt} = -\frac{\Lambda}{2\varepsilon} A \left(\frac{m}{\rho_m}\right)^{\frac{2}{3}} \rho_a V^3$$

V；流星の速度、m；流星の質量
ρ_a；大気密度

2. 流星物質の空間密度の求め方

通常行なわれている流星数の空間密度と同様な方法で行なう。密度を求めるにはまず、流星が観測できる領域の面積を求める必要がある。ラムカ観測では、この面積はすぐ計算できるが、今回は団体計数のデータしか手元になかったので出現星座の中心の天頂角が66.5度よりも小さいもののみを選んで計算した。この領域は半径230Km(地上100Km)である。Per群の流星物質は、この領域を60Km/Sで通過していく。輻射点高度の補正はあらかじめしておく。

流星物質の空間密度は次の様な式で求められる。

MSS-017

$$\left[\begin{matrix}\text{流星物質の}\\ \text{空間密度}\end{matrix}\right] = \frac{\left[\begin{matrix}\text{輻射点高度を補正した1時間あたりの流星物質の質量}\end{matrix}\right]}{\left[\begin{matrix}\text{流星出現領域の面積}\end{matrix}\right] \times \left[\begin{matrix}\text{流星の対地速度(秒速)}\end{matrix}\right] \times 3600}$$

3. 流星群に属する流星物質の量の推定

流星物質の空間密度は、その群の流星物質の総量を知る大きな手がかりとなると思われる。この総量を知ることに我々は大きな興味を持っている。しかし現在の段階では、次のような解決しなければならない困難がある。すなわち、流星の観測は、地球の軌道という"線"上でしか行なえず、断面を知ることができない。さらに、その線が分布のやく(分布の最も濃い所)を通っているのかどうかを知ることができないことである。

しかし、いくつかの仮定を通して総量を算出してみることも無意味な事ではないので例をあげて算出してみる。

○サンプル→1980年 8日、Per群 理大天文部 団体計数(5人)

太陽黄経	質量(g)
140.01	2.71
140.01	1.97
140.59	9.28
141.00	2.78
141.02	1.82
141.04	4.26
141.04	2.40

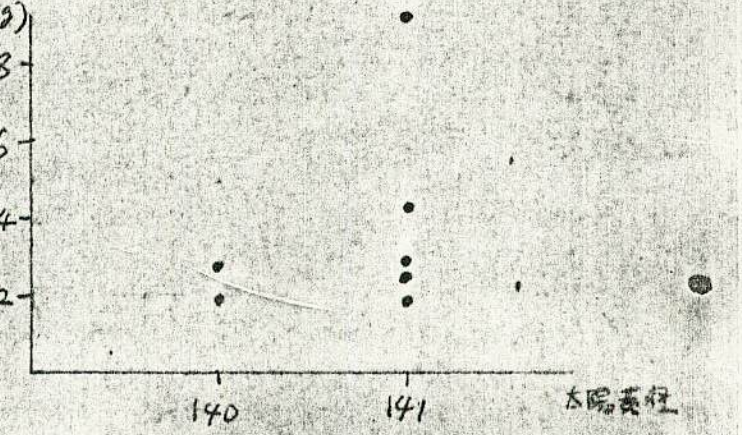

○計算例

⊙=140° の平均質量 2.34 g/hour　　⊙=141 の平均質量 4.11 g/hour

空間密度 6.5×10^{-26} g/cm³　　空間密度 1.14×10^{-25} g/cm³

○今、簡単のため 2g平均で10日間の出現があったとする。
またPer群の日心速度を41.5km/s、同期を12.0°とする。

流星物質が円筒形を一様に分布しているとし、その中心を地球が通るとすると

$S = 1.66\times10^{15}\,cm^2$　　$Volume/hour = S\times60\times10^5\times3600$

$= 3.59\times10^{25}\,cm^3/hour$

2g/hour $= 5.57\times10^{-26}$ g/cm³

$(2.6\times10^{12})\times\pi\times 4.15\times10^5\times120\times365.5\times24\times3600$

$\times 5.57\times10^{-26}$

$= 1.9\times10^{16}$ g //　(軌道全質量)

1.9×10^{10} t

1900億t

IRAS-ARAKI-ALCOCK彗星

Epock 1983.5.21
Ω 192.78
ω 48.39
i 73.38
q 0.991381 AU
e 1.0

「裏面参照」

日流研 オリエンテーション
6/12(日) 13h～
東京電機大 5号館

44人

26th MSS
1983.5.8.(日)

Cumulative flux

府川 正明 (日大)

1. Cumulative flux の紹介

Cumulative flux (キュムレイティブ フラックス) は直訳すると累積流量ということですが、図1はそのグラフです。グラフの横軸は流星の質量の対数 ($\log_{10}M$(kg)) を表わし、縦軸は毎秒・1m²の面積に上から下に通過 (2πsr) する流星数の対数を表わしています。(ただしある質量の流星数はそれ以上大きな質量の流星数をすべて含んだ値：累積流星数) つまりCumulative fluxとは流星物質の質量分布と言うことができます。

2. Cumulative flux の求め方

a. 惑星・衛星等の隕石クレーターの大きさ数、古さを調べることによって、その惑星の位置に於る太陽系内の隕石のCumulative fluxを知ることができる。

b. 人工衛星に平板を積み込み、宇宙空間に於てこれを広げ、平板に流星物質が衝突した時の平板の振動を感知してこの振動の大きさと数をカウントすればCumulative fluxを知ることができる。

c. 地上で流星を眼視または写真で観測し、その光度と個数の関数(光度関数)を求めた後、光度を質量に換算して流星のCumulative fluxを知ることができる。

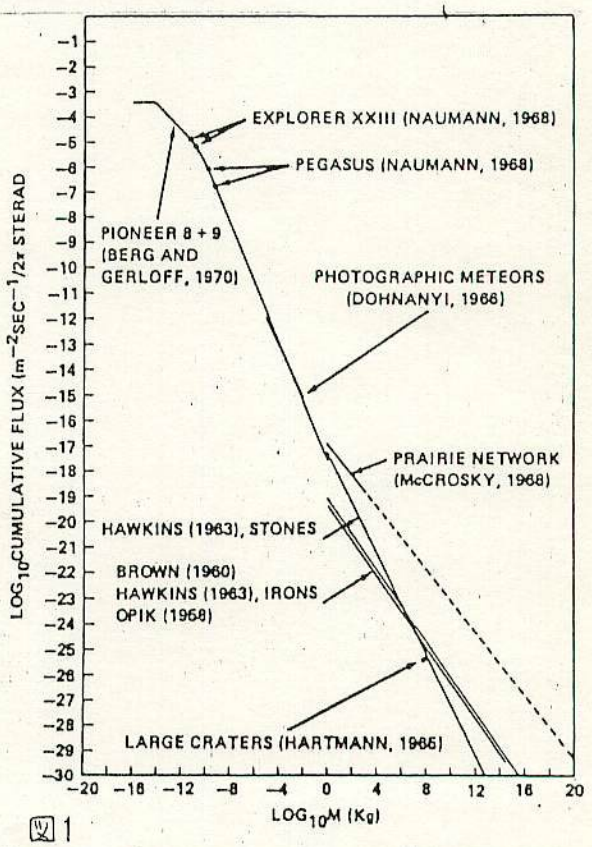

図1

FIGURE 1.—Cumulative flux (m^{-2} $s^{-1}/2\pi$ sr) of meteoroids into Earth's atmosphere having a mass of m (kg) or greater.

3. 流星の光度から質量を求める。

光度関数からCumulative fluxを求めるためには、まず流星の光度を質量に変換する必要があります。これに関しては流星物理セミナーに於て以下の様に考えることができる。

流星発光のエネルギーは流星物質が気化して減少した質量に比例するものと考えられます。気化した質量 $-M_p$ は $-\frac{1}{2}M_pV^2$ の運動エネルギーを持っていて写真域に対する光のエネルギー I_p、全エネルギーの写真域の光への変換割合を τ_p (光力係数) とすると

$$I_P = -\frac{\tau_P}{2} M_P V^2 \quad 1)$$

$$M_P = -\frac{2}{\tau_P}\frac{I_P}{V^2}$$

$$M_P(t) = \frac{2}{\tau_P}\int I_P(t)/\{V(t)\}^2\, dt$$ 発光点から消滅点まで積分

τについては

$$\tau = \frac{2\varepsilon}{\mu V^2 \beta} \quad 2)$$

ε：1個の原子を電離させるための平均エネルギー
(電離ポテンシャル)~7eV~1×10^{-11} erg
μ：流星原子1個あたりの質量 平均原子量 23→3.82×10^{-23}g
β：電離確率 $10^{-28}\ V^4$ (cgs)

$$\tau_P = 5.248\times10^{-10}\ V \quad (cgs)$$

よって 流星の光エネルギー I_P を測定して求め 速度Vを軌道計算から決定できれば、流星の質量を求めることができるわけです。

次に写真から流星の光度を求める方法を簡単に紹介します。[3] まずマイクロフォトメータを使用してフィルム上の流星の濃度(D)を測定し、この濃度を光の強度(I)に変換します。この変換は同じフィルム上に写された星の光度と写真濃度の関係や、光学ウェッジと写真濃度の関係を使って行います。そして、フィルム自体の分光感度、大気の吸収等を補正して流星の相対光度を決めこれを、見かけの等級に変換します。[4]

次に以上より求められた見かけの等級を絶対等級(流星を天頂100kmにもってきた時の等級)に標準化します。またこの時、流星までの距離の違いによる大気吸収の違いと、発光点と消滅点での観測地からの距離の違いも補正します。

ここまで計算してやっと 流星経路上の各点に於る絶対等級(m)が求められ

$$M_P = \frac{2}{\tau_m}\sum_{t=0}^{end} m(t)/\{V(t)\}^2\cdot\Delta t \qquad \tau_m = 10^{-19}\cdot V\ (cgs)$$

より 流星の測光質量(M_P)を求めることができます。

資料
1) 長沢工：流星質量計算についてのメモ (2-MSS)
2) 長沢工：流星の明るさについてのメモ (3-MSS)
3) 小笠原雅弘：流星写真測光 (1) (5-MSS)
4) 小笠原雅弘：流星写真測光 (2) (13-MSS)

IRAS-アラキ-アルコット彗星　　寺田（弟）　　26-MSS

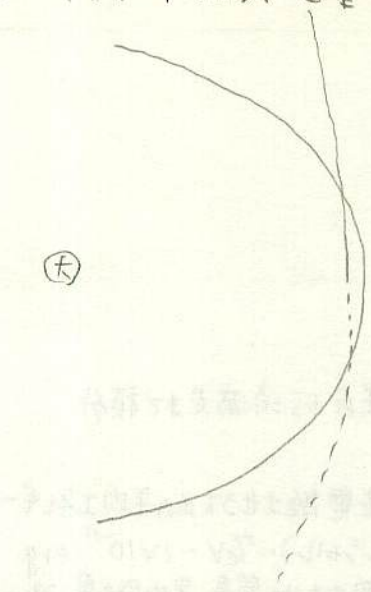

輻射点：α 288 δ 43　地心速度：45km

最接近　11日　0.031AU　500万km

地球が彗星の降交点通過　10日 6h 30m JST

降交点との距離　0.003 AU　50万km

彗星が降交点通過　12日

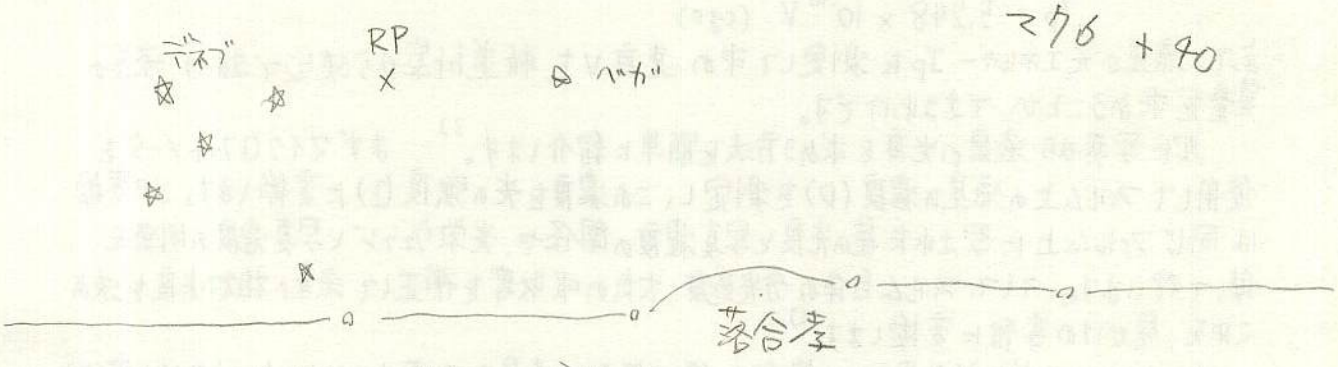

6月 うしかい ε 群　εBoo 突発群

R.P. { α：220～230
　　 { δ：30～35

速・微光

ソビエト　π CrB　HR 4074

6月15/16日 22h (UT)　(235, 34)
　　229, 34

落合 22h (JST)

4. 光度関数から Cumulative flux を求める

以上より流星の光度を質量に変化することが可能になりました。ただし観測上出た光度関数の光度は観測眼視等級であるのに対し、光度－質量変換式の光度は写真最大絶対等級だからその間に補正が必要となります。しかし今回は質量と個数との関係（グラフの傾き）だけに注目しその実数にはふれないことにします。よって本来絶対等級の明るい流星は暗く、暗い流星はより暗く見積ることになりますが、グラフの傾きは変化しないものと仮定します。

次に流星個数を毎秒 $1m^2$ あたり 上から下に通過する流星数に変換する必要がありますが、やはりこの場合も観測面積がはっきりしないこと、対象が群流星で突入角度がランダムでなく、また輻射点の位置によって数が大きく違うことなどより、補正はあまりめグラフの傾きだけに注目したいと思います。

これらを縦軸を $1m^2$ を毎秒、上から下へ通過（$2\pi sr$）する流星の個数の対数、横軸を流星の質量の対数としてグラフにすると、または、はっきりとした結論は出ませんが流星物質の質量と個数は大質量から小質量まで、だいたい log リニアな関係があるようです。

5. いろいろな観測からの Cumulative flux

表1に 太陽系内星間物質のさまざまな質量（又は直径）に対する観測対象を示しました。

表1. 太陽系内星間物質の観測対象とその質量（直径）分布

観測対象	DUSTの人工衛星直接測定	黄道光濃度	月マイクロクレータ
質量（直径）分布	$10^{-17} \sim 10^{-5}$ g	1～10 μm	$10^{-4} \sim 1$ mm

宇宙塵	流星眼視観測 光度関数	流星写真観測 測光質量	隕石	月クレータ	小惑星 質量分布
$1 \sim 10^2$ μm	$10^{-3} \sim 10$ g	$10^{-1} \sim 10^3$ g	$10^2 \sim$ g	$\sim 10^3$ m	$1 \sim 10^3$ km

- DUSTの人工衛星直接測定の方法

DUSTの衝突を電圧に変え測定する方法（マイクロフォン型）が1950年にTXMカでV-2ロケットにより行なわれて以来、最近ではパイオニア8/9号で大きな成果をあげています。

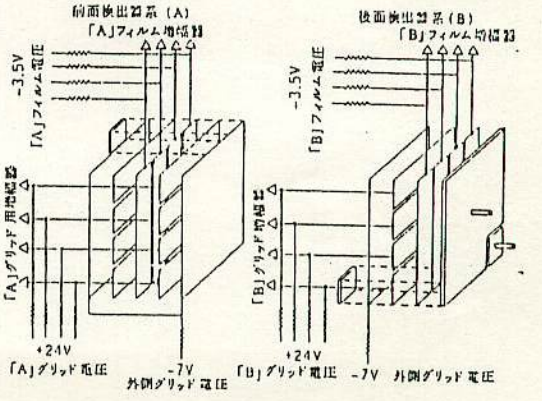

パイオニア8/9号の検出器

◦ 月のマイクロクレータ

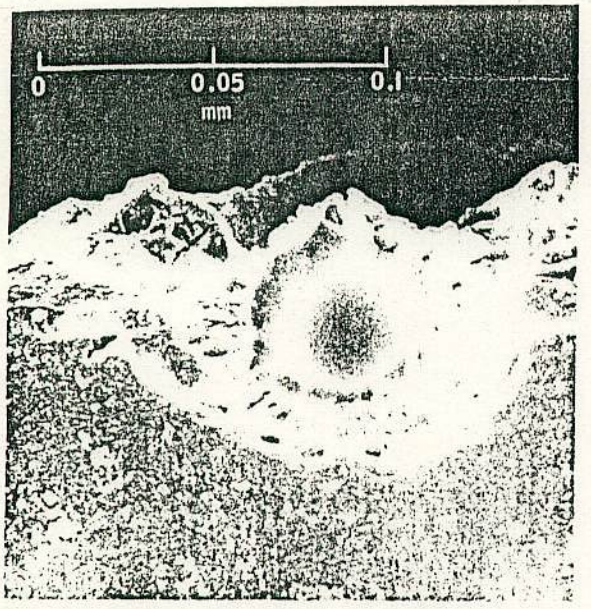

FIGURE 4.—A scanning electron micrograph of a small microcrater. The glass-lined pit and the spall area are nicely illustrated, but the microfractured halo zone is essentially invisible because the scanning electron microscope technique produces an image of the topography only and does not record any albedo differences present on the surface under study. In this case, the host rock is a millimeter-sized glass fragment from the lunar soil collected during the Apollo 11 mission. (Scanning electron micrograph courtesy of D. S. McKay, NASA MSC photograph 70-40177)

マイクロクレータの電子顕微鏡写真

アポロが採集した月の石の表面にはマイクロクレータと呼ばれる小さな穴(pit)があいています。(左図写真)
これは微粒子が月に石に直接衝突してあけたもので、その穴の直径と数を調べることで Cumulative flux を求めることができます。

以上のようにして求められた Cumulative flux を組合せていくと、0.1mm～10km に及ぶ太陽系内星間物質の Cumulative flux を知ることができます

1988 Part 1 Vol. 45

SOMSS from 下半年

104 Meteors, Meteor Streams

104.001 **A note on antimatter meteors.**
M. Beech.
Earth, Moon, Planets, Vol. 40, No. 2, p. 213 – 216 (1988).
It is argued here that unless antimatter meteors can be shown to possess some unambiguously unique characteristic not displayed by ordinary koinomatter meteors, it will be difficult to infer their existence given the standard interpretation of meteoroid structure. It is also argued, however, that the existence of antimatter meteors is extremely unlikely.

104.002 **Observing meteors: XII. Getting started with meteors.**
D. H. Levy.
Strolling Astron., Vol. 32, Nos. 7 – 8, p. 177 – 178 (1988).

104.003 **Boötiden 1987.**
M. Nolle, B. Koch.
Radiant, Jaarg. 10, Nr. 1, p. 4 – 5 (1988).

104.004 **Vuurbollen in April.**
P. Koning.
Radiant, Jaarg. 10, Nr. 1, p. 12 – 15 (1988).
The article deals with an analysis of over 600 observed fireballs brighter than –8 magnitude, observed between 1972 and 1987 all over the world. Data were used to carry out a statistical analysis concerning the distribution of fireball events over the year.

104.005 **Ursiden 1987.**
P. Jenniskens.
Radiant, Jaarg. 10, Nr. 2, p. 21 – 22 (1988).
The first results of the Ursid campaign 1987 are presented. Observer B. Rispens stayed in Lardier, France, from December 14 until 25. He noticed 1194 sporadic meteors, 98 Ursids and 108 Geminids. The observations are of special interest because they cover the full period of activity of the Ursid meteor shower.

104.006 **NAS–meteor section: Ursiden 1986.**
P. Jenniskens, T. E. Hillestad.
Radiant, Jaarg. 10, Nr. 2, p. 23 – 24 (1988).
10 minute counts are given for the Ursid outburst of 1986 as observed by NAS-MS members.

104.007 **De Leoniden in de rustige jaren.**
P. Jenniskens.
Radiant, Jaarg. 10, Nr. 2, p. 25 – 27 (1988).
Observations by visual observers of the Leonid meteor stream are analyzed. The observations cover the period 1981 – 1987 while the parent comet P/Tempel-Tuttle was near its aphelium.

104.008 **Procedure of interpretation of meteor observations accounting fragmentation.**
P. B. Babadzhanov, G. G. Novikov, V. N. Lebedinets, A. V. Blokhin.
Astron. Vestn., Tom 22, No. 1, p. 71 – 78 (1988). In Russian. English translation in Sol. Syst. Res.
Formulae describing the light curves I and ionization curves L of meteors accounting the theory of quasi-continuous fragmentation are obtained and analysed.

104.009 **On the Perseid meteor stream 1986 (II). Zenithal hourly rate data.**
P. Roggemans.
WGN, Vol. 16, Nr. 1, p. 12 – 31 (1988).
Using 39884 meteors observed from ten countries by 96 persons during 1456 man-hours, a rate profile of the Perseids 1986 is derived. Apart from a remarkably high activity around August 15.0, the 1986 return of the Perseids can be characterized as "normal".

104.010 **Soviet observations of the Perseids 1986.**
A. Grishchenyuk, A. Levina, V. V. Martynenko.
WGN, Vol. 16, Nr. 1, p. 32 – 34 (1988).

104.011 **The η–Aquarids 1987 in Australia.**
J. Wood.
WGN, Vol. 16, Nr. 2, p. 38 – 39 (1988).

104.012 **The η–Aquarids 1987 in Brazil.**
G. K. Renner.
WGN, Vol. 16, Nr. 2, p. 39 – 40 (1988).

104.013 **How high is a meteor?**
D. Olsson-Steel.
WGN, Vol. 16, Nr. 2, p. 41 – 48 (1988).
Some recent observations of the heights of meteors detected with backscatter radars operating at frequencies of 2, 6 and 54 MHz are reviewed, and it is shown that VHF radars detect only a small fraction of the total incident flux of small meteoroids. In addition the implications of these new results for the ecology of the smaller bodies in the solar system, and also the effect of the meteoroids upon the Earth's atmosphere, are discussed.

104.014 **The Perseids 1987 in the Soviet–Union.**
A. Grishchenyuk, A. Levina, V. Martynenko.
WGN, Vol. 16, Nr. 2, p. 49 – 50 (1988).

104.015 **The Perseids 1987 in the DDR.**
J. Rendtel.
WGN, Vol. 16, Nr. 2, p. 50 – 54 (1988).

104.016 **The Perseids 1987 in Belgium.**
G. Ticket.
WGN, Vol. 16, Nr. 2, p. 54 – 55 (1988).

104.017 **The Perseids 1987 in Florida.**
W. Simmons.
WGN, Vol. 16, Nr. 2, p. 56 – 57 (1988).

104.018 **The Quadrantids 1987 in Southern France.**
B. Koch.
WGN, Vol. 16, Nr. 2, p. 58 – 61 (1988).

104.019 **The Quadrantids 1987 in Denmark.**
P. T. Aldrich.
WGN, Vol. 16, Nr. 2, p. 61 – 62 (1988).

104.020 **Fall 1987 observations by Delphinus – The Netherlands.**
B. Rispens.
WGN, Vol. 16, Nr. 2, p. 62 – 64 (1988).

104.021 **Telescopic ε–Geminid observations.**
M. Vints.
WGN, Vol. 16, Nr. 2, p. 64 (1988).

104.022 **Meteor activity in September 1987 in Denmark.**
P. T. Aldrich.
WGN, Vol. 16, Nr. 2, p. 64 – 65 (1988).

104.023 **The Orionids 1987 from Denmark.**
P. T. Aldrich.
WGN, Vol. 16, Nr. 2, p. 66 (1988).

104.024 **The Geminids 1987 in Canada.**
P. Brown.
WGN, Vol. 16, Nr. 2, p. 67 (1988).

MSS-050

104.025 **Radar studies of cometary dust.**
W. J. Baggaley.
South. Stars, Vol. 32, No. 5, p. 145 – 148 (1987).
A programme of radar studies of meteoroids at Canterbury University has two avenues: (1) to measure the influx of meteors associated with known comets to yield stream structure, particle size distributions; (2) to determine the heliocentric orbits of radar meteors which may belong to previously unrecognised cometary nuclei which have been denuded of their gas and dust.

104.026 **The influence of ionospheric electric fields on the observed number of meteors and the mean heights of reflections during sunrise.**
A. E. Epishova, Z. M. Ioffe, L. N. Rubtsov.
Dokl. Akad. Nauk TadzhSSR, Tom 30, No. 1, p. 19 – 21 (1987).
In Russian. Abstr. in Ref. Zh., 51. Astron., 2.51.252 (1988).

104.027 **Meteore beobachten und auswerten.**
M. Nolle.
Sterne Weltraum, 27. Jahrg., Nr. 4, p. 242 – 245 (1988).

104.028 **A radar orbit search for meteors from comet Lexell.**
D. I. Olsson-Steel.
Astron. Astrophys., Vol. 195, No. 1/2, p. 338 – 344 (1988).
In this paper the 3759 radar meteor orbits determined from Adelaide, South Australia, in the 1960's are analysed using a new and powerful stream-search technique. Although there is some evidence for Lexell-related showers, this is not unambiguous due to the presence in the sporadic background of many orbits with similar orbital characteristics (very low inclinations, aphelia close to Jupiter), so that the reality of the stream cannot be proven. In a final section, the remarkable similarity between the characteristics of a hypothetical meteor shower in early December (put forward on the basis of weather records by Bowen, 1957) and the possible shower associated with Lexell occurring at that time, is briefly described.

104.029 **Gravitational breaking of meteor streams in resonance with Jupiter.**
H. Scholl, C. Froeschlé.
Astron. Astrophys., Vol. 195, No. 1/2, p. 345 – 349 (1988).
The authors investigate numerically the orbital evolution of seven meteor streams known to be located at mean motion resonances with Jupiter. The major goal was to find a splitting of the streams into arcs due to a resonance mechanism discovered previously by the authors for a model stream at the 2/1 resonance. None of the seven known meteor streams splits up into arcs due to this mechanism. On the other hand, close approaches to Jupiter of stream particles cause the formation of holes in some of the known meteor streams.

104.030 **Radar observations of Eta Aquarids in 1981 – 1986 at Dushanbe and Ondřejov.**
R. P. Chebotarev, S. O. Isamutdinov, A. Hajduk.
Bull. Astron. Inst. Czech., Vol. 39, No. 2, p. 82 – 85 (1988).
Results of simultaneous observations of radar meteor echoes during the period of the Eta Aquarid shower in 1981 – 1986 are given. The small changes in meteor activity in the consecutive returns of the shower and the relative stability of the position of the observed shower maxima with the characteristic double peak at solar longitudes of 44.4° and 47.8° show the independence of the particle space density within the stream of the position of the parent body on the orbit. The mass distribution of particles and other characteristics of the stream are also derived.

104.031 **A multiple-station Perseid over Norway.**
T. E. Hillestad.
WGN, Vol. 16, Nr. 3, p. 85 – 89 (1988).

104.032 **A triply-photographed meteor over Japan.**
K. Ohtsuka, Y. Shigeno.
WGN, Vol. 16, Nr. 3, p. 91 – 93 (1988).

104.033 **Japanese η-Aquarids observations in 1987.**
M. Koseki.
WGN, Vol. 16, Nr. 3, p. 94 – 96 (1988).

104.034 **Dutch video observations of a Leonid fireball in 1987.**
K. Jobse.
WGN, Vol. 16, Nr. 3, p. 97 – 98 (1988).

104.035 **Finnish observations – spring 1987.**
T. Hankamäki.
WGN, Vol. 16, Nr. 3, p. 99 – 100 (1988).

104.036 **Norwegian observations – spring 1987.**
T. E. Hillestad.
WGN, Vol. 16, Nr. 3, p. 101 – 102 (1988).

104.037 **An investigation into the association between Eta Aquarid meteor shower and Halley's comet.**
U. Mitra.
Bull. Astron. Soc. India, Vol. 15, No. 1, p. 23 (1987). Abstract. – See Abstr. 012.035.

104.038 **Inflow of sporadic meteor bodies to the earth.**
P. B. Babadzhanov, R. Sh. Bibarsov,
V. M. Kolmakov.
Dokl. Akad. Nauk SSSR. Ser. Mat. Fiz., Tom 296, No. 2, p. 307 – 309 (1987). In Russian. Abstr. in Ref. Zh., 51. Astron., 3.51.238 (1988).

104.039 **Report of IAU Commission 22: Meteors and interplanetary dust (*Météores et la poussière interplanétaire*).**
P. B. Babadzhanov.
Trans. IAU, Vol. XXA, p. 219 – 235 (1988). – See Abstr. 003.008.

104.040 **Cluster ions and the meteor head echo.**
J. Jones, J. B. A. Mitchell, B. A. McIntosh.
Mon. Not. R. Astron. Soc., Vol. 232, No. 4, p. 771 – 778 (1988).
Radar observations of a meteoroid entering the atmosphere occasionally exhibit a rapidly decaying echo which appears to come from, and move with, the region of the meteoroid itself. This head echo usually accompanies the normal meteor radar echo which is essentially stationary and may persist for several tens of seconds. The problem of the radar meteor head echo has remained unsolved for many years. This paper considers the possibility that the key to the enigma may lie in the very high recombination coefficients of molecular cluster ions and concludes that ionized trains containing a sufficient proportion of water cluster ions should exhibit this type of echo.

104.041 **Distribution of Lyrid meteoroids in a large range of echo durations.**
V. Porubčan, M. Šimek.
Bull. Astron. Inst. Czech., Vol. 39, No. 3, p. 165 – 168 (1988).
Radar observations of the Lyrid meteor stream made at the Ondřejov Observatory in 1980 – 1985, are analyzed and discussed from the viewpoint of determining the mass distribution exponent for overdense echoes in the range of 0.4 – 50 s. The mass exponent proved to be almost constant over the whole range of echo durations with $s \sim 1.58$. The contribution of larger particles, as compared with other meteor streams, was found to be more significant for the Lyrids. The almost constant value of s indicates a still active contribution of fresh cometary material to the stream.

104.042 **Lyrids in 1985.**
M. V. Gorshechnikov.
Astron. Vestn., Tom 22, No. 2, p. 184 – 186 (1988). In Russian. English translation in Sol. Syst. Res.
This work includes the results of the observations of the Lyrids meteor shower made in 1985 by using the multiplied counting method. The mass-distribution, index of activity, space density and other characteristics of the shower were determined. Very high activity of this shower was noticed.

MSS-050

104.043 **On the observable effect of maximum brightness shift in the direction of trajectory begin of a meteor.**
P. B. Babadzhanov, G. G. Novikov.
Dokl. Akad. Nauk TadzhSSR, Tom 30, No. 4, p. 219 – 222 (1987). In Russian. Abstr. in Ref. Zh., 51. Astron., 4.51.280 (1988).

104.044 **Quasi–continuous fragmentation of meteor bodies taking acceleration into account.**
P. B. Babadzhanov, G. G. Novikov, V. N. Lebedinets, A. V. Blokhin.
Izv. Akad. Nauk TadzhSSR. Otd–nie Fiz.–Mat., Khim., Geol. Nauk, No. 2, p. 16 – 29 (1987). In Russian. Abstr. in Ref. Zh., 51. Astron., 4.51.281 (1988).

104.045 **Theoretical meteor radiants of recently–discovered asteroids and comets, and twin showers of known meteoroid streams.**
D. Olsson–Steel.
Aust. J. Astron., Vol. 2, No. 3, p. 93 – 101 (1988). With a correction to 43.104.068.

In a previous paper (43.104.068) theoretical meteor radiants were calculated for all Earth–approaching asteroids and comets then known, and here that list is extended to include all such bodies discovered to the end of 1987. Of the new radiants, that of 1987 SY is of particular interest since it indicates that this asteroid may be the parent of the δ Leonid meteor shower.

104.046 **Results of observations of meteor streams originated by comet Halley.**
G. I. Zajtsev, V. S. Matsukova, K. P. Matsukov.
The 8th congress of the All–Union Astronomical–Geodetical Society, Astronomy, p. 28 – 30 (1987). In Russian. Abstr. in Ref. Zh., 51. Astron., 6.51.321 (1988). – See Abstr. 012.070.

104.047 **On the form of short–period meteor streams.**
P. B. Babadzhanov, Yu. V. Obrubov.
Dokl. Akad. Nauk TadzhSSR, Tom 30, No. 8, p. 486 – 491 (1987). In Russian. Abstr. in Ref. Zh., 51. Astron., 6.51.329 (1988).

104.048 **Low light level television meteor observations and simulations.**
T. Sarma.
Diss. Abstr. Int., Sect. B, Vol. 48, No. 9, p. 2680–B (1988). Thesis, The University of Western Ontario (Canada) (1987).

104.049 **Bright bolide above the Crimea Observatory.**
Ya. N. Chernykh.
Komet. Tsirk., No. 383 (1988). In Russian.

104.050 **On the origin of the Geminid meteor shower.**
O. I. Bel'kovich, E. D. Kondrat'eva, E. A. Reznikov.
Komet. Tsirk., No. 385 (1988). In Russian.

104.051 **The system of cometary–meteor orbits of Halley's family.**
E. N. Kramer, I. S. Shestaka.
Komet. Tsirk., No. 385 (1988). In Russian.

104.052 **On the possibility of observing the Draconid meteor stream in the years 1992 – 2025.**
E. A. Reznikov.
Komet. Tsirk., No. 385 (1988). In Russian.

104.053 **Die Quadrantiden.**
R. Arlt, I. Rendtel.
Astron. Raumfahrt, 26. Jahrg., Heft 3, p. 88 – 90 (1988).

BMS meteor observer's handbook. Vol. 1. Naked eye work.
See Abstr. 002.083.

Meteor showers. A descriptive catalog.
See Abstr. 002.122.

About an international meteor organization.
See Abstr. 013.043.

Een ZHR voor TV meteoren.
See Abstr. 036.048.

Die Ermittlung des Populationsindex von Meteorströmen. Eine ausführliche Anleitung.
See Abstr. 036.080.

On the determination of the probability of perception for visual meteors.
See Abstr. 036.107.

Hoeksnelheden en radiantbepaling.
See Abstr. 036.128.

Analytical approximation for the heat transfer coefficient.
See Abstr. 062.022.

Meteoroid bombardment of planetary rings.
See Abstr. 091.070.

Ballistic transport due to meteoroid erosion in planetary rings.
See Abstr. 091.071.

The Binningup H5 chondrite: a new fall from Western Australia.
See Abstr. 105.227.

52-MSS

散在流星の分類

EARTH'S INFLUX OF DIFFERENT POPULATIONS OF SPORADIC METEOROIDS FROM PHOTOGRAPHIC AND TELEVISION DATA

Zdeněk Ceplecha

Astronomical Institute, Czechoslovak Academy of Sciences, 251 65 Ondřejov Observatory, Czechoslovakia

Received 22 December 1987

ПРИТОК РАЗНЫХ ПОПУЛЯЦИЙ СПОРАДИЧЕСКИХ МЕТЕОРОИДОВ В ОБЛАСТЬ ЗЕМЛИ ПО ФОТОГРАФИЧЕСКИМ И ТЕЛЕВИЗИОННЫМ НАБЛЮДЕНИЯМ

Основу данной работы составляют точные фотографические и телевизионные данные с двух и более станций, полученные для 3624 спорадических метеоров в пределах масс от 2×10^{-5} г до 2×10^{7} г. Определяются и описываются критерии и процедуры их классификации по отдельным группам. Дан обзор известных в настоящее время 7 разных популяций спорадических метеоров (Табл. 1). Общее число и общая масса метеороидов как функции массы даются для отдельных групп и для всех спорадических метеоров. Абсолютная калибровка притока в область Земли была выполнена путем сравнения с результатами Halliday et al. (1984). При сравнении с визуальными данными и с данными о количестве кратеров на поверхности Луны было получено хорошее согласие лишь в узком интервале масс, соответствующем визуальным метеорам. В экстраполированных частях визуальной и кратерной кривых притока имеется значительное несоответствие результатам данной работы. Болиды после которых падает метеорит (тип I) имеют окончательно наклон кривой кумулятивных чисел —0,69 для массы большей чем 1 кг. Окончательная шкала масс, выведенная в настоящей работе, лежит между шкалами McCrosky и Halliday. Относительная значимость разных групп метеороидов изменяется с их массами весьма драматично (табл. 4 и 5, рис. 3). Общий приток спорадических метеороидов в область Земли по целому интервалу 12 порядков от 2×10^{7} до 2×10^{-5} г составляет 5×10^{9} г в год на всю земную поверхность. Большинство этого притока приходит в виде более крупных тел. Плотности и коэффициенты абляции даются для отедельных групп метеороидов так, как они вытекают из разных абляционных моделей нескольких авторов. Подвергаются критике некоторые крайние подходы к данному вопросу.

A. 発光点が低いグループ
C. 〃 高い
C1 黄道面に集中している
C2 でたらめな軌道傾斜角を持つ長周期
C3 〃 〃 〃 短周期

Precise photographic and television double- and multi-station data on 3624 sporadic meteors in the mass range from 2×10^{-5} grams to 2×10^{7} grams form the basis of this paper. The applied classification criteria and procedures are defined and described. A survey of 7 different populations of sporadic meteoroids known so far is presented (Tab. 1). The total numbers and masses of meteoroids as function of mass for individual groups and for all sporadic meteors are given. The absolute calibration of the influx to the Earth was carried out by comparison with the results of Halliday et al. (1984). The comparison with the visual and cratering (クレータからのデータ) data revealed good agreement in the narrow "visual" interval of masses and disagreement in the extrapolated parts of the visual and cratering flux curves. The slope of the cumulative number curve for the meteorite-dropping fireballs (type I) with masses larger than 1 kg was found as −0·69 in perfect agreement with the results of Halliday et al. (1984). The final mass scale derived in this paper is situated between the scale of McCrosky and the scale of Halliday. The relative significance of the different groups of meteoroids changes with the mass quite dramatically (Tabs 4 and 5, Fig. 3). The total influx of sporadic meteoroids in the mass interval of 12 orders from 2×10^{7} to 2×10^{-5} grams resulted in 5×10^{9} grams per year for the entire Earth's surface. Most of this mass comes in the form of larger meteoroids. Bulk densities and ablation coefficients for the individual meteor groups, depending on different ablation models of several authors, are presented and some extreme concepts of this problem are discussed.

5 Mt
最も重いものと軽いもので12桁もオーダーが違う

Key words: meteoroids: influx, populations, photographic data, TV - data.

1. Introduction

Thirty years ago meteoroids coming to the Earth's vicinity were assumed to be approximately of the same composition and structure: Verniani (1965, 1967) and Jacchia et al. (1965) argued in favour of all meteoroids being low density (0·2 Mg/m^3) friable bodies, when they analyzed the data on atmospheric trajectories of meteoroids photographed by Super-Schmidt cameras. This highly simplified view originated from biased statistical handling of the data. Different meteoroid populations were first recognized independently by Jacchia (1958) and Ceplecha (1958). The difference in beginning heights of luminous trajectories of meteoroids proved to be the most important tool for recognizing different meteoroid

populations among Super-Schmidt and small-camera meteors, when and if the correct dependence on velocity was considered (Ceplecha 1967, 1968, Cook 1973). Two main discrete levels of meteor beginning heights separated by 10 km difference have been found. The lower level was denoted A, the higher was denoted C. The C-group of meteoroids was recognized to contain two populations of orbits: the one with ecliptically concentrated short-period orbits was denoted C1 and the other with random orbital inclinations of long-period orbits was denoted C2. The classical meteor showers with known parent comets are of the type C1 and C2: thus the cometary origin of meteoroids of the whole C group is evident. The meteoroid masses of the Super-Schmidt and small-camera meteors are within the interval of 5×10^{-4} g to 5×10^{2} g. (McCrosky and Posen 1961).

After the photographic fireball networks yielded enough data, groups of meteoroids with widely different composition and structure were also recognized among these larger bodies up to the mass of 2×10^{7} g (Ceplecha and McCrosky 1976, Ceplecha 1985, Sekanina 1983, Wetherill and ReVelle 1981 a, b). A survey of results on all the meteoroid groups revealed, and of their relations to other bodies of the solar system was given by Ceplecha (1977). Since then, the observational materials has become substantially larger, and several changes in the classification scheme of meteoroids have taken place. This paper will survey all of this.

Recently new observational material of several hundreds of double-station meteors, observed by television systems, became available. The masses of these very small meteoroids are mostly within the interval of 2×10^{-5} to 5×10^{-3} g (Hawkes et al. 1984, Jones and Sarma 1985, Jones et al. 1985, Sarma and Jones 1985). The same methods of classification of atmospheric trajectories of TV-meteors as of that of Super-Schmidt meteors revealed a new group among the C-type meteoroids. It was denoted C3 and contains bodies of the C-type atmospheric trajectory with *short-period orbits of random inclinations*. They are quite numerous and comprise more than one quarter of all observed TV meteors. After this recognition, the C3 meteoroids were also detected among the Super-Schmidt and the small-camera meteors and also marginally among the fireballs (Hawkes et al. 1984, page 61) (this paper: 6%, 9%, 4% of all meteors, respectively). The C3 meteoroids were previously assumed to be a statistical flaw in the original analysis and were partly superposed by the C1 group.

This paper contains an up-to-date survey of all known populations of meteoroids as revealed within different observational materials. Definitions of the different groups of meteoroid populations are given for each observational material. Cumulative and incremental numbers as well as masses of meteoroids of individual groups are presented. The total meteoroid influx for the whole mass interval of 12 orders is given.

The observational material of photographic meteors and fireballs used in this paper was taken from the IAU meteor data archives (center A: B. Lindblad; Lund Observatory; center B: Z. Ceplecha, Ondřejov Observatory). Most of the data have already been published as well as data on double-station TV-meteors. The observational material consisted of 612 fireballs including 561 sporadic fireballs; of 1381 small-camera meteors including 812 sporadic meteors; of 2529 Super-Schmidt meteors including 1848 sporadic meteors; of 454 television meteors including 403 sporadic meteors. Altogether 3624 sporadic meteors were used over the whole mass interval. The masses of the individual meteoroids were obtained by integrating the whole light curve and, except for the question of changes in luminous efficiency, these masses are highly preferable over any estimates based only on one value of maximum brightness with some kind of average velocity, as is the case of interpretation of visual observations. Also radar data are severly limited in respect of determining the meteoroid mass from one value of intensity of the reflected signal not necessarily from the point of maximum ionization.

The mass scale of Halliday et al. (1984) was used and corrected for the ratio of all the meteoroids to the meteoroids of type I. Only a small correction of 0·2 in $\log m$ was found.

2. Definition of the Groups

The levels A, B, C, D are defined in the $h_B - v_\infty$ plot (h_B is the beginning height of the luminous trajectory, v_∞ the initial velocity; Ceplecha 1968). The problem of classification can be transformed to a one-dimensional parameter, K_B, by projecting the $h_B - v_\infty$ plot in the direction of the dependence of these two values. Then K_B is defined (Ceplecha 1967) as

$$K_B = \log \varrho_B + 2{\cdot}5 \log v_\infty - 0{\cdot}5 \log \cos z_R , \quad (1)$$

where ϱ_B is the air density at the beginning of the luminous trajectory expressed in g cm^{-3}, v_∞ is the initial velocity expressed in cm s^{-1} and z_R is the zenith distance of the radiant. Because of the statistical

fireballs identical with the same curve of Halliday et al. (1984) for meteorite-dropping fireballs: $\log(n_{all}/n_I) = 0{\cdot}64$ is our result within the mass interval of comparison with Halliday's cumulative numbers. Except for this small correction of mass and except for the possibility of absolute calibration

Table 2

Cumulative numbers.

Logarithms of meteoroid numbers for the whole Earth's surface per year are given.

larger mass than m log m (log g)	I "ast"	II A	B	IIIA C1	IIIA1 C2	C3	D	All meteoroids
6.8	(1.89)	2.71						
6.6	(2.03)	2.81						
6.4	2.17	2.92		(1.58)			2.43	3.14
6.2	2.31	3.02		(1.74)			2.51	3.24
6.0	2.45	3.12		(1.89)			2.60	3.34
5.8	2.59	3.23		(2.05)			2.68	3.44
5.6	2.73	3.33		(2.20)			2.76	3.55
5.4	2.87	3.44		(2.36)			2.84	3.65
5.2	3.01	3.55		(2.51)			2.92	3.76
5.0	3.15	3.65		2.66			3.00	3.87
4.8	3.29	3.75		2.82			3.08	3.98
4.6	3.42	3.86		2.97			3.16	4.09
4.4	3.56	3.96		3.12	2.77		3.24	4.20
4.2	3.69	4.07		3.27	2.85		3.32	4.32
4.0	3.82	4.17		3.43	2.94		3.40	4.43
3.8	3.95	4.28		3.58	3.02	2.55	3.48	4.55
3.6	4.08	4.38		3.73	3.10	2.71	3.56	4.66
3.4	4.20	4.49		3.89	3.19	2.88	3.64	4.78
3.2	4.31	4.59		4.04	3.27	3.04	3.72	4.89
3.0	4.43	4.70		4.19	3.35	3.20	3.81	5.01
2.8	4.54	4.80		4.34	3.43	3.35	3.90	5.12
2.6	4.66	4.91		4.50	3.52	3.52	4.00	5.24
2.4	4.77	5.01		4.65	3.61	3.68	4.10	5.36
2.2	4.88	5.12		4.80	3.73	3.84	4.22	5.48
2.0	4.99	5.23		4.95	3.89	4.00	4.34	5.60
1.8	5.11	5.33		5.09	4.08	4.16	4.47	5.72
1.6	5.22	5.44		5.24	4.30	4.32	4.61	5.84
1.4	5.33	5.54	3.95	5.37	4.55	4.48	4.76	5.96
1.2	5.44	5.65	4.15	5.50	4.82	4.64	4.91	6.09
1.0	5.56	5.75	4.36	5.62	5.11	4.80	5.06	6.22
0.8	5.67	5.87	4.57	5.73	5.39	4.97	5.21	6.36
0.6	5.78	6.02	4.78	5.82	5.67	5.13	5.35	6.51
0.4	5.90	6.22	4.99	5.91	5.94	5.29	5.50	6.67
0.2	6.01	6.46	5.20	6.03	6.17	5.45	5.66	6.87
0.0	6.12	6.76	5.41	6.17	6.40	5.61	5.82	7.09
-0.2	6.24	7.12	5.62	6.32	6.61	5.77	5.99	7.36
-0.4	6.35	7.53	5.83	6.49	6.80	5.93	6.17	7.69
-0.6	6.47	7.95	6.04	6.66	6.98	6.10	6.35	8.04
-0.8	6.58	8.21	6.25	6.85	7.15	6.29	6.54	8.29
-1.0	6.70	8.38	6.46	7.03	7.32	6.47	6.73	8.45
-1.2	6.81	8.49	6.66	7.22	7.48	6.67	6.93	8.58
-1.4	6.90	8.58	6.87	7.42	7.64	6.86	7.13	8.69
-1.6	6.97	8.64	7.07	7.62	7.80	7.05	7.33	8.78
-1.8	7.04	8.70	7.24	7.83	7.94	7.25	7.52	8.87
-2.0	7.11	8.76	7.39	8.05	8.08	7.44	7.72	8.96
-2.2	7.18	8.81	7.52	8.29	8.20	7.63	7.92	9.07
-2.4	7.25	8.87	7.64	8.55	8.31	7.83	8.07	9.19
-2.6	7.33	8.92	7.75	8.80	8.41	8.02	8.17	9.31
-2.8	7.40	8.98	7.85	9.03	8.52	8.21	8.25	9.45
-3.0	7.48	9.04	7.95	9.17	8.61	8.41	8.32	9.55
-3.2	7.55	9.10	8.05	9.25	8.71	8.60	8.37	9.64
-3.4		9.16	8.15	9.30	8.81	8.79	8.41	9.71
-3.6		9.22	8.25	9.33	8.90	8.98	8.45	9.78
-3.8		9.28	8.35	9.35	8.99	9.17	8.48	9.85
-4.0		9.33	8.45	9.37	9.07	9.36		9.93
-4.2		9.39	(8.55)	(9.38)	9.15	9.55		10.02
-4.4		9.45	(8.65)	(9.40)	9.22	9.73		10.12
-4.6		9.51	(8.75)	(9.41)	9.30	9.91		10.23

of all our meteoroid groups, the above procedure also provided a perfect check of validity expressed in the consistency of our results, based on more extensive observational material, with the independent results of Halliday et al. (1984). The mass scale of McCrosky, defined in chapter 2 section d) and used in all papers on PN and EN fireballs, is by 0·3 in log m above our final mass scale. Thus our final mass

scale used in this paper can be related to the two mentioned mass scales by

$$\log m\,(\text{this paper}) = \log m\,(\text{Halliday}) + 0{\cdot}2 = \log m\,(\text{McCrosky}) - 0{\cdot}3$$

The mass scale of this paper defines masses, which should be close to real masses. It contains the calibration with respect to the dynamic mass scale (well defined near the terminal point of the luminous trajectory of big meteoroids), verified by the actual

Table 3

Incremental numbers and masses.

Logarithms of numbers, log N, and logarithms of total masses, log(Nm), inside each mass interval of 0.2 in log m are given. Units: m in grams, N ... numbers of meteoroids for the entire Earth's surface per year.

mass interval log m		I "ent"		II A		B		IIIA C1		IIIAi C2		C3		IIIB D		All meteoroids	
from	to	log N	log Nm	log N	log Nm	log N	log Nm	log N	log Nm	log N	log Nm	log N	log Nm	log N	log Nm	log N	log Nm
6.8	6.6	(1.47	8.17)	2.14	8.84											(2.22	8.92)
6.6	6.4	(1.61	8.11)	2.24	8.74											(2.33	8.83)
6.4	6.2	1.75	8.05	2.35	8.65			(1.22	7.52)					1.76	8.06	2.55	8.85
6.2	6.0	1.89	7.99	2.45	8.55			(1.37	7.47)					1.84	7.94	2.66	8.76
6.0	5.8	2.03	7.93	2.56	8.46			(1.53	7.43)					1.91	7.81	2.77	8.67
5.8	5.6	2.17	7.87	2,67	8.37			(1.68	7.38)					1.99	7.69	2.88	8.58
5.6	5.4	2.32	7.82	2.77	8.27			(1.83	7.33)					2.07	7.57	2.99	8.49
5.4	5.2	2.46	7.76	2.88	8.18			(1.98	7.28)					2.15	7.45	3.11	8.41
5.2	5.0	2.59	7.69	2.98	8.08			2.14	7.24					2.23	7.33	3.22	8.32
5.0	4.8	2.72	7.62	3.08	7.98			2.29	7.19					2.30	7.20	3.33	8.23
4.8	4.6	2.84	7.54	3.19	7.89			2.44	7.14					2.39	7.09	3.44	8.14
4.6	4.4	2.99	7.49	3.29	7.79			2.59	7.09					2.47	6.97	3.56	8.06
4.4	4.2	3.12	7.42	3.40	7.70			2.75	7.05	2.09	6.39			2.54	6.84	3.69	7.99
4.2	4.0	3.24	7.34	3.50	7.60			2.90	7.00	3.18	6.28			2.62	6.72	3.80	7.90
4.0	3.8	3.36	7.26	3.61	7.51			3.05	6.95	2.26	6.16			2.70	6.60	3.91	7.81
3.8	3.6	3.47	7.17	3.71	7.41			3.20	6.90	2.34	6.04	2.21	5.91	2.78	6.48	4.03	7.73
3.6	3.4	3.58	7.08	3.82	7.32			3.36	6.86	2.43	5.93	2.37	5.87	2.87	6.37	4.14	7.64
3.4	3.2	3.69	6.99	3.92	7.22			3.51	6.81	2.51	5.81	2.53	5.83	2.96	6.26	4.26	7.56
3.2	3.0	3.80	6.90	4.03	7.13			3.66	6.76	2.59	5.69	2.69	5.79	3.06	6.16	4.37	7.47
3.0	2.8	3.91	6.81	4.14	7.04			3.81	6.71	2.67	5.57	2.85	5.75	3.18	6.08	4.49	7.39
2.8	2.6	4.02	6.72	4.24	6.94			3.97	6.67	2.78	5.46	3.01	5.71	3.30	6.00	4.61	7.31
2.6	2.4	4.13	6.63	4.35	6.85			4.12	6.62	2.89	5.39	3.17	5.67	3.44	5.94	4.73	7.23
2.4	2.2	4.24	6.54	4.46	6.76			4.27	6.57	3.12	5.42	3.33	5.63	3.58	5.88	4.86	7.16
2.2	2.0	4.35	6.45	4.56	6.66			4.41	6.51	3.37	5.47	3.49	5.59	3.73	5.83	4.98	7.08
2.0	1.8	4.46	6.36	4.67	6.57			4.55	6.45	3.62	5.52	3.65	5.55	3.89	5.79	5.11	7.01
1.8	1.6	4.58	6.28	4.77	6.47			4.68	6.38	3.90	5.60	3.81	5.51	4.05	5.75	5.23	6.93
1.6	1.4	4.69	6.19	4.88	6.38			4.80	6.30	4.19	5.69	3.97	5.47	4.21	5.71	5.36	6.86
1.4	1.2	4.80	6.10	4.98	6.28	3.72	5.02	4.91	6.21	4.49	5.79	4.13	5.43	4.37	5.67	5.50	6.80
1.2	1.0	4.92	6.02	5.08	6.18	3.94	5.04	5.02	6.10	4.79	5.89	4.30	5.40	4.53	5.63	5.63	6.73
1.0	0.8	5.03	5.93	5.24	6.14	4.15	5.05	5.07	5.97	5.08	5.98	4.46	5.36	4.67	5.57	5.78	6.68
0.8	0.6	5.14	5.84	5.49	6.19	4.36	5.06	5.09	5.79	5.35	6.05	4.62	5.32	4.81	5.51	5.97	6.67
0.6	0.4	5.26	5.76	5.78	6.28	4.57	5.07	5.21	5.71	5.59	6.09	4.78	5.28	4.97	5.47	6.18	6.68
0.4	0.2	5.37	5.67	6.09	6.39	4.78	5.08	5.40	5.70	5.80	6.10	4.94	5.24	5.14	5.44	6.42	6.72
0.2	0.0	5.49	5.59	6.45	6.55	4.99	5.09	5.60	5.70	6.01	6.11	5.10	5.20	5.31	5.41	6.70	6.80
0.0	-0.2	5.60	5.50	6.87	6.77	5.20	5.10	5.79	5.69	6.19	6.09	5.26	5.16	5.50	5.40	7.03	6.93
-0.2	-0.4	5.72	5.42	7.32	7.02	5.41	5.11	5.99	5.69	6.35	6.05	5.42	5.12	5.69	5.39	7.41	7.11
-0.4	-0.6	5.84	5.34	7.74	7.24	5.62	5.12	6.19	5.69	6.51	6.01	5.62	5.12	5.89	5.39	7.79	7.29
-0.6	-0.8	5.95	5.25	7.86	7.16	5.83	5.13	6.38	5.68	6.67	5.97	5.82	5.12	6.09	5.39	7.92	7.22
-0.8	-1.0	6.06	5.16	7.88	6.98	6.04	5.14	6.57	5.67	6.82	5.92	6.02	5.12	6.29	5.39	7.96	7.06
-1.0	-1.2	6.15	5.05	7.87	6.77	6.24	5.14	6.77	5.67	6.98	5.88	6.22	5.12	6.49	5.39	7.99	6.89
-1.2	-1.4	6.17	4.87	7.83	6.53	6.45	5.15	6.98	5.68	7.13	5.83	6.41	5.11	6.69	5.39	8.01	6.71
-1.4	-1.6	6.14	4.64	7.79	6.29	6.64	5.16	7.19	5.69	7.27	5.77	6.61	5.11	6.89	5.39	8.05	6.55
-1.6	-1.8	6.20	4.50	7.80	6.10	6.76	5.05	7.41	5.71	7.40	5.70	6.80	5.10	7.09	5.39	8.15	6.45
-1.8	-2.0	6.29	4.39	7.83	5.93	6.85	4.95	7.63	5.73	7.50	5.60	7.00	5.10	7.29	5.39	8.26	6.36
-2.0	-2.2	6.37	4.27	7.89	5.79	6.93	4.83	7.85	5.85	7.58	5.48	7.19	5.09	7.48	5.38	8.41	6.31
-2.2	-2.4	6.46	4.15	7.95	5.65	7.02	4.72	8.10	5.99	7.66	5.36	7.38	5.08	7.53	5.23	8.56	6.26
-2.4	-2.6	6.53	4.03	8.01	5.51	7.10	4.60	8.44	5.94	7.75	5.25	7.58	5.08	7.50	5.00	8.72	6.22
-2.6	-2.8	6.60	3.90	8.07	5.37	7.18	4.48	8.64	5.94	7.84	5.14	7.77	5.07	7.42	4.78	8.86	6.16
-2.8	-3.0	6.68	3.78	8.14	5.24	7.27	4.37	8.81	5.91	7.92	5.02	7.96	5.06	7.45	4.58	8.89	5.99
-3.0	-3.2	6.75	3.65	8.20	5.10	7.36	4.26	8.47	5.87	8.01	4.91	8.15	5.05	7.42	4.32	8.93	5.78
-3.2	-3.4			8.26	4.96	7.45	4.15	8.33	5.83	8.10	4.80	8.34	5.04	7.40	4.10	8.90	5.60
-3.4	-3.6			8.32	4.82	7.55	4.05	8.18	5.88	8.18	4.68	8.53	5.03	7.38	3.88	8.96	5.46
-3.6	-3.8			8.38	4.68	7.66	3.96	8.03	4.33	8.25	4.55	8.72	5.02	7.35	3.65	9.05	5.35
-3.8	-4.0			8.44	4.54	7.76	3.86	7.95	4.05	8.31	4.41	8.91	5.01			9.16	5.26
-4.0	-4.2			8.50	4.40	7.86	3.76	7.91	3.81	8.37	4.27	9.09	4.99			9.29	5.19
-4.2	-4.4			8.56	4.26	7.96	3.66	7.88	3.58	8.43	4.13	9.27	4.97			9.43	5.13
-4.4	-4.6			8.62	4.12	8.06	3.56	7.88	3.38	8.48	3.98	9.45	4.95			9.57	5.07

masses of Lost City and Innisfree, and it depends on artificial meteor experimens by Ayers et al. (1970).

The results of all these computations are given in Tab. 2. The mass intervals are 0·2 in log m from 6·8 to −4·6 (in log g). For each group separately, Tab. 2 contains logarithms of the cumulative numbers already calibrated to the whole Earth's surface per one year. In the last column, the logarithms of cumula-

tive numbers are given for all sporadic meteoroids, as they resulted from summing up the numbers of meteoroids of all groups within each mass interval.

Table 3 contains the incremental numbers, as they resulted from Tab. 2. For each 0·2 log m interval, Table 3 contains logarithms of the numbers and logarithms of masses within each of the 0·2-wide log-mass interval, for each group of meteors separately. The last column gives the same for all meteors as it resulted from summing up the incremental numbers and masses of all the meteor groups.

The results of Tab. 3 for "all meteors" are compared in Fig. 1 with the "visual data" published by Hughes (1978, p. 155) (denoted c) and d) in Fig. 1). The absolute values in the typically visual interval from 0·1 to 10 g agree almost perfectly, but the incremental masses in the other intervals (log $M < -1$, and log $M > 1$) differ by orders of magnitude. This only emphasizes danger of any extrapolation of cumulative numbers beyond the region of actual full-sensitivity of a receptor It is interesting that the incremental mass has the absolute maximum at the largest mass boundary of our observational material and a local maximum just at the "visual" meteors (they are close to the "Super-Schmidt" meteors). The local maximum at log $m = -0{\cdot}5$ (in grams) is mostly caused by the A-group bodies. They comprise half of all the meteors in the whole "Super-Schmidt" region and almost 90% of all meteors at log $m = -0{\cdot}5$. Details will be discussed in the next chapter.

The discrepancy between the "visual" and the "photographic and TV" data could be in the definition of the mass scale. Certainly the "visual" mass scale contains meteoroids of the same brightness un-

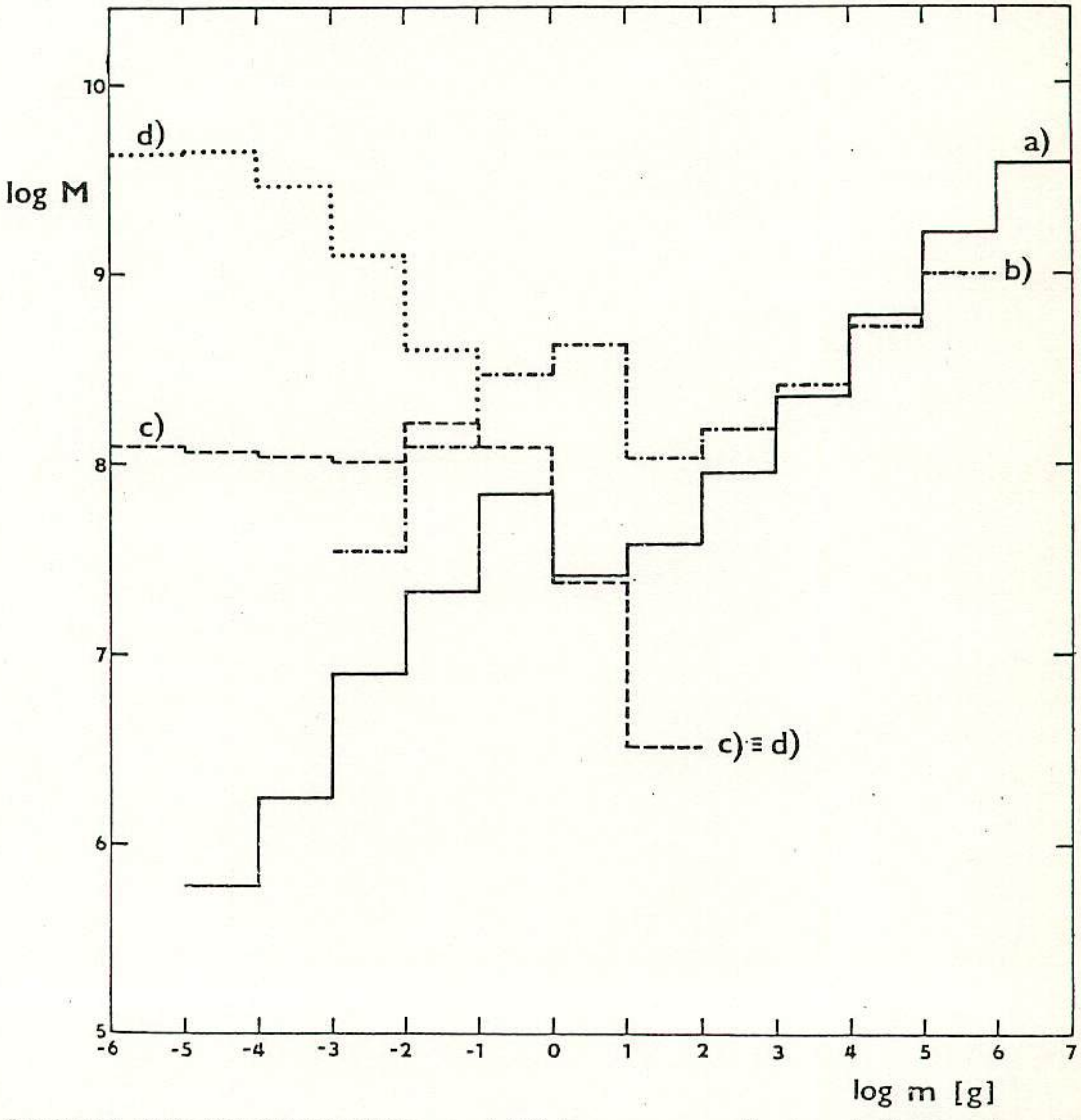

Fig. 1. Incremental masses M in intervals of $\Delta \log m = 1$. M is in grams per year for the entire Earth's surface. a) the results of this paper, b) the results of this paper with the luminous efficiency variable with mass according to Eq. (5), c) and d) the results from visual observations (Hughes 1978).

resolved, but with the mass ratios up to 200, which causes incorrect slopes of cumulative curves (they are steeper than the cumulative curves with resolution of the mass-velocity dependence). But on the other hand, the luminous efficiences applied to detailed velocity and brightness data of the photographic and TV meteors, may be only rough values and also mass dependent (the velocity dependence was taken into account for each meteor separately in integrating the light curves according to Eq. (2)).

As an extreme (and very improbable) assumption of the mass dependence of the luminous efficiency we took the expression

$$\log \tau_0 = 0{\cdot}2 \log m - 18{\cdot}70 \tag{5}$$

(in the system of cgs units combined with $I = 1$ for 0 stellar magnitude), where $\tau = \tau_0 v$ is the luminous efficiency. This assumption actually means a 10 times smaller luminous efficiency for $\log m = -3$ than for $\log m = 2$, which is highly improbable. At $\log m = 3{\cdot}5$ both luminous efficiencies (the above equation and the average efficiency corresponding to the final mass scale used in this paper) are identical. In Fig. 1 the incremental mass curve denoted b) corresponds to this extreme crude assumption. The absolute maximum at the most massive bodies remains. The local maximum is shifted to larger masses and the discrepancy with the visual interval is evident. On the other hand, the bodies with $\log m = -1$ to $\log m = -3$ are closer to the extrapolated visual values c).

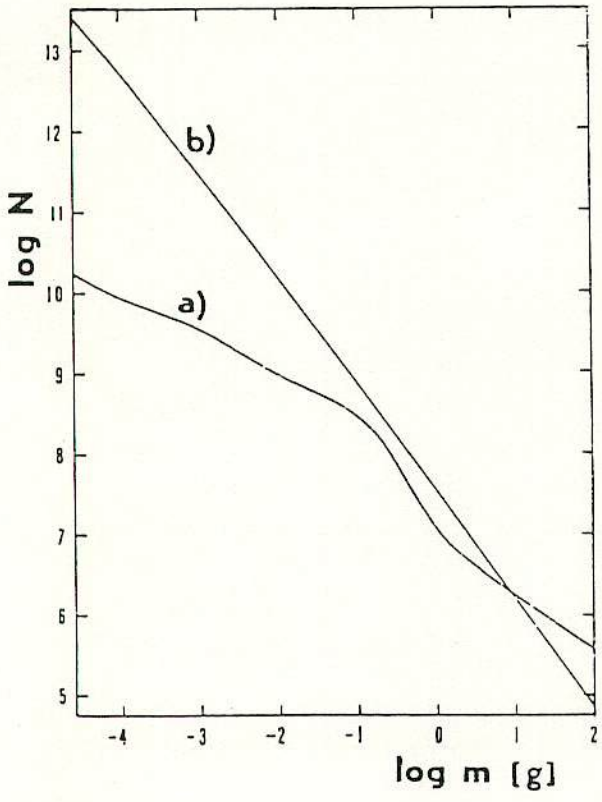

Fig. 2. Cumulative numbers N of meteoroids of mass greater than m (in grams). N is given for the entire Earth's surface per year. a) the results of this paper, b) the flux model of Grün et al. (1985). The a) curve is extremely well defined for meteoroids with $\log m$ greater than -3. The discrepancy of a) and b) at $\log m = -3$ is almost 2 orders of magnitude

The results of Tab. 2 are compared in Fig. 2 with the model of meteoroid fluxes given by Grün et al. (1985), based on lunar microcratering and Whipple's (1967) interpretation of meteor statistics within the mass interval of 10^{-4} to 10^{2} grams. The same order of discrepancy as with Hughes' values was found. The average slope is identical between $\log m = 0{\cdot}7$ and $\log m = -1{\cdot}3$, which is a typical interval for visual meteor observations (and close to Super-Schmidt sensitivity interval), and on which the slope given by Whipple (1967) mostly depends.

The dimension of a crater, when related to the mass of its projectile, has a similar large spread due to the velocity of the projectile as in the case of the "maximum brightness of a visual meteor". Again more populated ranges of smaller projectiles of high velocity are added to the ranges of a few larger projectiles of low velocity at the same dimension of their craters, unresolved. This makes the cumulative slope seemingly steeper.

The curve of incremental mass, resulting from all available photographic and TV-data and denoted a) in Fig. 1, is distinctly preferable to all "visual", "visual-extrapolated" and "cratering-extrapolated" data with the following precautions: The extreme wings below $\log m = -3$ and above $\log m = 5$ are close to the boundaries of the sensitivity of all the used systems and may contain less bodies than in reality. Within the interval from $\log m = 5$ to $\log m = -3$ the incremental masses can differ from reality maximally by $\pm 0{\cdot}3$ in $\log m$, but the relative change from one interval to the next has a precision better than $\pm 0{\cdot}1$ in $\log m$.

The method of dividing the meteors into groups, treating the groups separately and summing the meteoroid numbers of all groups in the final step, gives better results than if the whole observational material were treated as one statistical body without classification. We feel that group A is still a composite (Hawkes et al. 1984) and future, improved classification systems may treat this group as several groups. The results would then be refined, but we do not expect this refinement to bring larger changes to our present results.

Table 4

Relative percent cumulative numbers of meteoroids of individual groups.

All meteoroids of the group larger than mass m;
m in grams.

log m (log g)	I "Ast"	II A	B	IIIA C1	IIIAi C2	C3	IIIB D
6.8	(13)	(87)	-	-	-	-	-
6.6	(14)	(86)	-	-	-	-	-
6.4	11	65	-	(3)	-	-	21
6.2	13	64	-	(3)	-	-	20
6.0	14	63	-	(4)	-	-	19
5.8	15	63	-	(4)	-	-	18
5.6	16	63	-	(4)	-	-	17
5.4	17	62	-	(5)	-	-	16
5.2	18	62	-	(5)	-	-	15
5.0	19	61	-	6	-	-	14
4.8	20	60	-	7	-	-	13
4.6	21	59	-	8	-	-	12
4.4	22	57	-	8	3	-	10
4.2	23	55	-	9	3	-	10
4.0	24	54	-	10	3	-	9
3.8	25	53	-	11	3	-	8
3.6	26	51	-	12	3	-	8
3.4	26	50	-	13	3	1	7
3.2	26	50	-	14	2	1	7
3.0	26	49	-	15	2	2	6
2.8	26	48	-	16	2	2	6
2.6	26	46	-	18	2	2	6
2.4	26	45	-	19	2	2	6
2.2	25	44	-	21	2	2	6
2.0	25	43	-	22	2	2	6
1.8	25	41	-	23	2	3	6
1.6	24	39	-	25	3	3	6
1.4	23	38	1	25	4	3	6
1.2	22	36	1	25	5	4	7
1.0	21	34	1	25	8	4	7
0.8	20	32	2	24	11	4	7
0.6	19	33	2	20	15	4	7
0.4	17	35	2	17	18	4	7
0.2	14	39	2	15	20	4	6
0.0	11	47	2	12	20	3	5
-0.2	7	57	2	9	18	3	4
-0.4	5	70	1	6	13	2	3
-0.6	3	80	1	4	9	1	2
-0.8	2	83	1	4	7	1	2
-1.0	2	83	1	4	7	1	2
-1.2	2	82	1	4	8	1	2
-1.4	2	78	2	5	9	1	3
-1.6	1	73	2	7	11	2	4
-1.8	1	68	2	9	12	3	5
-2.0	1	62	3	12	13	3	6
-2.2	1	55	3	17	13	4	7
-2.4	1	48	3	23	13	4	8
-2.6	1	41	3	31	12	5	7
-2.8	1	34	3	38	12	6	6
-3.0	1	30	3	41	12	7	6
-3.2	(1)	29	3	41	12	9	5
-3.4	(1)	28	3	39	13	12	5
-3.6	(1)	27	3	35	13	16	5
-3.8	(<1)	27	3	31	14	21	(4)
-4.0	(<1)	25	3	27	14	27	(4)
-4.2	(<1)	23	3	23	14	34	(3)
-4.4	(<1)	22	3	19	13	41	(2)
-4.6	(<1)	19	3	15	12	49	(2)

5. Changes of Significance of Meteoroid Groups with Mass

The change of importance of the individual groups with the mass of meteoroid is strongly impressing and there is no way of dealing with the entire meteoroid complex in the whole mass interval of Tab. 1 as with one statistical body. The detailed quantification in the preceding chapter is represented in Tabs 4 and 5 in percent numbers of meteoroids in the 0·2 – log m intervals. Tab. 4 contains the cumulative numbers and Tab. 5 the incremental numbers. The following results of relative changes of population of the individual groups with the meteoroid masses can be specified by using the incremental numbers.

The short-period randomly inclined orbits of the C3

Table 5

Relative percent incremental numbers of meteoroids of individual groups. Meteoroids of the group inside the given mass interval of 0.2 in log m; m in grams.

log m (log g) from	to	I "Ast"	II A	B	IIIA C1	IIIAi C2	C3	IIIB D
6.8	6.6	(18)	(82)	-	-	-	-	-
6.6	6.4	(19)	(81)	-	-	-	-	-
6.4	6.2	16	64	-	(4)	-	-	16
6.2	6.0	17	63	-	(5)	-	-	15
6.0	5.8	18	62	-	(6)	-	-	14
5.8	5.6	20	61	-	(6)	-	-	13
5.6	5.4	21	60	-	(7)	-	-	12
5.4	5.2	22	59	-	(8)	-	-	11
5.2	5.0	24	58	-	8	-	-	10
5.0	4.8	25	57	-	9	-	-	9
4.8	4.6	25	56	-	10	-	-	9
4.6	4.4	27	54	-	11	-	-	8
4.4	4.2	27	52	-	12	-	-	7
4.2	4.0	28	50	-	13	2	-	7
4.0	3.8	28	50	-	14	2	-	6
3.8	3.6	28	48	-	15	2	1	6
3.6	3.4	27	47	-	17	2	2	5
3.4	3.2	27	46	-	18	2	2	5
3.2	3.0	27	45	-	19	2	2	5
3.0	2.8	26	44	-	21	2	2	5
2.8	2.6	26	43	-	23	1	2	5
2.6	2.4	25	42	-	24	1	3	5
2.4	2.2	24	40	-	26	2	3	5
2.2	2.0	24	38	-	27	2	3	6
2.0	1.8	23	37	-	28	3	3	6
1.8	1.6	22	35	-	28	5	4	6
1.6	1.4	21	33	-	28	7	4	7
1.4	1.2	20	31	2	26	10	4	7
1.2	1.0	19	28	2	23	15	5	8
1.0	0.8	17	29	2	19	20	5	8
0.8	0.6	15	34	2	13	24	5	7
0.6	0.4	12	40	2	11	25	4	6
0.4	0.2	9	47	2	10	24	3	5
0.2	0.0	6	57	2	8	20	3	4
0.0	-0.2	4	70	1	6	14	2	3
-0.2	-0.4	2	81	1	4	9	1	2
-0.4	-0.6	1	89	1	2	5	1	1
-0.6	-0.8	1	87	1	3	6	1	1
-0.8	-1.0	1	83	1	4	8	1	2
-1.0	-1.2	1	76	2	6	10	2	3
-1.2	-1.4	1	66	3	9	13	3	5
-1.4	-1.6	1	54	4	14	16	4	7
-1.6	-1.8	1	45	4	18	18	5	9
-1.8	-2.0	1	37	4	25	17	5	11
-2.0	-2.2	1	30	3	33	15	6	12
-2.2	-2.4	1	24	3	43	13	7	9
-2.4	-2.6	1	20	2	53	11	7	6
-2.6	-2.8	1	16	2	60	9	8	4
-2.8	-3.0	1	18	2	53	10	12	4
-3.0	-3.2	1	21	3	39	14	19	3
-3.2	-3.4	-	23	4	27	16	27	3
-3.4	-3.6	-	23	4	17	17	37	2
-3.6	-3.8	-	21	4	10	16	47	2
-3.8	-4.0	-	19	4	6	14	57	-
-4.0	-4.2	-	16	(4)	(4)	12	64	-
-4.2	-4.4	-	14	(3)	(3)	10	70	-
-4.4	-4.6	-	11	(3)	(2)	8	76	-

group are virtually absent among meteoroids larger than a few hundred grams. At 10 g they reach 5% of all bodies and again became relatively insignificant (due to the overwhelming position of the A-meteors over the other groups) from 1 to 0·1 gram. They then steadily and rapidly increase up to 76% at the end of our mass interval at 2×10^{-5} g. If we compare the C3-group with the C1-group of short-period ecliptically concentrated orbits, we see that the number of C1-meteors is larger by one order than that of the C3-meteors for masses larger than 100 grams. The C3-bodies reach the same number as the C1-bodies at 5×10^{-4} grams, where both the C1- and the C3-meteors already outnumber all the other groups. The C1-group becomes quite insignificant for masses smaller than 10^{-4} grams.

The C1 and IIIA-group alone reaches the first maximum of relative numbers up to 28% between

400 g and 10 g and the second maximum up to 60% at 2×10^{-3} g. Its significance then rapidly decreases to a few percent at 10^{-4} g.

The C2 and III Ai-group with the long-period randomly inclined orbits is negligible for bodies larger than 100 g. It reaches its maximum of 25% between 10 grams and 1 gram; for smaller masses it mostly remains between 10% and 20%. The minimum at 0·3 grams is caused by the maximum of the relative importance of the A-group.

The source of the C2 and C3 bodies seems to be the same: long-period comets. Thus the short-period orbits of the C3-bodies may originate due to higher ejection velocities from the parent comets. The ejection velocity is an function of meteoroid mass and the change of the regime of transit from long-period to short-period orbit may take place within a relatively small mass interval. If the C2 and C3-meteoroids are of the same origin in long-period comets, the ejection velocity for masses larger than 0·01 g is then small enough to change only an insignificant number of orbits to short-period orbits and, on the contrary, the ejection velocity for bodies smaller than 0·001 g is large enough to change most of the original orbits to short periods. At the meteoroid mass the of 2×10^{-3} g, the relative number of the C2 and the C3-bodies is identical.

The steadiest population of meteoroids belongs to the *A* and II group. Within the mass range of 2×10^{7} to 5×10^{-3} g, it never sinks below one quarter of all the observed meteoroids. At the mass of 0·3 g, the relative number of meteoroids of the A and II population reaches the maximum of 89% of all meteoroids. The steady importance of this meteoroid system may be due to two different sources of its bodies, which we suspect to be carbonaceous bodies: comets and asteroids. Larger meteoroids of the A and II group may be mostly derived from asteroids, while the smaller meteoroids of the same group may mostly come from comets.

On the contrary, group I and the group of "asteroidal" meteors display a steady increase of relative meteoroid numbers from small to large bodies. Below 1 g these bodies are virtually absent but, in contrast, they comprise 28% of all fireballs at 10 kg.

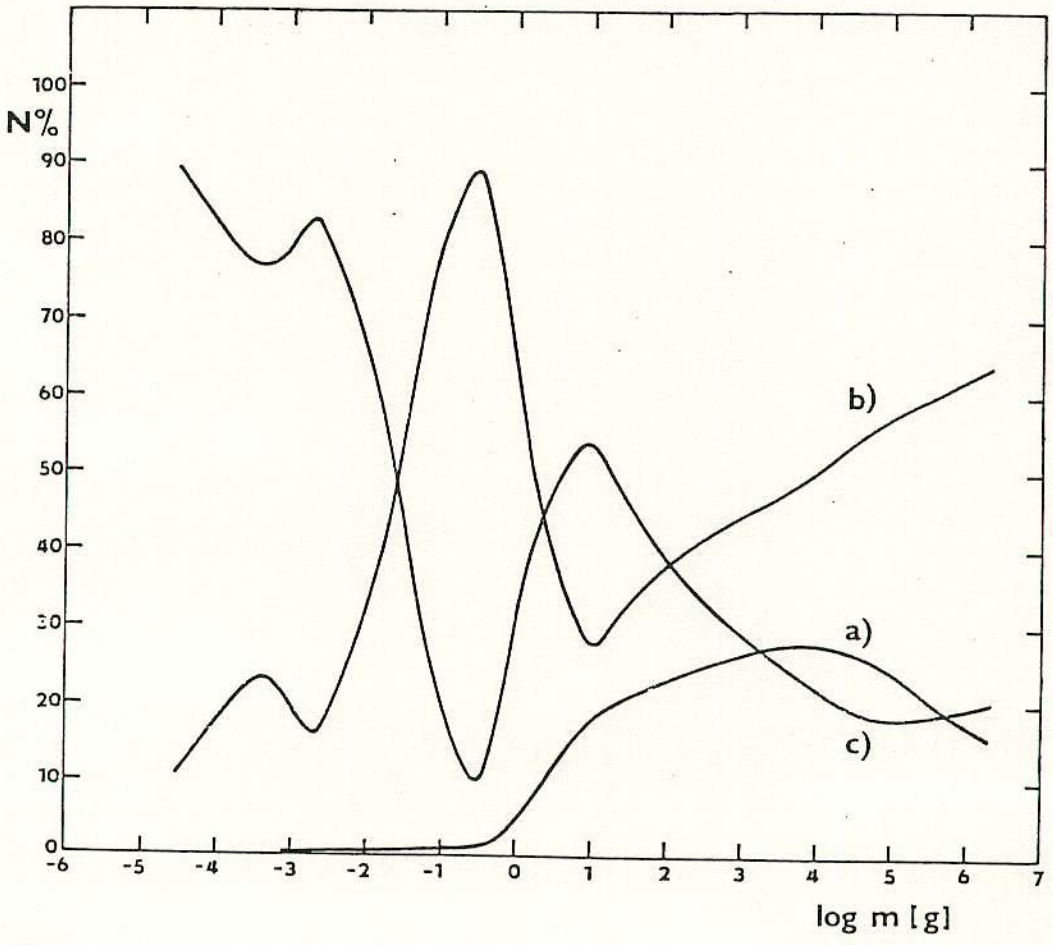

Fig. 3. Relative percentage of incremental numbers (N%) of three types of meteor bodies as a function of the meteorid mass: a) stony material, b) A-group material (carbonaceous bodies), c) cometary material.

Between 10 g and 1000 kg this system of group I bodies has a steady contribution of 20% to 30% of all the bodies.

The B group seems to be generally a weak population, not exceeding 4% in incremental numbers at any mass. Orbits of the B-group bodies always have a small perihelion distance of less than 0·3 A. U. This paper deals with sporadic meteors, but it is worthwhile to remind the reader that Geminids are typical members of the B-group.

Surprisingly, the D and III B group is quite strong up to 16% for the largest bodies of more than 100 kg. This group still has mostly more than 5% of its bodies in the huge interval of 100 kg to 1 g. This system becomes insignificant for bodies smaller than 0·001 g. The maximum of 12% at 0·01 g may be only seeming due to the overwhelming importance of the A-group at 0·3 g, where the D-group sinks to 1% of all meteoroids (practically 1% of the A-group at 0·3 g).

The large density changes inside a cometary body (Donn 1988) may form potential meteoroids of quite diverse densities, but with a generally similar chemical composition. Meteoroids of the B, C and D groups manifest this feature quite well.

Figure 3 represents the percentage change of three types of meteor bodies expressed in incremental numbers: a) stony material, b) A-group material (carbonaceous bodies), c) cometary material. It suggests that most internal discrepancies in the results of studying meteors by objective optical means in the past, originated from the very fact that we first learned about meteoroids from the mass interval of the complicated interlaced systems of meteor bodies.

The total influx of all sporadic meteoroids of 5×10^9 grams per year for the entire Earth's surface resulted within the mass interval of 12 orders from 2×10^7 grams to 2×10^{-5} grams. Most of this mass comes in the form of bigger meteoroids.

6. Densities and Ablation Coefficients of the Individual Groups

The average bulk densities of meteoroids and the average ablation coefficients given in Tab. 1 are values derived on several theoretical assumptions. They are calibrated using these values derived for all the 3 meteorite falls, which belong to the photographic fireballs of group I: Příbram, Lost City and Innisfree. But the values of bulk densities and ablation coefficients deduced by different authors from widely different theoretical concepts, agree rather well (Ceplecha 1986). The average values given in Tab. 1 should be closer to the actual average values than about ±30%. Tab. 6 contains the intervals of one standard deviation both sides of the average values of ϱ_M and σ in Tab. 1. These standard deviations contain two inseparable components superposed: the random errors of determination of the individual ϱ_M and σ and the actual distribution of the numbers of bodies of different densities and ablation coefficients.

Table 6

Interval of ± one standard deviation of average ϱ_M(g cm^{-3}) and σ(s^2 km^{-2}) of Tab. 1.

Group	ϱ_M from	ϱ_M to	σ from	σ to
"ast" + I	2·7	5·9	0·007	0·028
A + II	1·4	2·7	0·028	0·056
B	0·65	1·7	0·05	0·11
C + IIIA	0·55	0·91	0·08	0·13
D + IIIB	0·18	0·38	0·17	0·26

Recently Padevět (1983a, 1983b, 1987) argued values of the bulk densities and ablation coefficients different from the values in Tab. 1. His theoretical concept yields results at variance with all other investigators. He claims that all the groups of Tab. 1 can be explained using the known meteorite types. But his theoretical concept should be applied to all the detailed data on the velocity change of the individual well observed fireballs. Padevět applied his theoretical concept only to the terminal-point and to the beginning-point data. Before this theoretical concept will be checked by well observed fireball velocities over the entire trajectories, his results should be taken with enough precaution.

The detailed knowledge of the dynamics of the ablating meteoroid along its whole luminous trajectory makes the absolute values of the ablation coefficients for types I and II fireballs not only realistic, but also quite accurate (Tab. 6). If the type I fireballs belong to ordinary chondrites with a bulk density of 3·7 g/cm^3, then 2·0 g/cm^3 is the bulk density which fits the ablation coefficient and velocity change of the type II fireballs. The classification of the type I and II fireballs in Tab. 1 is based not only on their terminal heights, but it also contains all the details of the observed velocity change represented by one "total ablation" coefficient for each fireball. In this sense, the distinction using the ablation coefficient is very much preferable and the rough criteria a) to g) of chapter 2 cannot compete.

But Tab. 1 contains data not only on fireballs. In this sense, all the Super-Schmidt-camera meteors

have Padevět's undercritical mass and should not contain bodies of the C and D type. But they do! And even for the A-group of the Super-Schmidt meteors, the luminous trajectory is shorter than it should be for compact stones. Jacchia (1958) explained the difference in the ablation coefficient between "asteroidal meteors" and C-type meteors introducing a process of "progressive fragmentation", which puts them, like Padevět's "overcritical mass" cases, in clear controversy with the small masses of the Super-Schmidt meteoroids.

The old interpretation of Super-Schmidt meteors by Verniani (1965, 1967) assigned very low bulk densities to all meteoroids. Although his results based on the simple equalization of photometric and dynamic masses in Hoppe's theory (single-body theory) have been critically rejected many times, we can still hear or read the following universal statement: "all meteoroids are low-density friable fluffy particles of cometary origin". This is evidently a false statement and the reason mostly lies in the "double biased" statistical treatment of the data. Most of the Super-Schmidt meteors were published by McCrosky and Posen (1961) without any selection at all. This material contains 50% of the A-type bodies and 45% of the C-type bodies. Jacchia and Whipple (1961) were interested in precise data on initial velocities, on orbits and thus on good atmospheric trajectories: they chose the longer trajectories for this purpose. Their selection of 413 Super-Schmidt meteors contains 32% of the A-type bodies and 62% of the C-type bodies. Verniani (1967) in his final analysis used 189 "best" meteors selected from Jacchia's and Whipple's 413: among other criteria for his rather narrow selection he used the "regular" statistical distribution of the ratio of dynamic to photometric mass, expressed as $\log(\tau_0/\varrho_M^2)$. This selection worked exactly in the same way as Jacchia's and Whipple's selection. Among the 189 meteors of Verniani's selection from Jacchia's and Whipple's selection of 413 meteors there remained only 20% of the A-type bodies and 75% of the C-type bodies. Verniani actually recognized these 20% of meteors as bodies of densities higher that the rest, but he then used an average dependence of his $\log(\tau_0/\varrho_M^2)$ on $\log v$ (an incorrect exponent resulted, because of two superposed statistical distributions) thus smoothing these 20% into the overwhelming rest of 75% of the C-bodies. His statement that all meteoroids are low-density friable bodies of cometary origin should be attributed, as a first approximation, only to the C-type bodies. Also the absolute values of the bulk densities of "all meteors" of Verniani are too low due to the above mentioned smoothing over two different statistical distributions and due to the applied but uncalibrated equivalence of photometric and dynamic mass.

One more selection of Super-Schmidt data is available: that of Hawkins and Southworth (1958), which contains 316 randomly selected meteors. This random selection contains 48% of the A-type bodies in very good agreement with 50% of the A-type bodies in the almost complete Super-Schmidt observational material published by McCrosky and Posen (1961). The "double bias" described above, which suppressed the actual 50% of the A-type bodies to the 32% and finally to the 20%, is an example of "do not do any least-squares study without paying attention to the statistical distribution" and of "do not represent any whole by selecting from something, which somebody has already formed from the same whole in the same way".

REFERENCES

Ayers W. G., McCrosky R. E., Shao C.-Y. 1970 *Smithson. Astrophys. Spec. Rep.* 317

Ceplecha Z. 1958 *Bull. Astron. Inst. Czechosl.* 9, 154

— 1967 *Smithson. Contr. Astrophys.* 11, 35

— 1968 *Smithson. Astrophys. Obs. Spec. Rep.* 279

— 1977 Meteoroid Populations and Orbits, in *Comets, Asteroids, Meteorites* (Ed. A. H. Delsemme, The University of Toledo, USA), p. 143

— 1980 in *Solid Particles in the Solar System* (Eds I. Halliday and B. A. McIntosh), IAU Symp. 90, 171

— 1983 New Aspects in the Classification of Meteoroids, in *Asteroids, Comets, Meteors* (Eds C. I. Lagerkvist, H. Rickman, Astron. Obs. Uppsala, Sweden), p. 435

— 1985 *Bull. Astron. Inst. Czechosl.* 36, 237

— 1986 in Photographic Fireball Networks, in *Asteroids, Comets, Meteors II* (Eds C.-I. Lagerkvist et al. The Uppsala University, Sweden), p. 575

Ceplecha Z., McCrosky R. E. 1976 *J. Geophys. Res.* 81, 6257

Ceplecha Z., Rajchl J. 1965 *Bull. Astron. Inst. Czechosl.* 16, 15

Cook A. F. 1976 *Smithson. Contr. Astrophys.* 14

Donn B. 1988 *Astron. Astrophys.*, in press

Grün E., Zook H. A., Fechtig H., Giese R. H. 1985 *Icarus* 62, 244

Halliday I., Blackwell A. T., Griffin A. A. 1984 *Science* 223, 1405

Halliday I., Griffin A. A. 1982 *Meteoritics* 17, 31

Hawkes R. L., Jones J., Ceplecha Z. 1984 *Bull. Astron. Inst. Czechosl.* 35, 46

Hughes D. W. 1978 in *Meteors, in Cosmic Dust* (Ed. J. A. M. McDonnell, John Wiley and sons, Chichester, England), p. 123

Jacchia L. G. 1958 *Smithson. Contr. Astrophys.* 2, 181

Jacchia L. G., Verniani F., Briggs R. E. 1965 *Smithson. Astrophys. Obs. Spec. Rep.* 175

Jacchia L. G., Whipple, F. L. 1961 *Smithson. Contr. Astrophys.* 4, 97

Jones J., Sarma T. 1985 *Bull. Astron. Inst. Czechosl.* 36, 103

MSS-052

Jones J., Sarma T., Ceplecha Z. 1985 *Bull. Astron. Inst. Czechosl.* 36, 116
McCrosky R. E., Posen A. 1961 *Smithsonian Contr. Astrophys.* 4, 15
Padevět V. 1983 a *Bull. Astron. Inst. Czechosl.* 34, 360
— 1983 b *Meteoritics* 18, 369
— 1987 *Bull. Astron. Inst. Czechosl.* 38, 156
Pecina P., Ceplecha Z. 1983 *Bull. Astron. Inst. Czechosl.* 34, 102
— 1984 *Bull. Astron. Inst. Czechosl.* 35, 120
ReVelle D. O. 1983 *Meteoritics* 18, 386
Sarma T., Jones J. 1985 *Bull. Astron. Inst. Czechosl.* 36, 9
Sekanina Z. 1983 *Astron. J.* 88, 1382
Verniani F. 1965 *Smithson. Contr. Astrophys.* 8, 141
— 1967 *Smithson. Contr. Astrophys.* 10, 181
Wetherill G. W. 1985 *Meteoritics* 20, 1
Wetherill G, W., ReVelle D. O. 1981 a *Icarus* 48, 308
— 1981 b Relationship Between Comets, Large Meteors and Meteorites, in *Comets* (Ed. L. Wilkening, Univ. of Arizona Press, USA)
Whipple F. L. 1967 On Maintaining the Meteoritic Complex, in *Zodiacal Light and Interplanetary Medium*, NASA-SP 150, p. 409

TWO-COMPONENT MODELS OF INDIVIDUAL SUNSPOT UMBRAE

M. Sobotka

Astronomical Institute, Czechoslovak Academy of Sciences, 251 65 Ondřejov, Czechoslovakia

Received 27 November 1987

ДВУХКОМПОНЕНТНЫЕ МОДЕЛИ ТЕНЕЙ ОТДЕЛЬНЫХ СОЛНЕЧНЫХ ПЯТЕН

В работе приводятся полуэмпирические двухкомпонентные модели 11 теней разного размера (радиус 2″—8″) и обсуждаются их общие свойства. Модели, построенные на основе профилей линий Fe I 543,5 нм и Na I D_2, имеют яркие составляющие холоднее невозмущенной фотосферы, в большинстве случаев описываемые модельным параметром $\Delta\Theta = 0{,}10$. Температуры темных составляющих находятся в диапазоне $\Delta\Theta = 0{,}35-0{,}50$. Фактор наполнения яркой составляющей в больших тенях остается практически постоянным ($\leqq 0{,}05$), тогда как в малых тенях он существенно изменяется (0,05—0,30). Зависимость температуры обеих составляющих, так же как фактора наполнения, от стадии развития пятна не наблюдалась.

Semi-empirical two-component models of 11 umbrae differing in size (radii 2″—8″) are presented and their general characteristics are discussed. The models, based on the profiles of the Fe I 543·5 nm and Na I D_2 lines have bright components cooler than the undisturbed photosphere, with a temperature down-scaling factor $\Delta\Theta = 0{\cdot}10$ in most cases. The temperature of dark components fluctuate in the range of $\Delta\Theta = 0{\cdot}35$ to 0·50. The filling factor of the bright component remains practically constant ($\leqq 0{\cdot}05$) in large umbrae ($r_u > 4''$), whereas in small umbrae it changes considerably (0·05—0·30). No dependence of the temperature of both components as well as the filling factor on the phase of evolution of the spot was observed.

Key words: sunspot umbra: models — photosphere

1. Introduction

High resolution photographs of sunspot umbrae reveal their complex photometric structure caused by the inhomogeneity of physical conditions. In addition to dark cores we observe brighter regions, extensions of penumbral filaments and embryos or remainders of light bridges. This photometrically variable "background" is superposed by bright umbral dots. The spatial distribution of the umbral dots resembles photospheric granulation very much (Bumba and Suda 1970). Due to relatively long exposure time, spectroscopic observations enable umbral inhomogeneities to be solved only in extremely rare cases (Adjabshirzadeh and Koutchmy 1983) and in sufficiently large umbrae. Such data are usually not available for studying individual and evolutionary characteristics of umbrae. In such cases we may try to describe the complex structure of the umbra by

第54回流星物理セミナー　文献資料　　from 国立天文部

3・流星数の調査

表1は異なった観測方法で捕らえられた全流星数の観測結果を表している。流星体質量の全域（$2*10^{-5}$g～$2*10^{7}$g）をカバーし、観測された全流星中のグループごとの流星数の割合をも表している。軌道の特徴がグループごとに出ているが、大部分は非常に広範囲で不規則な値を統計的に分類した代表値（ときどき中央値）である。ρM、σは、CeplechaやMcCrosky、ReVelleらによって生まれた値で、表1の最終欄に予想される”構成とその物質”とともに、各々のグループについて求められている。表1によると、グループIの母天体は小惑星であり、3：1のKirkwood gap（Wetherill 1985）に接近していることが最も重要視されるであろう。以下は表の通りである。

各々のグループの軌道の特徴はeに最も規則的な違いがあることであろう。表によると、普通の隕石と炭素質の隕石は0．6と最も小さく、Draconid typeは0．7、黄道に集中している周期彗星物質は0．8、彗星物質の密集したBグループは0．9、そしてrandomに傾斜したeが1に近い長周期軌道を描く彗星物質へと続いている。これは0．1g以上の質量がある。A，C1，C3，Dの中の小流星体は他よりも小さいeとaをもち、0．1g以下の流星体についてはしばしば0．5～1A．U．のaをもち、0．1g以上の質量を完全に除外している。

4・各グループの総流星数と流星体の質量

表1の中で最も目立つ特徴は全流星に関する個々のグループ内の質量%の変化である。これにより、logmが0．1か0．2の小段階で全体の質量間隔をわけていくことによって累積流星数の更につっこんだ研究が行なわれた。質量間隔が重なる為、簡単に4つの違う観測機材を比べることが出来る。ある型の機材で観測された微光天体はその隣接機材の輝天体である。流星の質量と数の確実な目盛りを定めることは、火球に有効である為（Halliday et al．1984）私達は火球の最も明るく巨大な天体の相対数の研究を始めた。火球の観測物質、流星の相対数における各グループの比較、更には35mmカメラでの観測流星の個々のグループ間の相対数も観測より直接得られた。仮に、観測機材の違う2つのグループの 流星の累積数曲線を流星の全質量範囲を通じて1つに結び付ける為にはグループの累積カーブが4つの異なった観測機材間をうまく続けられるような、ある定数をさがさねばならないのである。そして、与えられた観測機材の低感度のために検出数の減少した、微量発見流星体の一部は、1つの定数をすべての流星グループに当てはめた、隣接した観測機材への累積数曲線の延長線でうまく説明された。これにより全ケースにおいて、とらえられた隣接観測機材間の相対的変化の1つの値（logm＝±0．1）を得ることが出来た。このように累積数曲線はすべてのグループでかなり大きい質量間隔で構成されていたのである。

確実な目盛り定めはHalliday et al．（1984）の研究から引用された。第一に私達は独自にタイプIの火球と同じ累積数曲線の傾きを発見した。私達の範囲の違いは彼の質量スケールに従って、質量対数log0．2の小さい値を過ぎて増加するスケールにより、最終的な質量スケールに修正された。そしてこれもまた流星数対数を修正した。そして、タイプIの火球の累積数曲線を用い、Hallidayの累積数の質量間隔比較の結果が、log（naII／nI）＝0．64である。この細かい質量補正と私達の流星グループの確実な目盛り定めの実現性を除いては、上記の手順もまた私達の結果のコンシステンシーをしめした、より広範囲の観測機材に基づいた妥当性の完全チェックがHalliday et al．（1984）の結果の独立性を与えたのである。McCroskyの質量スケールは私達の最終的な質量スケール上のlogm＝0．3に近い。このように、この資料を使った私達の最終質量スケールは

logm（this paper）＝logm（Halliday）＋0．2＝logm（McCrosky）－0．3

により2つの言及された質量スケールと関係があるのである。

表1　写真及びＴＶ流星数の調査

観測機材	ＴＶカメラ				ｓシュミットカメラ				小型 ~~3-5m~~カメラ				火球ネット					流星体構成物質の特質		
質量範囲 b)	$2*10^{-5}$～$5*10^{-3}$g				$5*10^{-4}$～1g				10^{-1}～$5*10^{2}$g				10^{2}～$2*10^{7}$g							
グループ	%	軌道の特徴			%	軌道の特徴			%	軌道の特徴			群	%	軌道の特徴			ρM	σ	仮定上の母天体の構成
		a	e	i		a	e	i		a	e	i			a	e	i	g/cm³	s²/km²	
小惑星型流星	<1	0.7 a)	0.39 a)	18° a)	1	2.4	0.64	15°	5	2.5	0.64	10°	I	29	2.4	0.68	6°	3.7	0.017	通常のいん鉄の小惑星
A	27	1.6	0.55	14°	50	2.3	0.61	1°	39	2.5	0.64	4°	II	33	2.3	0.61	5°	2.0	0.041	炭素質いん石の彗星･小惑星
B	2	2.1	0.95	29°	3	2.4	0.92	5°	5	2.5	0.90	6°	−	−	−	−	−	1.0	0.08	彗星内部の彗星物質の密集；パエトン？
C1 c)	21	1.7	0.63	16°	7	2.2	0.80	6°	11	2.5	0.80	5°	IIIA c)	14	2.4	0.82	4°	0.75	0.10	通常の彗星物質の短周期彗星
C2	18	≈∞	0.99	r.	32	≈∞	0.99	r.	21	≈∞	0.99	r.	IIIAi	11	≈∞	0.99	r.	0.75	0.10	通常の彗星物質の長周期彗星
C3 c)	23	1.3	0.60	r.	6	1.9	0.72	r.	9	2.1	0.77	r.	C3 c)	4	2.7	0.67	r.	0.75	0.10	通常の彗星物質の長周期彗星
D	3	2.6	0.66	18°	1	3.3	0.70	25°	10	3.1	0.77	10°	IIIB	9	3.0	0.70	13°	0.27	0.21	微量彗星物質のＧＺ型短周期彗星

a・短半径　　e・離心率　　i・軌道傾斜角　　ρM・流星体の密度　　σ・融発係数　　%obs.・比較観測流星数

a）No.811104060の流星のみが小惑星型と認められた；よってその要素が与えられている。
b）総質量範囲：個々のグループは速度分布の相違の結果である。
c）Ｃ１からＣ３群の対応部分を加えることによってＣ３群はrandom(r.)i(i>35° を除く)に修正される。

MSS-78

Dust from beyond the Solar System

David W. Hughes

A sensitive radar in New Zealand has for the first time detected the faint meteors produced by interstellar dust grains hitting the Earth. It even points to nearby, young stars as being among the sources.

DUST particles are continually striking the Earth's upper atmosphere. Each meteoroid rapidly loses mass and velocity, leaving behind it a train of excited and ionized gas. This train can be seen as a meteor (colloquially known as a shooting star), and can also reflect radar pulses (when it is known as a radio meteor).

Almost all meteoroids have incident velocities between 11 and 73 km s^{-1}. The former is the Earth's escape velocity, so anything falling to Earth will be travelling at least that fast. The latter velocity is reached in a head-on collision with a meteoroid in a parabolic orbit around the Sun; that is, one with just enough energy to be on the border between a bound, closed orbit and an unbound one. Meteoroids in the above velocity range are members of the Solar System, and have been produced by the decay of comets and by collisions between asteroids.

Throughout the history of meteor science, people have wondered whether any incident meteoroids have hyperbolic orbits (with enough energy to be unbound). Rather than being miniature planets of our own Sun, hyperbolic meteoroids would have an origin beyond the Solar System. The easiest way of detecting them is by looking for a geocentric velocity in excess of the upper limit of 73 km s^{-1} given above. Öpik estimated[1] that between 60 and 70 per cent of the meteoroids that were not associated with the well-known showers were hyperbolic. Lovell[2] thought that this value was far too high, and by the 1960s Öpik[3,4] had reduced his value to around 3 per cent.

It is clear that our Solar System must be a source of hyperbolic meteoroids for other planetary systems. Consider comet Swift–Tuttle, the parent of the Perseid meteor shower that is active throughout most of August. Swift–Tuttle has an orbital period of 130 years and at perihelion it has a velocity of 42.2 km s^{-1}, very close to the parabolic limit. At perihelion the 'dirty snowball' cometary nucleus is sublimating furiously, and millimetre and submillimetre dust particles are being blown away from its surface at a relative velocity of around 0.9 km s^{-1}. Any dust that is emitted in the direction of the comet's motion moves off on a hyperbolic orbit[5], and typically 40 per cent of the dust lost by this comet leaves the Solar System and moves off through the Galactic disk.

The proportion of hyperbolic meteoroids produced increases as the meteoroid mass decreases. Comets with shorter orbital periods and with nuclei that have direct rather than retrograde spin will be considerably less prolific when it comes to producing hyperbolic meteoroids.

On page 323 of this issue, Taylor, Baggaley and Steel[6] recount how they have used a powerful radar telescope near Christchurch, New Zealand, to measure the orbits and sizes of incident meteoroids. Just under 1 per cent of all the meteoroids they detected had velocities in excess of 100 km s^{-1}. As this is far above the parabolic limit, the authors are confident that these meteoroids are from beyond the Solar System. The typical diameters of the detected meteoroids were between 15 and 40 μm.

What is even more exciting is that the annual variability of the hyperbolic meteoroid flux reveals the direction of the sources of these particles. Three major sources are identified. One is a group of nearby luminous A-type stars; another is a local group of even brighter B-type stars and young star clusters moving past the Sun; and the third is associated with the direction in which the Sun is moving around the Galaxy.

It is interesting to note that massive, fast-spinning A- and B-type stars are unlikely to have planetary systems because their original stellar nebulae are too hot for planets to condense[7]. Planetary systems with large numbers of gas giant planets, and thus decaying comets, are prevalent around single G and K stars with masses in the 1 to 0.25 solar mass range. Maybe the New Zealand high-velocity particles are produced by a different mechanism from the one seen in our own Solar System.

It also seems that the fraction of hyperbolic meteoroids decreases as the particle size goes up. Still, it is refreshing to know that even though more than 99 per cent of the dust in the Solar System is 'home grown', at least a fraction of a per cent comes from beyond. □

David Nunuk/SPL

The trail of a Perseid meteor at dusk. The dust particle that produced this meteor came from a comet within our Solar System, but tiny meteors from other stars have now been detected by radar. No visible shooting stars have yet been shown to be of interstellar origin.

David W. Hughes is in the Department of Physics, University of Sheffield, Sheffield S3 7RH, UK.

1. Öpik, E. J. *Publ. astr. Obs. Tartu* **30**, No. 6 (1941).
2. Lovell, A. C. B. *Meteor Astronomy* 212–247 (Clarendon, Oxford, 1954).
3. Öpik, E. J. *Contr. Armagh Obs.* **26**, 1–82 (1958).
4. Öpik, E. J. *Ir. astr. J.* **9**, 156–159 (1969).
5. Harris, N. W., Yau, K. K. C. & Hughes, D. W. *Mon. Not. R. astr. Soc.* **273**, 999–1015 (1995).
6. Taylor, A. D., Baggaley, W. J. & Steel, D. I. *Nature* **380**, 323–325 (1996).
7. Hughes, D. W. *New Scient.* **136**, No. 1851, 29–33 (1992).

Discovery of interstellar dust entering the Earth's atmosphere

A. D. Taylor*†‡, W. J. Baggaley§ & D. I. Steel*‖

* Department of Physics and Mathematical Physics, University of Adelaide, SA 5005, Australia
† Unit for Space Sciences, University of Kent, Canterbury, UK
§ Department of Physics and Astronomy, University of Canterbury, Christchurch, New Zealand
‖ Anglo-Australian Observatory, Private Bag, Coonabarabran, NSW 2537, Australia

ALL known asteroids and comets are believed to have been gravitationally bound to the Sun since they formed (together with the Sun and planets) from the solar nebula. This is because no such object has been observed with a speed exceeding the solar escape velocity, although some comets have been close to this limit[1]. As comets are occasionally ejected from the Solar System, interstellar comets might be expected to arrive every few centuries, having been ejected from similar systems around other stars[2]. The flux of interstellar dust into the Solar System should be much higher, but its detection poses significant technological challenges. Recently, the Ulysses spacecraft detected a population of dust particles near Jupiter, identified as being of interstellar origin on the basis of their speeds and trajectories[3,4]. Here we report the radar detection of interstellar particles in the Earth's atmosphere. From intra-annual variations in particle flux, we infer the existence of two discrete sources, one associated with nearby A-type stars, and the other with the Sun's motion about the Galactic Centre. The data also suggest the presence of a third source, possibly associated with local B-type stars and young stellar clusters.

We are conducting a survey of the orbits of very faint radar meteors using the AMOR radar in New Zealand[5]. So far over 350,000 individual meteoroid orbits have been determined, many more than the total of ~69,000 from the previous surveys stored at the IAU Meteor Data Center[6]. Previous radar meteor orbit systems used Fresnel diffraction echo profiles to measure meteor speeds, and such profiles are sensitive to pulse aliasing effects, especially at high speeds, as we discuss elsewhere[7]. We determine meteor speeds from time lags between spaced receiver sites and thus can measure, with reasonable accuracy, meteor speeds exceeding the parabolic limit for orbits bound to the Solar System (~73 km s^{-1}: 42.1 km s^{-1} to which is added the Earth's speed and the effect of the terrestrial gravitational field).

We find that ~14% of all our orbits have in-atmosphere speeds $V > 73$ km s^{-1}, and these we term pseudohyperbolic particles (PHPs); here we use V for the measured speeds, and v for actual speeds. Previous optical and radar meteor surveys have rendered catalogues containing up to 30% PHPs[7]. The problem lies in identifying which are true interstellar particles (ISPs) and are not just bound orbits with large measurement errors[8,9]. Most PHPs have geocentric speeds close to the parabolic limit so that a small error in the measured speed (or radiant coordinates) would result in a hyperbolic orbit being indicated, but if real ISPs exist then some should be detected with geocentric speeds well below that limit[8].

The results presented here use a high-quality set of 1,508 meteors with measured speeds $V > 100$ km s^{-1} and similar echo profiles at all receiver sites. This data set, collected between February 1990 and November 1991, comprises only 0.9% of the orbits measured in that period, owing to the stringent selection criteria applied[5]. Comparison between Fresnel and time-lag speed determinations for meteors with $V < 50$ km s^{-1} leads to an estimated uncertainty $\sigma \approx 6$ km s^{-1} in the speeds near $V = 73$ km s^{-1}, a value substantiated by inspection of the measured speeds in the ~65 km s^{-1} η-Aquarid shower[5,7]. The data set therefore comprises meteors with speeds $>3\sigma$ above any possible bound Solar System orbit. This means that an ISP whose real (not measured) geocentric speed was $v = 90$ km s^{-1} would not have been gathered into the data set used here unless its speed was erroneously measured as being $V > 100$ km s^{-1}; thus the majority of ISPs were probably excluded from the data set analysed but this was necessary in order to exclude mis-measurements of meteoroids from bound orbits. The mean speed for this ISP data set is $\bar{V} \approx 164$ km s^{-1} with an uncertainty of ±30 km s^{-1}, in agreement with a crude estimate of $\bar{V} \approx 140$ km s^{-1} derived solely from their mean ionization height[7].

The meteoric ionization produced is a strong function of speed, so ISPs near our limiting magnitude ($M_{\rm lim} = 12.5$) will be smaller than the typically ~100 μm meteoroids from bound orbits we detect. Verniani[10] determined an empirical relation $q = 0.0509\, m^{0.92}\, v^{3.91}$ between the mass (m in g), the speed (v in m s^{-1}), and the electron line density (q, electrons per metre). Our $M_{\rm lim}$ corresponds to $q = 2.5 \times 10^{11}$ m^{-1}. At $v = 100$ km s^{-1} the diameter of the smallest detectable meteoroid (assumed spherical with density 1 g cm^{-3}) is ~40 μm; at $v = 200$ km s^{-1} it is ~15 μm. Far-infrared observations require a substantial ~30-μm interstellar grain component[11], and Pioneer 10 and 11 dust impact data, indicating a constant flux at heliocentric distances from 3 to 18 AU, have been interpreted as being due to ~10-μm interstellar grains penetrating the Solar System[4]. Interstellar particles of order tens of micrometres are therefore not unexpected.

Our data set displays strong seasonal variations (Fig. 1), arguing against these meteors being merely Solar System particles for which exceptional errors accumulated. The strongest evidence for these particles having come from interstellar trajectories lies in the relative absence of detections between days 260 and 350, when the Earth is moving away from the apex of the solar motion. The trends seen in Fig. 1 may be explained as being due to seasonally changing relative geometries between the terrestrial motion vector and discrete source directions. We tentatively identify a bimodal distribution with peaks near days 32 and 170. The raw

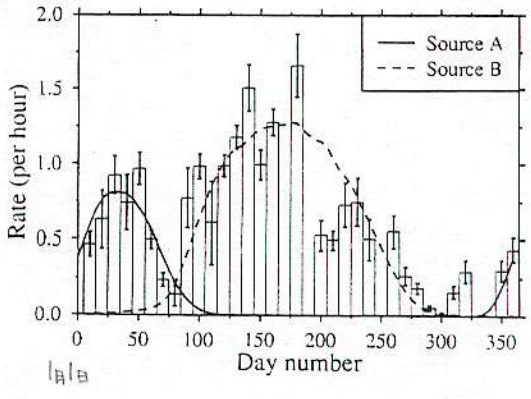

FIG. 1 Detection rates of meteors with observed velocities $V > 100$ km s^{-1} in ten-day bins (histogram). Uncertainty bars indicate the square roots of the count statistics. Expected distributions from two models of discrete interstellar sources are shown: ecliptic latitude $\beta = 30°$, longitude $\lambda = 240°$, and initial speed $v_\infty = 40$ km s^{-1} (source A, peak at day of year 32; solid line), and $\beta = 30°$, $\lambda = 0°$, $v_\infty = 80$ km s^{-1} (source B, peak at day 170; dashed line). As discussed in the text, an alternative possibility is that there is a source B′ giving a peak near day 150, and another source C resulting in a peak near day 224.

‡ To whom correspondence should be addressed at Adelaide.

MSS-78

observational data render mean time lags for meteors detected between days 340 and 80 which are significantly shorter than those between days 80 and 280. The difference is equivalent to ~20 km s^{-1}, suggesting a slower ISP source for the peak at day 32 than that at day 170.

We developed a model of the ISP influx for comparison with the observations, taking into consideration gravitational focusing by the Sun, flux enhancements resulting from the Earth's orbital motion, and increased ionization production by high-speed meteoroids. This renders an estimate of the fraction of meteors detected with $V > 100$ km s^{-1}. We assume that ISPs flow into the Solar System from a direction defined by its ecliptic latitude (β) and longitude (λ) with a single initial speed (v_∞). Electromagnetic and radiation effects are insignificant for these particle sizes. Gravitational focusing increases the spatial density over that in interstellar space, and concentrates ISPs behind the Sun compared to positions between the Sun and the source. Figure 2*a* shows the spatial density at 1 AU as a function of the terrestrial ecliptic longitude (L) with respect to the influx for a hypothetical source emanating from $\beta = 30°$, $\lambda = 0°$, with $v_\infty = 40$ km s^{-1}. A northern radiant was chosen because the solar motion is towards a point well north of the ecliptic (see later). Due to the geographical latitude and antenna patterns of our radar, most of our meteor radiants are in the declination range $+5° > \delta > -30°$ (ref. 5); thus only ISPs from low northern latitudes can appear in our data, so we chose $\beta = 30°$ for our source models. Varying β in the range 0–60° makes little difference to the results. The model particles are then propagated to the Earth, the geocentric velocity of each calculated, and a normalized flux derived. When $180° < L < 360°$ the terrestrial motion is towards the source, producing the flux enhancement seen in Fig. 2*a*.

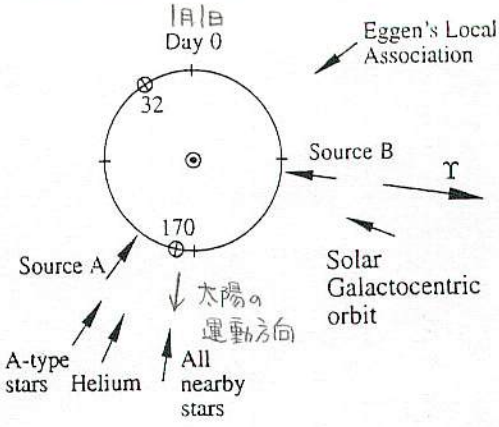

FIG. 3 Summary of possible sources of interstellar meteoroids and the influx observed, projected onto the ecliptic. The symbol Υ shows the vernal equinox. Days of year 32 and 170 correspond to peaks in the count rates shown in Fig. 1 and are marked on the Earth's orbit. These peaks are explicable by our model sources A (~110° in longitude from day 32) and B (~95° in longitude from day 170); the differential longitude shifts are due to the different speeds used for A and B. Source A may plausibly be associated with the motion of the Solar System relative to nearby A-type stars[13] rather than the motion relative to all other local stellar types[12]. Source B is near-aligned with the Sun's Galactocentric orbit[14], but temporal gaps in the data used here do not allow us to exclude the possibility that the larger peak fitted in Fig. 1 actually comprises two separate components, one (source B') centred near day 150 and then more closely associated with the solar Galactocentric orbit, whilst the other (source C) centred near day 225, is derived from Eggen's local association of star clusters and B-type stars[15,16].

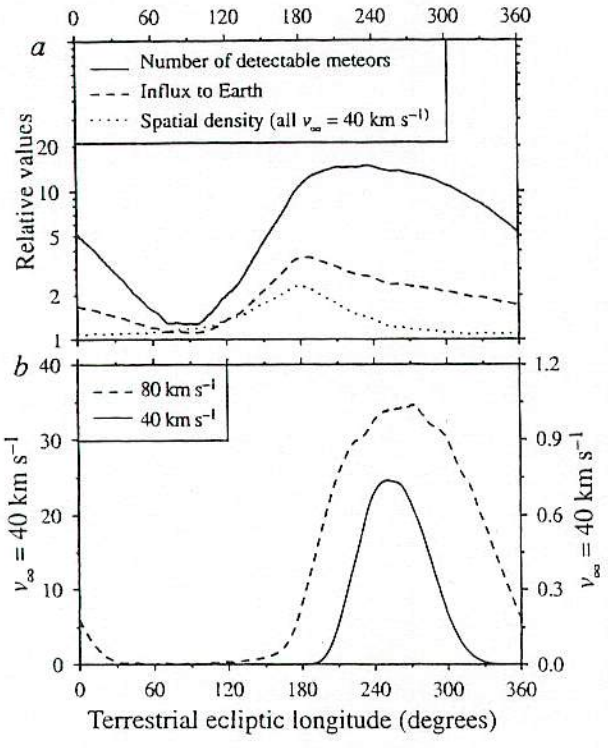

FIG. 2 *a*, The relative spatial density, flux to the Earth, and number of meteors above a given detection threshold, for a hypothetical interstellar source emanating from $\beta = 30°$, $\lambda = 0°$ with $v_\infty = 40$ km s^{-1}. While the spatial density is enhanced by gravitational focusing behind the Sun (terrestrial ecliptic longitude $L = 180°$), most meteors would be detected during the half-year as the Earth approaches the interstellar influx ($180° < L < 360°$). *b*, The relative numbers of interstellar meteors expected to be detected with measured speeds $V > 100$ km s^{-1} for two source models, one with $v_\infty = 40$ km s^{-1}, as in *a*, and the other emanating from the same direction but with $v_\infty = 80$ km s^{-1}.

For any limiting line density q and specified v, a minimum mass m_{min} producing a detectable meteor may be derived. The number of detections is $N(m > m_{min}) = k m_{min}^{-\alpha}$; α is the cumulative mass index and k a constant. We cannot determine α from our ISP sample owing to speed measurement uncertainties and the speed-dependence of ionization production, so we adopt $\alpha = 0.6$ as representative of ISPs. Varying α has little effect on the relative shape of different velocity populations and does not affect the longitude L at which peak influxes are anticipated. The value of α does, however, affect the relative strength of sources with different v_∞, making any estimate of that speed very model-sensitive.

The uppermost curve in Fig. 2*a* shows the relative numbers of ISPs that would be detected as a function of L. As the Earth approaches incoming ISPs ($L = 270°$), the geocentric speeds will generally be ~(60 cos β) km s^{-1} greater than six months later while moving away from the source direction. For a heliocentric speed of 58 km s^{-1} at 1 AU (corresponding to $v_\infty = 40$ km s^{-1}), this variation represents a factor of 3 in the geocentric speeds and thus a change in detectable mass by a factor of ~100, leading to $\sim 100^\alpha \approx 16$ times more ISPs being detected. Most of these, though, would have $V < 100$ km s^{-1} and so would be rejected from our data set. Figure 2*b* shows only those test ISPs with $V > 100$ km s^{-1}; note that the terrestrial encounter speeds are actually $v \approx 90$ km s^{-1}, but we have applied random experimental errors in the model to deduce how many of those test particles would have $V > 100$ km s^{-1} measured. For $v_\infty = 40$ km s^{-1}, the model predicts a peak detection rate when $L = 250°$ ($\lambda - L = 110°$). For a source in the direction but with $v_\infty = 80$ km s^{-1} the peak occurs at $L = 265°$ ($\lambda - L = 95°$) and is much broader, although there remains an absence of detections around $L = 90°$. Earth encounter speeds are $v \approx 120$ km s^{-1} for ISPs from this source detected near the peak. If $v_\infty = 80$ km s^{-1} then ISPs are 47 times more likely to be detected and counted within our data set than those with $v_\infty = 40$ km s^{-1} ($\alpha = 0.6$); for $\alpha = 0.2$ or 1.0 the ratios are 27 and 80 times, respectively. ISPs with $v_\infty = 20$ km s^{-1} are over 100 times less likely to be selected

than if $v_\infty = 40\,\mathrm{km\,s^{-1}}$. Clearly high-speed interstellar sources are strongly favoured by the speed selection ($V > 100\,\mathrm{km\,s^{-1}}$) imposed here.

Next we compare these model calculations with our data set. $L \approx 100°$ on 1 January, allowing the day-of-year to be easily deduced from L. In Fig. 1 we model a fit to the data with two populations, emanating from $\beta = 30°$, $\lambda = 240°$ with $v_\infty = 40\,\mathrm{km\,s^{-1}}$ (source A), and from $\beta = 30°$, $\lambda = 0°$ with $v_\infty = 80\,\mathrm{km\,s^{-1}}$ (source B); these are the hypothetical sources plotted in Fig. 2*b* differentially shifted in longitude and scaled by factors of 1.1 (source A) and 0.037 (source B) to fit the observational data. The scaling suggests that the spatial density in interstellar space of source A is $\sim 10^3$ times greater than that of Source B.

Figure 3 provides a graphical summary of these source directions, which require identification with plausible producers of ISPs. The solar motion relative to nearby stars[12] is directed towards a galactic latitude $b = 23°$, longitude $l = 52°$ (that is $\beta = 50°$, $\lambda = 269°$), near the location of source A. For late A-type stars only[13], the apex is towards $\lambda \approx 243°$, even closer to source A, and would produce a peak near day 34. Such stars are excellent candidates as ISP producers because they possess protoplanetary particulate disks, collisions and radiation pressure leading to dust ejection. Source A is also close to the flow of neutral helium through the Solar System, as associated with the $\sim$0.4-μm interstellar grains detected with Ulysses[4], but the ISPs we have detected are too large to have come into equilibrium with that gas.

We now consider source B, associated with the faster ISPs. These ISPs might come from a direction associated with the solar galactocentric orbit[14], thus emanating from $b = 0°$, $l = 90°$ ($\beta = 60°$, $\lambda = 347°$). That direction would give a peak detection rate at day 154; the observed peak is near day 170 for source B (Figs 1 and 3). Alternatively this source might comprise two discrete components: B′ centred at day 150 and C centred at day 225 (compare Fig. 1). Eggen[15,16] describes a local association of young star clusters and B-type stars moving past the Sun. These would produce ISPs coming from $\beta = 19°$, $\lambda = 121°$, and a peak detection rate around day 224.

Our analysis of stringently selected radar-detected meteors demonstrates that there is a near-Earth flux of small meteoroids (sizes $\sim$15–40 μm) arriving from interstellar space; these meteoroids originate from a few discrete sources in the vicinity of the Sun. We plan further data collection, and analysis of data in hand, to refine our knowledge of plausible source directions for these particles. □

Received 18 July 1995; accepted 1 February 1996.

1. Kresák, Ľ. *Astr. Astrophys.* **259,** 682–691 (1992).
2. Hughes, D. W. *J. Br. astr. Assoc.* **101,** 119–120 (1990).
3. Grün, E. *et al. Nature* **362,** 428–430 (1993).
4. Grün, E. *et al. Astr. Astrophys.* **286,** 915–924 (1994).
5. Baggaley, W. J., Bennett, R. G. T., Steel, D. I. & Taylor, A. D. *Quart. Jl. R. astr. Soc.* **35,** 293–320 (1994).
6. Lindblad, B. A. & Steel, D. I. in *Asteroids, Comets, Meteors 1993* (eds Milani, A., Di Martino, M. & Cellino, A.) 497–501 (IAU Symp. 160, Kluwer, Dordrecht, 1994).
7. Taylor, A. D., Baggaley, W. J., Bennett, R. G. T. & Steel, D. I. *Planet. Space Sci.* **42,** 135–140 (1994).
8. Jones, J. & Sarma, T. *Bull. astr. Inst. Czechoslov.* **36,** 103–115 (1985).
9. Hajduková, M. Jr in *Meteoroids and their Parent Bodies* (eds. Štohl, J. & Williams, I. P.) 61–64 (Slovak Acad. Sci., Bratislava, 1993).
10. Vernani, F. *J. geophys. Res.* **78,** 8429–8462 (1973).
11. Rowan-Robinson, M. *Mon. Not. R. astr. Soc.* **258,** 787–799 (1992).
12. Jaschek, C. & Valbousquet, A. *Astr. Astrophys.* **255,** 124–129 (1992).
13. Jaschek, C. & Valbousquet, A. *Astr. Astrophys.* **242,** 77–84 (1991).
14. Mihalas, D. & Binney, J. *Galactic Astronomy: Structure and Kinematics* (Freeman, San Francisco, 1981).
15. Eggen, O. J. *Mon. Not. R. astr. Soc.* **204,** 377–390 (1983).
16. Eggen, O. J. *Mon. Not. R. astr. Soc.* **204,** 391–403 (1983).

ACKNOWLEDGEMENTS. This work was supported in part by the Australian Research Council.

Semiconducting superlattices templated by molecular assemblies

Paul V. Braun*, Paul Osenar* & Samuel I. Stupp*†‡

Departments of * Materials Science and Engineering and † Chemistry, and Beckman Institute for Advanced Science and Technology and Materials Research Laboratory, University of Illinois at Urbana-Champaign, Urbana, Illinois 61801, USA

ORGANIC–INORGANIC nanostructured composites provide a rich source of new materials[1–14] for a host of technological applications. For example, the incorporation of organic molecules in an inorganic lattice can toughen an otherwise brittle material[15–17], or be used to tailor its electronic properties[14], and cooperative interactions between organic and inorganic molecules are being used to generate a range of porous materials for separation and catalytic technologies[4–10]. Here we describe the growth of stable semiconductor–organic superlattices based on cadmium sulphide and cadmium selenide. The template for the structures is provided by a liquid-crystalline phase formed from non-ionic organic amphiphiles, water and precursor ions for the inorganic semiconductor. Precipitation of the organic–inorganic solid takes place within the ordered environment of the mesophase, and both the symmetry and long-range order of the liquid crystal are preserved. We anticipate that materials of this type can be tailored, through the electronic properties of the organic amphiphiles, for photosynthetic and photocatalytic applications.

‡ To whom correspondence should be addressed.

A promising route to nanostructured composites uses the ordered environment of a preformed amphiphile-solvent mesophase to nucleate and grow inorganic structures. In such a system, the ordered assembly of organic molecules in the mesophase partitions the solvent and may therefore confine the reactive species, providing a controlled environment for the formation of nanostructures. In the few experiments that have attempted to harness the order of a mesophase in the synthesis of inorganic materials, precipitates with unique morphology were obtained, including oblong crystallites[11] and macroporous crystalline networks[12]. The mesoporous oxide methodology has been applied to a concentrated system in a recent study[13] in which the mesoporous oxide was derived from an isotropic liquid (formed by adding tetramethyl orthosilicate to a mesophase). Here we report the growth of a non-oxide, nanocomposite material templated directly by a hexagonal mesophase yielding a superlattice with matching symmetry and periodicity (Fig. 1). We believe this is the first example of a reaction leading to a nanostructure templated with the characteristic spacings and symmetry of the precursor mesophase. In our system the nature of the mesophase does not change at any time throughout the synthetic pathway leading from precursor to product. This is in contrast to earlier work based on the cooperative assembly of condensing oxide precursors with amphiphilic molecules, in which nanocomposites were precipitated from dilute solutions or isotropic solutions formed by adding precursor to a mesophase[6–10,13]. However, in none of these cases did the precipitation take place in the preordered environment of a mesophase.

We have targeted the synthesis of nanocomposites containing II–VI semiconductors. The organized, molecular dispersion of organic in a semiconductor lattice could provide materials with properties not attainable by conventional techniques, as the intimate association of organic and inorganic components in a

MSS-93

Ongoing Meteor Work

Leonid Dust Trails and Meteor Storms

Robert H. McNaught and David J. Asher

Leonid storms are caused by the Earth intersecting dense trails of dust ejected from Comet 55P/Tempel-Tuttle. Here, we extend existing studies by examining the higher ejection-velocity regions of young dust trails and the circumstances around the 2031 return of 55P/Tempel-Tuttle. A model of dust trail density is successfully fitted to the observed ZHR of storms. Based on this, predictions are made for encounters in the next few years and around 2031, giving both the times and rates of maxima. The most likely prospects for encounters are from 1999–2002, especially 2001 and 2002. Details of a storm in 1869 are presented and confirm that the time of maximum is predictable to 10 minutes accuracy or better. The consequences of these findings are applied to the satellite threat and to the methods of global analysis of Leonid rates.

1. Introduction

Meteor storms occur when the Earth passes through dense trails of meteoroids and dust such as those observed by the Infra-Red Astronomical Satellite [1]. The motion of Comet 55P/Tempel-Tuttle only has relevance, with regard to Leonid storms, in defining the initial orbits of the meteoroids at ejection. To understand Leonid activity requires a study of the perturbed motion of these meteoroids. It has been known for some time [2–4] that perturbations can be significantly different on Leonid meteoroids that are separated in mean anomaly. Extensive calculations about swarm/trail encounters covering the 19th and 20th centuries were first done by Kondrat'eva et al. [5] and later (without prior knowledge) by Asher [6].

The natural tendency is for the spatial density of meteoroids to decrease, trails becoming dispersed after many orbital revolutions. However, there does exist a dynamical mechanism, namely a mean motion resonance, that can cause meteoroids in the Leonid and other streams to remain very concentrated on longer time scales [7]. Thus, a second source of Leonid storms is meteoroids many revolutions old in the 5/14 resonance with Jupiter. Meteoroids from every return of the comet ultimately add to this, if ejection is within a suitable initial range of semi-major axes. This has been investigated for the 1998 Leonid fireball shower [8], the observed time of maximum for that outburst [9] being demonstrated to be consistent with the prediction from the resonant meteoroids and quite discrepant from the comet node (a difference of 0.8 day). Further study is required on these resonant meteoroids, but this source appears to have been involved in the fireball display of 1965 and maybe also in the storms of 1799 and 1832. These resonant meteoroids cover only around 10° of mean anomaly and so could generally be encountered at high strength only once per comet orbit.

It is not coincidental that the resonant mechanism leads to outbursts that are rich in fireballs. Larger particles, which produce brighter meteors, are expected to have lower ejection speeds from the comet nucleus. This means that they go on to orbits more similar to that of the comet (which is itself in the resonance) and so are more likely to be resonant. However, smaller particles are more numerous, and the highest ZHR storms result from younger trails, which are our subject here.

2. Extended table of dust node

Readers should refer to [6] for a description of why our method is appropriate for calculating dust trail positions. Briefly, the model has meteoroids ejected from 55P/Tempel-Tuttle at each perihelion and integrated until nodal crossing in any specific year. Thus, at the time of ejection, taken to be exactly at perihelion, the perihelion distance and the angular orbital elements are set equal to those of the comet, and the process iterates to find the precise value of the semi-major axis at ejection, a_0, that gives passage through the descending node at the time when the Earth reaches the orbital plane. We used the 15th order Radau integrator [10] in the

MERCURY integration package [11], kindly provided to us by John Chambers, with accuracy parameter 10^{-11} and perturbations from eight planets (Mercury to Neptune). Particles affected by radiation pressure must have smaller a_0 than listed in Table 1 in order to cross the ecliptic at the correct time. For example, $\beta = 0.001$ (ratio of the forces of radiation pressure and solar gravity) means that the correct effective a_0 is 0.2 smaller than that listed (cf. [6,12]). Possible variations in the trail geometry due to ejection away from perihelion or radiation pressure are discussed later (Sections 3 and 5).

Table 1 is an extended version of (some columns of) that given in [6], which included data for trails generated 1, 2, and 3 revolutions earlier, in the two years prior to, and four years after, the perihelion passage of 55P/Tempel-Tuttle. In the present paper, trails 4, 5, and 6 revolutions old are considered in the same years, and a larger range of ejection velocities (allowing nodal crossing to occur in years further from the comet's perihelion) are considered for the 1–3-revolution trails. As more revolutions are considered, the range of Δa_0 over these six years contracts, and encounters with trails of this age outside these years could still produce notable activity, albeit the ZHR will tend to decrease the older the trail. To save extensive further computation, reference was made to [5] for other possible years and trails older than 6 revolutions worthy of consideration; we selected for inclusion the 7-revolution trails in 1832 and 2001 and the 8-revolution trail in 2000 (the values in Table 1 being derived by ourselves).

Table 1 – Data for dust trails generated a reasonably small number of revolutions previously. Below, Δa_0 is the initial difference in semi-major axis from the comet that allows the nodal crossing to occur at exactly the relevant time in November of the year in question; r_D and r_E are the heliocentric distances of the dust trail's descending node and of the Earth at the same longitude; and f_M, the "mean anomaly factor," is inversely proportional to the stretching in mean anomaly that has occurred since ejection, normalized to a fixed, small interval in a_0 centered on the value of Δa_0 in question (refer to Section 5). The spatial density of a trail encountered by the Earth depends on Δa_0 (ejected meteoroids being concentrated towards orbits nearer the comet), $r_E - r_D$ (which gives a measure of the distance between the Earth and the center of the trail), and f_M (since the particle density decreases as the trail lengthens), as investigated quantitatively in Section 5. Finally, Ω is equal to the longitude of the Sun at the time of nodal crossing (calculated for orbit of Earth at relevant date, but expressed in J2000). A dash indicates that the relevant part of the trail had been disrupted to a greater or lesser extent (cf. [6]), a blank space simply that we did not attempt to calculate the data.

Year	Trails 1 rev. old				Trails 2 rev. old				Trails 3 rev. old			
	Δa_0	$r_E - r_D$	f_M	Ω	Δa_0	$r_E - r_D$	f_M	Ω	Δa_0	$r_E - r_D$	f_M	Ω
1798	−0.28	+0.0043	1.08	233°.04	−0.15	+0.0058	0.53	233°.02	−0.09	+0.0017	0.41	232°.15
1799	−0.07	+0.0032	1.00	233°.04	−0.04	+0.0035	0.52	233°.03	−0.02	+0.0018	0.27	232°.84
1800	+0.14	+0.0028	1.00	233°.03	+0.07	+0.0020	0.52	233°.06	+0.02	+0.0060	0.17	233°.32
1801	+0.35	+0.0029	0.95	233°.02	+0.19	+0.0006	0.53	233°.17	+0.06	+0.0105	0.15	233°.58
1802	+0.56	+0.0029	0.95	233°.04	+0.31	−0.0011	0.55	233°.49	+0.09	+0.0134	0.18	233°.95
1803	+0.76	+0.0022	0.95	233°.18	+0.42	−0.0008	0.43	234°.45	+0.12	+0.0208	0.11	234°.84
1831	−0.25	+0.0034	1.00	233°.16	−0.13	+0.0051	0.55	233°.17	−0.10	+0.0068	0.40	233°.16
1832	−0.04	+0.0014	1.00	233°.18	−0.02	+0.0017	0.55	233°.18	−0.02	+0.0019	0.39	233°.17
1833	+0.17	−0.0003	0.95	233°.18	+0.09	−0.0015	0.53	233°.18	+0.07	−0.0028	0.45	233°.21
1834	+0.38	−0.0017	0.95	233°.18	+0.20	−0.0044	0.52	233°.17	+0.15	−0.0070	0.61	233°.27
1835	+0.59	−0.0026	0.95	233°.18	+0.31	−0.0065	0.50	233°.16	+0.24	−0.0107	0.39	233°.42
1836	+0.79	−0.0033	0.95	233°.18	+0.42	−0.0083	0.50	233°.18	+0.33	−0.0142	0.43	233°.80
1864	−0.25	+0.0124	1.06	233°.96	−0.13	+0.0138	0.55	233°.94	−0.10	+0.0156	0.41	233°.95
1865	−0.04	+0.0072	1.00	233°.32	−0.02	+0.0074	0.59	233°.31	–	–	–	–
1866	+0.17	+0.0036	1.00	233°.30	+0.09	+0.0026	0.55	233°.31	+0.07	+0.0012	0.40	233°.31
1867	+0.37	−0.0002	1.00	233°.42	+0.20	−0.0026	0.55	233°.43	+0.15	−0.0057	0.45	233°.42
1868	+0.58	+0.0012	0.95	234°.06	+0.31	−0.0044	0.54	234°.03	+0.24	−0.0096	0.40	234°.01
1869	+0.78	+0.0103	0.95	233°.43	+0.43	+0.0055	0.53	233°.49	+0.32	−0.0005	0.44	233°.54
1897	−0.35	−0.0020	1.00	234°.24	−0.18	+0.0008	0.45	234°.93	−0.12	+0.0013	0.25	235°.26
1898	−0.14	+0.0155	1.06	234°.84	−0.07	+0.0167	0.55	234°.96	−0.05	+0.0176	0.41	235°.04
1899	+0.07	+0.0138	1.02	235°.02	+0.04	+0.0132	0.54	234°.98	+0.03	+0.0126	0.41	234°.98
1900	+0.28	+0.0199	1.00	234°.07	+0.15	+0.0182	0.55	234°.02	+0.11	+0.0168	0.41	234°.05
1901	+0.48	+0.0146	1.00	233°.85	+0.25	+0.0125	0.53	233°.82	+0.19	+0.0097	0.46	233°.85
1902	+0.68	+0.0114	0.95	233°.85	+0.36	+0.0086	0.59	233°.85	+0.28	+0.0035	0.45	234°.03

Table 1 – Data for dust trails (continued).

Year	Trails 1 revolution old				Trails 2 revolutions old				Trails 3 revolutions old			
	Δa_0	$r_E - r_D$	f_M	Ω	Δa_0	$r_E - r_D$	f_M	Ω	Δa_0	$r_E - r_D$	f_M	Ω
1930	−0.36	+0.0075	1.00	235°09	−0.17	+0.0071	0.40	235°24	−0.12	+0.0018	0.32	235°39
1931	−0.14	+0.0065	1.08	235°09	−0.08	+0.0105	0.53	234°90	−0.06	+0.0125	0.37	235°09
1932	+0.07	+0.0060	0.95	235°09	+0.03	+0.0059	0.46	235°36	+0.02	+0.0059	0.31	235°43
1933	+0.28	+0.0054	1.00	235°15	+0.11	+0.0118	0.27	236°01	+0.07	+0.0135	0.16	235°99
1934	+0.49	+0.0040	0.95	235°50	+0.16	+0.0173	0.28	236°24	+0.10	+0.0182	0.21	235°95
1935	+0.69	+0.0182	1.00	235°96	+0.23	+0.0342	0.39	236°20	+0.16	+0.0327	0.41	235°66
1961	−0.75	+0.0109	1.14	235°03	−0.39	+0.0160	0.57	235°10	−0.25	+0.0078	0.42	234°93
1962	−0.53	+0.0083	1.08	235°06	−0.28	+0.0116	0.55	235°10	−0.18	+0.0114	0.28	235°27
1963	−0.31	+0.0059	1.00	235°09	−0.17	+0.0077	0.55	235°11	−0.13	+0.0136	0.34	235°10
1964	−0.10	+0.0038	1.00	235°12	−0.05	+0.0043	0.53	235°12	−0.04	+0.0063	0.44	234°95
1965	+0.11	+0.0023	1.00	235°13	+0.06	+0.0017	0.59	235°13	+0.04	+0.0015	0.37	235°45
1966	+0.32	+0.0016	0.95	235°13	+0.17	−0.0001	0.52	235°16	+0.09	+0.0033	0.19	235°94
1967	+0.53	+0.0012	0.95	235°13	–	–	–	–	+0.12	+0.0063	0.16	236°21
1968	+0.73	+0.0010	0.95	235°15	+0.39	−0.0036	0.55	235°44	–	–	–	–
1969	+0.93	0.0000	0.95	235°27	+0.51	−0.0058	0.54	236°09	+0.20	+0.0136	0.13	237°37
1992									−0.45	+0.0176	0.43	235°41
1993									−0.36	+0.0109	–	235°54
1994					−0.38	+0.0102	0.57	236°40	−0.28	+0.0155	0.12	236°43
1995					−0.26	+0.0168	0.57	235°48	−0.19	+0.0211	0.42	235°47
1996	−0.28	+0.0099	1.08	235°29	−0.15	+0.0126	0.55	235°27	−0.11	+0.0149	0.41	235°27
1997	−0.06	+0.0085	1.00	235°26	−0.04	+0.0091	0.55	235°26	−0.03	+0.0095	0.40	235°26
1998	+0.14	+0.0068	1.00	235°26	+0.08	+0.0055	0.55	235°27	–	–	–	–
1999	+0.35	+0.0047	0.95	235°28	+0.19	+0.0019	0.53	235°27	+0.14	−0.0007	0.38	235°29
2000	+0.55	+0.0031	0.95	235°29	+0.30	−0.0012	0.55	235°27	+0.22	−0.0051	0.38	235°32
2001	+0.76	+0.0022	0.95	235°29	+0.41	−0.0034	0.52	235°25	+0.30	−0.0086	0.39	235°39
2002	+0.96	+0.0018	0.95	235°27	–	–	–	–	+0.39	−0.0119	0.45	235°56
2003	+1.16	+0.0019	0.90	235°27	+0.63	−0.0061	0.49	235°23	+0.48	−0.0151	0.78	236°03
2004					+0.74	−0.0074	0.78	235°30	+0.56	−0.0167	0.32	237°14
2005					+0.85	−0.0099	0.50	235°63	+0.61	−0.0111	0.13	238°90
2006					+0.96	−0.0001	0.53	236°62	+0.63	+0.0106	0.08	240°21
2007									+0.65	+0.0214	0.08	238°99
2008									+0.67	+0.0254	0.12	238°24
2009									+0.70	+0.0264	0.18	237°46
2025									−0.38	+0.0026	0.10	237°13
2026									−0.34	+0.0122	0.20	237°19
2027					−0.39	+0.0126	0.57	235°82	−0.29	+0.0170	0.31	236°57
2028					−0.28	+0.0104	0.37	235°66	−0.22	+0.0156	0.42	235°90
2029	−0.32	+0.0071	1.00	235°88	−0.17	+0.0083	0.55	235°93	−0.13	+0.0112	0.42	235°97
2030	−0.11	+0.0219	1.00	236°21	−0.06	+0.0224	0.95	236°21	−0.04	+0.0232	0.44	236°21
2031	+0.10	+0.0183	1.00	235°42	+0.05	+0.0179	0.53	235°42	+0.04	+0.0171	0.41	235°42
2032	+0.30	+0.0154	0.95	235°36	+0.16	+0.0140	0.55	235°35	+0.12	+0.0114	0.46	235°36
2033	+0.51	+0.0133	0.95	235°38	+0.27	+0.0107	0.53	235°37	+0.21	+0.0063	0.42	235°36
2034	+0.71	+0.0112	0.90	235°40	+0.38	+0.0072	0.53	235°40	+0.29	+0.0010	0.44	235°37
2035	+0.91	+0.0094	0.95	235°43	+0.49	+0.0040	0.53	235°41	+0.38	−0.0039	0.39	235°35
2036					+0.60	+0.0013	0.52	235°41	+0.46	−0.0079	0.38	235°31
2037					+0.71	−0.0007	0.52	235°38	+0.54	−0.0111	0.40	235°26
2038					+0.82	−0.0021	0.50	235°34	+0.62	−0.0135	0.38	235°24
2039					+0.93	−0.0033	0.50	235°33	+0.70	−0.0158	0.36	235°30
2040									+0.78	−0.0192	0.38	235°56
2041									+0.87	−0.0229	0.41	236°73
2042									–	–	–	–

Year	Trails 4 revolutions old				Trails 5 revolutions old				Trails 6 revolutions old			
	Δa_0	$r_E - r_D$	f_M	Ω	Δa_0	$r_E - r_D$	f_M	Ω	Δa_0	$r_E - r_D$	f_M	Ω
1798	−0.09	+0.0044	0.38	232.15	−0.08	+0.0069	0.29	232.36	−0.03	−0.0039	0.11	232.49
1799	−0.02	+0.0015	0.24	232.80	−0.01	+0.0015	0.25	232.77	−0.01	−0.0001	0.10	232.80
1800	+0.01	+0.0066	0.13	233°32	+0.01	+0.0068	0.10	233°32	0.00	+0.0083	0.04	233°25

Table 1 – Data for dust trails (continued).

Year	Trails 4 revolutions old				Trails 5 revolutions old				Trails 6 revolutions old			
	Δa_0	$r_E - r_D$	f_M	Ω	Δa_0	$r_E - r_D$	f_M	Ω	Δa_0	$r_E - r_D$	f_M	Ω
1801	+0.03	+0.0114	0.10	233°47	+0.03	+0.0114	0.09	233°42	+0.01	+0.0144	0.04	233°24
1802	+0.06	+0.0139	0.15	233°72	+0.05	+0.0134	0.14	233°60	+0.02	+0.0174	0.10	233°21
1803	+0.08	+0.0218	0.09	234°45	+0.08	+0.0213	0.33	234°25	+0.04	+0.0252	0.08	233°56
1831	−0.07	+0.0035	0.34	232°50	−0.07	+0.0056	0.42	232°34	−0.07	+0.0091	0.08	232°47
1832	−0.01	+0.0012	0.20	233°10	−0.01	+0.0011	0.17	233°09	−0.01	+0.0010	0.16	233°07
1833	+0.02	+0.0010	–	233°47	–	–	–	–	–	–	–	–
1834	+0.05	+0.0013	0.12	233°69	+0.03	+0.0022	0.08	233°61	+0.02	+0.0023	0.07	233°56
1835	+0.08	+0.0013	0.13	233°90	+0.05	+0.0021	0.10	233°72	+0.04	+0.0018	0.10	233°63
1836	+0.11	+0.0022	0.12	234°50	+0.07	+0.0032	0.09	234°27	+0.06	+0.0029	0.09	234°17
1864	−0.09	+0.0178	0.37	233°93	–	–	–	–	−0.08	+0.0188	0.61	233°07
1865	–	–	–	–	–	–	–	–	–	–	–	–
1866	+0.06	−0.0004	0.37	233°33	+0.02	+0.0029	–	233°60	–	–	–	–
1867	+0.14	−0.0093	0.44	233°51	+0.05	−0.0019	0.12	233°93	+0.03	−0.0010	0.08	233°86
1868	+0.21	−0.0147	0.35	234°22	+0.07	−0.0037	0.12	234°73	+0.05	−0.0030	0.10	234°56
1869	+0.29	−0.0078	0.36	234°05	+0.10	+0.0058	0.13	234°80	+0.07	+0.0069	0.10	234°62
1897	−0.10	+0.0023	0.12	235°45	−0.09	+0.0039	0.17	235°54	−0.07	+0.0008	0.17	234°85
1898	−0.05	+0.0187	0.35	235°12	−0.05	+0.0201	0.36	235°17	−0.03	+0.0187	–	234°91
1899	+0.02	+0.0119	0.36	234°97	+0.02	+0.0110	0.34	234°98	+0.01	+0.0124	0.15	235°13
1900	+0.10	+0.0145	0.59	234°05	+0.10	+0.0112	0.35	234°11	+0.04	+0.0165	0.05	234°49
1901	+0.17	+0.0048	0.40	233°87	+0.18	−0.0017	0.49	234°11	+0.06	+0.0077	0.14	234°67
1902	+0.25	+0.0044	0.24	234°46	+0.24	+0.0062	0.44	234°69	+0.09	+0.0187	0.11	235°14
1930	−0.10	+0.0011	0.23	235°55	−0.08	+0.0018	0.18	235°70	−0.08	+0.0031	0.16	235°82
1931	−0.05	+0.0134	0.31	235°26	−0.05	+0.0143	0.13	235°40	−0.05	+0.0154	0.24	235°54
1932	+0.02	+0.0058	0.25	235°48	+0.02	+0.0054	0.23	235°52	+0.02	+0.0049	0.23	235°57
1933	+0.05	+0.0137	0.13	235°98	+0.05	+0.0132	0.12	235°96	+0.05	+0.0121	0.15	235°95
1934	+0.08	+0.0175	0.25	235°81	+0.08	+0.0158	0.23	235°69	+0.09	+0.0128	0.28	235°59
1935	+0.14	+0.0299	0.35	235°43	–	–	–	–	–	–	–	–
1961	−0.20	+0.0126	0.26	235°42	−0.14	+0.0124	0.12	235°90	−0.12	+0.0122	0.08	236°07
1962	−0.14	+0.0054	0.32	235°31	−0.12	+0.0064	0.20	235°59	–	–	–	–
1963	−0.09	+0.0111	0.19	235°48	−0.08	+0.0087	0.16	235°66	–	–	–	–
1964	−0.04	+0.0088	0.04	234°99	–	–	–	–	−0.04	+0.0128	0.27	235°30
1965	+0.03	+0.0018	0.21	235°57	+0.02	+0.0019	0.19	235°66	+0.02	+0.0016	0.04	235°71
1966	+0.06	+0.0051	0.11	236°00	+0.05	+0.0056	0.09	236°02	+0.04	+0.0053	0.08	236°03
1967	+0.08	+0.0082	0.11	236°10	+0.06	+0.0084	0.10	236°04	+0.06	+0.0075	0.14	235°98
1968	+0.11	+0.0096	0.16	236°30	–	–	–	–	–	–	–	–
1969	+0.13	+0.0157	0.11	237°00	+0.12	+0.0157	0.12	236°81	+0.13	+0.0135	0.17	236°60
1996	−0.10	+0.0215	0.33	235°15	−0.08	+0.0217	0.18	235°55	−0.07	+0.0195	0.14	235°78
1997	−0.03	+0.0107	0.40	235°14	−0.03	+0.0130	0.59	235°11	–	–	–	–
1998	+0.04	+0.0040	0.29	235°63	+0.03	+0.0044	0.18	235°79	+0.03	+0.0044	0.04	235°85
1999	+0.08	+0.0016	0.17	236°04	+0.06	+0.0034	0.10	236°13	+0.05	+0.0039	–	236°16
2000	+0.11	+0.0008	0.13	236°28	+0.07	+0.0028	0.09	236°23	+0.06	+0.0030	0.08	236°19
2001	+0.14	+0.0002	0.13	236°46	+0.09	+0.0017	0.11	236°29	+0.08	+0.0014	0.13	236°20
2002	+0.17	0.0000	0.15	236°89	+0.12	+0.0015	0.12	236°72	+0.11	+0.0014	0.13	236°67
2003	+0.20	+0.0031	0.10	237°62	+0.14	+0.0059	0.08	237°29	+0.12	+0.0062	0.08	237°12
2029	−0.11	+0.0144	0.49	236°02	−0.12	+0.0228	0.34	236°05	−0.09	+0.0204	0.19	236°53
2030	−0.04	+0.0242	0.38	236°21	–	–	–	–	−0.05	+0.0321	0.50	236°18
2031	+0.03	+0.0161	0.36	235°42	–	–	–	–	+0.03	+0.0150	–	235°84
2032	+0.11	+0.0086	0.36	235°36	+0.07	+0.0092	0.14	236°02	+0.05	+0.0107	0.10	236°15
2033	+0.18	+0.0016	0.35	235°39	+0.11	+0.0054	–	236°29	+0.07	+0.0072	0.09	236°29
2034	+0.25	−0.0054	0.36	235°43	+0.13	+0.0012	0.13	236°46	+0.09	+0.0028	0.10	236°33

Year	Trails 7 revolutions old				Trails 8 revolutions old			
	Δa_0	$r_E - r_D$	f_M	Ω	Δa_0	$r_E - r_D$	f_M	Ω
1832	0.00	+0.0004	0.06	233°09				
2000					+0.06	+0.0008	0.27	236°10
2001	+0.08	−0.0004	–	236°11				

3. Use of comet and dust node to predict peak time

Much of the uncertainty in predicting Leonid storms in the past has been due to the reliance on the comet's nodal longitude and distance, to predict activity. Based on the dust trail data in [6] and the observed times of maxima in [13], it has been shown [14] that the comet's orbit only gives a first approximation to predicting storms, but that the dust trails represent the time of maximum of a storm to within the uncertainty of the observed maximum (±8 minutes in the best observed cases).

It must be stated that the priority in these calculations belongs to Reznikov for the general technique and to Kondrat'eva, Murav'eva, and Reznikov [5] for application to the Leonids. However, the independent work by Asher [6] provided a resolution in nodal longitude of 0°.01 (about 15 minutes) as opposed to the $\sim 0°.1$ (2.4 hours) of [5]. It is this additional resolution in the nodal longitude that has allowed a critical check on past showers [14] and gives us reason to be confident in predicting the time of maximum of future Leonid storms. The results in [6] and in this paper confirm the times and distances of encounters given in [5] with only some minor differences. Between 100 and 200 years in the past, there appears to be a slight but systematic and unexplained difference in encounter distance ($r_E - r_D$) of between +0.0001 and +0.0002 AU ([5] relative to [6]). One date in [5] appears to be wrong: from [6], we find November 13.8 UT for 1802, whereas Kondrat'eva et al. [5] have November 13.2 UT, possibly duplicated in error from their line immediately above. The encounter distance for the 1866 trail in 2000 is misprinted in [5] and should be +0.00078 AU (Emel'yanenko, *private communication*), confirmed in Table 1.

The validity of a 5th decimal in r_D is questionable as a result of various unconsidered factors like ejection away from perihelion and solar radiation pressure. Preliminary simulations incorporating these suggest that the structure of the dust trail is not uniform. On these grounds, we believe the true center of the dust trail is slightly beyond r_D, but that the peak density is towards the inside of the trail (see Figure 1, later). For these reasons, the 5th decimal in r_D is only partly justifiable. Comparison of our values of $r_E - r_D$ and those in [5] also suggest the differences in this 5th decimal are partly random.

In Table 2, the observed and calculated nodes are given to 3 decimal places for the four showers with well-observed maxima. The simulations just mentioned suggest that the longitude is less sensitive to the unconsidered factors than r_D is, and, even if the accuracy is not quite 1 in the 3rd decimal, the very small residuals against the observed time of maximum given in [13] seem instructive. Even the worst of these well-defined maxima has an O−C of only 7 minutes! The maximum in 1833 is poorly defined and the large residual (45 minutes) may be unimportant.

McNaught [14] showed that, for years with maximum ZHR smaller than around 500, the time of maximum may be poorly defined using predictions based on distant dust trails. This is largely a result of the background dominating the activity curve. However, hidden within the activity, a peak due to the dust trails (the "storm peak") can sometimes be discerned. This was the case in 1965 and 1998 with a peak of faint meteors present close to the correct longitude, but of lower rates than the fireball shower. Several years from the comet's return, when the background rates of Leonids are sufficiently low, a close approach to a dust trail can produce a distinct, short-lived and well-predictable shower. This occurred in 1969 [13], when the observed peak reached a ZHR of 300, and differed in time by only 7 minutes from the calculated dust trail node.

4. Storms since 1833

Over the next four years, the Earth will closely encounter individual dust trails at various distances. To predict the circumstances, it is necessary to examine the past close approaches to such dust trails. Table 2 lists the circumstances of storms using the dust trail data from Table 1 and the observed ZHR from [13]. The ZHRs quoted in [13] are not fully corrected owing to the heterogeneous data and lack of information in many of the primary sources used, but the uniform analysis by Brown makes the data set as uniform as might ever be expected. The data for 1867 have been adjusted to correct for moonlight interference using the value suggested in [13].

Table 2 – Data for storms (excluding 1799 and 1832) and the well-defined 1969 outburst.

Year	Trail	Obs. node (J2000)	Calc. node (J2000)	O − C	Δa_0 (AU)	$r_E - r_D$ (AU)	f_M	ZHR
1966	2 rev	235°.160	235°.158	+0°.002	+0.17	−0.00014	0.52	90 000
1833	1 rev	233°.15	233°.184	−0°.03	+0.17	−0.00029	0.95	60 000
1866	4 rev	233°.337	233°.333	+0°.004	+0.06	−0.00036	0.37	8 000
1867	1 rev	233°.423	233°.420	+0°.003	+0.37	−0.00021	1.00	4 500
1969	1 rev	235°.277	235°.272	+0°.005	+0.93	−0.00005	0.95	300

Since 1833, specific attention has been paid to recording Leonid activity; so, looking for other years that had close approaches to dust trails would be a useful check on the validity of using the dust trails as the main predictor of high activity. The circumstances of encounter with trails up to 6 revolutions old and passing within 0.0010 AU of the Earth are given in Table 3.

Table 3 – All additional approaches to dust trails since 1833 that are within 0.0010 AU and up to 6 revolutions old.

Year	Trail	Obs. node (J2000)	Calc. node (J2000)	O − C	Δa_0 (AU)	$r_E - r_D$ (AU)	f_M	ZHR
1869	3 rev	233°.533*	233°.536	−0°.003*	+0.32	−0.00053	0.44	1 000
1897	6 rev		234°.852		−0.07	+0.00079	0.17	
1897	2 rev		234°.929		−0.18	+0.00075	0.43	
1968	1 rev	235°.65	235°.147	+0°.50	+0.73	+0.00095	0.95	~ 110

* Time assumed to be local and converted from longitude. See text.

Activity in 1869 could have been expected around November 14.02 UT from western Asia, eastern Europe, and the Middle East. This shower is mentioned by Kronk [15], and the author was contacted regarding the details. We are most indebted to Gary Kronk for his immediate reply giving the full text from his primary reference [16]. Mr. Meldrum and six other observers at Port Louis Observatory and other parts of the island of Mauritius in the Indian Ocean made a specific watch for Leonids on the nights of November 12-13, 13-14, and 14-15. It was on the morning of the November 13-14 night, just at the start of twilight that the peak was observed. Meldrum wrote the following:

> *"I have not had time to analyze the observations carefully, but the time of maximum intensity was about* 4^h09^m *a.m. The only source of doubt in this subject arises from the circumstance that after* 4^h15^m *daylight was setting in."*

Observations continued until 4^h40^m a.m. On the assumption that the time system used was local, as was the function of such observatories for the setting of ship's chronometers, we have corrected these times to UT using a longitude of $\lambda = 57°30'$ for Port Louis as given in the *Times Atlas of the World*. This is 3^h50^m ahead of UT, and the observed time of maximum converts to November 14, 0^h19^m UT. The calculated longitude for the responsible dust trail was $\lambda_\odot = 233°.536$ (J2000), which converts to November 14, 0^h24^m UT. As Meldrum notes that twilight could have affected the time of maximum, the influence through loss of meteors in the morning twilight would act to make the true maximum later than observed, if it had any influence at all. This could bring the observed and predicted times into even closer agreement. Nautical twilight is calculated to have started at 4^h20^m a.m., in accord with Meldrum's statement.

Meldrum quotes a number of watch durations and meteor counts from which an effective ZHR at maximum of close to 1000 seems to be a reasonable conclusion after making appropriate corrections for factors they mention. It is probable that the rates at maximum were double those half an hour earlier. A fuller account of this shower will be presented as a separate paper.

The two trails in 1897 represent meteoroids on orbits with smaller semi-major axis than 55P/Tempel-Tuttle, something that is known to be less common following ejection. Hasegawa [17] mentions strong activity as seen from Beijing Observatory on November 14–15, 1897, but the maxima predicted from the dust trails are November 15.50 and November 15.57. These would have been visible from western North America, but it would appear that nothing substantial was observed.

The trail in 1968 is of meteoroids with high ejection velocity, although of lower velocity than in the 1969 outburst. This trail and the two trails of 1897 are not approached closely. With values of Δa_0 somewhat outside the range of known storms no substantial activity would be expected. The 1-revolution trail in 1968 is evidently not what was observed at longitude $\lambda_\odot = 235°.65$.

5. A model of the relative spatial density

As noted in the Introduction, Leonid storms can result from two causes: close approaches to a single recent dust trail or an encounter with the dense resonant zone. As the storms of 1799 and 1832 were rich in fireballs and probably contain a component of such resonant meteoroids, they are excluded from this analysis. It is also clear from [5] that both these storms comprised encounters with multiple dust trails.

Here, making the assumption that all recent dust trails are created equal, an attempt is made to fit the dust trail parameters, Δa_0, $r_E - r_D$, and f_M, of the storms listed in Tables 2 and 3, to the observed ZHR. If this can be done, then storm ZHRs can be predicted.

All the observed storms had small negative values of $r_E - r_D$. This need have no special significance as there simply happen to be no values of $r_E - r_D$ between -0.0001 and $+0.0008$ since 1833. The values for 1799 and 1832 were -0.0005 and $+0.0005$, respectively, for the several dust trails given in [5] that are older than the ones we considered here. An attempt to fit the observed ZHRs for storms was made initially on the assumption that the density profile in $r_E - r_D$ is a Gaussian distribution centered on zero. The simulations mentioned earlier (Section 3) produce an elliptical cross section on intersection with the ecliptic, but with a concentration towards the inside of the ellipse (Figure 1). Thus, calculations were also made with the center of the dust trail at distances $r_D + 0.0001$ AU and $r_D + 0.0002$ AU, values that seem appropriate for the possible outward shift of the trail center.

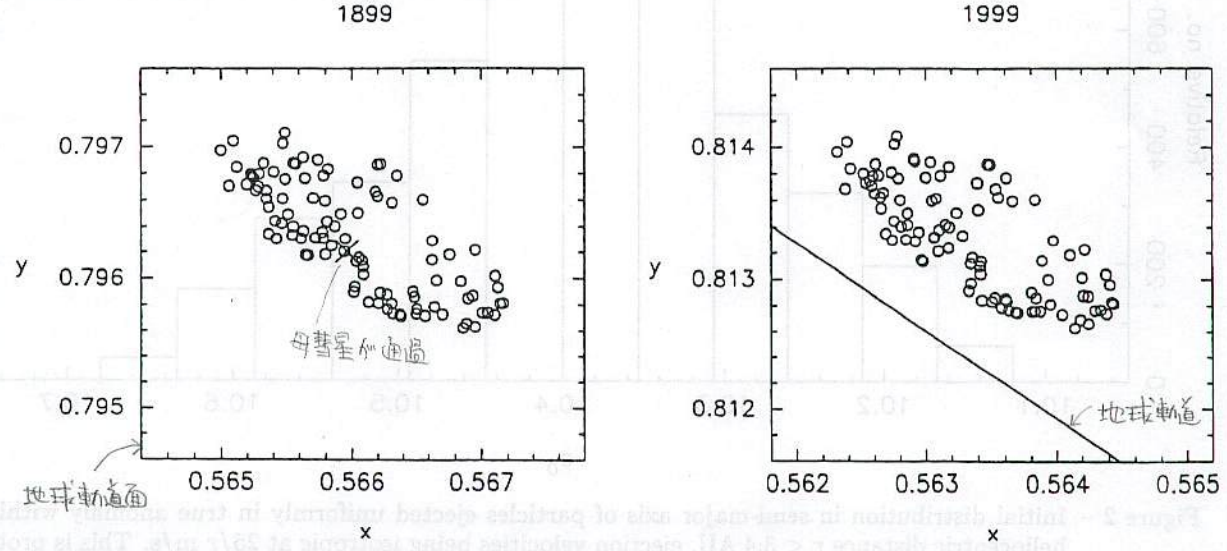

Figure 1 – Cross section in (x, y) ecliptic coordinates of trail generated in 1899, at epoch of ejection and at nodal crossing in 1999. Initial elements of particles were generated by assuming ejection uniform in true anomaly, isotropic, and at $25/r$ m/s (cf. Figure 2), but only particles with appropriate a_0 were integrated and plotted. In the 1899 plot, the cross is the comet's node (which is in a different part of the ecliptic and so not on the 1999 plot). The line on the 1999 plot is the Earth's orbit; slightly higher ejection speeds would bring orbits to Earth intersection.

MSS-093

To fit the observed ZHR to the dust trails, it is necessary to have a relationship defining the relative spatial density of the trails. In a given trail encounter, particles have a tightly constrained value of Δa_0 (Section 2). Therefore, trails' relative densities depend on the relative amount of material ejected on to orbits with different values of Δa_0 (Figure 2), with an effective value of Δa_0 of about +0.2, believed to be a good representation for the bulk of the meteoroids in the stream that are of a size that produce visual meteors. Lower and higher values of Δa_0 will be represented by lower spatial densities and also by a variation in mass. Higher mass meteoroids will tend to be at values of Δa_0 closer to zero.

The initial density is diluted by the stretching of the trail as it evolves. The contribution of this stretching factor to the density can be derived from integrations. Unlike the $r_E - r_D$ and Δa_0 factors, it is not dependent on the ejection model, and no parameters need fitting. To calculate the stretch of a particular trail, a few particles were ejected at perihelion with orbits identical except for increments in e of 0.000 001, all of which crossed the ecliptic very close to the correct time in November in the relevant year (Earth encounter occurring if $|r_E - r_D|$ is small). The average difference in mean anomaly M between these particles at the time of encounter gives an indication of the linear stretching, and we introduce a "mean anomaly factor" f_M (Table 1) which decreases as the stretch increases.

Examination of Figure 1 indicates that, to a high degree of accuracy, the dispersion in the other elements does not increase from that at formation during the early evolution of dust trails. It would appear, therefore, that the spatial density decreases linearly with the stretch in M. Thus the variable that is fitted is ZHR/f_M, where f_M normalizes the data to the median stretch value of a 1-revolution trail. No account of dispersion of particles with size due to radiation pressure is considered although it undoubtedly occurs and has the effect of a small outward shift of the center. This would indicate that the mass index will be higher for encounters at positive $r_E - r_D$.

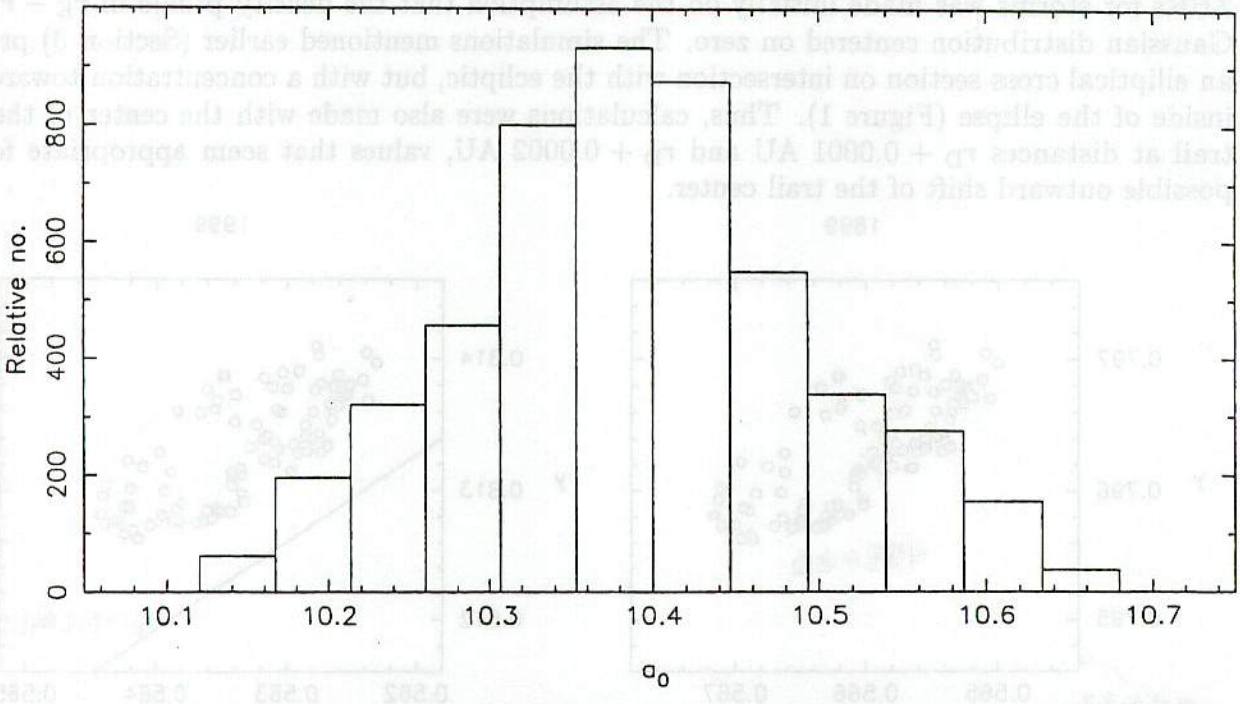

Figure 2 – Initial distribution in semi-major axis of particles ejected uniformly in true anomaly within heliocentric distance $r < 3.4$ AU, ejection velocities being isotropic at $25/r$ m/s. This is probably a reasonable ejection model (see [18]) but there are still free parameters. For example, lower ejection velocities would narrow the distribution. The distribution is centered on the comet's a_0. Particles affected by radiation pressure having the same a_0 as the comet will fall behind the comet, i.e., their *effective* value of a_0 will be greater. This shifts the distribution to the right, but the shift depends on the radiation pressure parameter, which varies among meteoroids. However, to keep our model manageable, it appears acceptable to use a Gaussian distribution, with mean and dispersion to be fitted.

The fit to the data was by a two dimensional Gaussian profile to Δa_0 and $r_E - r_D$. With the observed ZHR being only proportionately correct, a least-squares fit to the fractional residuals was made. This put the maximum in Δa_0 at +0.16 to +0.17 for radial profiles with the center assumed to be in the range r_D to $r_D + 0.0002$ AU. These fits are good for most of the storm data (mean fractional error 10–15%). These data and the observed ZHRs (normalized to 1 revolution) are plotted in Figure 3. It is clear that there is both a paucity of data and a paucity of potential data from past encounters to help refine the fit. The center of the Gaussian can be fitted to a center as small as $r_D - 0.0002$ AU, but with errors of around 25%. Larger values of $r_E - r_D$ are fitted with decreasing errors, but then an anomaly arises that a major storm should have occurred over western Europe in 1801, when at present no activity is known. This is discussed later (Section 7).

The parameters of the fit are given in Table 4. The peak ZHR is the rate that would be encountered by passage through the center of a 1-revolution old dust trail. This potential peak value has to be reduced by the f_M for a specific dust trail.

Table 4 also displays the drop off in rates over the radius of the Earth (0.000043 AU) on the flanks of the profile of a 1-revolution trail. This has significance in the global analysis of meteor rates. The effect is modified by f_M for older trails, and would have to be calculated individually for every storm. With the indication that parts at least of dust trails retain their shape over many revolutions (at least in the case of the Leonid trail cross section simulation mentioned here), this effect will have to be considered for a short outburst from any shower. The center and shape of the profile would have to be known for the specific correction factor to be calculated.

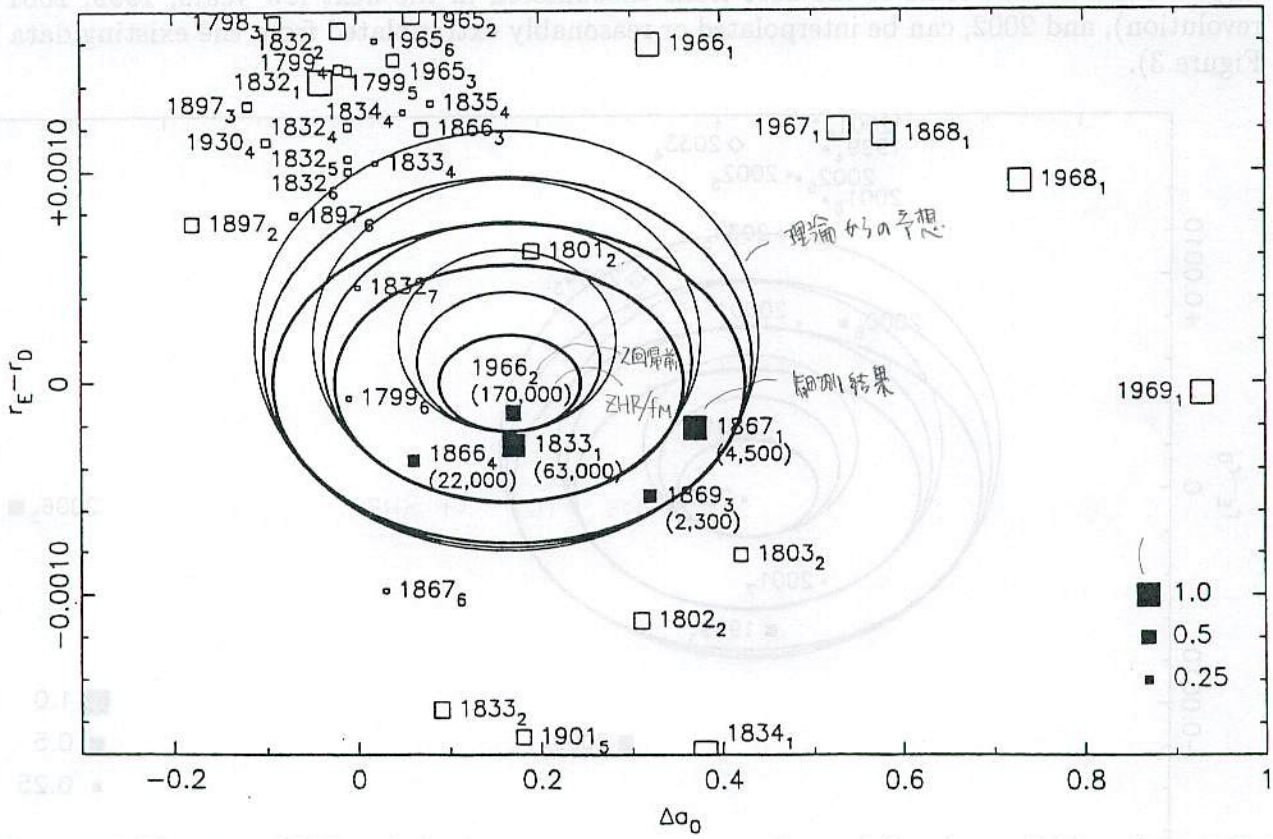

Figure 3 – Variation of ZHR with the three parameters, $r_E - r_D$, Δa_0, and f_M, given in Table 1. As the effect of f_M on the ZHR is calculable from integrations, ZHR/f_M is fitted to $r_E - r_D$ and Δa_0. The five solid squares are the points (Tables 2 and 3) used to derive the fit (observed ZHR/f_M in parentheses), and the elliptical contours represent the fit itself. Three fits have been done, successively assumed to be centered on r_D, $r_D + 0.0001$ AU, and $r_D + 0.0002$ AU, shown as lines of decreasing thickness. In each case the inner, middle, and outer contours correspond respectively to values of ZHR/f_M of 10^5, 10^4, and 10^3. Larger squares are drawn for larger values of f_M, the size of square being illustrated for values of f_M of 1.0, 0.5, and 0.25. Multiplying the fitted ZHR/f_M by f_M gives the estimated ZHR.

Δa_0 が 0.2 近くが多い

Table 4 – Characteristics and consequences of the fit. Fit 0 is centered radially on r_D, Fit 1 on r_D + 0.0001 AU, and Fit 2 on $r_D + 0.0002$ AU.

Fit no.	Mean fractional error, %	Peak ZHR	Δa_0	FWHM Δa_0	FWHM r	Percentage drop over 1 Earth radius at distance from trail center, AU			
						0.0002	0.0004	0.0006	0.0008
0	14	160 000	+0.17	0.19	0.00056	13%	25%	35%	45%
1	11	210 000	+0.16	0.19	0.00062	10%	21%	30%	37%
2	10	290 000	+0.16	0.19	0.00064	8%	17%	25%	32%

Extrapolation of the double Gaussian storm profile predicts a ZHR of zero for the 1-revolution trail encountered in 1969, when, as mentioned, the observed peak ZHR was 300. This is hardly surprising, with the sparse and unreliable data used in the fit, and the likelihood that a Gaussian is not a good representation of the spread in Δa_0 this far from the dense storm region. The wings of the Gaussian profiles represented in [13] in every case show activity enhanced above the profile. Whilst the storm peak seems well presented, it appears necessary to use another profile for the overall structure of the dust trail. One such attempt has been made by Jenniskens [19].

6. Predicting time and ZHR of maximum

Encounters at the current epoch

Figure 4 shows that some of the dust trails encountered in the next few years, 1999, 2001 (7-revolution), and 2002, can be interpolated or reasonably extrapolated from the existing data (cf. Figure 3).

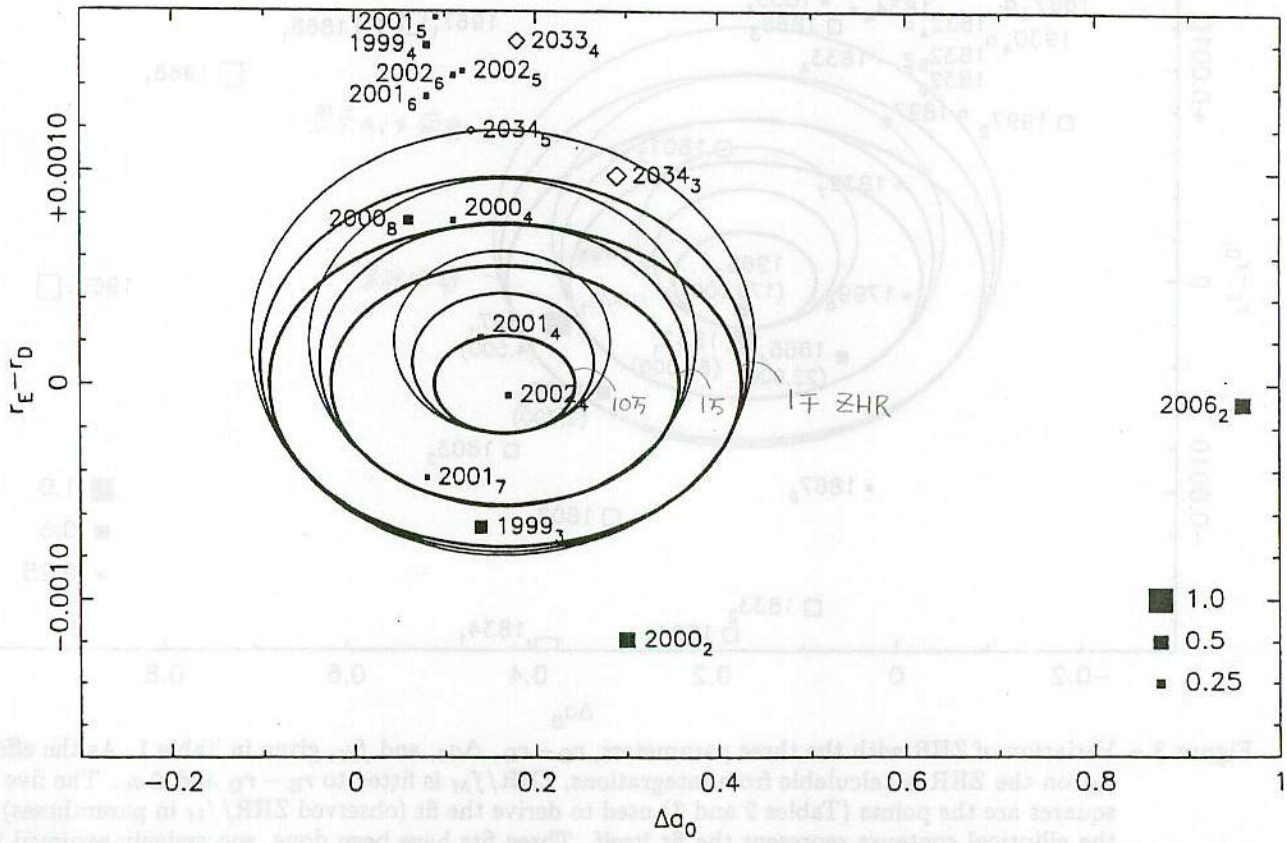

Figure 4 – Values of $r_E - r_D$, Δa_0, and f_M (Table 1) for future trails plotted against the fitted contours of Figure 3. The estimated value of ZHR/f_M is shown by a point's position relative to the contours (see caption to Figure 3), and this should be multiplied by f_M (shown by size of square as in Figure 3) to yield the ZHR.

It is also clear that several trails will be encountered in the previously unobserved zone, 2000 and 2001 (4-revolution). The trails in 2000 probably lie beyond the uncertain peak and on the steep descending profile, making any rate prediction for these years rather uncertain. As previously mentioned, the effect of radiation pressure may increase the number of smaller meteoroids encountered in these years.

The data from each year will allow the fit to be recalculated, or a better model developed. It is possible that before the potential storms of 2001 and 2002 the predictions could be very well defined.

Based on the dust trail parameters in Table 5, predictions for the next few years are given in Table 6. As the trails encountered in 1999 and 2000 (8-revolution) were responsible for the 1966 and 1866 storms, respectively, we should be confident that the cores of these streams are dense. Trails that have never previously been encountered are assumed to be similar to other trails and for our simple analysis all are necessarily assumed equal. Encounters with the same trails at different values of Δa_0 will allow the structure and evolution of specific dust trails to be investigated.

Table 5 – Circumstances of dust trail encounters for the current epoch. The last column indicates previous encounters with the same dust trail.

Year	Trail	Δa_0	$\tau_E - \tau_D$	f_M	Previous encounters
1999	3 rev	+0.14	−0.00066	0.38	1966 storm
2000	8 rev	+0.06	+0.00077	~ 0.27	1866 storm
2000	4 rev	+0.11	+0.00077	0.13	none
2001	7 rev	+0.08	−0.00043	~ 0.14	1869 storm, 1893*
2001	4 rev	+0.14	+0.00022	0.13	none
2002	4 rev	+0.17	−0.00005	0.15	none
2006	2 rev	+0.96	−0.00009	0.53	1969

* Mentioned in [5] ($\Delta a_0 = -0.10$, $\tau_E - \tau_D = -0.00019$).
Outside range of years considered as potentially storm-producing.

Table 6 – Predictions for the current return of 55P/Tempel-Tuttle.

Time (UT)	Estimated ZHR	Trail	Moon age	Visible from
1999, Nov 18.089 (02^h08^m)	1500	3 rev	10	Europe, Middle East, Africa
2000, Nov 18.156 (03^h44^m)	100–5000?	8 rev	22	Europe, Africa
2000, Nov 18.327 (07^h51^m)	100–5000	4 rev	22	E. USA, E. Canada, Atlantic
2001, Nov 18.417 (10^h01^m)	2500?	7 rev	3	Americas
2001, Nov 18.763 (18^h19^m)	10000–35000	4 rev	3	E. Asia, W. Pacific, Australia
2002, Nov 19.442 (10^h36^m)	25000	4 rev	15	Americas
2006, Nov 19.198 (04^h45^m)	150	2 rev	28	W. Europe, W. Africa

The 8-revolution trail in 2000 has nearby sections both in front and behind that have been disrupted owing to close approaches to Earth between 1733 and the present, albeit the section with the critical mean anomaly for intersection with the Earth should just survive. For the 7-revolution trail in 2001, f_M is quite rapidly varying at the critical M. The derived ZHRs for these two trails are therefore denoted with a question mark in Table 6. No other close encounters to dust trails 6 or less revolutions old occur prior to 1999 in the current return of 55P, consistent with observations. Kondrat'eva et al. [5] do mention an 8-revolution trail on 1991 Nov 20.2 UT at $\Delta a_0 = -0.16$ and $\tau_E - \tau_D = -0.00041$. We would expect activity from this to have been low, but probably detectable.

The time of maximum is derived from the nodal longitude of the dust trails. The uncertainty of these predictions is probably better than 10 minutes (see Tables 2 and 3 and reference [14]).

MSS-093

1999に出ても2000～2002の予報にならない。ストリームが違う。
2000が出ると2001～2002も出る可能性が高い。

ZHR predictions may be "reliable" (within a factor of 2?) for 1999 and 2002. It is in the region of Figure 3 at positive $r_E - r_D$ that the data are extrapolated with the largest uncertainty. This includes the 4- and 8-revolution trails in 2000 and the same 4-revolution trail in 2001.

Observations in 1999 may not affect the predictions for following years, due to the constraining effect of the steeply rising profile fitted through the storm data. However, the observations of the trails in 2000 should dramatically lower the uncertainty for future years. One especially interesting feature is that the same (4-revolution) trail will be encountered in 2000, 2001, and 2002. Following observation in 2000, predictions for this trail in 2001 and 2002 should be especially well-defined. The assumption that all trails are created equal is certainly the case here, although the mass distribution will probably change over the three years and will be an important observational result.

In 2006, the Earth encounters an adjoining section of the same dust trail that produced the 1969 outburst. The circumstances in these two years are almost identical, but the stretch in M is double in 2006, giving a prediction of half the ZHR of 1969. This prediction is unrelated to the profile fitted to the storm data.

The Last-Quarter Moon will reduce the observed rates in 2000 and the near-Full Moon will be a bigger problem in 2002. The highest observable rates at this epoch may be in 2001, despite the uncertain rates, as no moonlight will be present.

Encounters around the 2031 return

It has long been assumed that no significant activity could occur around the next perihelion passage of 55P/Tempel-Tuttle. However, this conclusion was based on the use of the comet's orbit alone. The data in Table 7 are for three outlying trails approached in 2033 and 2034. These are plotted in Figure 4. Unfortunately, they are probably too distant for any reasonable chance of high activity, but, again, the region is one of very uncertain extrapolation. Predictions based on this data appear in Table 8. The substantial data that can be gathered between 1999 and 2006, with seven close approaches to dust trails during that period, should allow a realistic assessment of activity to be made before this next return. In particular, the possibility of a storm in 2034 will likely be decided by the strength of activity in 2000. The prediction of zero ZHR is from an unreasonable extrapolation of the model, and it refers only to that particular dust trail and not the shower that year as a whole. Some activity from such a dust trail will probably occur, but strong activity is highly improbable. Background activity will still be present, but this will also be rather uncertain in the changed circumstances.

Table 7 – Circumstances of dust trail encounters for next return of 55P/Tempel-Tuttle. The last column indicates previous encounters with the same dust trail.

Year	Trail	Δa_0	$r_E - r_D$	f_M	Previous encounters
2033	4 rev	+0.18	+0.00161	0.35	1966 storm, 1999
2034	3 rev	+0.29	+0.00098	0.44	1969, 2006
2034	5 rev	+0.13	+0.00119	0.13	2000, 2001, 2002

Table 8 – Predictions for the next return of 55P/Tempel-Tuttle.

Time (UT)	Estimated ZHR	Trail	Moon age	Visible from
2033, Nov 17.904 (21^h42^m)	0	4 rev	26	E. Asia, W. Pacific, W. Australia
2034, Nov 18.139 (03^h20^m)	0–1000	3 rev	7	Europe, Africa
2034, Nov 19.222 (05^h19^m)	0–100	5 rev	8	W. Europe, W. Africa

MSS-093

7. Historical studies

The form of this analysis could profitably be carried back to examine the dust trail characteristics of Leonid storms throughout history. This would provide more data on the parameters relevant to storm production and give information on dust trail evolution. In fact, such data could locate the position of the center of the dust trail. They could also be used to check the dates ascribed to storms from historical references. Some apparent discrepancies between dates of storms as reported in different parts of the world could conceivably be the result of multiple storms separated by a day or more.

The circumstances of approaches to Leonid dust trails within 0.005 AU in the last 200 years and up to the year 2039 are given in Table 9. This lists the encounters in chronological order giving the nodal crossing time, revolution number, and the ZHR derived from the fits to the storm data using three assumed center positions. As previously mentioned, a value of zero does not indicate the Leonid ZHR was zero in that year, but only that the contribution of that specific dust trail to the overall ZHR was zero. It has also been noted that this extrapolation to well outside the storm region is unwarranted.

Table 9 – Predictions of time of nodal crossing and ZHR for individual dust trails up to 6 revolutions old (and selected older ones) passing within 0.0050 AU of the Earth. The three ZHR predictions are for the highest density in the dust trail assumed to be centered at r_D (ZHR_0), r_D + 0.0001 AU (ZHR_1), and r_D + 0.0002 AU (ZHR_2). The factor f_M represents the extent of dispersion of the trail relative to the median density of a 1-revolution trail and has been used in the calculation of the ZHRs. The symbol "*" refers to trail encounters used in the ZHR fit (Section 5).

Date (UT)	Trail	f_M	ZHR_0	ZHR_1	ZHR_2	Moon age
1798, Nov 11.431 (10^h20^m)	3	0.41	0	0	0	3
1798, Nov 11.431 (10^h20^m)	4	0.38	0	0	0	3
1798, Nov 11.772 (18^h32^m)	6	0.11	0	0	0	4
1798, Nov 12.317 (07^h36^m)	1	1.08	0	0	0	4
1799, Nov 12.306 (07^h21^m)	5	0.25	0	0	1	15
1799, Nov 12.339 (08^h08^m)	6	0.10	1 500	2 000	2 000	15
1799, Nov 12.336 (08^h04^m)	4	0.24	0	0	0	15
1799, Nov 12.377 (09^h02^m)	3	0.27	0	0	0	15
1799, Nov 12.567 (13^h37^m)	2	0.52	0	0	0	15
1799, Nov 12.575 (13^h48^m)	1	1.00	0	0	0	15
1800, Nov 12.823 (19^h45^m)	1	1.00	0	0	0	25
1800, Nov 12.856 (20^h33^m)	2	0.52	0	0	0	25
1801, Nov 13.065 (01^h34^m)	1	0.95	0	0	0	7
1801, Nov 13.211 (05^h04^m)	2	0.53	2 500	15 000	50 000	7
1802, Nov 13.344 (08^h15^m)	1	0.95	0	0	0	18
1802, Nov 13.795 (19^h04^m)	2	0.55	0	1	1	18
1803, Nov 13.737 (17^h41^m)	1	0.95	0	0	0	29
1803, Nov 14.995 (23^h53^m)	2	0.43	2	2	3	0
1831, Nov 13.244 (05^h52^m)	4	0.34	0	0	0	9
1831, Nov 13.897 (21^h31^m)	1	1.00	0	0	0	9
1832, Nov 13.076 (01^h50^m)	6	0.16	0	10	100	20
1832, Nov 13.088 (02^h07^m)	5	0.17	0	6	80	20
1832, Nov 13.091 (02^h11^m)	7	0.06	200	800	2 000	20
1832, Nov 13.103 (02^h28^m)	4	0.20	0	1	20	20
1832, Nov 13.176 (04^h14^m)	2	0.55	0	0	0	20
1832, Nov 13.175 (04^h13^m)	1	1.00	0	0	3	20
1832, Nov 13.174 (04^h11^m)	3	0.39	0	0	0	20
1833, Nov 13.429 (10^h17^m)	2	0.53	0	0	0	2
*1833, Nov 13.435 (10^h26^m)	1	0.95	70 000	70 000	70 000	2
1833, Nov 13.455 (10^h56^m)	3	0.45	0	0	0	2

Table 9 – Predictions of time of nodal crossing and ZHR (continued).

Date (UT)	Trail	f_M	ZHR_0	ZHR_1	ZHR_2	Moon age
1834, Nov 13.681 (16^h20^m)	2	0.52	0	0	0	12
1834, Nov 13.692 (16^h37^m)	1	0.95	0	0	0	12
1834, Nov 14.070 (01^h40^m)	6	0.07	0	0	0	13
1834, Nov 14.112 (02^h42^m)	5	0.08	0	0	0	13
1834, Nov 14.192 (04^h36^m)	4	0.12	0	1	15	13
1835, Nov 13.948 (22^h44^m)	1	0.95	0	0	0	23
1835, Nov 14.396 (09^h30^m)	6	0.10	0	0	0	23
1835, Nov 14.487 (11^h42^m)	5	0.10	0	0	0	23
1835, Nov 14.667 (16^h00^m)	4	0.13	0	0	15	24
1836, Nov 13.202 (04^h51^m)	1	0.95	0	0	0	4
1836, Nov 14.181 (04^h20^m)	6	0.09	0	0	0	5
1836, Nov 14.281 (06^h45^m)	5	0.09	0	0	0	5
1836, Nov 14.507 (12^h10^m)	4	0.12	0	0	0	5
1866, Nov 14.017 (00^h24^m)	1	1.00	0	0	0	7
1866, Nov 14.022 (00^h31^m)	3	0.40	0	9	200	7
1866, Nov 14.024 (00^h34^m)	2	0.55	0	0	0	7
*1866, Nov 14.046 (01^h06^m)	4	0.37	8 000	8 000	8 000	7
*1867, Nov 14.392 (09^h25^m)	1	1.00	4 500	4 500	4 500	18
1867, Nov 14.401 (09^h38^m)	2	0.55	0	0	0	18
1867, Nov 14.829 (19^h54^m)	6	0.08	1	1	2	18
1867, Nov 14.896 (21^h30^m)	5	0.12	0	0	0	18
1868, Nov 14.252 (06^h02^m)	2	0.54	0	0	0	29
1868, Nov 14.281 (06^h45^m)	1	0.95	0	0	0	29
1868, Nov 14.777 (18^h39^m)	6	0.10	0	0	0	30
1868, Nov 14.940 (22^h33^m)	5	0.12	0	0	0	30
*1869, Nov 14.016 (00^h24^m)	3	0.44	900	900	1 000	10
1897, Nov 14.890 (21^h22^m)	1	1.00	0	0	0	20
1897, Nov 15.498 (11^h57^m)	6	0.17	2	20	100	20
1897, Nov 15.574 (13^h47^m)	2	0.45	0	1	4	21
1897, Nov 15.907 (21^h46^m)	3	0.25	0	0	0	21
1897, Nov 16.086 (02^h04^m)	4	0.12	0	0	0	21
1897, Nov 16.184 (04^h25^m)	5	0.17	0	0	0	21
1901, Nov 15.557 (13^h21^m)	4	0.40	0	0	0	4
1901, Nov 15.790 (18^h57^m)	5	0.49	0	0	0	4
1902, Nov 15.971 (23^h18^m)	3	0.45	0	0	0	16
1902, Nov 16.391 (09^h23^m)	4	0.24	0	0	0	16
1930, Nov 17.497 (11^h56^m)	3	0.32	0	0	0	27
1930, Nov 17.657 (15^h46^m)	4	0.23	0	0	2	27
1930, Nov 17.804 (19^h18^m)	5	0.18	0	0	0	27
1930, Nov 17.917 (22^h01^m)	6	0.16	0	0	0	27
1932, Nov 17.189 (04^h33^m)	6	0.23	0	0	0	19
1934, Nov 17.628 (15^h04^m)	1	0.95	0	0	0	10
1964, Nov 16.946 (22^h43^m)	2	0.53	0	0	0	13
1964, Nov 16.944 (22^h40^m)	1	1.00	0	0	0	13
1965, Nov 17.219 (05^h16^m)	2	0.59	0	0	0	24
1965, Nov 17.215 (05^h10^m)	1	1.00	0	0	0	24
1965, Nov 17.527 (12^h40^m)	3	0.37	0	0	1	24
1965, Nov 17.653 (15^h41^m)	4	0.21	0	0	0	24
1965, Nov 17.739 (17^h44^m)	5	0.19	0	0	0	24
1965, Nov 17.786 (18^h52^m)	6	0.04	0	0	0	24
1966, Nov 17.467 (11^h12^m)	1	0.95	0	0	1	5
*1966, Nov 17.495 (11^h53^m)	2	0.52	70 000	75 000	75 000	5
1966, Nov 18.270 (06^h28^m)	3	0.19	0	0	0	6

Table 9 – Predictions of time of nodal crossing and ZHR (continued).

Date (UT)	Trail	f_M	ZHR_0	ZHR_1	ZHR_2	Moon age
1967, Nov 17.721 (17^h18^m)	1	0.95	0	0	0	16
1968, Nov 17.000 (23^h59^m)	1	0.95	0	0	0	26
1968, Nov 17.293 (07^h02^m)	2	0.55	0	0	0	26
1969, Nov 17.374 (08^h58^m)	1	0.95	0	0	0	7
1998, Nov 18.168 (04^h02^m)	4	0.29	0	0	0	29
1998, Nov 18.329 (07^h54^m)	5	0.18	0	0	0	29
1998, Nov 18.392 (09^h24^m)	6	0.04	0	0	0	29
1999, Nov 18.072 (01^h44^m)	2	0.53	0	0	0	10
1999, Nov 18.078 (01^h53^m)	1	0.95	0	0	0	10
1999, Nov 18.089 (02^h08^m)	3	0.38	1 200	1 400	1 500	10
1999, Nov 18.830 (19^h55^m)	4	0.17	0	0	0	11
1999, Nov 18.916 (21^h59^m)	5	0.10	0	0	0	11
2000, Nov 17.329 (07^h53^m)	2	0.55	0	0	1	21
2000, Nov 17.348 (08^h22^m)	1	0.95	0	0	0	21
2000, Nov 18.156 (03^h44^m)	8	0.27	90	1 000	5 000	22
2000, Nov 18.244 (05^h51^m)	6	0.08	0	0	0	22
2000, Nov 18.280 (06^h44^m)	5	0.09	0	0	0	22
2000, Nov 18.327 (07^h51^m)	4	0.13	80	1000	5 000	22
2001, Nov 17.559 (13^h24^m)	2	0.52	0	0	0	2
2001, Nov 17.595 (14^h17^m)	1	0.95	0	0	0	2
[1] 2001, Nov 18.417 (10^h01^m)	7	0.14	2 500	2 500	2 500	3
2001, Nov 18.505 (12^h08^m)	6	0.13	0	0	10	3
2001, Nov 18.595 (14^h18^m)	5	0.11	0	0	0	3
2001, Nov 18.763 (18^h19^m)	4	0.13	13 000	25 000	35 000	3
2002, Nov 17.842 (20^h13^m)	1	0.95	0	0	0	13
2002, Nov 19.225 (05^h24^m)	6	0.13	0	0	4	14
2002, Nov 19.274 (06^h35^m)	5	0.12	0	0	3	14
2002, Nov 19.442 (10^h36^m)	4	0.15	25 000	25 000	30 000	15
2003, Nov 18.100 (02^h23^m)	1	0.90	0	0	0	24
2003, Nov 20.425 (10^h11^m)	4	0.10	0	0	0	26
[2] 2006, Nov 19.198 (04^h45^m)	2	0.53	150	150	150	28
2025, Nov 19.582 (13^h58^m)	3	0.10	0	0	0	29
2033, Nov 17.904 (21^h42^m)	4	0.35	0	0	1	26
2034, Nov 18.139 (03^h20^m)	3	0.44	4	130	1 200	7
2034, Nov 19.094 (02^h15^m)	6	0.10	0	0	0	8
2034, Nov 19.222 (05^h19^m)	5	0.13	0	6	120	8
2035, Nov 18.379 (09^h06^m)	3	0.39	0	0	0	18
2035, Nov 18.447 (10^h43^m)	2	0.53	0	0	0	18
2036, Nov 17.691 (16^h35^m)	2	0.52	0	0	0	29
2037, Nov 17.918 (22^h01^m)	2	0.52	0	0	0	10
2038, Nov 18.143 (03^h26^m)	2	0.50	0	0	0	21
2039, Nov 18.382 (09^h10^m)	2	0.50	0	0	0	2

[1] The 7-revolution trail in 2001 has a slightly uncertain value of f_M causing the predictions for that year to be additionally uncertain.

[2] In 2006, the formal prediction based on the Gaussian fit to Δa_0 predicts a ZHR of 0 as in 1969. However, the circumstances are almost identical as in 1969 and the encounter is with the same trail. The ZHR given is from the *observed* 1969 ZHR corrected by f_M.

Most years of substantial activity in Table 9 correspond to known showers. One year does stand out, though. Some activity should have occurred in 1801 from a 2-revolution trail with low stretch in M. This is of particular interest as the circumstances are similar to both trails in 2000. The $r_E - r_D$ of +0.0006 is an intermediate value missing from the encounters since 1833 when more attention has been paid to Leonid activity. A strong shower or minor storm could have occurred as seen from western Europe or western Africa on November 13.21 UT in 1801.

An initial examination by Mark Bailey and John McFarland of the observing log of Armagh Observatory indicates that observations were in progress that night, but no mention was made of meteor activity. Examination of other records in western Europe and western Africa for that date would be useful. Reports that can put constraints on the meteor activity at that time will have a substantial bearing on what to expect over the next several years. It would seem unlikely that a major storm was overlooked in a moonless sky, and this does tend to rule out Fit 2 and possibly even Fit 1. This would unfortunately mean that activity in the next several years would be at the lower end of the predictions.

8. Threat to satellites

Should the Earth pass through the center of a 1-revolution trail at $\Delta a_0 \approx +0.17$, the predicted peak ZHR would likely be in the range 150 000–300 000. The higher rates would be predicted if the maximum density were located beyond our calculated value of r_D. Whilst the Earth is 8.6×10^{-5} AU in diameter, and presents a small target (nominally, "collision" if $|r_E - r_D| < 4.3 \times 10^{-5}$ AU), the region inhabited by satellites is very much larger. Geostationary (GEO) satellites can pass through this dense zone of meteoroids when $|r_E - r_D| < 2.7 \times 10^{-4}$ AU. This will occur in 2001 and 2002, when the same 4-revolution trail is encountered.

The maximum density in the center of these trails is likely to have an equivalent ZHR of 20 000–40 000. These estimates are much lower than what was actually encountered in 1966 (about 90 000), although the effective rates in parts of the GEO region in that year could have been some 50% higher still. The risk to an individual satellite is probably much lower than in 1966, when no satellites were damaged, but GEO and low-Earth orbit (LEO) space is now much more crowded with active satellites.

In 2001, the densest part of the dust trail at the time of encounter is almost certainly near the GEO satellite belt over the Far-Eastern Pacific. GEOs over the Indian Ocean and Indonesia will be least affected. Should the densest part of the dust trail be beyond r_D, GEO satellites at intermediate longitudes will be most affected.

The most threatened GEO satellites in 2002 are on the leading (South-American) and trailing (Indonesian) longitudes of the Earth. If the densest part of the trail is further out than r_D, this will affect GEO satellites closer to the central Pacific. This potential "direct hit" of a dust trail with the Earth in 2002 will result in LEO satellites being directly threatened.

Given that we may be able to predict the time of Leonid maximum activity to a few minutes accuracy, and that the direction and distance of the closest approach to the dust trail are known (to a somewhat lesser accuracy), there are two strategies that satellite operators could use to minimize the threat. These are only available to satellites other than GEOs. The first is to position the satellite in its orbit furthest from the dust trail at the time of maximum. This position would be at the satellite's maximum distance towards or away from the Sun, the Leonid dust stream at its node being nearly perpendicular to the direction of the Sun. For a circular orbit, this point would be the longitude given in Table 10 for a trail that passes inside the Earth's orbit (2000, 4-revolution and 8-revolution, and 2001, 4-revolution), but would be 180° opposite (and latitude negated) for trails that pass outside the Earth's orbit (1999 and 2001, 7-revolution). If the peak flux in 2001 and 2002 is encountered on one side of the GEO belt (either towards or away from the Sun), the other side may only experience about 10% of that flux.

GEO satellites (0° inclination) will lie some 14 000 km below the ecliptic at the longitude opposite the Sun. They will experience the peak some 25 minutes earlier than the times given; so the longitude would be modified by +6°. GEO satellites towards the Sun have maximum 25 minutes later centered at a longitude $\lambda = +174°$ from that given.

The instant of maximum appears to be predictable with around 10 minutes uncertainty or better.

Encounters with multiple trails in a single year can be separated by several hours or days. Rate analysis would require separate profiles fitted to each trail. If the time of maximum is confirmed to be very close to the prediction of when single dust trails are encountered, then, for years with multiple encounters, use of the predicted time of maximum for each trail could help fit overlapping profiles. The general background activity would require an additional profile to be fitted as the activity from the dust trails exists within the population of older Leonid meteoroids that have an indistinct or disrupted trail structure. The spatial density in radius vector can drop off by up to 40% over the radius of the Earth whilst rates are still high. This has implications for global analyses of observations. At the instant of maximum, the greatest separation in radial distance is between the point on the Earth's surface at latitude $\varphi = 19°$ N with the radiant rising, and all points with the radiant in the sky at around morning twilight. If the trail passes inside the Earth's orbit, the gradient in the profile results in the morning twilight region of the Earth having an enhanced incident flux over regions further into darkness at that same moment.

With the intensity contours plotted in Figure 3 being based on ZHRs derived from visual observations, they are directly comparable with the activity curve observed in a single shower. The observed stream duration in any year, when measured at a suitable intensity level, allows the ellipticity of the dust trail cross-section to be derived. This will be presented in a separate paper.

References

[1] Ľ. Kresák, *Astron. Astrophys.* 279, 1993, pp. 646–660.

[2] A. Berberich, *Astron. Nachr.* 147, 1898, pp. 359–360.

[3] G.H. Stoney, A.M.W. Downing, *Proc. R. Soc. London, Ser. A* 64, 1899, pp. 403–409.

[4] C.P. Olivier, "Meteors", Williams amd Wilkins, Baltimore, 1925.

[5] E.D. Kondrat'eva, I.N. Murav'eva, E.D. Reznikov, *Solar System Research* 31, 1997, pp. 489–492.

[6] D.J. Asher, "The Leonid meteor storms of 1833 and 1966", *MNRAS*, 1999, *in press*.

[7] V.V. Emel'yanenko, M.E. Bailey, in *ASP Conf. Ser.* 104, *Physics, Chemistry and Dynamics of Interplanetary Dust*, B.Å.S. Gustafson, M.S. Hanner, eds., Astron. Soc. Pacific, San Francisco, 1996, pp. 121–124.

[8] D.J. Asher, M.E. Bailey, V.V. Emel'yanenko, *MNRAS* 304, 1999, pp. L53–L56.

[9] R. Arlt, *WGN* 26, 1998, pp. 239–248.

[10] E. Everhart, in *Dynamics of Comets: Their Origin and Evolution*, A. Carusi, G.B. Valsecchi, eds., Reidel, Dordrecht, 1985, pp. 185–202.

[11] J.E. Chambers, F. Migliorini, *Bull. Amer. Astron. Soc.* 29, 1997, p. 1024.

[12] I.P. Williams, *MNRAS* 292, 1997, pp. L37–L40.

[13] P. Brown, "The Leonid meteor shower: historical visual observations", *Icarus* 138, 1999, pp. 287–308.

[14] R.H. McNaught, *The Astronomer* 35, 1999, pp. 279–283.

[15] G.W. Kronk, "Meteor Showers: A Descriptive Catalog", Enslow, Hillside, NJ, 1988.

[16] C. Meldrum, *Nature* 1, 1869, pp. 220–221.

[17] I. Hasegawa, in *Meteoroids and their Parent Bodies*, J. Štohl, I.P. Williams, eds., Slovak Academy of Sciences, Bratislava, 1993, pp. 209–223.

[18] P. Brown, J. Jones, *Icarus* 133, 1998, pp. 36–68.

[19] P. Jenniskens, *Astron. Astrophys.* 295, 1995, pp. 206–235.

Table 10 – Orientation of Earth during forthcoming trail encounters.

Date (UT)	Trail	Point opposite Sun		Center Leonid "shadow"	
		λ	φ	λ	φ
1999, Nov 18.089	3 rev	324° E	19° N	245° E	22° S
2000, Nov 18.156	8 rev	300° E	19° N	220° E	22° S
2000, Nov 18.327	4 rev	238° E	19° N	158° E	22° S
2001, Nov 18.417	7 rev	205° E	19° N	126° E	22° S
2001, Nov 18.763	4 rev	80° E	19° N	1° E	22° S
2002, Nov 19.442	4 rev	196° E	19° N	116° E	22° S

The second strategy would apply to satellites whose orbits pass into Leonid "eclipse." For satellites with this potential geometry, it is simple for the satellite to pass through this zone at the predicted time of maximum. Slight maneuvers in height are made to alter the mean anomaly to the appropriate value. The satellite would then maximize its time in the shadow, shielded from any storm. The maximum duration a satellite could be in the Earth's shadow is around 36 minutes for LEO satellites out to around 5000 km. Above this, the duration increases, reaching 70 minutes at GEO distances. However, GEO satellites, with inclinations of 0°, orbit totally outside the Leonid shadow. Estimates of several storms (given in [13]) give a FWHM of around 0°.011 to 0°.022 in solar longitude (15 to 30 minutes). Given a probable uncertainty in the predicted time of maximum of less than 10 minutes, a satellite with optimum geometry, placing it in the middle of the Leonid "shadow" at the time of predicted maximum, would have a vastly reduced overall threat.

One possible caveat is that, as a satellite enters and leaves the Leonid shadow, meteoroids will be encountered that have passed through the Earth's tenuous outer atmosphere. It might be expected that a dustball structure would fragment under such circumstances increasing the flux of particles in this narrow zone. The maximum gravitational deflection such a Leonid would experience on skirting the atmosphere is 1°.4.

Satellites a considerable distance perpendicularly out of the ecliptic will have the time of encounter altered by 1.8 minutes per 1000 km. This is earlier than the predicted maximum if below the ecliptic and later if above. The cause is the 163° inclination of the dust trail to the ecliptic. GEO satellites at the same (opposite) longitude as the Sun during the Leonids are 14 000 km above (below) the ecliptic and will thus experience the peak some 25 minutes after (before) the Earth. GEO satellites leading (trailing) the Earth have the maximum about 40 minutes earlier (later). This interval is partly due to the GEO satellites in these directions being over 9000 km out of the ecliptic, but also being in front of (behind) the Earth in its orbit. GEO satellites ahead and behind the Earth will experience identical rates, unless passage through the near-Earth environment led to a breakup of particles. The trailing GEO satellites are well outside the Leonid shadow.

9. Conclusion

Study of the perturbed motion of dust trails from 55P/Tempel-Tuttle indicates that the Earth will begin a series of close approaches to trails starting with a possible minor storm in 1999. Storms can be expected in the years 2001 and 2002, but estimation of their intensity is strongly limited by the lack of observational data. The effect of the Full Moon in 2002 will reduce the observed rates making 2001 potentially the year of highest observed rates at this epoch.

During the next return, activity is likely to be low, but a storm in 2034 is possible. Data from the current epoch will allow a much better assessment of what may occur.

参考「天体の位置計算」長沢工（1981）より

5.4 日心直交座標系で表わした天体の位置

5.3節で，2体問題として運動する天体の楕円軌道上の位置を計算する方法を述べた．でも，これだけの計算では，その天体がどこに見えるかを知ることはできない．それには，もう少しの計算が必要である．その計算の第1段階として，天体の軌道上の位置を，太陽を原点とする，日心直交座標系で表わし直すことを考えよう．

5.4.1 日心直交座標系

ここで計算に使われる日心直交座標系には2種類のものがある．日心黄道直交座標系と，日心赤道直交座標系である．これは，前に説明をした，黄道直交座標系，赤道直交座標系をそれぞれ平行移動して，原点を太陽の重心に移したものである．念のために，ここでもう一度定義をし直しておくと，両座標系とも原点は太陽の重心で，

日心黄道直交座標系 (heriocentric ecliptic rectangular coordinates)

「1950.0においての黄道面を $X_c Y_c$ 面とし，その面上の平均春分点方向に X_c 軸，黄径90°の方向に Y_c 軸をとり，さらに黄道の北極方向に Z_c 軸をとったもの．」

日心赤道直交座標系 (heriocentric equatorial rectangular coordinates)

「1950.0においての平均赤道面を $X_q Y_q$ 面とし，その面上の平均春分点方向に X_q 軸，赤経6時方向に Y_q 軸をとり，天の北極方向に Z_q 軸をとったもの．」

となる．混乱しないように，黄道座標系に対しては添字cを，赤道座標系には添字qをつけて表わすことにする．X_c 軸と X_q 軸は完全に一致している．

まず，楕円軌道上で計算した位置 (x, y) を，日心黄道直交座標系による位置 (X_c, Y_c, Z_c) に変換しよう．そのためには，5.3節の〔5-3図〕で示した xy 直交座標系と，この $X_c Y_c Z_c$ 直交座標系を，はっきり関係づけなければならない．これを，〔5-5図〕によって考えていこう．

5.4.2 軌道要素

xy 系も $X_c Y_c Z_c$ 系も太陽の重心が原点であるから，原点は一致している．ここで楕円軌道を含む平面（xy 面）を考えると，この面が黄道面（$X_c Y_c$ 面）と一致していない限り，必ず，黄道面と原点を通る直線NSN′でまじわる．もし仮に，太陽重心から天体の動きを観察できたとすれば，天球上の天体の経路が必ず黄道と交わるといっても同じことである．この交点2つのうち，天体が黄道の南側から北側へと通過する点Nをこの軌道の**昇交点** (ascending node)，反対に北側から南側へと通過していく点N′を**降交点** (descending node) という．そしてNの黄経，つまり∠γSNを**昇交点黄経** (the longitude of the ascending node) といい，通常 Ω（オメガ）で表わしている．

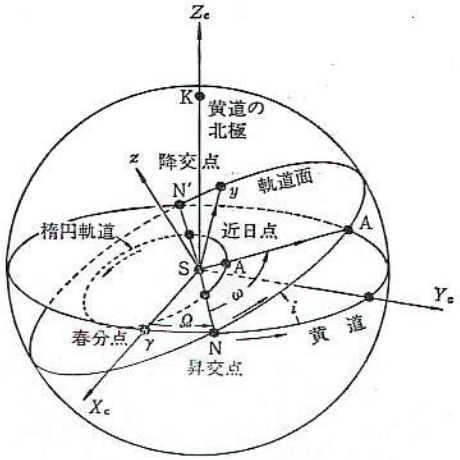

【5-5図】 楕円軌道と日心黄道直交座標系の関係

つぎに，軌道平面と黄道面の交わりの角を，この軌道の**軌道傾斜角** (inclination) といい，ふつうは i で表わす．この i は，昇交点Nで考えて，黄道上で黄経の増加する向きと，軌道上で天体の運動する向き（〔5-5図〕でともに矢印のついている向き）の間にはさまれる角として示す．したがって，$0° \leqq i \leqq 180°$ である．

昇交点黄経 Ω，軌道傾斜角 i が与えられれば，楕円軌道面の位置が日心黄道直交座標系の中ではっきりと決まる．しかし，まだ，この軌道面上で，楕円軌道の向きが決まっていない．これを指定するために，軌道面の x 軸を定める近日点の方向をAとし天球上に示すことにしよう．Aはもちろん楕円軌道面上にある．このときに作られる∠NSAを**近日点引数** (the argument of periherion, きんじつてんいんすう) といい．ω（オメガ）で書き表わす．（同じオメガでも，Ω はギリシャ大文字，ω は小文字である）．こうして，Ω, i, ω の3つの量を決めると，楕円軌道を表わした xy 座標系と，日心黄道直交座標系の $X_c Y_c Z_c$ との関係がすべて確定することになる．

今までに出てきた量で，軌道長半径 a，離心率 e，昇交点黄経 Ω，軌道傾斜角 i，近日点引数 ω，元期の平均近点角 l_0（あるいは天体の近日点通過時刻 t_0）の6つを，楕円軌道の**軌道要素** (orbital elements) という．2体問題では，これはすべて一定の定数である．一般的にいって，2体問題によって位置計算をするには，まずこの軌道要素の値を知っていなければならない．

2000.10.15.流星物理セミナー

眼視観測における観測方向と流星数

内山茂男

要旨

流星の眼視観測をおこなう場合、観測方向によって流星数がどのように変わるのかを調べた。その結果、流星群の輻射点がたとえば南天にあった場合、東西南北のどの方向を観測しても流星数はほとんど変わらないことがわかった。また、観測方向の天頂距離と流星数の関係は、流星の光度比と大気減光率によって大きく変化し、天頂距離が大きくなることによって流星数が多くなる場合と少なくなる場合があることがわかった。

《1.輻射点方向と流星数》

流星群の流星は輻射点方向から平行に、地球大気に突入し、上空 100km 付近で発光する。流星が出現する位置は、確率的には上空 100km 付近のどこでも同じと考えられる。この様子を図 1 に示す。

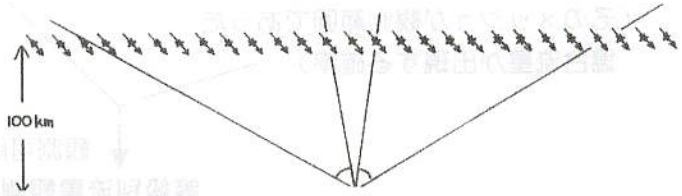

図 1. 輻射点方向・観測方向と流星数

★印は最大光度点を示す。

この図を読みとって、観測方向による流星数の違いをまとめたのが、表 1 である。最大光度点は全くの同数であるが、この最大光度点は、あくまでも“点”であるから輻射点方向に関係ないのは当然である。

観測方向		輻射点方向と反対	輻射点と反対方向
流星数	最大光度観測視野内	10 個	10 個
	全経路　観測視野内	9 個	8 個
	一部経路観測視野内	1 個	3 個

表 1. 輻射点方向・観測方向と流星数（図 1 より）

- 結論 -

◎例えば輻射点が南天にある場合に、南天を観測しても東天・北天・西天を観測しても、流星数はだいたい同じになる。

ただし、輻射点から離れた方が流星数はやや多くなる可能性がある。理由は次の２つである。

(1)輻射点から離れると経路の一部が視野に入る流星数が増える。

(2)同じ明るさであれば、経路が長い流星の方が認識しやすい可能性がある(第 41 回流星会議千種高校発表より)。

《2.観測方向の天頂距離と流星数》

2-1 天頂距離によって流星数が変化する原因

(1)低空の流星を増やす効果

◎上空 100km での可視領域が増大する（図 2)。

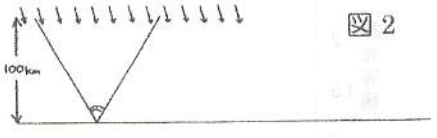

図 2

(2)低空の流星数を少なくする効果

◎流星の距離が増大する

◎大気減光が大きくなる

↓

ともに、流星が暗くなる。

結果的にもともと暗い流星が見えなくなる。

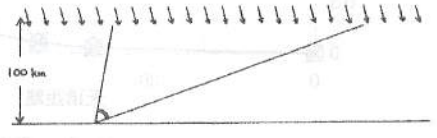

2-2 計算方法

流星は上空 100km 付近に出現することが多い。そこで、上空 100km の平面を 5km×5km のメッシュで区切り、各メッシュに同じ確率で流星が出現するとし、下の流れのようにエクセルで計算した。計算対象としたのは、観測地点真上から半径 1000km 程度のメッシュである。

地球の丸みについては、影響が大きいと思われる大気減光だけはこれを考慮し、それ以外では計算方法が非常に複雑になるのでこれを無視した。

メッシュ毎の流星出現出現率は同じ
↓ 補正：観測地点からの距離
　　大気減光
　　光度比
メッシュ等級別流星出現率
（そのメッシュが観測範囲であった場合流星が出現する確率）

観測可能視野（左右 120°、上下 100° の楕円と仮定）
↓ 補正：IMO 流星可視面積比
等級別観測可能視野
↓ 幾何学的に計算
等級別観測可能メッシュ

↓ 観測可能メッシュの流星出現率を加算
等級別流星観測率
↓ 加算
全流星観測率
（これを観測方向毎に求めて比較する）

2-3. 大気減光による補正

参考にしたのは「天文年鑑の天体写真データ」にある「大気減光による補正」の表である。しかし、表のままでは扱いにくいので、表の値に近くなる計算式をいろいろと捜して、作ったのが次の式である。（Z：天頂距離）

$$\text{露出倍数} = 1 + 0.294(\sqrt{\tan^2 Z + 2.15^2} - 2.15) + 0.686(\sqrt{\tan^2 Z + 30^2} - 30)$$

この式の計算結果と天文年鑑の値を減光等級に直して比較したのが、図 3 である。

さて、これを見ると、天頂距離 80°、すなわち、地平線から高度 10° でちょうど 1 等級の減光である。これは、低空の光害増加を考慮していないものであると考えられるので、流星観測としては、もう少し減光等級の大きいものも検討すべきであろう。そこで、上記の式の係数を変更して、天頂距離 80°（高度 10°）での減光が 1,2,3,4 等級の 4 通りを、それぞれ、「減光度 1,2,3,4」と呼び（図 4）、それらについて調べて行った。

図 3. 大気減光

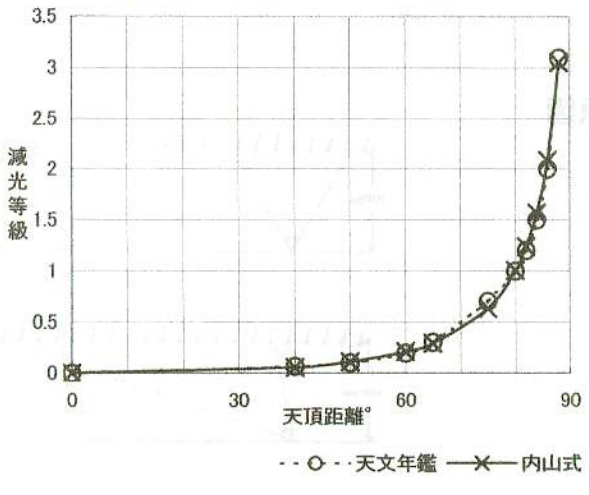

図 4. 減光度と減光等級

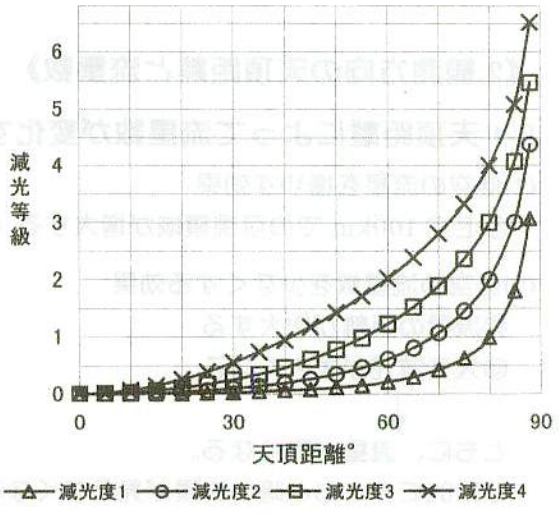

2-4. IMO 可視面積比補正

天文ガイド 2000 年 5 月号、6 月号に高梨氏が紹介した以下の値（表 2）を使用。1 等級毎の可視面積を求め、視野中心付近のその面積内の流星だけ観測可能と仮定した。計算上は、最微等級 6.0 等とし、5 等級流星から 1 等級毎に求めた。（最微等級が変わっても、結果には影響しないはず）

表 2.
最微等級と
可視面積比

Mag	5	4	3	2	1	0	-1	<-2
Lm - Mag	1.0	2.0	3.0	4.0	5.0	6.0	7.0	>8.0
可視面積比	0.023	0.079	0.24	0.52	0.74	0.85	0.94	1

※Lm：最微等級。Mag：流星等級

図 5. 可視面積計算例
天頂方向を観測した場合。
上空 100km の平面で各領域の内側の流星が観測できる。（5km×5km メッシュを用いているため凸凹している）

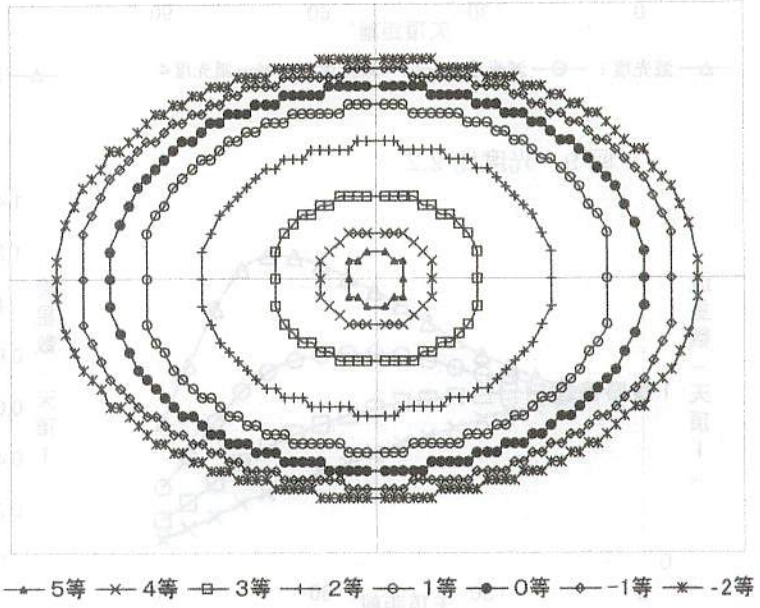

2-5. 計算結果

実際に観測する際の空の条件として減光度 2 程度のケースが多いと思われるので、まずこの場合の計算結果を図 6 に示す。

これを見てわかるように、流星の光度比によって、全く結果が異なっている。光度比が 2.0 よりも小さくなると、天頂方向よりも低空を観測したほうが明らかに多くの流星が観測できる。

次ページには光度比別の計算結果を示す。

図 6. 天頂距離と流星数
- 減光度 2 の場合 -

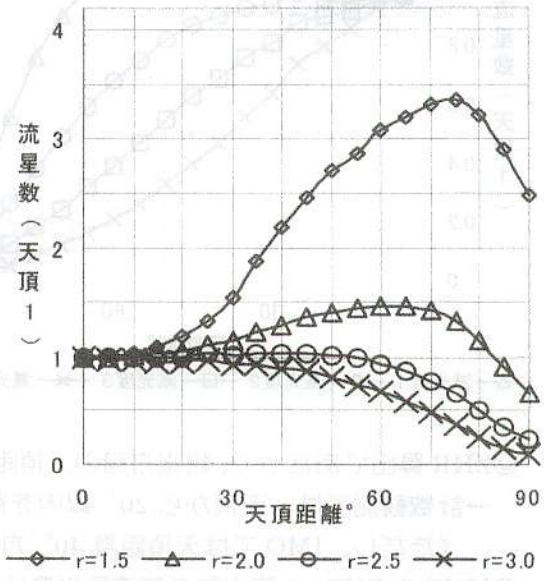

表 3. 極大付近の流星の光度比（IMO の Web site より）

1998 年しし座流星群（欧州火球ナイト）	1.2～1.4
1999 年しし座流星群（欧州大出現時）	2.1～2.4
1996 年ペルセウス座流星群	1.7～2.2
1997 年ペルセウス座流星群	主に 2.0～2.2
1993 年ふたご座流星群	2.3 程度
1996 年ふたご座流星群	1.9～2.4
1997 年みずがめ座 η 流星群	2.0～2.4
散在流星（1999 年しし座流星群観測時）	3.0

図 7. 光度比 1.4

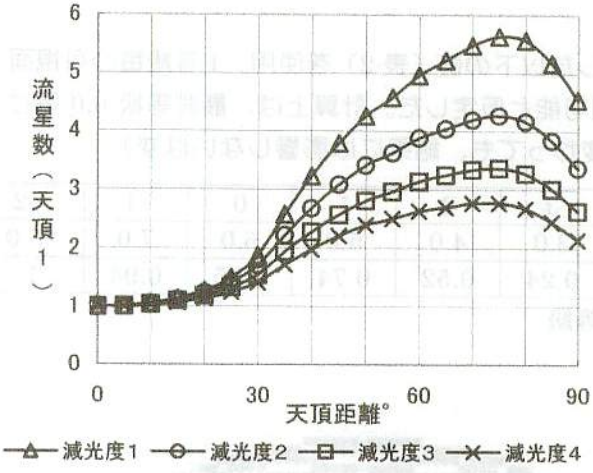

図 8. 光度比 1.8

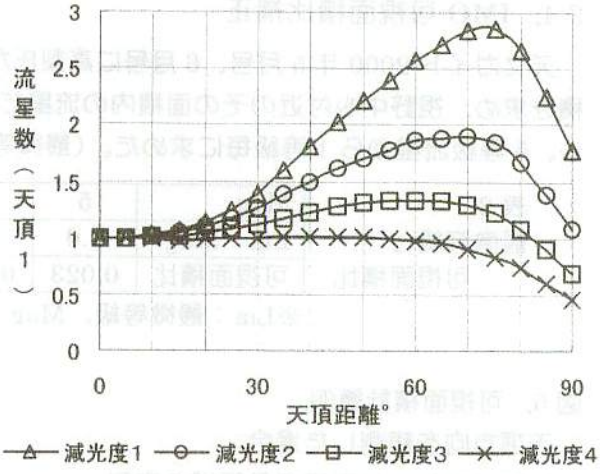

図 9. 光度比 2.2

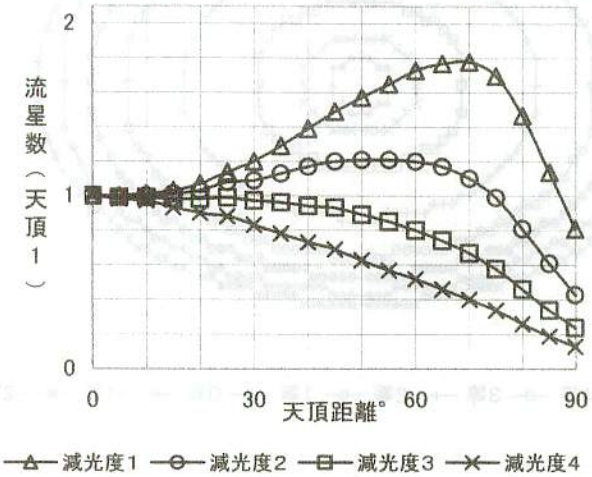

図 10. 光度比 2.6

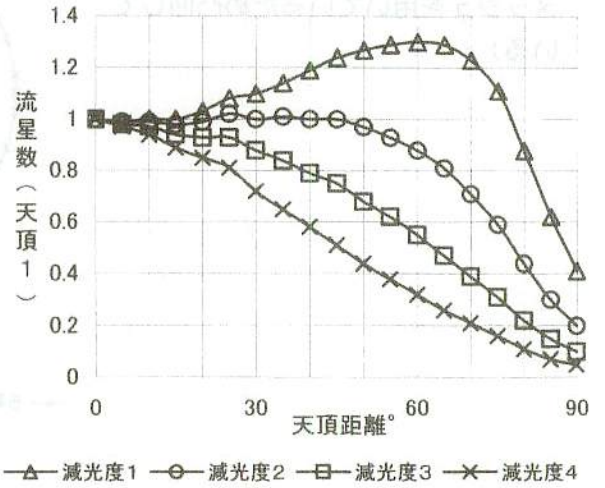

図 11. 光度比 3.0

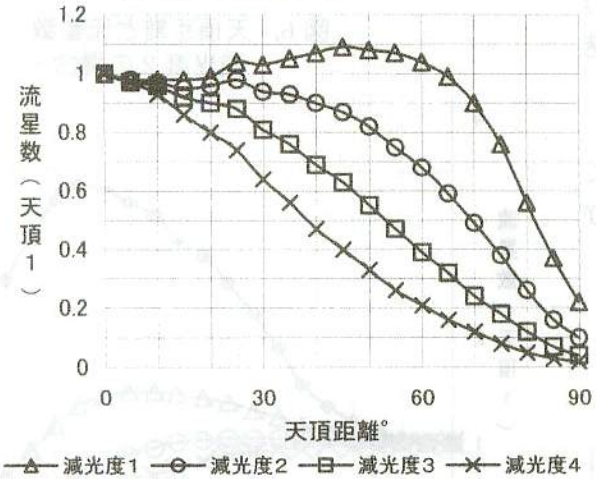

《まとめ》

◎流星数は輻射点からの離角にはほとんど関係ない。

◎流星数は観測方向の天頂距離によって変化する。この変化の様子は流星の光度比と大気の減光度によって大きく変化する。

◎光度比が小さい場合や減光度が小さい場合は、地平線が十分に見える方向を観測すると流星数が増える。一方、光度比が大きい場合や減光度が大きい場合は、天頂方向が流星数が多い。

◎観測方向の天頂距離が 20° 以内の場合の流星数は、天頂方向とあまり変わらない。

◎ZHR 算出にあたって、観測方向の天頂距離による流星数の変化を補正することは事実上無理である。

→計数観測では、天頂から 20° 以内を視野中心とすべきでは？

（ただし、IMO では天頂距離 40° 方向を観測することを推奨している。）

◎NMS の ZHR1.6 算出時の群流星光度比 1.6 は問題ないか？

←光度比 1.6 では、低空を観測したほうがずっと多くの流星が観測できるはずである。現実にそうなっているだろうか。

○ '00しし座流星群昼間観測のお誘い

昨年、私達は図らずも(？)昼間に流星観測をして、昼間流星を観測してしまいました。しかしながら、まだ十分なサンプルがないために、私達が見たものは全て紛れもない流星であると言うことはできないでいます。そこで今年は、この観測を全国的に展開し、新たな観測として確立させたいと思います。

○方法

以下の方法を提案します。各自で可能な方法を選んで観測して下さい。

（イ） 眼視観測

11月18日はAM5:00頃から薄命が始まります。日の出は6:19ですので、昼間火球観測は通常の観測(最微4.5以上)ができなくなってから、しし座流星群の輻射点の沈むPM1:00頃までとなります。観測時はできる限り太陽光を直接視野に入れないようにし、正確な時計、あるいはストップウォッチを用いるといいでしょう。

（ロ） 電波観測

電波観測は眼視との同定や等級の目安を導くのに不可欠です。出来うるならば眼視と平行して、同地点観測を行ってみて下さい。注意点は、リスン法でもパソコンを利用する方法でも、時間を正確に把握してもらうことです。特にパソコンを利用する場合は内部時計に誤差があると、結果が著しく変わる可能性があります。時報等を用いて正確な時刻での観測をお願いします。

（ハ） ビデオ観測

普通の家庭用ビデオカメラを空に向けて撮影をしてみて下さい。JJYの音声を同時に録音するようにすれば正確な時刻が求まるでしょう。

これらの観測をされた方は是非ご報告下さい。

報告先 〒338-0826
埼玉県浦和市大久保領家173-3ベルフォーレ浦和201

芹澤寛隆 FAX 048-857-8465
E-mail aaf80100@pop17.odn.ne.jp

MSS-095

MSS-097

2001.4.15　第97回 流星物理セミナー

73P/Schwassmann-Wachmann 3 彗星関連流星群出現予報

橋本岳真

1930年に発見され、地球に0.0617AUまで大接近して微光流星雨を降らせたとされる73P/Schwassmann-Wachmann 3 彗星は、その後長い間行方不明となっていましたが、1979年に再検出されました。そして1990年、1995年と順調に回帰が確認されましたが、1995年9月22日に近日点を通過した同彗星はA～D核の4個に核分裂を起こし、10月上旬には5等台まで増光しました。今回の回帰は、彗星が降交点を通過した134日後の2001年5月31日に地球が降交点から0.056AU(地球ー月間距離の約22倍)のところを通過する予定です。これまでの観測から、前回回帰時に分裂した核もB,C,E核の3つが確認されたばかりか、2000年5月23/24～29/30日にかけては関連流星群と思われる5月うしかいα群の出現が観測されました。このように、今後の回帰にともなう流星雨出現の可能性が出てきた今年は、流星群進化のエポックとして観測の重要性が増してきました。

表1:73P/Schwassmann-Wachmann 3 彗星関連流星群出現予報(MPC発表の2001年の軌道を使用)

METH.	ALPHA	DELTA	VG	L	DATE-MAX.	Q	E	PERI.	NODE	INCL.	
-Q	208.9	29.3	12.21	69.9	MAY 31.3	0.9918	0.6939	198.8	69.9	11.4	qアジャストメント法
-H	209.1	21.0	13.89	54.3	MAY 15.1	0.9374	0.6939	214.7	54.3	11.0	ωアジャストメント法
-P	210.7	25.4	13.10	61.2	MAY 22.3	0.9647	0.6850	207.8	61.2	11.6	従来法

ADDITIONAL INFORMATION : (-) DIST. = 2.497 AU; DT = 134.0 DAYS; MIN. DIST. = .0420 AU

NESLUSAN L., SVOREN J., PORUBCAN V., 1998, "A COMPUTER PROGRAM FOR CALCULATION OF A THEORETICAL METEOR-STREAM RADIANT", ASTRON. ASTROPHYS. 331, 411-413. で公開されたプログラムDOSMETH.EXEを使用

図1　73P/Schwassmann-Wachmann 3 彗星関連流星群予想輻射点位置(MPC発表の2001年の軌道を使用)

日付	5/11	5/16	5/21	5/26	5/31	6/6	6/11	6/16
Ls	50	55	60	65	70	75	80	85
α	208	209	209	210	209	207	205	202
δ	+19	+22	+24	+27	+29	+32	+34	+36
r-R	-0.070	-0.051	-0.042	-0.046	-0.056	-0.069	-0.081	-0.092

重野好彦氏作成のRVO.EXEよりqアジャストメント法を使用して作成

■2000年5月に観測されたうしかい座α群の出現数変化

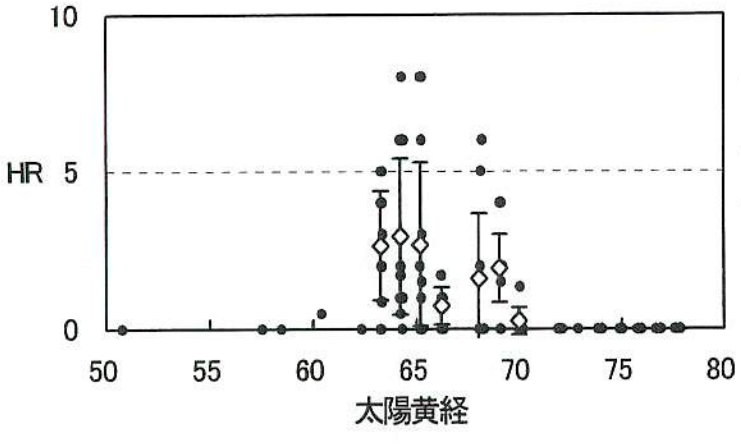

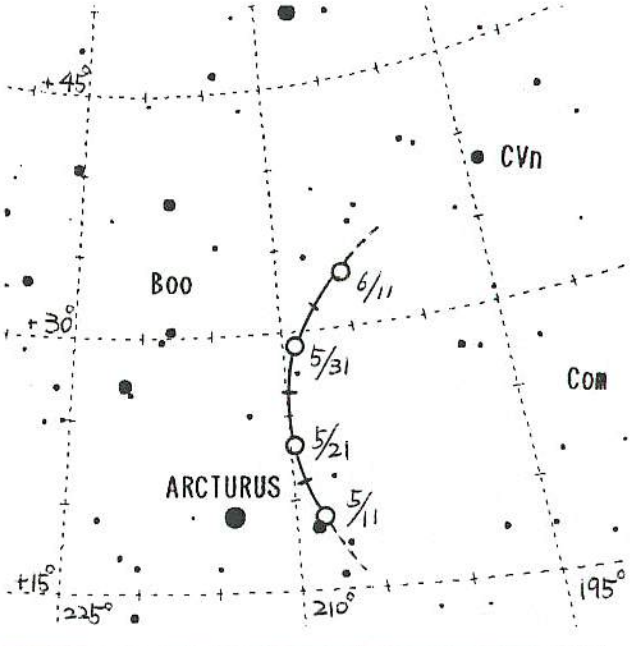

■5～6月にうしかい座周辺で活動する流星群

流星群名	活動期間	極大日	輻射点	備考	出典
5-6月Boo群	5月下旬 - 6月下旬		Boo付近	73P/SW3, 7P/PW彗星関連群を含む	H1993
5月αBoo群	5/17 - 5/31		212, +20	緩, 微光, 1970年突発, '69, '71出現	H1993
5月εBoo群	5/21 - 5/30	5月21日	220, +29	緩, 微光, 1930年突発	H1993
τHer群	5/19 - 6/14	6月 3日	229, +39	緩, 微光, 1930年突発	C1973
6月εBoo群	6/10 - 6/16	6月中旬	220, +31	緩, 微光, 1930, 1982, 1983年突発	KM1979
6月Boo群	6/28 - 6/28	6月28日	219, +49	緩, 微光, 1916, 1921, 1927年突発	C1973

C1973=A. F. Cook, 1973 KM1979=小関正広, 1979 H1993=橋本岳真, 1993

MSS-097

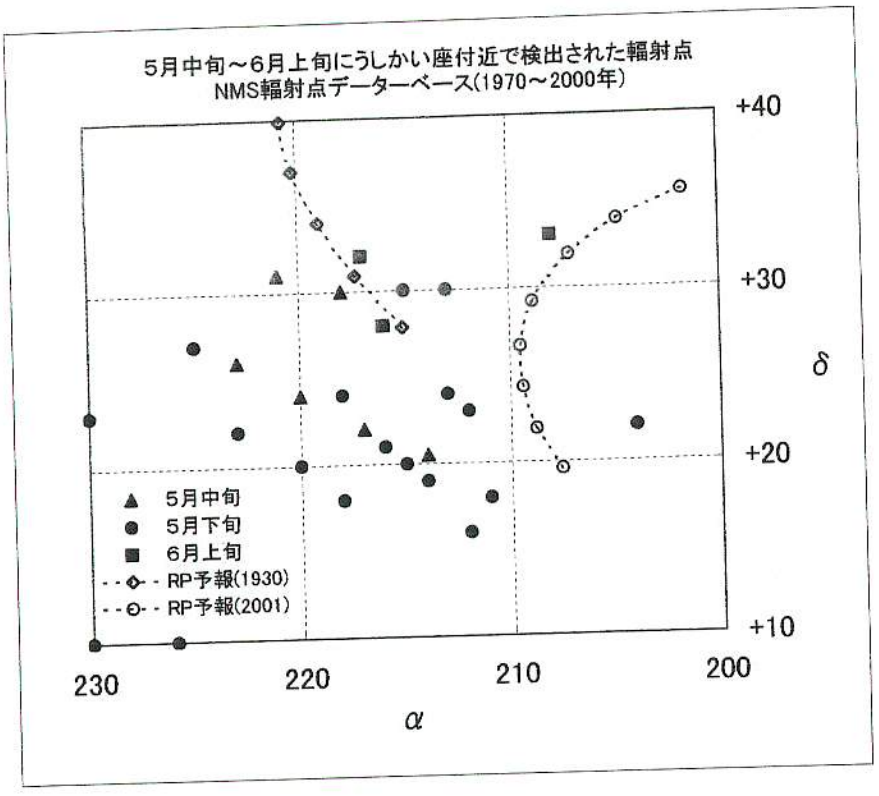
5月中旬～6月上旬にうしかい座付近で検出された輻射点
NMS輻射点データーベース(1970～2000年)
+40
+30
+20
+10
δ
230
220
210
200
α
5月中旬
5月下旬
6月上旬
RP予報(1930)
RP予報(2001)

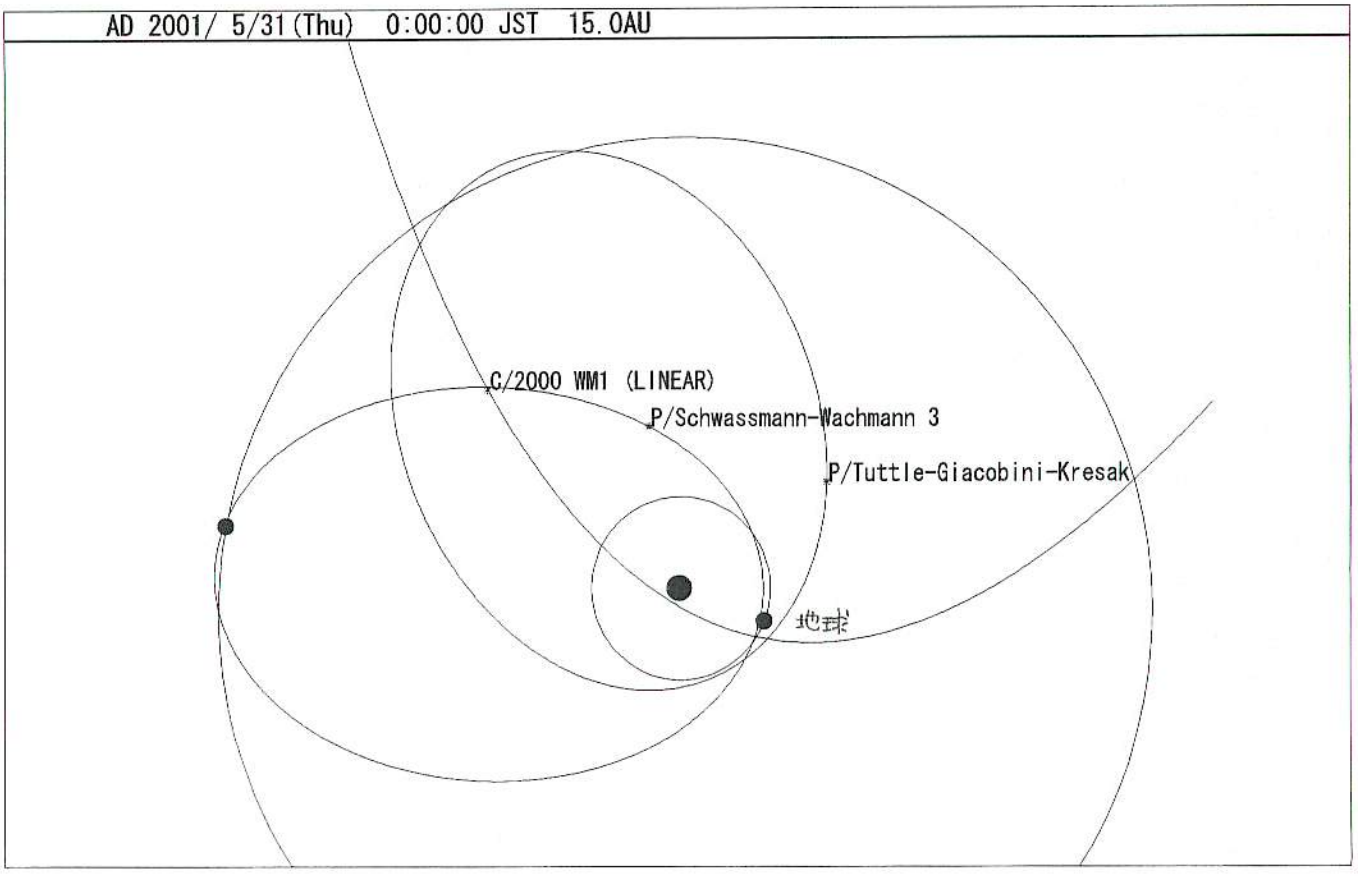
AD 2001/ 5/31 (Thu) 0:00:00 JST 15.0AU
C/2000 WM1 (LINEAR)
P/Schwassmann-Wachmann 3
P/Tuttle-Giacobini-Kresak
地球

太陽系外からの流星

海老塚 昇（甲南大）、阿部 新助（神戸大）、前田 幸治（宮崎大）、中村 卓司（京大）

第118回 流星物理セミナー　2007年2月17日

太陽系における星間物質の検出

- Ulysses：太陽極軌道人工惑星
  Particle counterにて双曲線軌道の粒子を検出。
  10^{-19}-10^{-11}Kg
- Arecibo: プルトリコ、口径300m?, 430MHz
  143/3000(4.8％) が双曲線軌道@ 1997 Nov. 15-20と1998 。
  10^{-14}-10^{-9}Kg
- AMOR (Advanced Meteor Orbital Radar): ニュージーランド
  1,600/350,000 (0.46％)が対地速度100Km/s。
  >10^{-10}Kg
- MARS: ウクライナ、31.1MHz
  7,911/250,000 (3.2％)が双曲線軌道@1972-1978
  10^{-8}-10^{-6}Kg (>5x10^{-9} Kg)

Kharikiv (ウクライナ)のレーダ観測

B.L. Kashcheyev, S.V. Kolomiyets, “Interstellar particle detection and selection criteria of meteor streams”, *Proceedings of the Meteoroids 2001 Conference*, **ESA SP-495**, 643 - 650, 2001

- Kharikiv 電波技術研究所(ウクライナ)のレーダ (MARS) によって1972-1978の7年間に250,000個の流星の軌道を決定。(**10^{-6}-10^{-8} Kg: 2-7等**@50Km/sec)
- 7,911/250,000 (2.8%) が放物線あるいは双曲線軌道。
- 太陽向点方向から到来する星間物質は**1<e<1.1**、1102個が該当。
- 双曲線軌道の流星は0.9<e<1の楕円軌道とは分布が本質的に異なる。(軌道傾斜角が大きく、逆行が多い？)

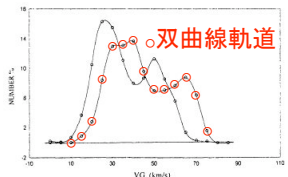

楕円と双曲線軌道流星の速度分布

Fig.1. Distribution number of meteors against geocentric velocity V_g for elliptic (shift left) and hyperbolic (shift right) orbits

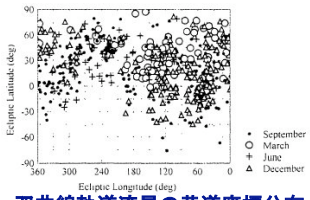

双曲線軌道流星の黄道座標分布

Fig.3. Contribution of radiants (β', λ') of the hyperbolic orbits (1<e<1.1) from four seasons

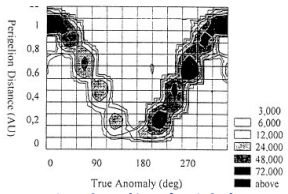

近日点距離と真近点角

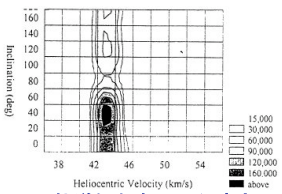

軌道傾斜角と日心速度

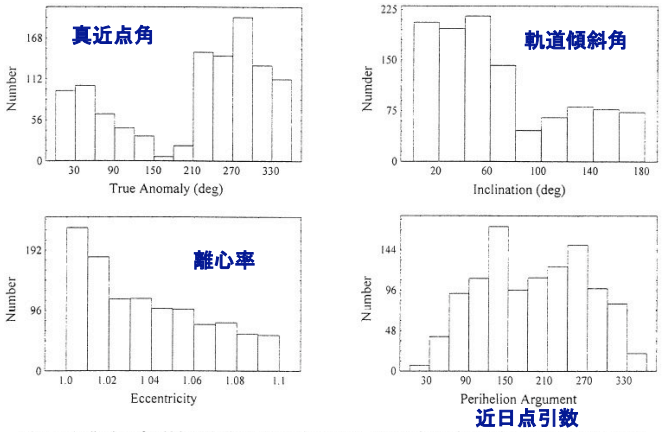

Fig. 4. Distribution of 1102 hyperbolic meteor orbits (1< e <1.1) on heliocentric velocity and on orbits elements

1<e<1.1の流星の到来方向

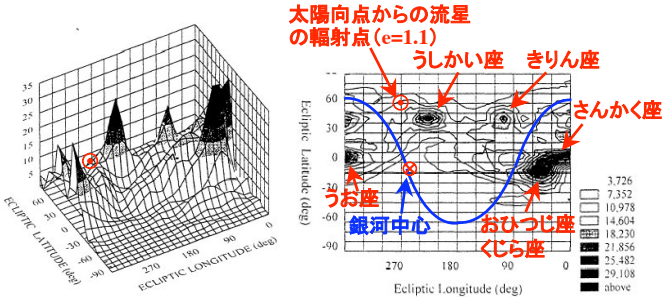

Fig. 2. N=N (β', λ') of 1102 hyperbolic orbits with1 < e < 1.1 (1972-1978) in Kharkiv

Arecibo (プルトリコ)のレーダ観測

D.D. Meisel, D. Janches, J.D.Mathews, “Extrasolar Micrometeors Radiating from the Vicinity of the Local Interstellar Bubble”, ApJ, **567**, 323-341, 2002.

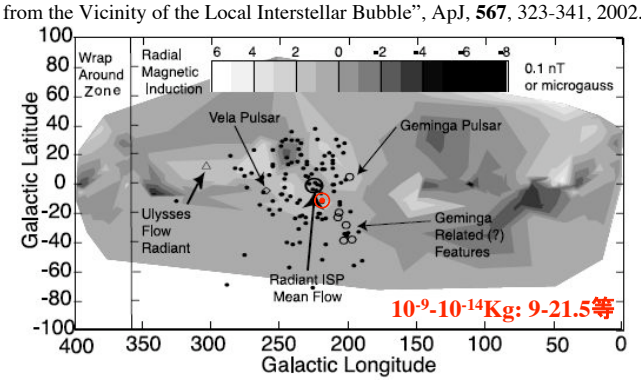

高速流星の発光高度と明るさ

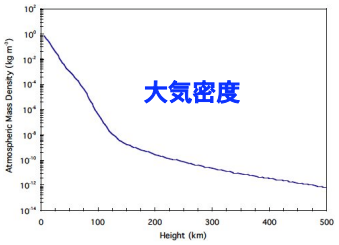

Fig. 1. Atmospheric mass density as a function of height, based on averaged data from the MSISE-90 atmospheric model.

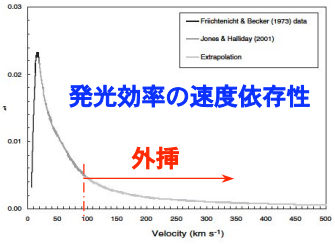

Fig. 2. Velocity dependence of the luminous efficiency factor, τ_I, for radiation in the visible region of the electromagnetic spectrum.

K.A. Hill, L.A. Rogers, R.L. Hawkes, “High geocentric velocity meteor ablation”, A&A **444**, 615-624 (2005)

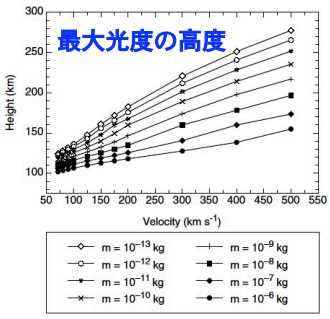

Fig. 4. Meteor heights at the point of peak light intensity (H_{max}) for cometary structure meteoroids.

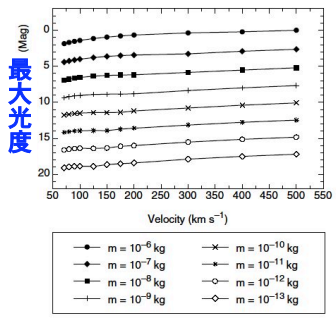

Fig. 10. The maximum light intensity (I_{max}) of cometary structure meteoroids expressed in absolute astronomical magnitude.

彗星のような物質(0.25g/cm^3)

10^{-6}Kg∽2.0mm, 10^{-7}Kg∽910μm, 10^{-8}Kg∽420μm
10^{-9}Kg∽200μm, 10^{-10}Kg∽91μm, 10^{-11}Kg∽42μm

星間物質の空間密度

[個/Km^3]

直径 (a)	$a^{-3.5}$	a^{-4}	$a^{-4.5}$
91μm (10^{-10}Kg, 11.5等)	$4.4x10^{-4}$	$1.5x10^{-5}$	$4.8x10^{-7}$
200μm (10^{-9} Kg, 9.0等)	$2.8x10^{-5}$	$6.3x10^{-7}$	$1.4x10^{-8}$
420μm (10^{-8} Kg, 6.5等)	$2.1x10^{-6}$	$3.2x10^{-8}$	$5.0x10^{-10}$

0.1μm ($2.5x10^{-16}$ Kg@0.25g/cm^3): 10^7個/Km^3,
N(a)∝$a^{-3.5}$ @0.005<a<0.25μm, Mathis, Rumpl, & Nordsieck (1977)
視野φ28° →φ60Km@高度120Km: $30^2\pi = 2.8x10^3$Km^2
太陽系の速度: 20km/sec

[個/Hour]

等級	$a^{-3.5}$	a^{-4}	$a^{-4.5}$
11.5	89,000	3,000	97
9.0	5,600	127	2.8
6.5	420	6.5	0.1

I.I.-HDTV カメラ

業務用HDシステムからHDハンディカムに改造。

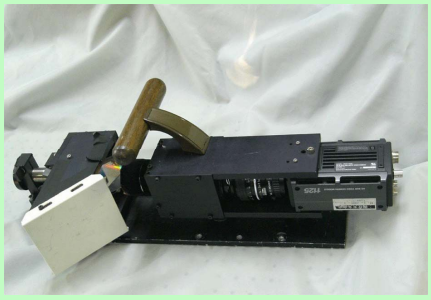

グリズム等の対物分光器(左)および紫外線分光システム(右)

I.I.-ハイビジョンカメラの限界等級

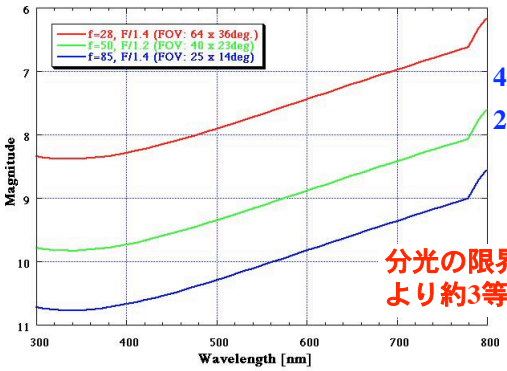

420μm: 6.5等
200μm: 9.0等
91μm: 11.5等

分光の限界等級は撮像より約3等明るい。

Limiting magnitude of color I.I.-HDTV
(t=0.033sec., R=3, Eff.=0.05, S/N=3)

UFOキャプチャー

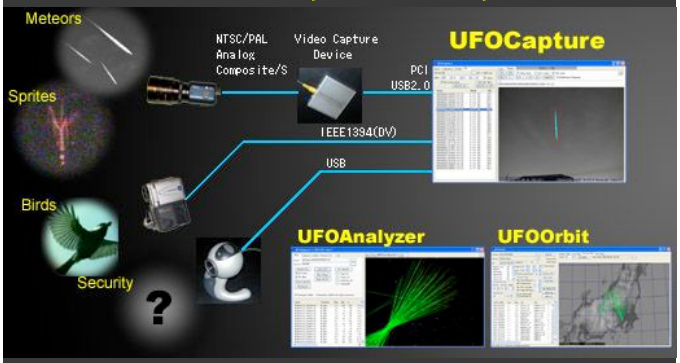

http://sonotaco.com/

前田さんの観測機材（宮崎）

ほぼ同方向に向けた2台のカメラ (WAT-902H)

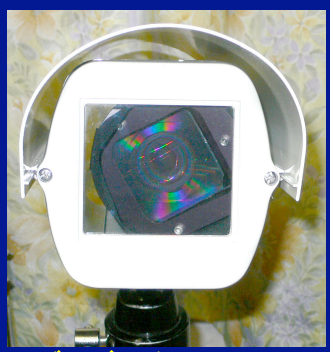

グリズムを取付けたカメラのハウジング

自動検出された流星のスペクトル

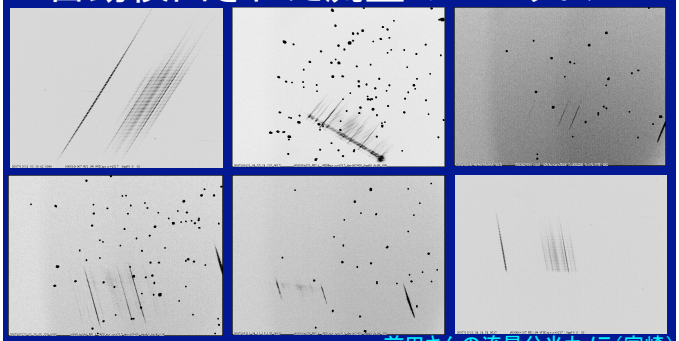

前田さんの流星分光カメラ（宮崎）

双曲線軌道の流星の分光観測は
太陽系外の物質組成比を直接測定できる手段

まとめ

- レーダ観測、探査機によって双曲線軌道の流星あるいは粒子を検出。
- 双曲線軌道の流星の輻射点は太陽向点付近が多く、20Km/secで到来する星間物質は1<e<1.1。
- 420μm (10^{-9}Kg)の粒子は6.5等@50Km/sec。
- I.I.-HDTVの対物分光システムの限界等級(視野30°)は7等。
- 双曲線軌道の流星の分光観測は太陽系外の物質組成比を直接測定できる手段。

宇宙から見た流星嵐の想像図

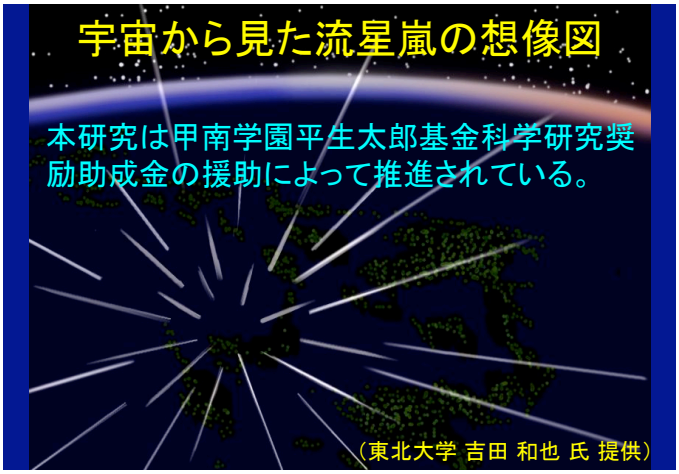

本研究は甲南学園平生太郎基金科学研究奨励助成金の援助によって推進されている。

（東北大学 吉田 和也 氏 提供）

系外流星の起源

海老塚 昇（名古屋大学／理研）

1. はじめに

前回（120 回）の流星物理セミナーのときに発表した「太陽系外からの流星の分光観測」[1]に対して、後日、重野さんから「太陽から 1AU と 10 光年の距離の比が約 50 万倍あるので近傍星からの粒子密度は悲観的に少ないのではないか。」とのコメントをいただきました。そこで最も近いαCen 星（4.4 光年）について粒子密度を検討してみました。中心星から粒子が等速で放射状に広がる場合に密度比は距離の 2 乗に反比例します。そのため一点から等速で粒子が放出された場合に 1AU と 4.4 光年の比が 1:280,000 なので密度比は、

$1/280{,}000^2=1.3\times10^{-13}$ ・・・(1-1)

になり、近傍星からの系外流星が到来する確率は悲観的な値になりそうです。

私の発表では、「銀河中心方向や外縁部の物質の組成比が太陽系近傍と異なると面白い。」と締めくくり、また、「星によって物質比が異なると思うか？」という質問に対して、「近傍星と太陽系の物質比はあまり変わらないのではないか、一方、おうし座とオリオン座の分子雲では物質比が異なるかもしれない。」と答えました。重野さんのコメントをきっかけに近傍星や分子雲、赤色巨星等から、それぞれどのくらいの系外流星が到来するか検討をしてみました。

2. 近傍星

質量放出のプロセスとして彗星やダスト・トレイルが木星に接近したときにはじき飛ばされる場合が支配的ではないかと思われます。直径 10km の彗星（10^{15} kg）が年間に 1 個太陽に接近して彗星質量の 1/1,000 のダスト（水を含まない。彗星質量の 80%が水の氷とした場合に直径 1km の彗星 5 個分。）を放出すると仮定します。木星から 1AU 以内を通過するダストの半分が太陽系外に飛び出すと仮定すると、その質量放出は木星の軌道長半径が 5.2AU なので、

$10^{15}*0.5*\pi*1^2/(1{,}000*4\pi*5.2^2)=4.6*10^9$ kg/年 ・・・(2-1)

になります。ダストのサイズ分布を直径の-3.5 のベキとすると、各サイズの合計質量は直径の-0.5 のベキになります。この場合に最小サイズのダストの合計質量が全体の 68%を占めます。最小サイズの粒子が直径 0.1μm, 質量 $2*10^{-19}$ kg（彗星の密度 1 g/cm^3 の 1/5、0.2 g/cm^3 を仮定）とすると、

$4.6*10^9*0.68/(2*10^{-19})=1.6*10^{28}$ 個/年 ・・・(2-2)

の粒子が太陽系から放出されることになります。サイズ分布を直径の-3.5 乗のベキとすると直径 1.7mm の粒子（10^{-6} kg 、2 等級の流星サイズ）の放出は、

$1.6*10^{28}*(1.7*10^4)^{-3.5}=2.5*10^{13}$ 個/年 ・・・(2-3)

すなわち、

$2.5*10^{13}/(365*24*60*60)=7.9*10^5$ 個/秒 ・・・(2-4)

になります。粒子が等方的に秒速 1km/s で放出されたとして 4.4 光年の距離における空間密度は、

$7.9*10^5/\{1*4\pi*(4.4*300{,}000*60*60*24*365)^2\}=3.6*10^{-23}$ 個/km^3 ・・・(2-5)

になります。面積 10,000km（直径 112 km、高度 112km において 1 ステラジアン）を 1 時間あたりに 1km/s で通過するフラックスは、

$3.6*10^{-23}*1*10{,}000*60*60=1.3*10^{-15}$ 個/時 ・・・(2-6)

すなわち、

$1/(1.3*10^{-15}*365*24)=8.8*10^{10}$ 年/個 ・・・(2-7)

になって、宇宙年齢を超えてしまいます。

3. 分子雲

惑星形成の標準モデル[2]では木星サイズの惑星が誕生する段階において 1/100,000ー1/1,000 太陽質量のダストや微惑星を系外に放出する可能性があります。イメージとして星生成領域すなわち分子雲が太陽系における彗星のようにチリをまき散らしながら、銀河にダスト・トレイルを形成しているといった感じでしょうか。おうし座分子雲（距離 430 光年）やオリオン座分子雲（1,200 光年）等では、それぞれ現在約 100 個と数 1,000 個の星・惑星形成が行われています。これらから粒子が秒速 30km/s で放出されたとすれば、それぞれ 430 と 1,200 万年かけて太陽系に到達することになります。

太陽系の各惑星の固体質量および軌道半径から、その母体となった原始太陽系円盤の半径は 40au 程度で、その範囲の固体質量が 1/10,000 太陽質量（円盤総質量の 1ー2%）、固体面密度分布は中心星（太陽）からの距離を r とすると $r^{-3/2}$ に比例すると推測されています。太陽系惑星形成の標準モデルではいくつか問題点を指摘されていますが、原始太陽系円盤の 40au の範囲で乱流が収まると 1,000ー10,000 年かけて赤道面にダストが沈殿し、その間にダストは直径 1cm くらいに成長して、重力不安定によって 1ー10 年くらいで一気に 1ー

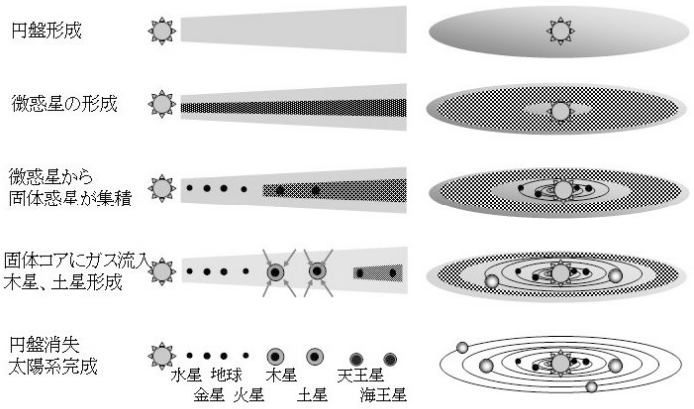

図 1. 惑星形成の標準モデル (東京工業大学 井田研究室のホームページ[2]より)

10km くらいの微惑星に成長すると考えられています。5AU（木星軌道）においては微惑星形成から 1,000 万年くらい経って地球質量の 5 倍以上の岩石惑星ができると周囲の円盤ガスが流れ込んで暴走的に地球質量の数 100 倍のガス惑星に成長します。また、5AU 近傍に多くのダストが残っていると、惑星の外側の軌道にある天体は加速されるためにガスの抵抗を受けないサイズ（10μm 以上?）の大量のダストが太陽系外に放出されると考えられます。さらに木星の内側では木星によって加速（減速）された微惑星同士の高速衝突によって破片が飛び散り、多数の小惑星ができるとともに、その一部が太陽系外に放出されるプロセスも考えられます。

太陽程度の中質量の星形成が行われている、おうし座分子雲において木星質量の惑星が成長する段階の恒星系が 10 個あり、1 恒星系あたり 100 万年間に 1/100,000 太陽質量の固体成分（80%が水の氷）が放出され、粒子の最小サイズが直径 10μm, 質量 10^{-12} kg（密度 1g/cm^3 を仮定、多少怪しい？）とすると、

$2*10^{30}*10/10^5/10^6*0.68/10^{-12}=1.4*10^{32}$ 個/年 ・・・(3-1)

の粒子がまき散らされることになります。サイズ分布を直径の-3.5 乗のベキ（この仮定も多少怪しい）とすると直径 1.7mm（$5*10^{-6}$ kg ）の粒子（氷が蒸発すると 10^{-6} kg）の放出は、

$1.4*10^{32}*(1.7*10^2)^{-3.5}=2.2*10^{24}$ 個/年 ・・・(3-2)

になります。粒子が等方的に放出されたとして 430 光年の距離における面積 10,000km を 1 時間あたりに通過するフラックスは、

$2.2*10^{24}*10{,}000/(365*24)/\{4\pi*(430*300{,}000*60*60*24*365)^2\}=1.2*10^{-8}$ 個/時 ・・・(3-3)

すなわち、9,500 年に 1 個になり、残念ながら 7 桁くらい増えないと観測に引っかからないでしょう。

4. 晩期型星

AGB 星（漸近巨星枝）は太陽質量程度の晩期型赤色巨星であり、その質量の半分を放出してやがて白色矮星になります。AGB 星では 0.01ー1,000μm 程度のダスト（密度 0.01g/cm^3 以下、グラファイトや SiO_2 が主成分で、主に原子間力によって結合されている）が大量に生成されると考えられています。なお、星間ダストの一部は起源が超新星爆発の残骸であるとされていますが、0.01μm より大きなダストが生成されないと考えられています。

1 恒星系あたり 10 億年間に 1/10 太陽質量の固体成分が放出されると仮定して、粒子の最小サイズが直径 0.01μm, 質量 10^{-23} kg（密度 0.01g/cm^3 を仮定）とすると、

$2*10^{30}/10/10^9*0.68/10^{-23}=1.4*10^{43}$ 個/年 ・・・(4-1)

の粒子がまき散らされることになります。サイズ分布を直径の-3.5 乗のベキとすると直径 4.6mm（10^{-6} kg ）の粒子の放出は、

$1.4*10^{43}*(4.6*10^5)^{-3.5}=2.1*10^{23}$ 個/年 ・・・(4-2)

になります。粒子が等方的に放出されたとして 500 光年の距離（ベテルギウス）における面積 10,000km（直径 112 km）を 1 時間あたりに通過するフラックスは、

$2.1*10^{23}*10{,}000/\{365*24*4\pi*(500*300{,}000*60*60*24*365)^2\}=8.5*10^{-10}$ 個/時 ・・・(4-3)

すなわち、13 万年に 1 個になります。

5. 終わりに

いずれの見積もりでも放出される質量や粒子の直径、ベキ等のさじ加減で値が大きく変わります。しかし、近傍星の見積もりではこの値より 10 桁以上も大きな質量放出プロセス（ー10^{20} kg/年）は考えにくいので、近傍の恒星系からの寄与はほとんど無いといえそうです。

分子雲の見積もりでは固体質量の半分が惑星や小天体として残っている太陽系の惑星形成（標準モデル）を想定していますが、エキセントリック・プラネットが形成されるような原始惑星系円盤（原始太陽系円盤の数倍重いと考えられている）等からは数桁も多くのダストが放出されている可能性があります。さらにオリオン座分子雲は、おうし座分子雲よりも約 1,000 倍重く、多数の大質量星を形成していますが、大質量星における惑星形成のプロセスはよくわかっていません。大質量星の近傍では強力な紫外線によりダストが蒸発してしまうと考えられておりますが、オリオン座分子雲では褐色矮星や木星質量の数倍程度の浮遊惑星も発見されており、大量のダストが放出されている可能性もあります。

晩期型星起源のダストは密度が極めて小さいので、地球大気との衝突によって破砕され、流星として観測することができないかも知れません。一方で、タールのような有機物が主成分のダストは 200K 以上で粘着性が高くなり、3AU（スノーライン）より内側ではコンパクトになって、彗星ダストに近い密度なっている可能性もあります。また、AGB 星は最晩期に激しい質量放出（新星爆発）を起こして、それ以前に放出されたダストをかき集めて球殻状（惑星状星雲）や砂時計状に広がります。この部分では密度が何桁あるいは十何桁も高くなっていると思われます。このような領域が太陽系を通過する際には大量の系外流星が降り注ぐことでしょう。そして氷河期？

今回の見積もりでは f30mm 口径 25mm の光学系と I.I.-TV による分光の限界等級として 2 等としていますが、最新の電波観測では 10^{-10} kg （12 等程度）の流星軌道を求めることができ、流星数を約 5 桁稼ぐことができます。また、銀河面の体積と天文学的な時間を積分すると、かなり大きな値になります。太陽系は銀河系のオリオン腕にありますが、近傍の腕に沿った方向と鉛直方向に系外流星の異方性が見られるかも知れません。そこで、電波観測による系外流星の到来方向に関する文献を調査しました。図 2 のキエフの電波観測データ[3]は 1<e<1.1 なので太陽系天体が多く含まれていると思われますが、おひつじ座から、さんかく座あたりのピークは、おうし座分子雲やオリオン座腕、ペルセウス腕の方向とほぼ一致します。一方、New Zealand のデータ[4]には、いて座（λ : 260°，β : 0°）近傍にピークが見られ、いて座腕や銀河中心方向になります。ただし、双方のデータには、うお座近傍以外の相関が見られません。

現時点では写真やビデオ等の光学観測によって系外流星を捉えた例 [5, 6]は多くありませんが、分光観測による物質組成比の統計的なデータが得られるようになると、その起源についての描像が浮かび上がってくることでしょう。

参考文献

[1] 海老塚 昇, 前田 幸治, 中村 卓司, “太陽系外からの流星の分光観測”, 第120回流星物理セミナー集録, (2008)

[2] http://www.geo.titech.ac.jp/lab/ida/STUDIES/basic_process.html

[3] B.L. Kashcheyev, S.V. Kolomiyets, “Interstellar particle Detection and Selection Criteria of Meteor Streams”, *Proc. the Meteoroids 2001 Conference*, **ESA SP-495**, 643 - 650, (2001).

[4] Baggaley, W. Jack, “Advanced Meteor Orbit Radar observations of interstellar meteoroids”, JGR, **105**, 10353-10362, (2000)

[5] R.L. Hawkes, S.C. Woodworth, “Optical detection of two meteoroids from interstellar space”, J. R. Astron. Soc. Can., **91**, 218, (1997)

[6] S.C. Woodworth, R.L. Hawkes, “Optical Search for High Meteors in Hyperbolic Orbits”, ASP Conf. Ser., **104**, 83, (1996)

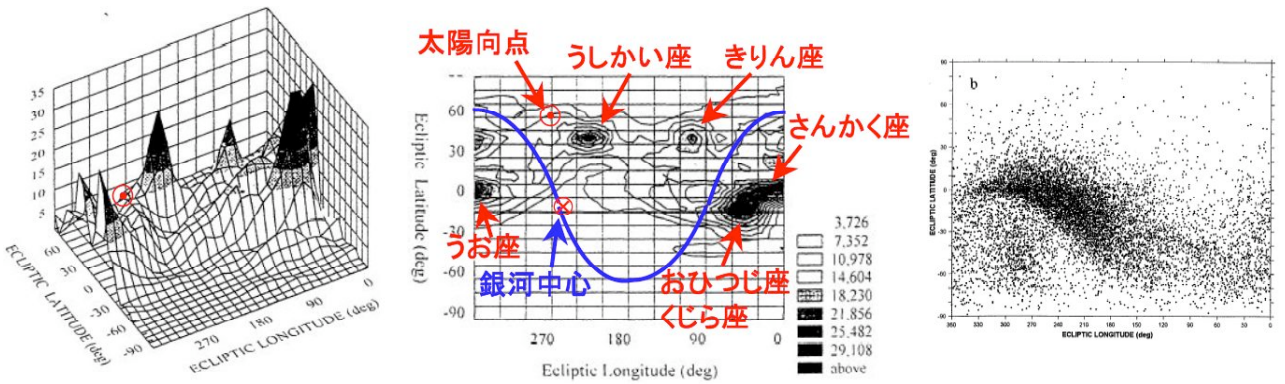

Fig. 2. N=N (β', λ') of 1102 hyperbolic orbits with 1 < e < 1.1 (1972-1978) in Kharkiv　　AMOR, 45<Vh<60 (1995-1998)

図2 Kharivにおける1<e<1.1の双曲線軌道の流星の到来方向分布（左と中央）[3]。
New Zealandにおける日心速度45ー60 km/sの流星の到来方向分布（右）[4]。

太陽系外から飛来する流星
Extra-Solar Meteor

GCOE研究会「太陽系外惑星とその形成」 3, September, 2009

海老塚 昇 (名大・プラズマナノ工学研究センター)
EBIZUKA, Noboru
(Plasma Nanotechnology Research Center, Nagoya Univ.)

重野 好彦 (流星物理セミナー)
SHIGENO, Yoshihiko
(Meteor Science Seminar)

Detection of interstellar media in the solar system

Particle with 10^{-19}~10^{-11}kg (Radius: 0.005~2 μm@1g/cm^3) are detected by particle counters of spacecrafts.
3~30% of particles at 1au are assumed to be interstellar media.
[M. Baguhl et.al. 1996]

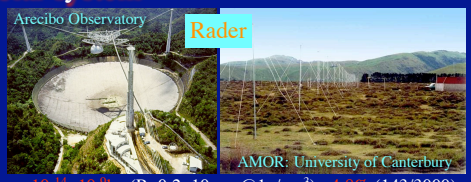

- 10^{-14}~10^{-9}kg (R: 0.2~10 μm@1g/cm^3), 4.8% (143/3000) → e >1.0 (Arecibo, Puerto Rico, D=300m, 430MHz).
- $5x10^{-9}$~10^{-6}kg (R: 10~100 μm@1g/cm^3), 3.2% (7,911 /250,000) → e >1.0 (MARS: Ukraine, 31.1MHz).
- >10^{-10}kg (R: >5 μm@1g/cm^3), 0.46% (1,600/350,000) → Ve > 100 km/s (e >2.5, AMOR, New Zealand).

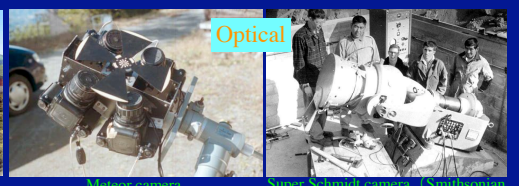

Meteor camera
http://www.ne.jp/asahi/meteor/star/index.html
Super Schmidt camera (Smithsonian Astronomical observatory, 1950s era)

10^{-4}~10^{-1} kg (R: 0.5~ 5 mm@1g/cm^3, Mag.: -3~ -10) : 1.3% (59/4,581, IAU/MDC Photograph),
10^{-9}~10^{-4}kg (R: 10~500 μm@1g/cm^3, Mag.: 9.5~ -3) : 1~2% (2/160, Video@Canada) → e>1.45 (Ve > 46.6 km/s).
e STD: ~ 0.1

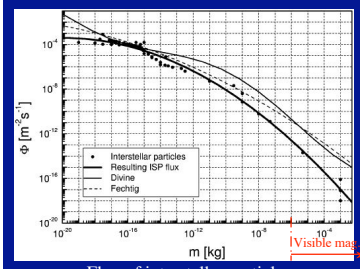

Flux of interstellar particles
[M. Hajduková Jr., et.al. (2006)]

Optical meteor observations of Mr. Shigeno

- Photograph in 1983, 1987, 1989 and 1991
- I.I. Video camera from 1992 to 2009.
- 3787 trajectory data of meteors.
- Data could download from http://www004.upp.so-net.ne.jp/msswg/ .

3722 meteors (~20, May.,2007) were investigated.

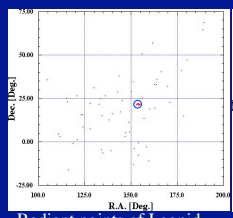

Radiant points of Leonid @18, Nov., 2001.
R.A. × Dec. : 2° × 1°

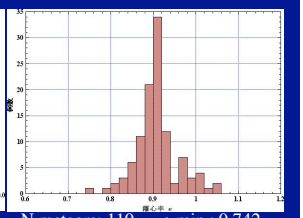

N meteors: 110 e min.: 0.742
e average: 0.908 e max. : 1.056
e STD of Leonid: 0.051

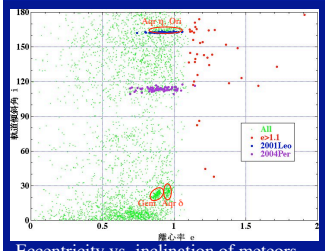

Eccentricity vs. inclination of meteors

Candidates of extra solar meteors

No.	q	e	Ω	ω	i	Ve	Vh	L abs	Precision, Asymptote direction
1	1.012	1.909	146.4	181.6	177.9	80.0	50.5	3.6	△ Leo (Approached to Saturn)
2	0.822	1.382	211.5	225.5	118.7	65.4	46.9	3.4	◎ CVn
3	0.882	1.244	54.2	36.4	134.5	68.7	45.2	0.9	◎ Ant
4	0.979	1.208	140.1	200.2	143.0	69.5	44.0	4.6	◎ Aur
5	0.916	1.180	54.7	329.8	153.3	71.9	44.3	-0.7	○ Psc
6	0.926	1.160	32.9	211.5	82.2	49.7		2.9	◎ Cas
7	0.964	1.146	140.3	155.3	116.4	62.1	43.4	3.8	○ Leo (Approached to Jupiter)

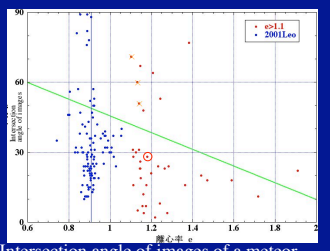

Intersection angle of images of a meteor trajectory projected on the celestial sphere.

q: 1.012 e: 1.909
Ω: 146.4 ω: 146.4
i : 177.9
Asymptote direction: Leo
Approached 5 au to Saturn

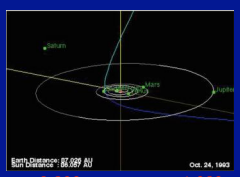

q: 0.822 e: 1.382
Ω: 211.5 ω: 225.5
i : 118.7
Asymptote direction: Cvn

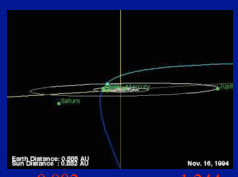

q: 0.882 e: 1.244
Ω: 54.2 ω: 36.4
i : 134.5
Asymptote direction: Ant

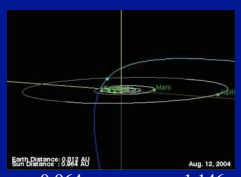

q: 0.964 e: 1.146
Ω: 140.3 ω: 155.3
i : 116.4
Asymptote direction: Leo
Approached 2 au to Jupiter

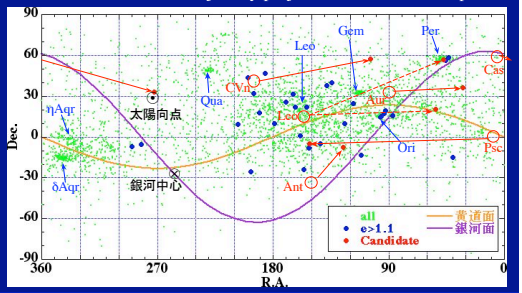

Stereoscopic and spectroscopic observation system for extra-solar meteors

UV-HDTV camera (UV sensitive I.I. -HDTV camera, above) and I.I.-HDTV camera with grism (Direct vision grating, below).

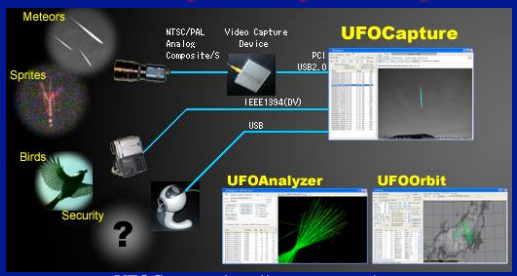

UFOCapture, http://sonotaco.com/

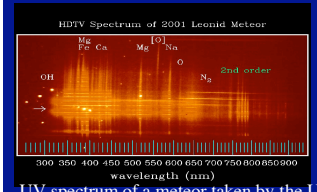

UV spectrum of a meteor taken by the UV-HDTV camera above and an objective spectrometer of reflection grating.

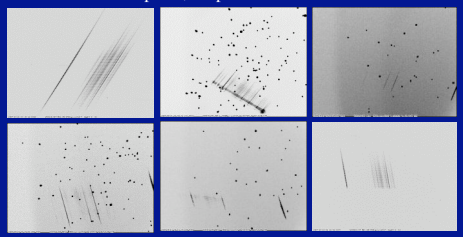

Meteor spectra taken automatically by a grism, CCTV camera and UFOCaptur. (Dr. K. Maeda, Mikyazaki Univ.)

- I.I.-HDTV camera is sensitive about 1 magnitude fainter than a I.I.-CCTV camera since a HDTV camera have 6 times pixels as a CCTV camera.
- 3 sets of I.I. HDTV cameras will be placed with 20~50 km in distance.
- Remote observations and automatic detection.
- ~240,000 (150 meteors x 8 hours x 200 nights) of meteors brighter than 8 magnitude will be detectable in a year?
- I.I. HDTV camera : ~$15,000/camera
  Initial costs : $100,000 ~ $200,000?
  Maintenance costs : ~ $20,000?
  Human resouce : 2 → 0.5 persons?

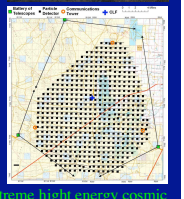

Telescope Array for observations of extreme hight energy cosmic ray. (Institute for Cosmic Ray Research, Univ. Tokyo, Utah, USA)

Conclusions

- 0.99% (37/3722) of meteors on Sigeno's observations are e>1.1.
- Trajectory of 2 meteors have been influenced by Jupiter or Saturn, nevertheless, 5 meteors (0.13%) are supposed to be extra-solar meteor, among the 7 candidate meteors.
- Several 100,000 of meteors (< 8 mag.) will be detectable in a year by stereoscopic observations with I.I.-HDTV camea.
- Spectral observations for meteors with hyperbolic trajectory provide direct information of abundance of extra-solar systems.

太陽系外から飛来した流星

海老塚 昇 (名大・プラズマナノ工学研究センター)、
重野 好彦 (流星物理セミナー)

第123回　流星物理セミナー　　2009年10月4日

太陽系における星間物質の検出

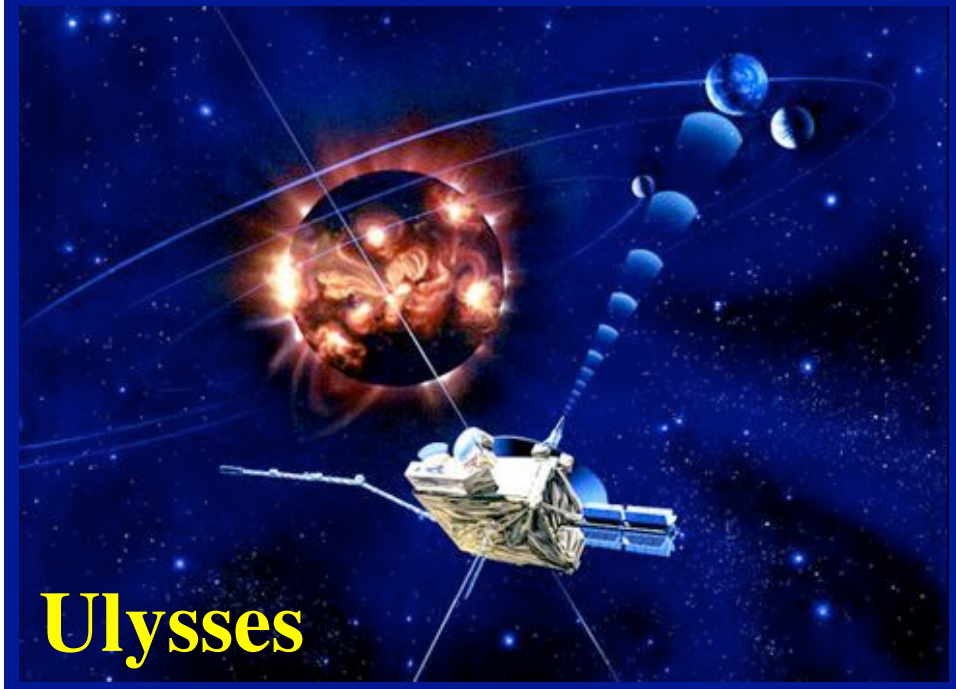

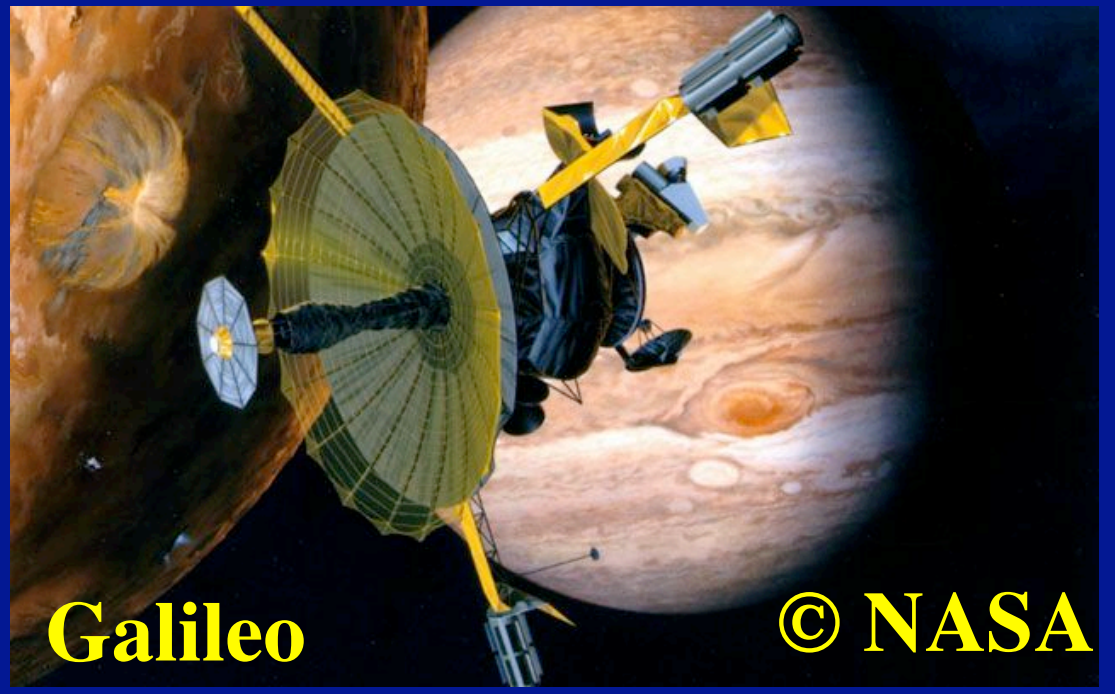

探査機等のParticle counterによって10^{-19}~10^{-11}kg
(直径: 0.005~2 μm@1g/cm^3) の粒子を検出。

半数以上が星間ダストと思われる。

流星レーダ観測

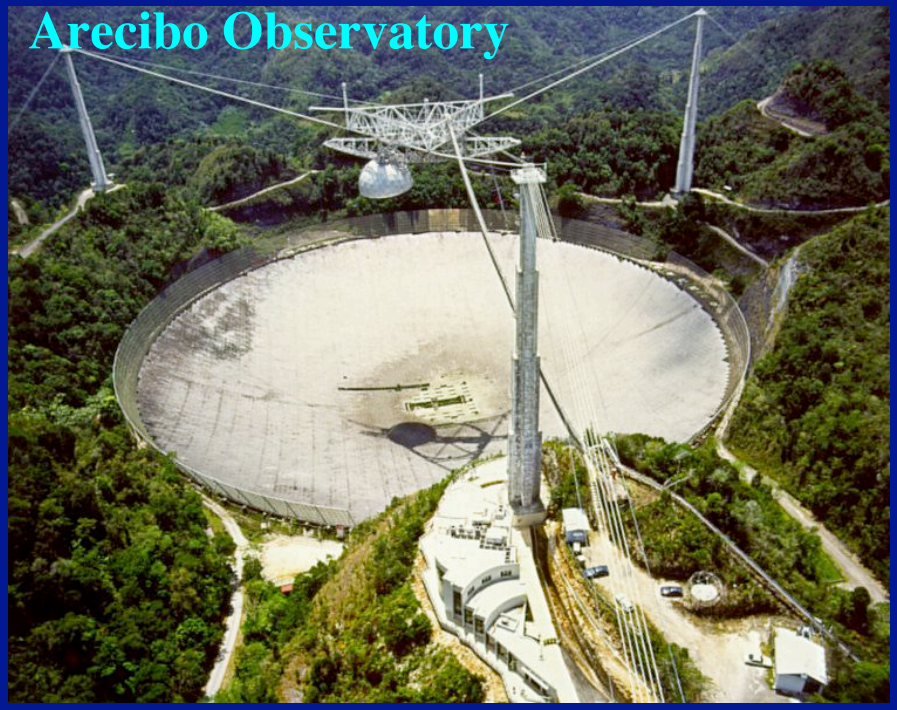

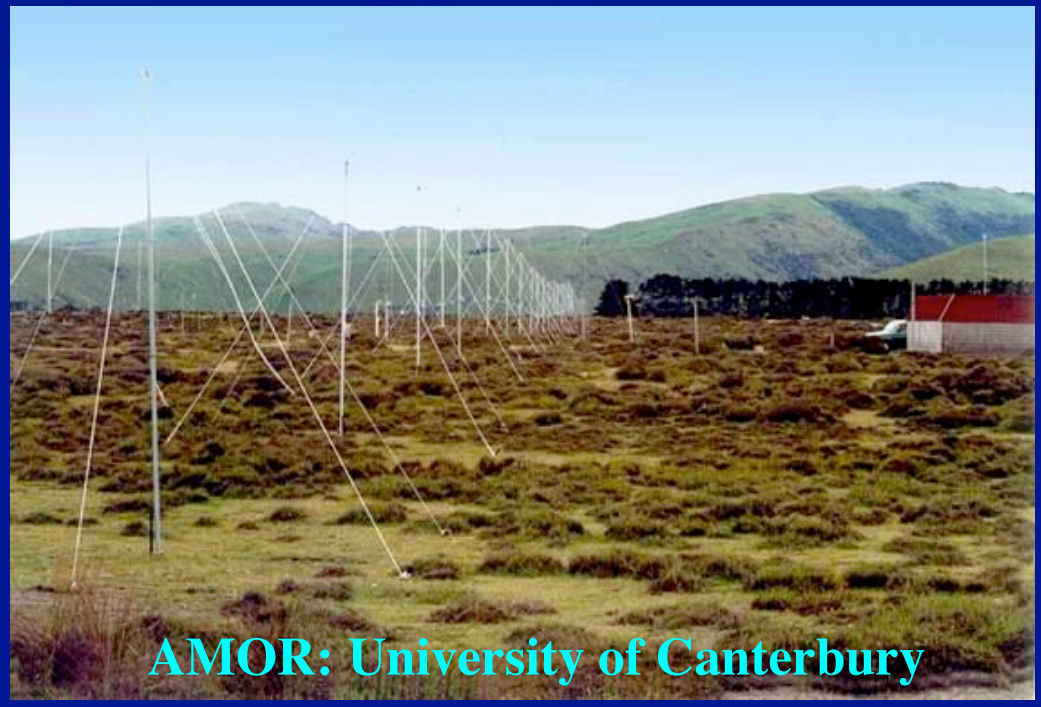

- 10^{-14}~10^{-9}kg (直径: 0.2~10 μm@1g/cm^3) : 4.8% (143/3000) が e>1.0 (Arecibo,プルトリコ, 口径300m, 430MHz)。
- $5x10^{-9}$~10^{-6}kg (直径: 10~100 μm@1g/cm^3) : 3.2% (7,911/250,000)がe>1.0 (MARS: ウクライナ, 31.1MHz)。
- >10^{-10}kg (直径: >5 μm@1g/cm^3) : 0.46% (1,600/350,000) が地心速度 > 100 km/s (e>2.5, AMOR, ニュージーランド)。

光学観測

10^{-4}~10^{-1} kg (-3~ -10等): 1.3% (59/4,581)と10^{-9}~10^{-4} (9.5~ -3等) kg:1~2% (2/160)がe>1.45 (日心速度＞46.6 km/s、IAU/MDC銀塩写真、カナダのビデオ観測)。

四連写真儀
http://www.ne.jp/asahi/meteor/star/index.html

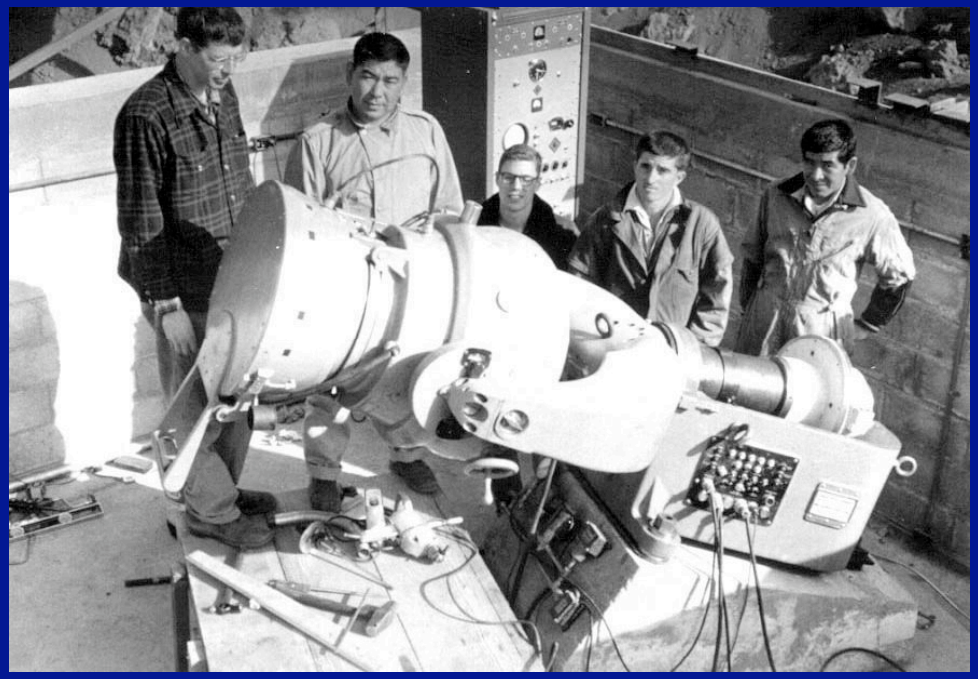

SAOのSuper Schmidt camera
（1950年代）

写真観測の精度

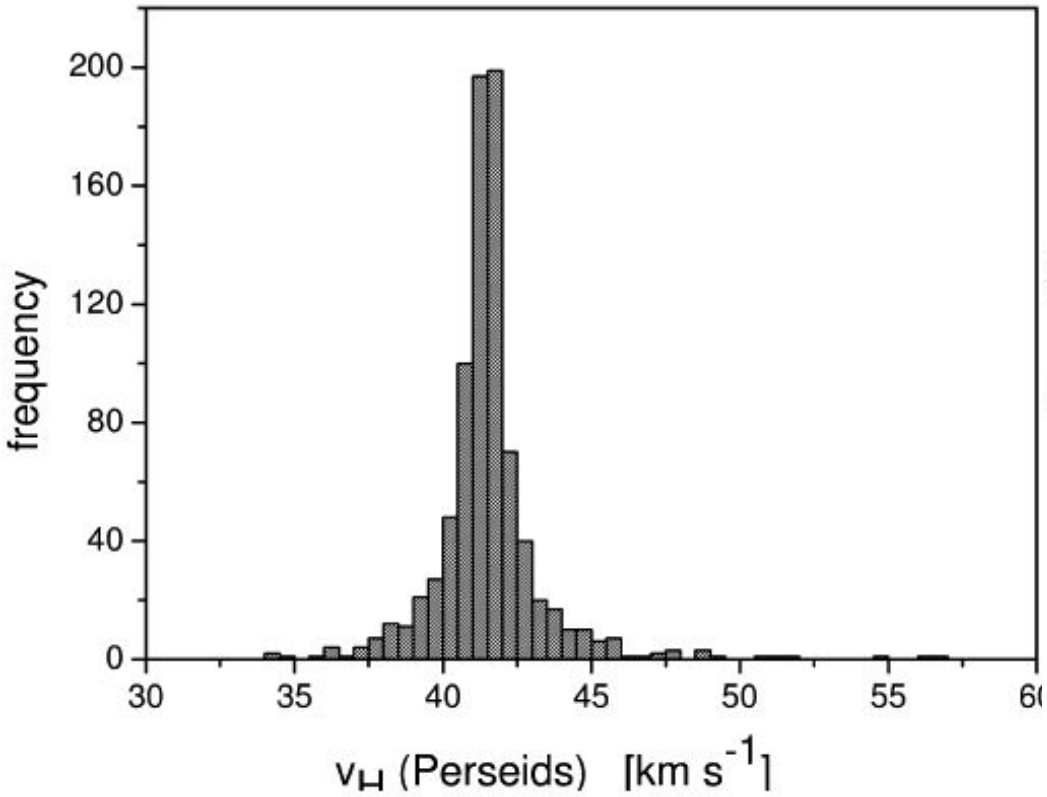

ペルセウス座流星群 (41.7 km/s) の速度分布。224/835 (27%)が > 42.1 km/s (e>1)、5/835 (0.6%)が > 46.6 km/s (e>1.45)。
標準偏差：1.3km/s (e: 0.11)?

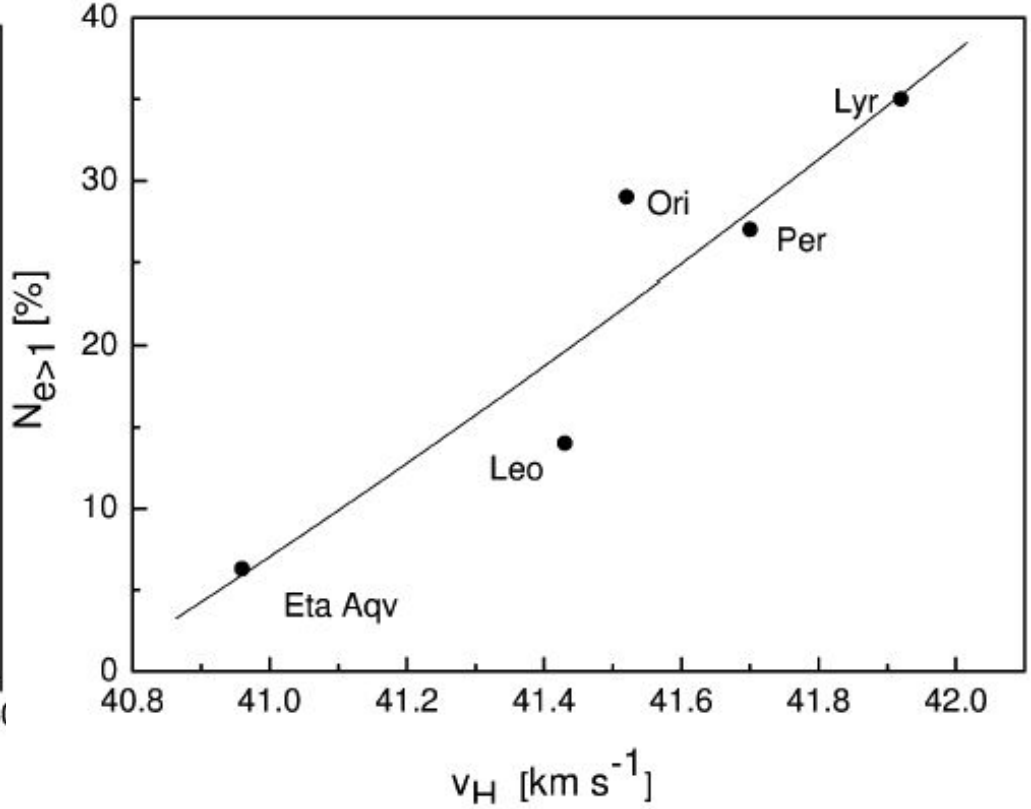

高速流星群の日心速度と e > 1の割合。

IAU/MDCの銀塩写真カタログ

M. Hajduková Jr., et.al. (2006)

重野 好彦氏等の流星ステレオ観測および軌道データ

- 3787個の流星軌道データ。
- 1983, 1987, 1989, 1991年は銀塩写真。
- 1992 ~2008年は主にI.I.+ビデオカメラ。
- http://www004.upp.so-net.ne.jp/msswg/ からダウンロード可能。

3722個の流星軌道データ（~2007.5.20）を使用。

しし座流星群の離心率分布

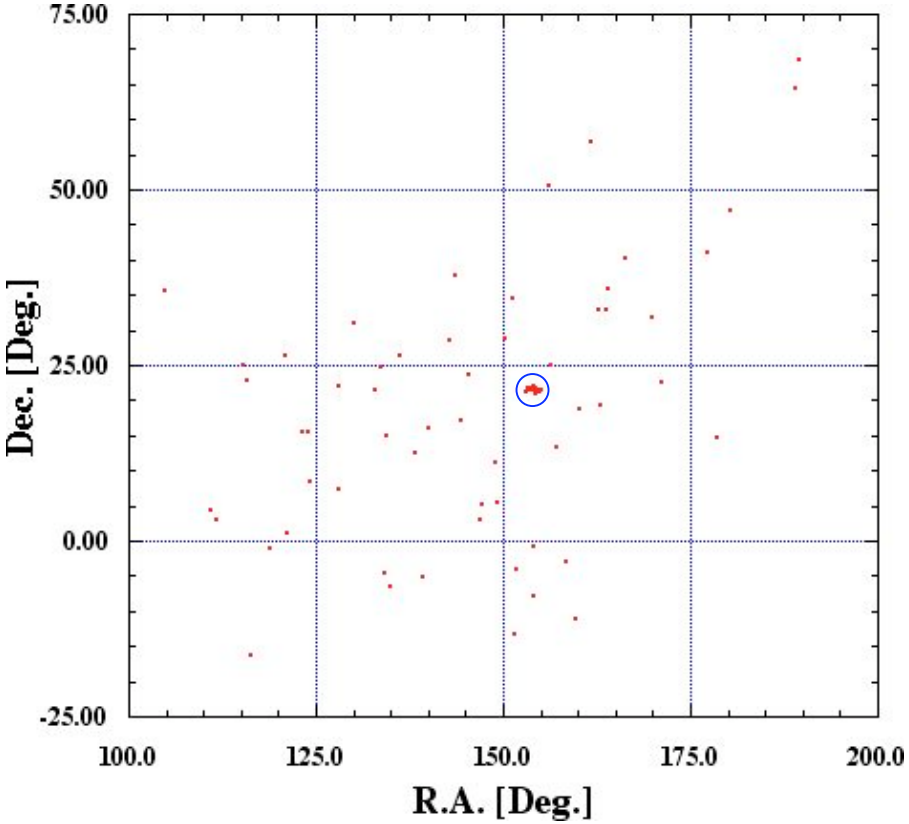

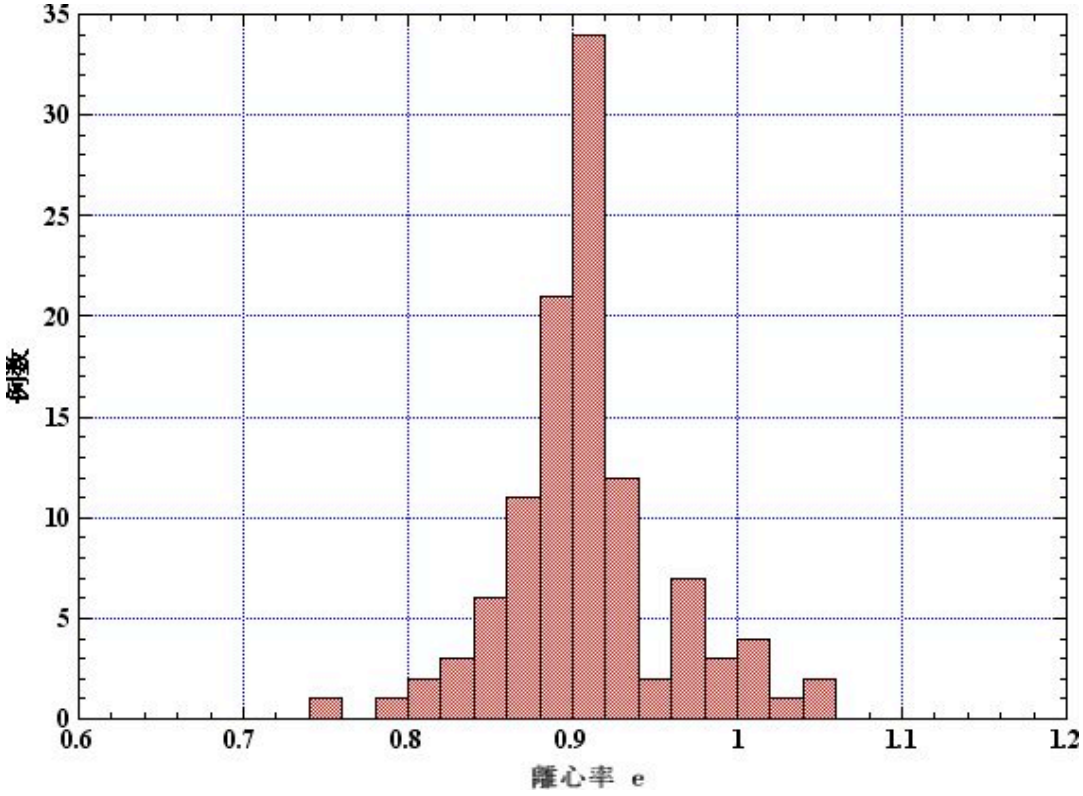

2001. 11. 18の輻射点、
R.A: 2°× Dec.: 1°の範囲。

流星数：110　　最小：0.742
平　均：0.908　　最大：1.056
標準偏差：0.051

離心率vs.軌道傾斜角

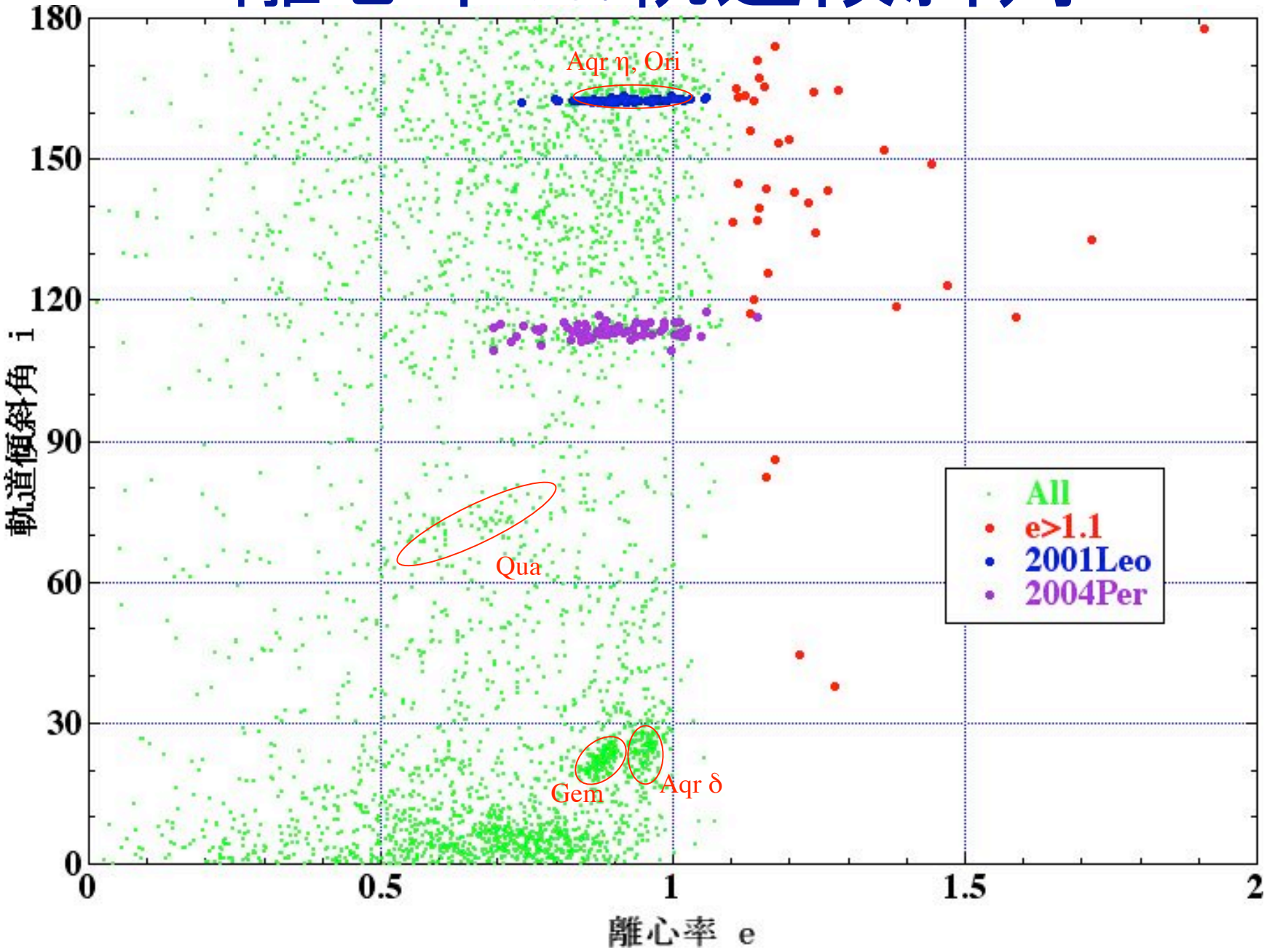
180
150
120
90
60
30
0
0
0.5
1
1.5
2
軌道傾斜角 i
離心率 e
Aqr η, Ori
Qua
Gem
Aqr δ
All
e>1.1
2001Leo
2004Per

地心速度vs.軌道傾斜角

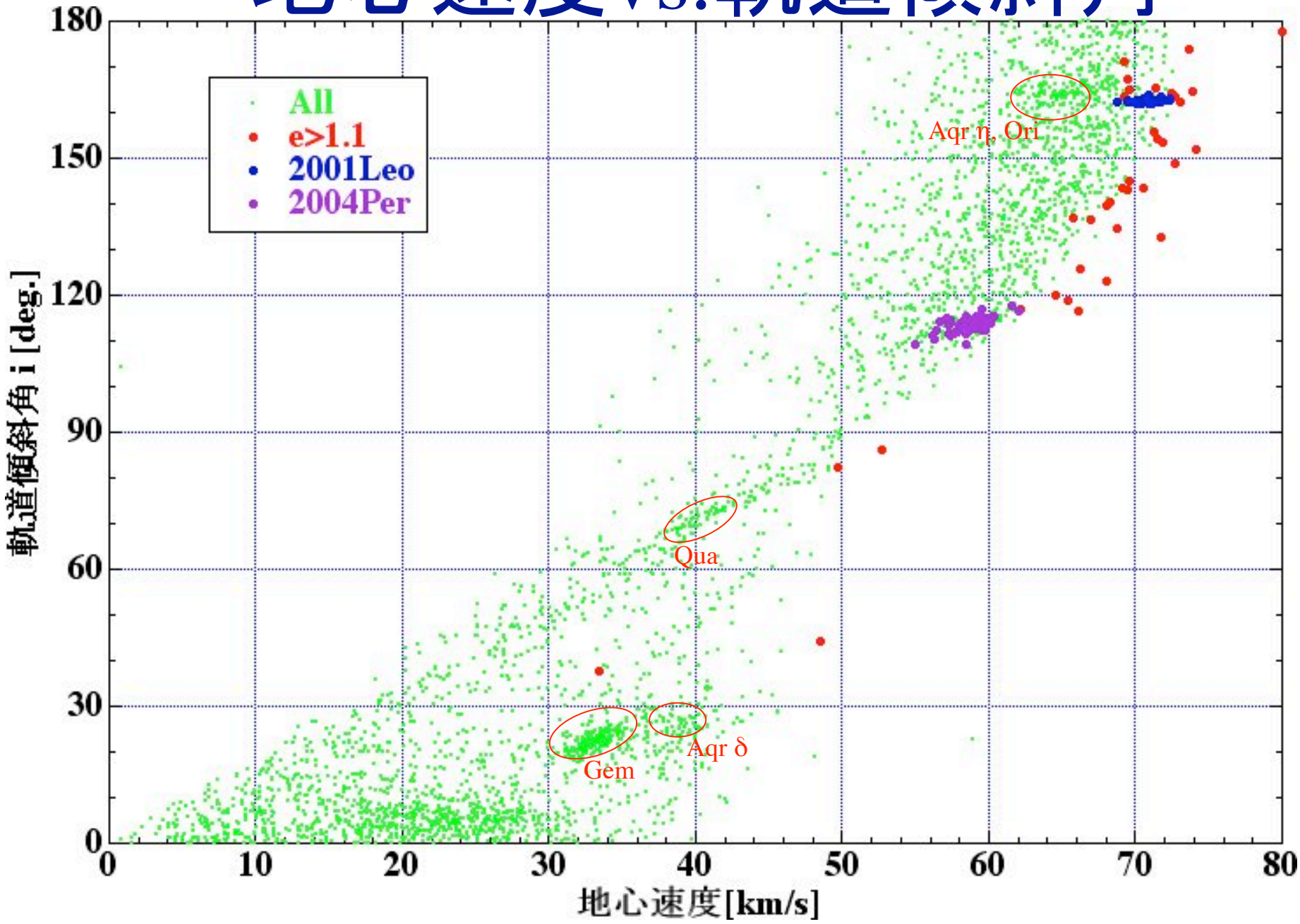

離心率 vs. 測定点数

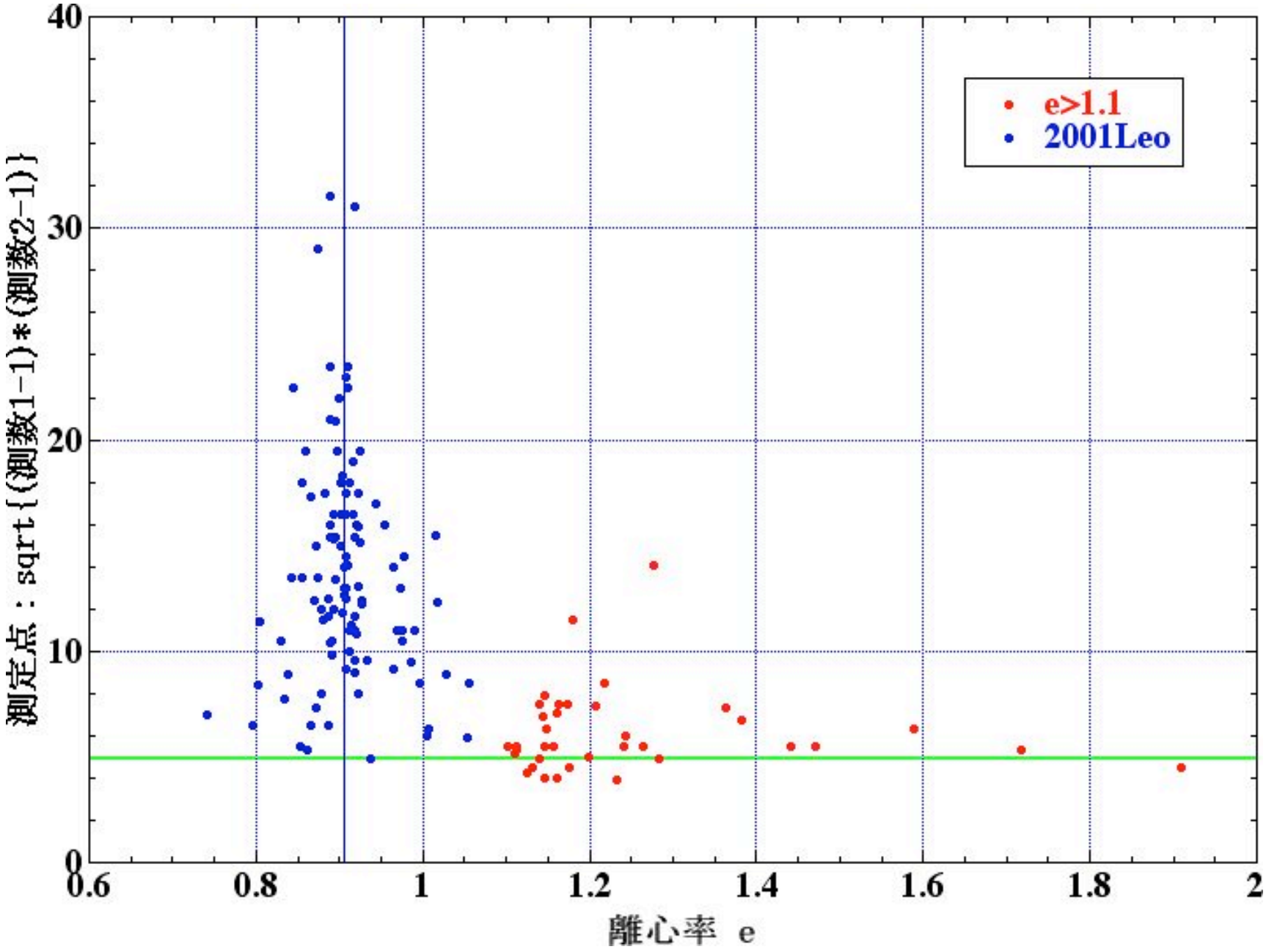
e>1.1
2001Leo
測定点：sqrt{(測数1−1)*(測数2−1)}
離心率 e
0
10
20
30
40
0.6
0.8
1
1.2
1.4
1.6
1.8
2

離心率 vs. 交差角

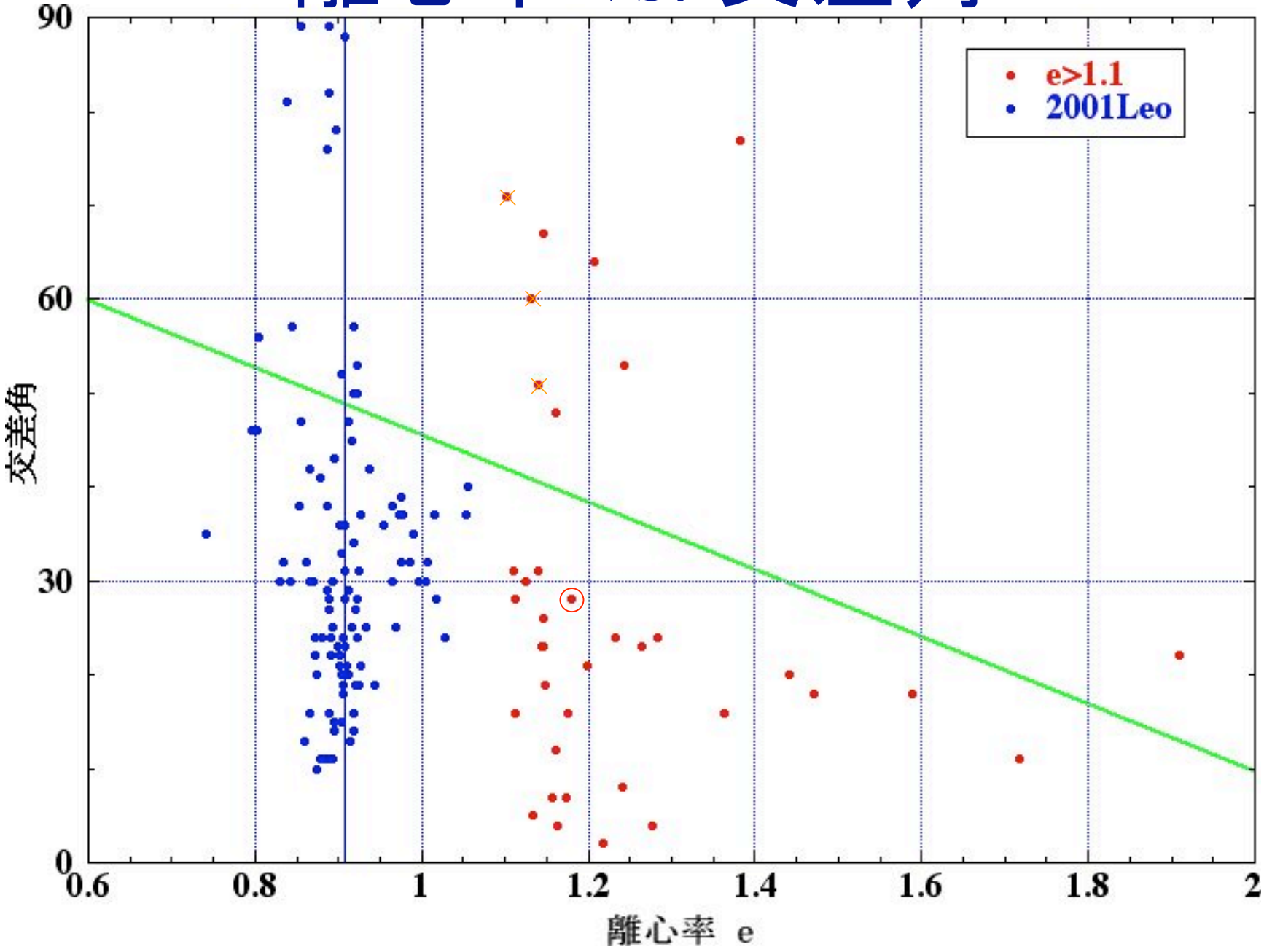

系外流星候補

No.	q	e	ω	Ω	i	Ve	Vh	L abs	精度、到来方向
1	1.012	1.909	181.6	146.4	177.9	80.0	50.5	3.6	△ しし座（土星に接近）
2	0.822	1.382	225.5	211.5	118.7	65.4	46.9	3.4	◎ りょうけん座
3	0.882	1.244	36.4	54.2	134.5	68.7	45.2	0.9	◎ ポンプ座
4	0.979	1.208	200.2	140.1	143.0	69.5	44.0	4.6	◎ ぎょしゃ座
5	0.916	1.180	329.8	54.7	153.3	71.9	44.3	-0.7	○ うお座
6	0.926	1.160	211.5	32.9	82.2	49.7		2.9	◎ カシオペア座
7	0.964	1.146	155.3	140.3	116.4	62.1	43.4	3.8	○ しし座（木星に接近）

系外流星候補1の軌道

q: 1.012　　e: 1.909

Ω: 146.4　　ω: 181.6

i : 177.9

到来方向：しし座

土星に約5 au接近

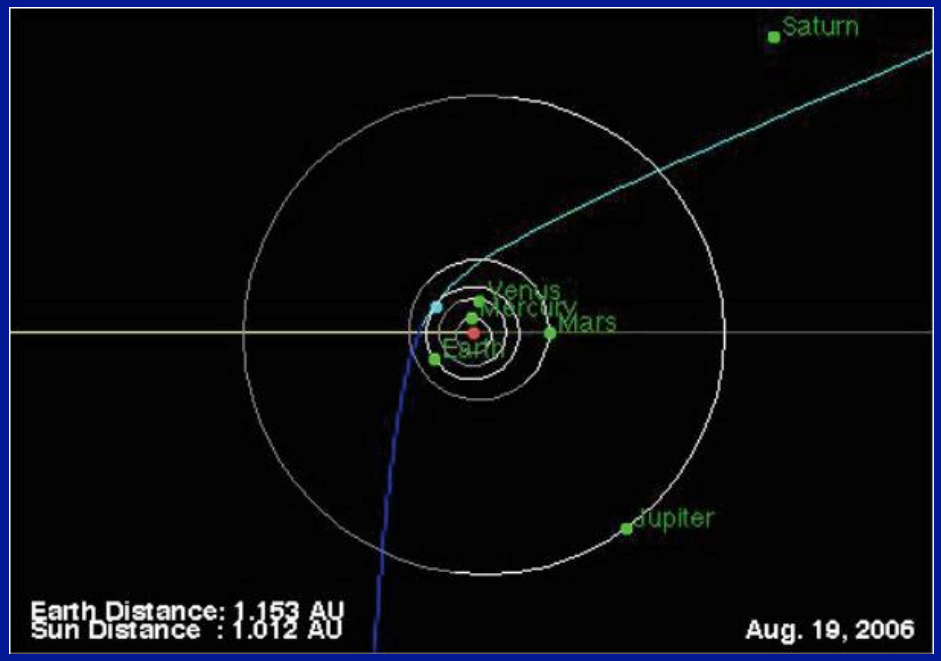

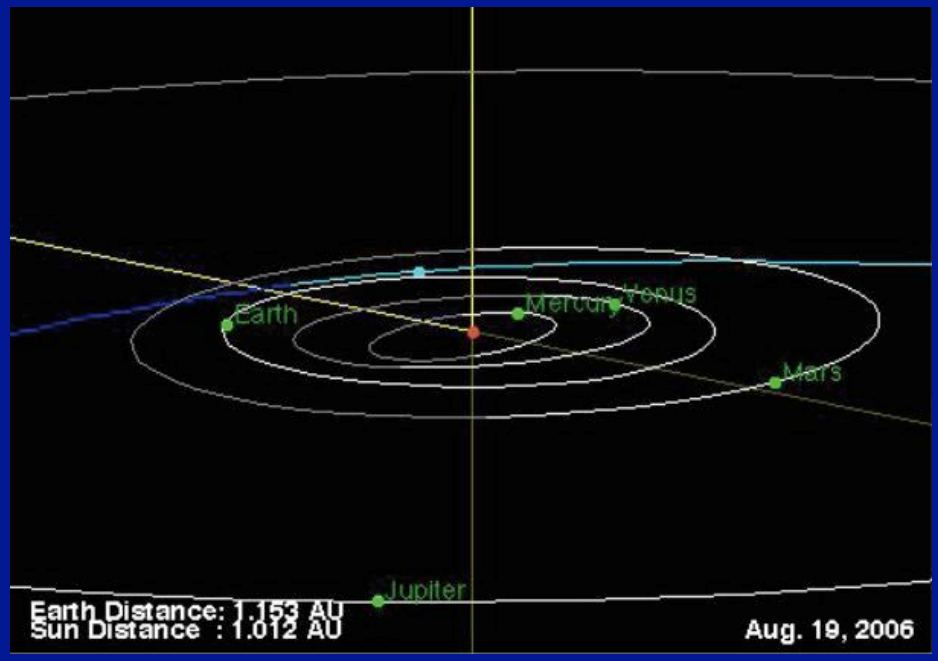

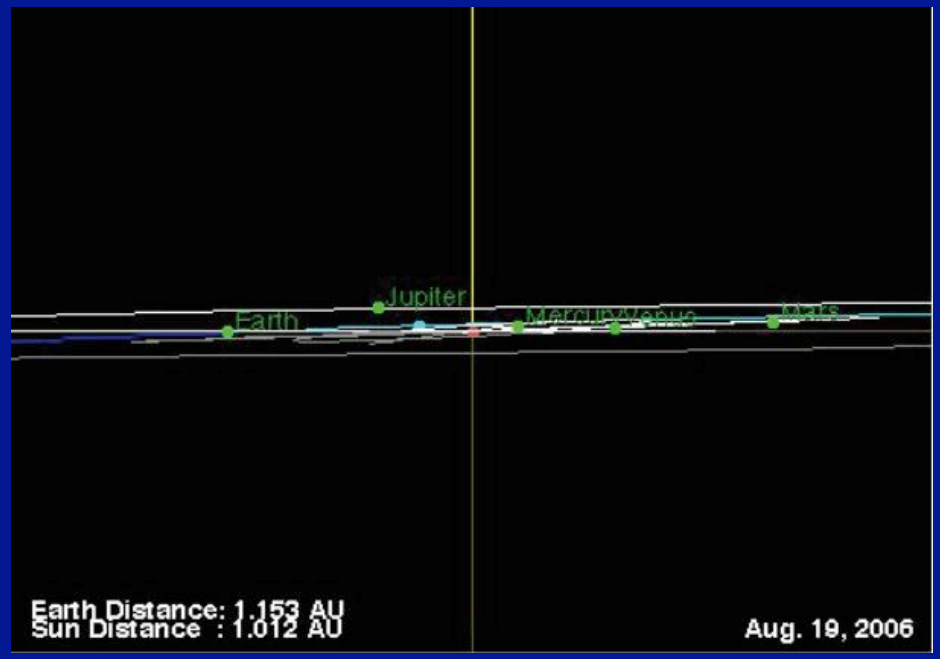

水星軌道ビュアー ©アストロアーツ

系外流星候補2の軌道

q: 0.822　　e: 1.382

Ω: 211.5　　ω: 225.5

i : 118.7

到来方向：りょうけん座

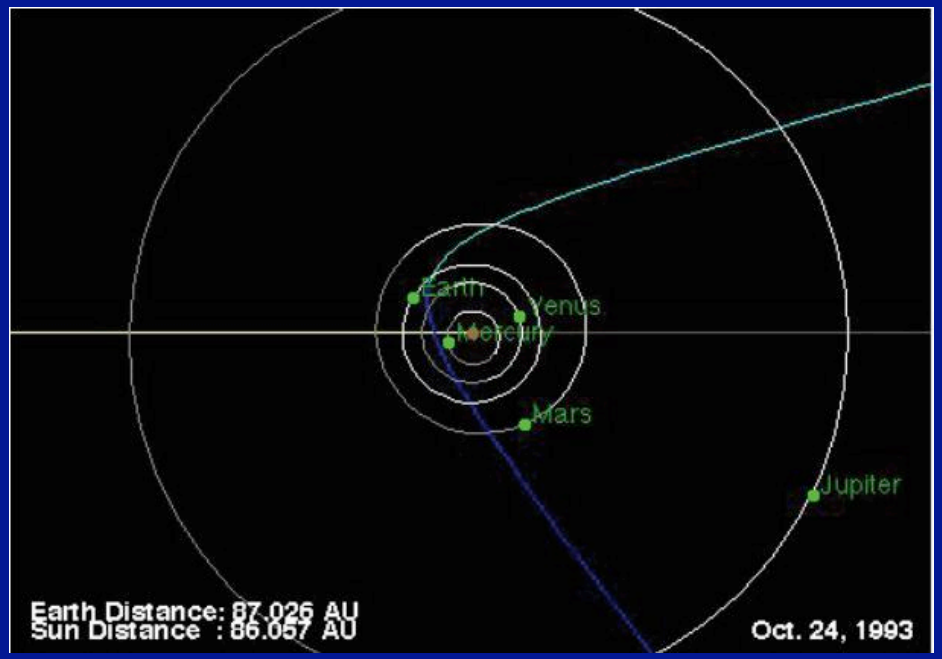

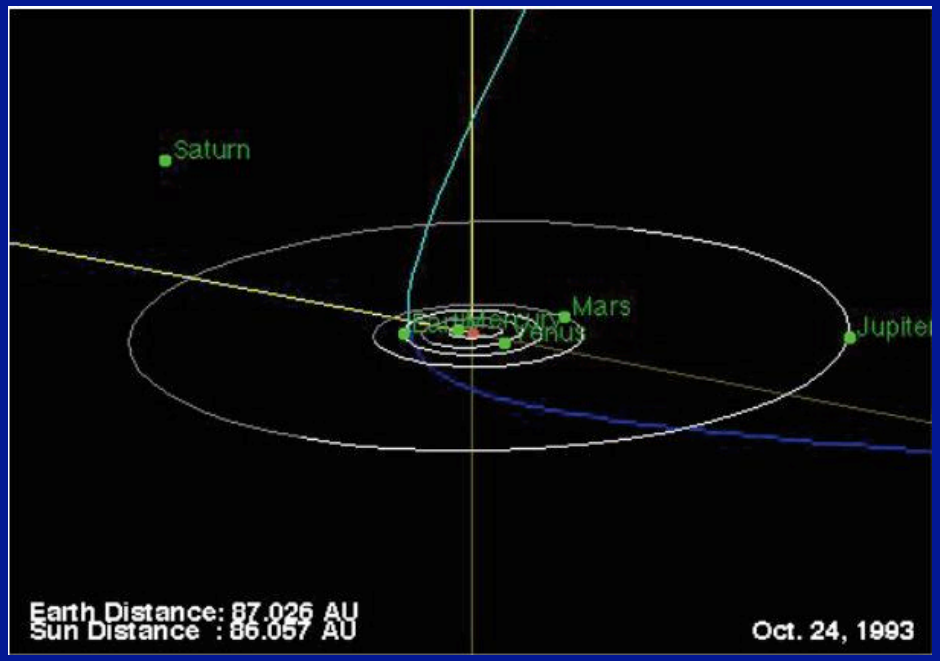

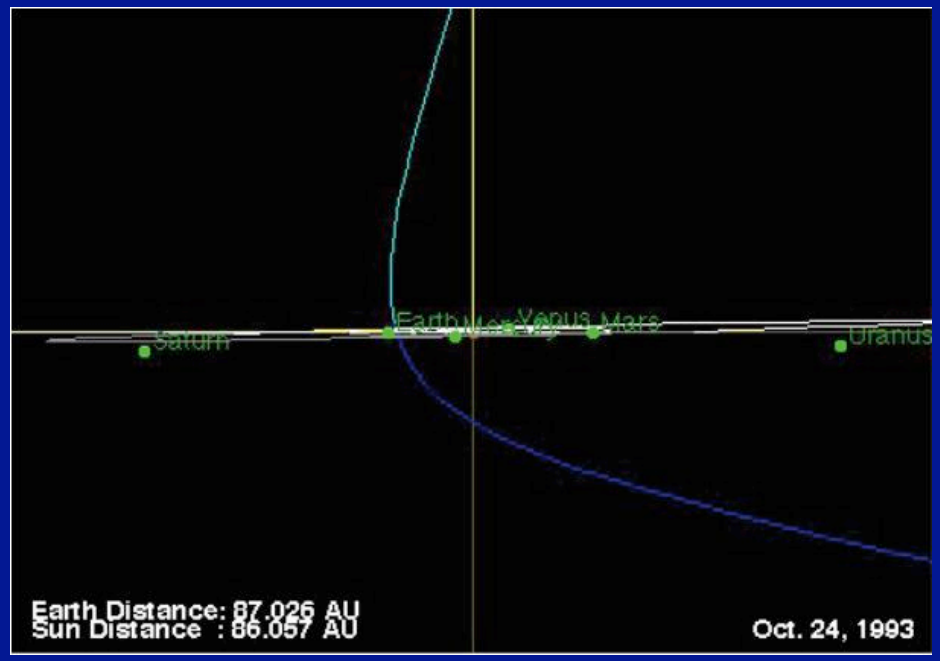

水星軌道ビュアー ©アストロアーツ

系外流星候補3の軌道

q: 0.882　　e: 1.244

Ω: 54.7　　ω: 36.4

i : 134.5

到来方向：ポンプ座

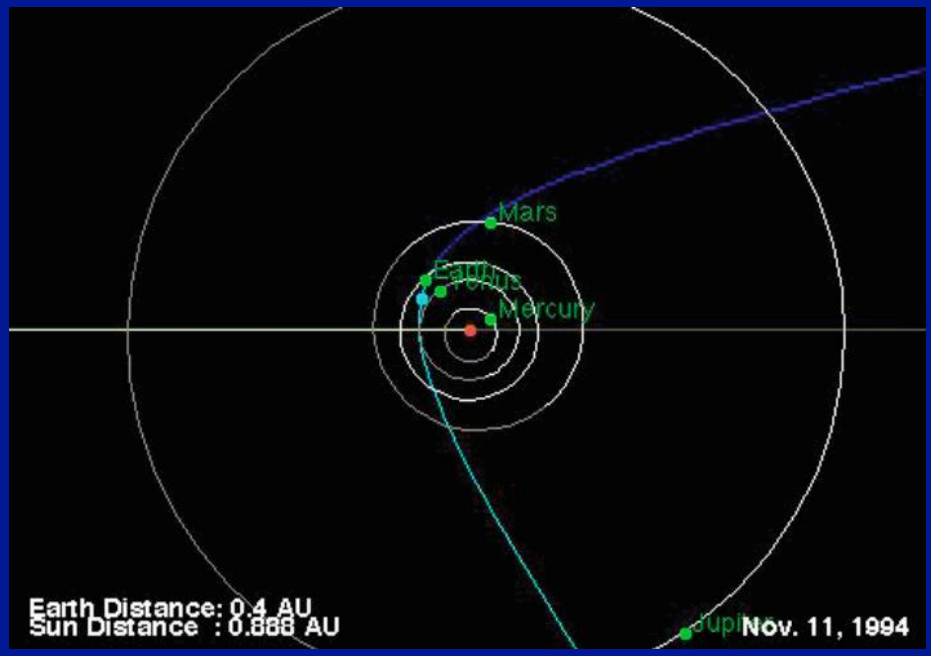

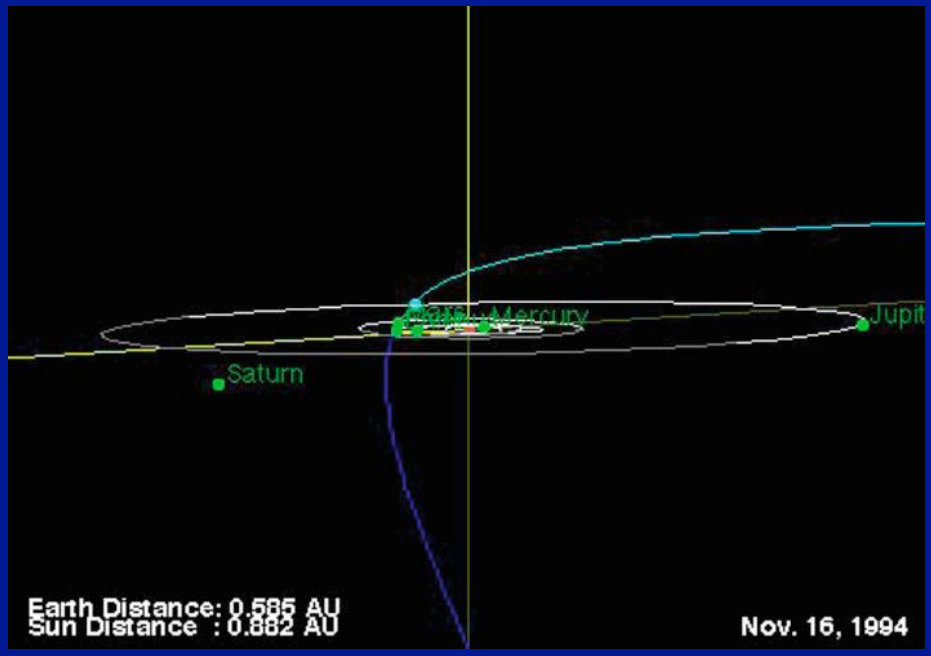

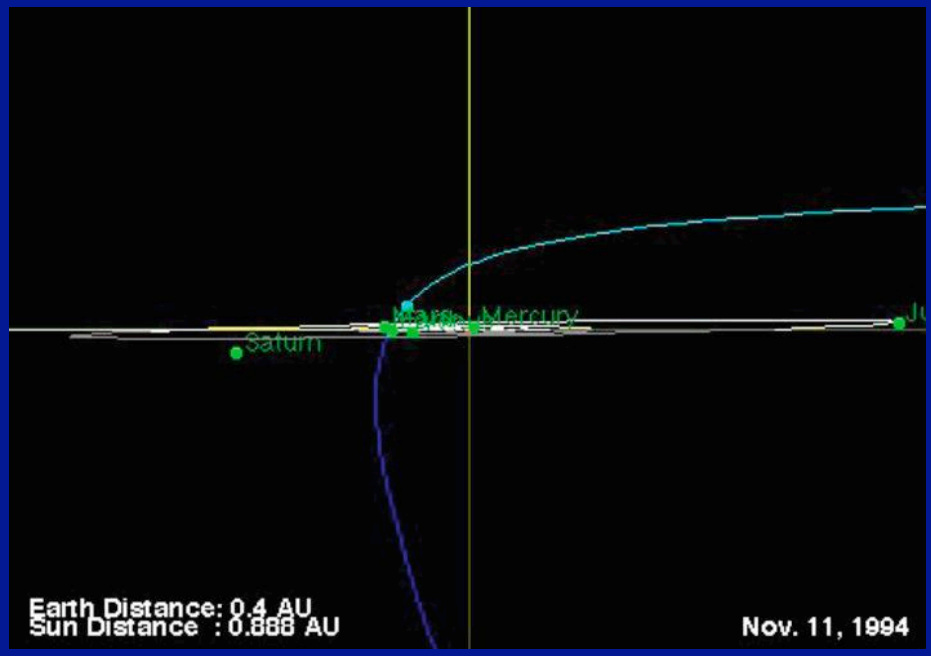

水星軌道ビュアー ©アストロアーツ

系外流星候補4の軌道

q: 0.979　　e: 1.208

Ω: 140.1　　ω: 200.2

i : 143.0

到来方向：ぎょしゃ座

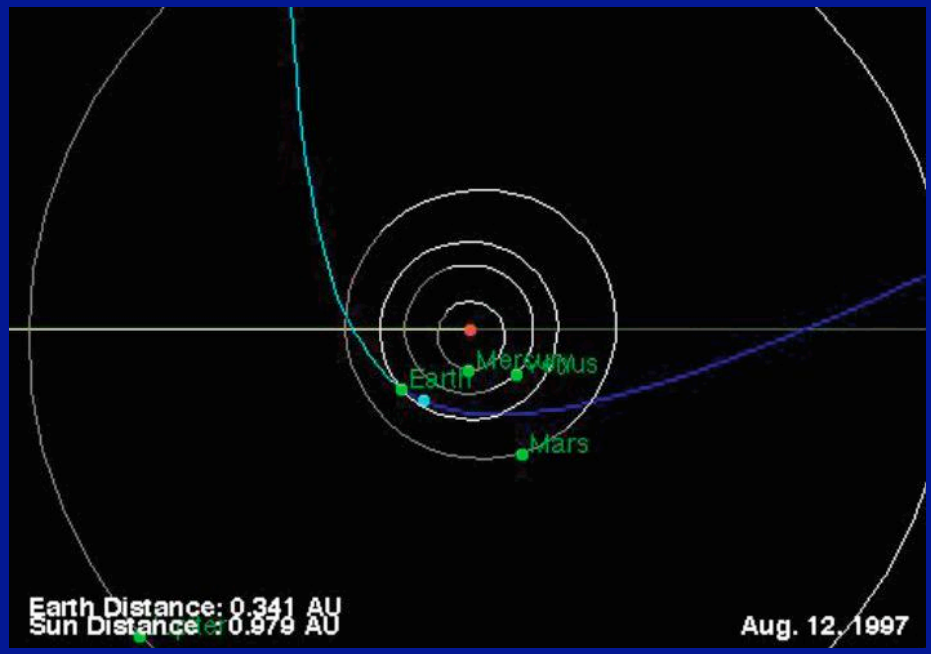

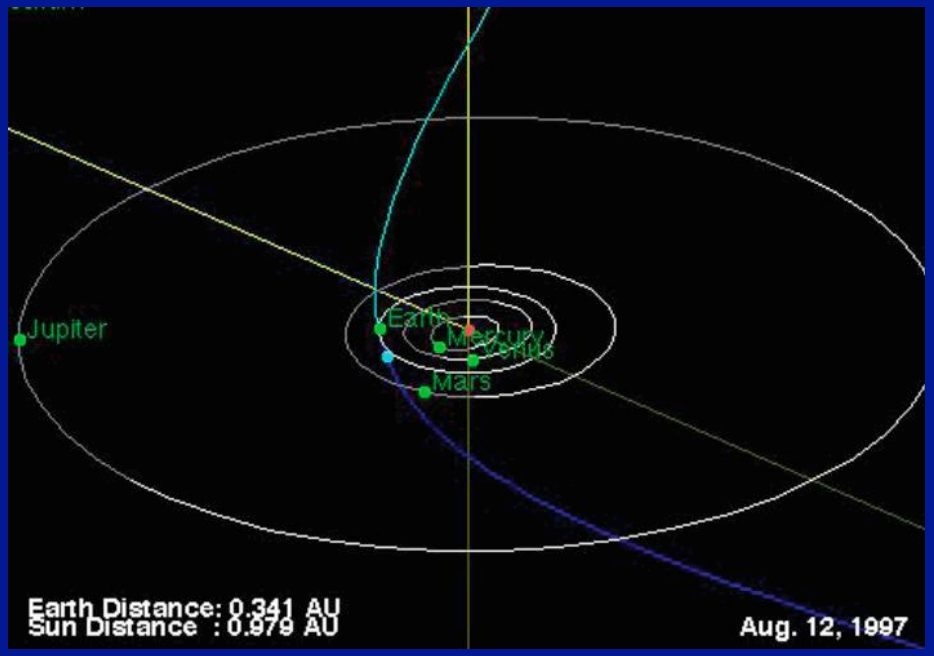

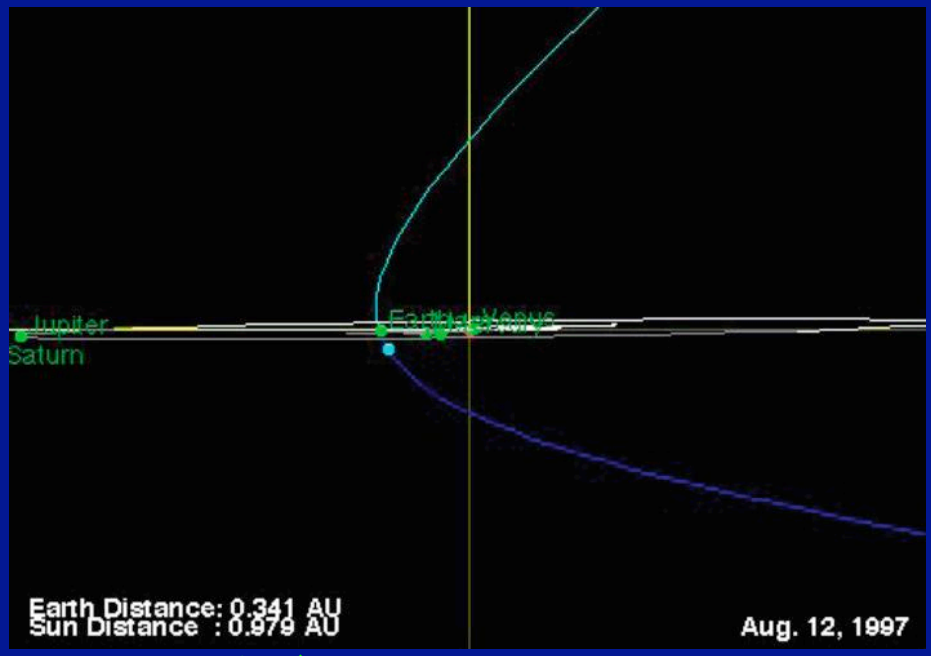

水星軌道ビュアー ©アストロアーツ

系外流星候補5の軌道

q: 0.916　　e: 1.180

Ω: 54.7　　ω: 329.8

i : 153.3

到来方向：ポンプ座

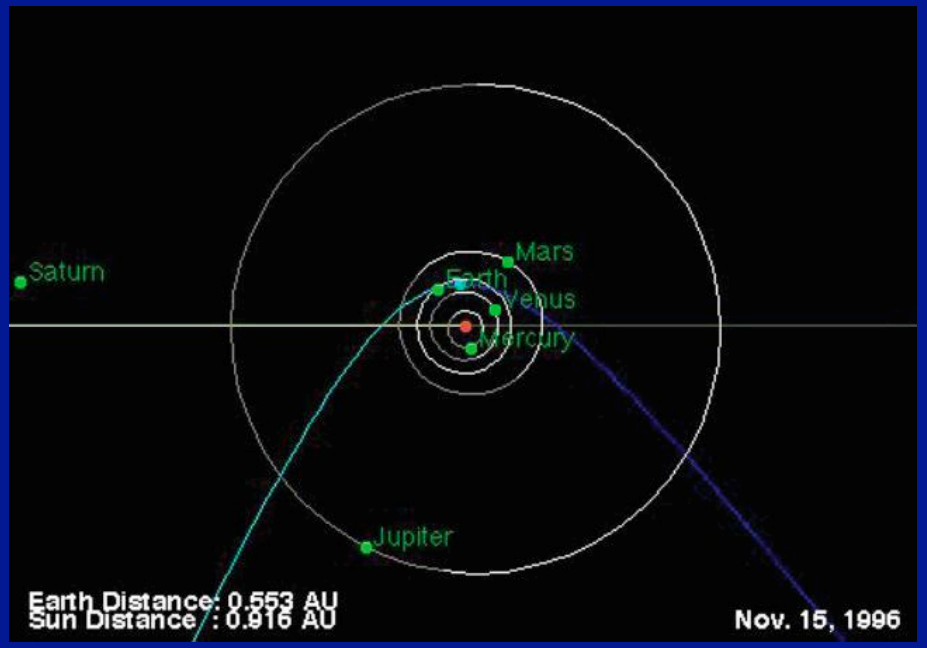

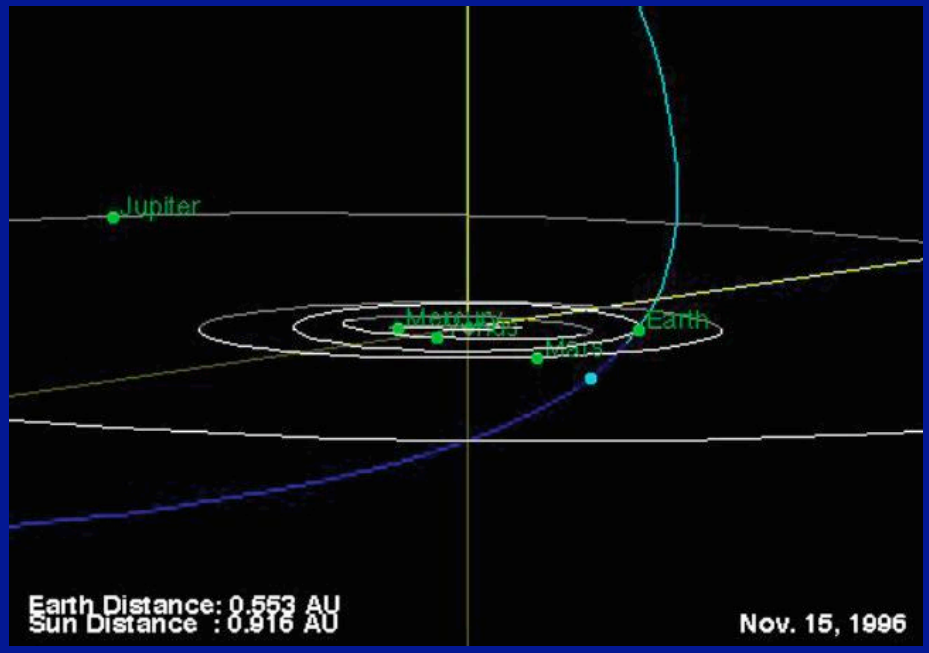

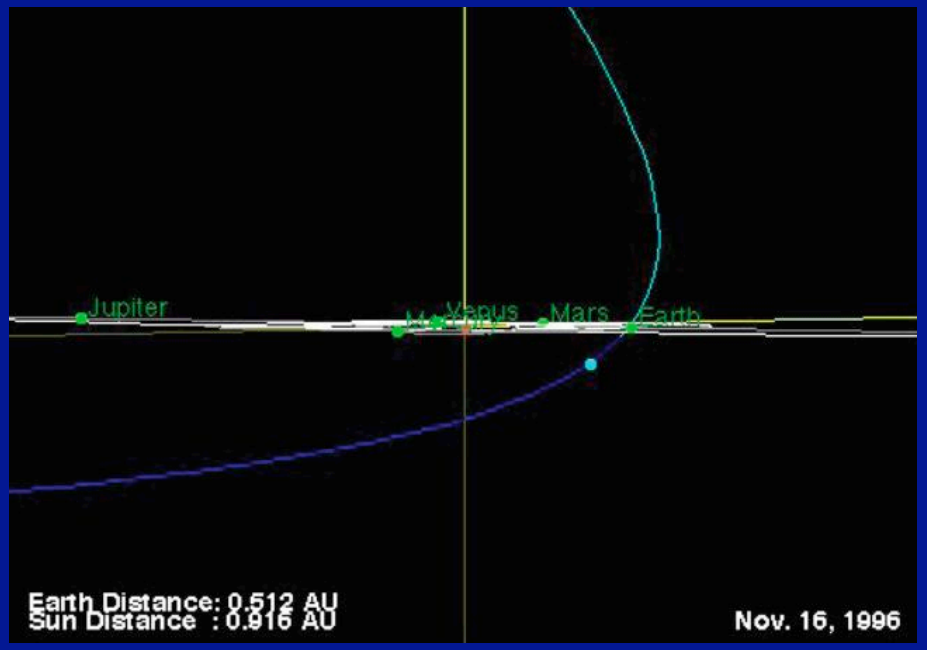

水星軌道ビュアー ©アストロアーツ

系外流星候補6の軌道

q: 0.926　　e: 1.160

Ω: 32.9　　ω: 211.5

i : 82.2

到来方向：カシオペア座

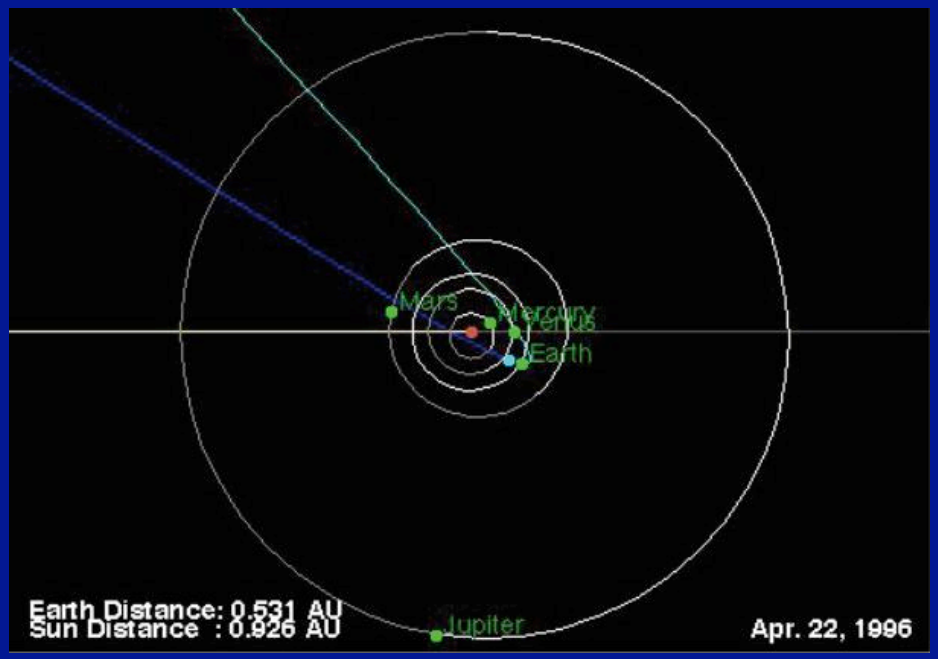

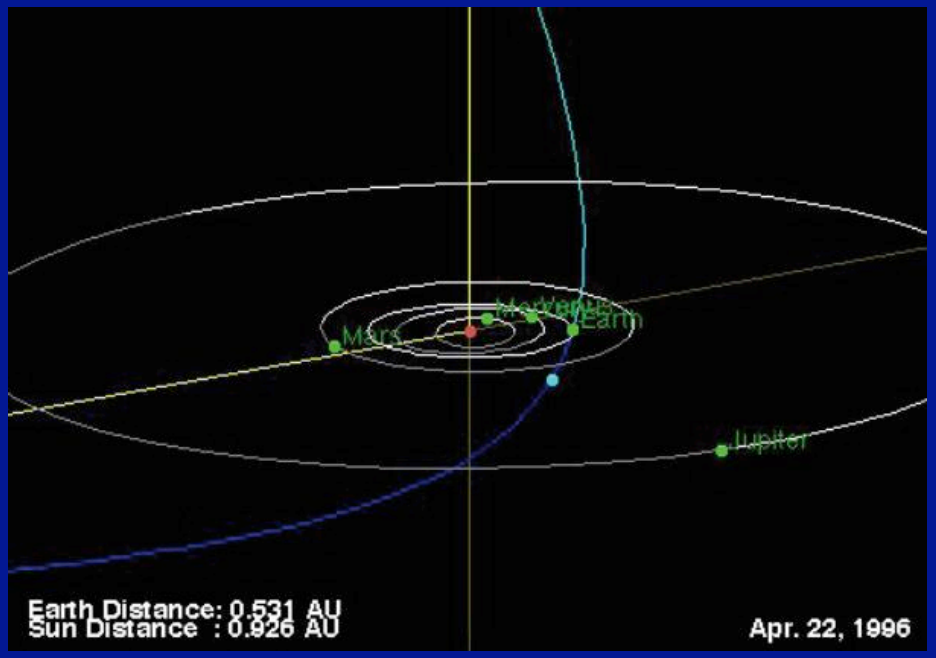

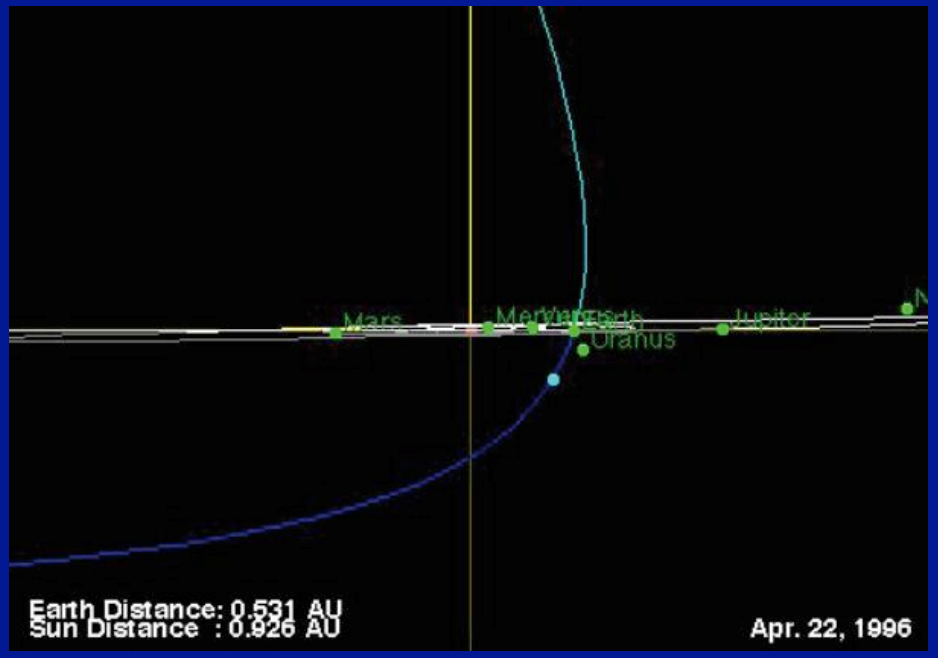

水星軌道ビュアー ©アストロアーツ

系外流星候補7の軌道

q: 0.964　　e: 1.146

Ω: 140.3　　ω: 155.3

i : 116.4

到来方向：しし座

木星に約2 au接近

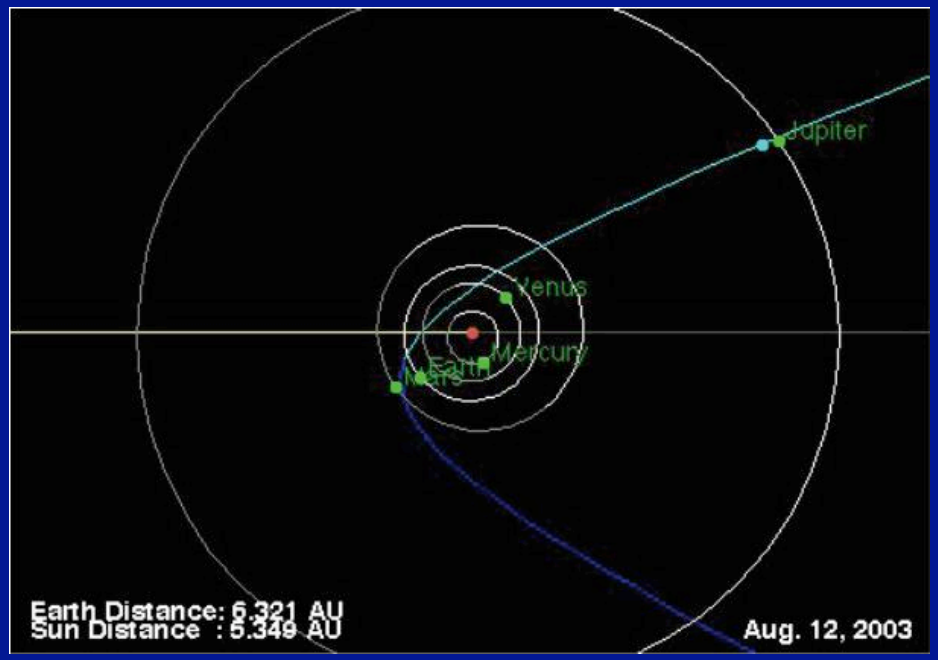

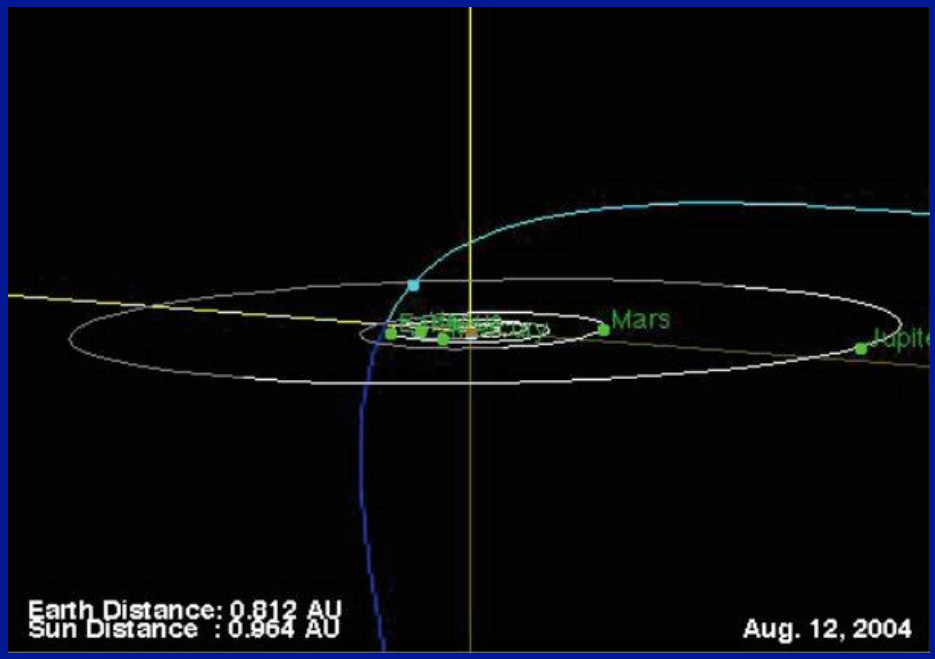

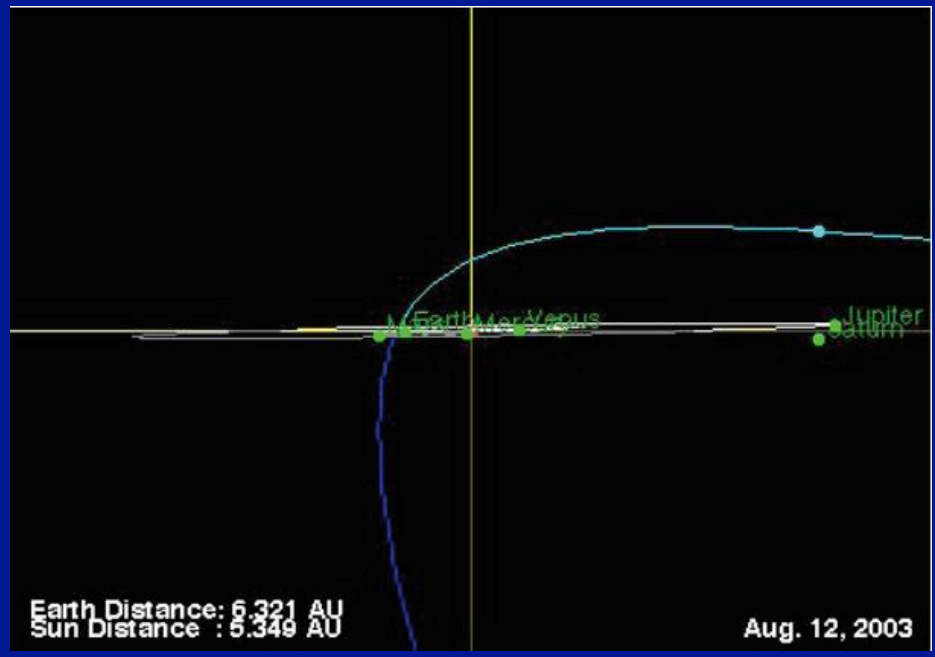

水星軌道ビュアー ©アストロアーツ

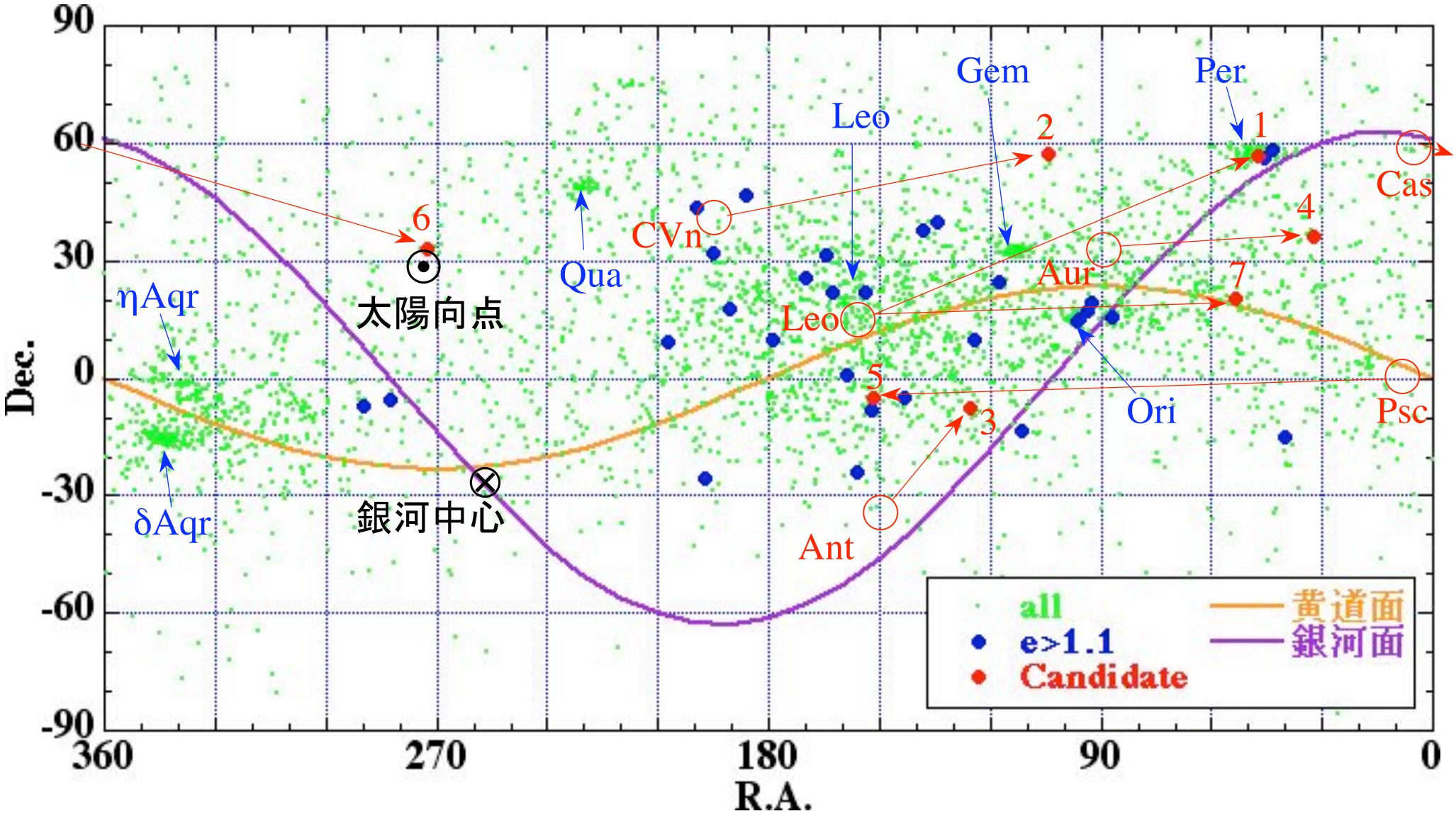
90
60
30
0
-30
-60
-90
Dec.
360
270
180
90
0
R.A.
Gem
Per
Leo
2
1
Cas
6
CVn
4
Qua
Aur
7
Leo
ηAqr
太陽向点
5
Ori
Psc
3
δAqr
銀河中心
Ant
all
e>1.1
Candidate
黄道面
銀河面

天球上の流星分布

ステレオ観測の結果

- しし群における離心率eの標準偏差: $\sigma = 0.05$。
- 37/3722 (1.0%) がe>1.1。
- 候補7流星のうち、
  - 2流星は木星や土星の影響を受けたと考えられる。
  - 5流星 (0.13%) は太陽系外から到来?

I.I.-ハイビジョンカメラの限界等級

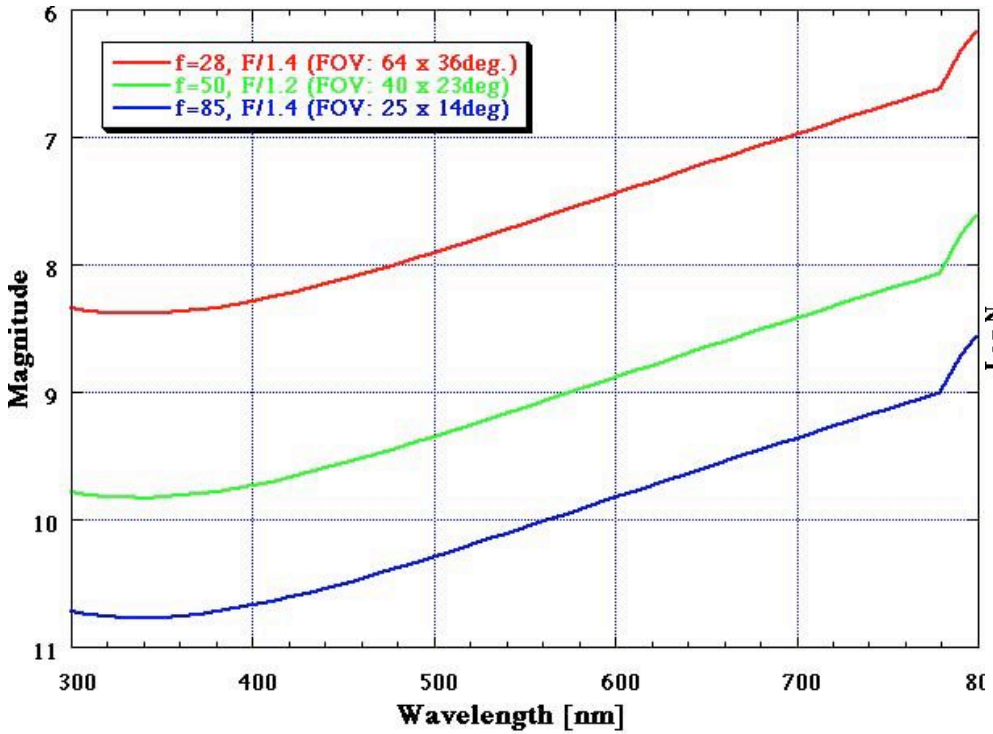

Limiting magnitude of color I.I.-HDTV
(t=0.033sec., R=3, Eff.=0.05, S/N=3)

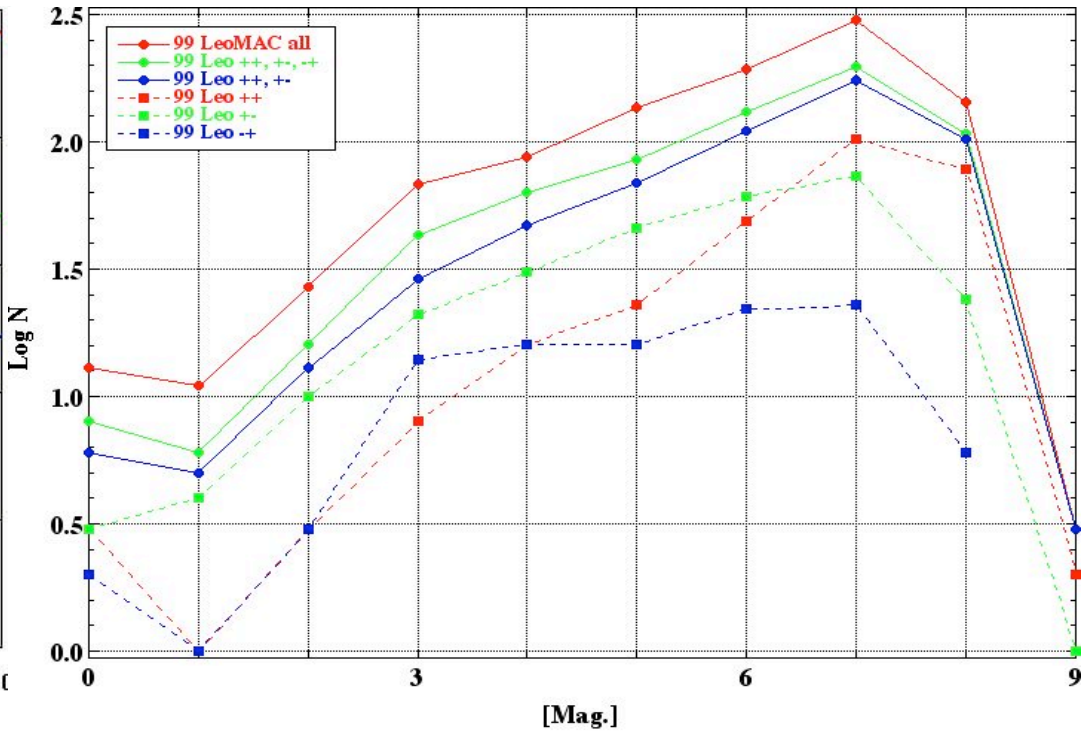

I.I.-HDTV (NHK)による、しし座流星群（1999年、地中海上空）の光度分布。

標準レンズの撮像限界等級は8等。

R=200の分光の限界等級は3等。

UFOキャプチャー

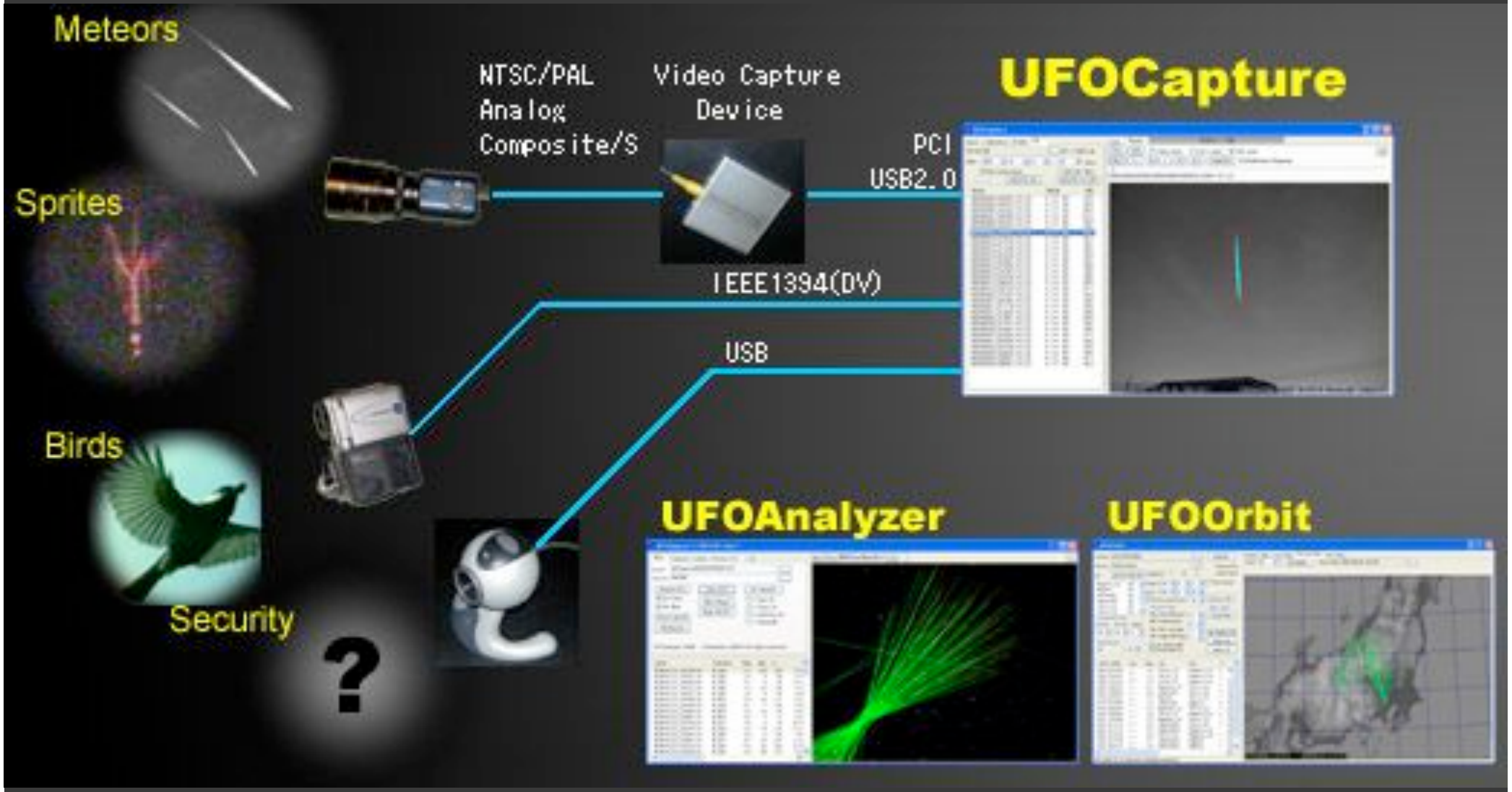

http://sonotaco.com/

自動検出された流星のスペクトル

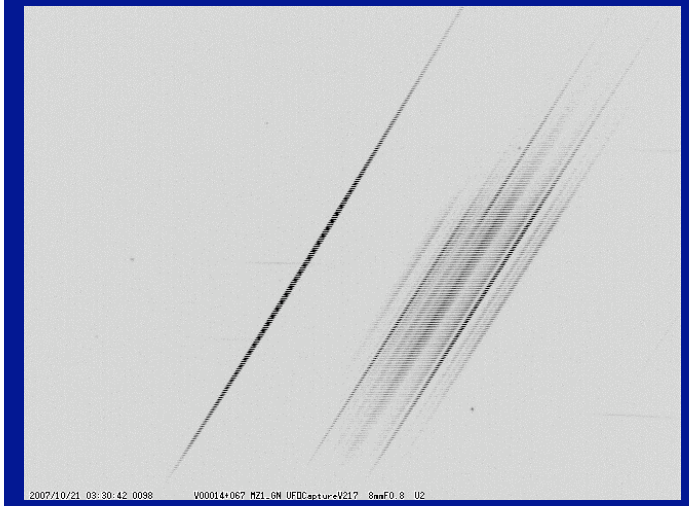

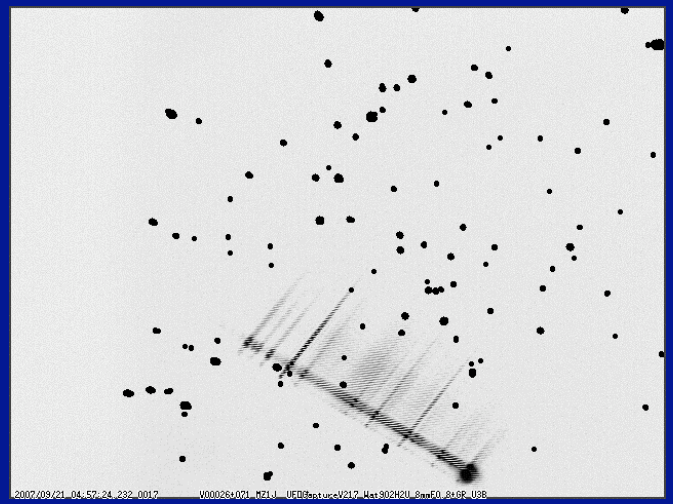

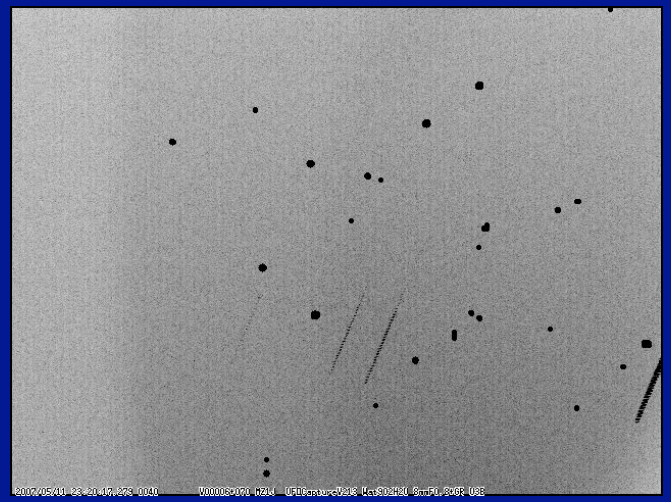

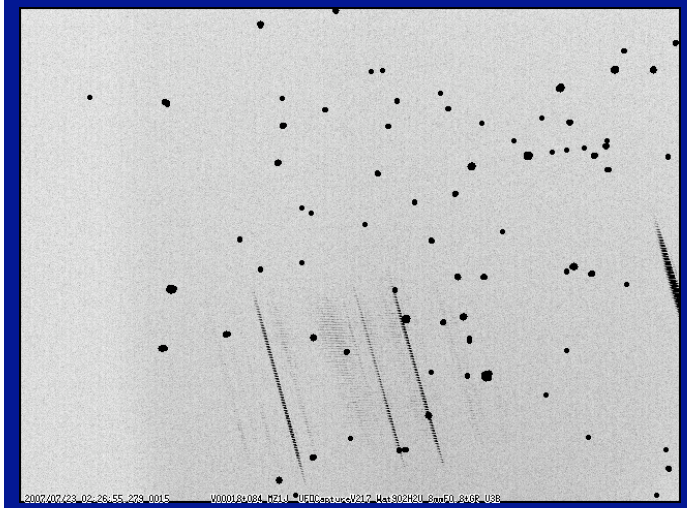

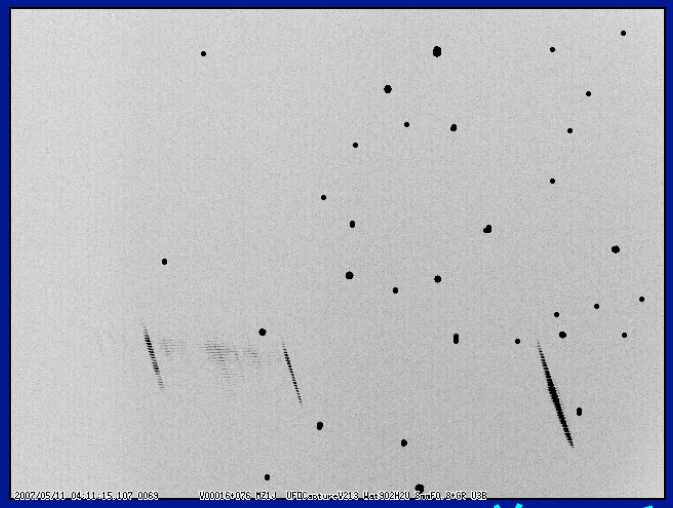

前田氏の流星分光カメラ

双曲線軌道の流星の分光観測は太陽系外の物質組成比を直接測定できる手段

系外流星のステレオ観測

- 3台のI.I. HDTVカメラを20~ 50 km離して配置。
- 自動検出・リモート観測。
- 8等までの流星を年間に~240,000（150個×8時間×200夜）検出可能?
- I.I. HDTVカメラ: ~150万円/台。
  初期費用：1,000 ~ 2,000万円?
  維持費　：~ 200万円／年?
  人件費　：2 → 0.5人?

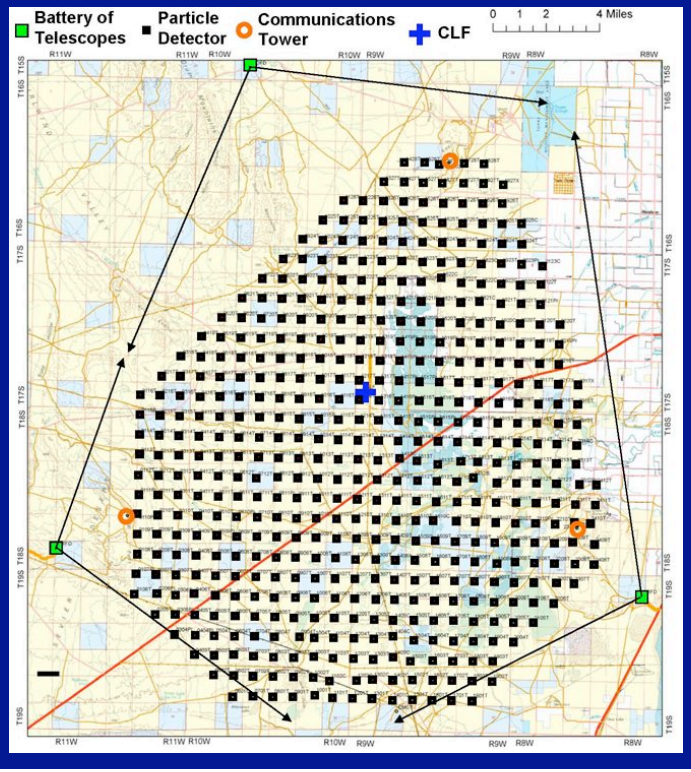

極限エネルギー宇宙線観測用
Telescope Array（東大宇宙線研、米国ユタ州）

AMOR (ニュジーランド)のレーダ観測

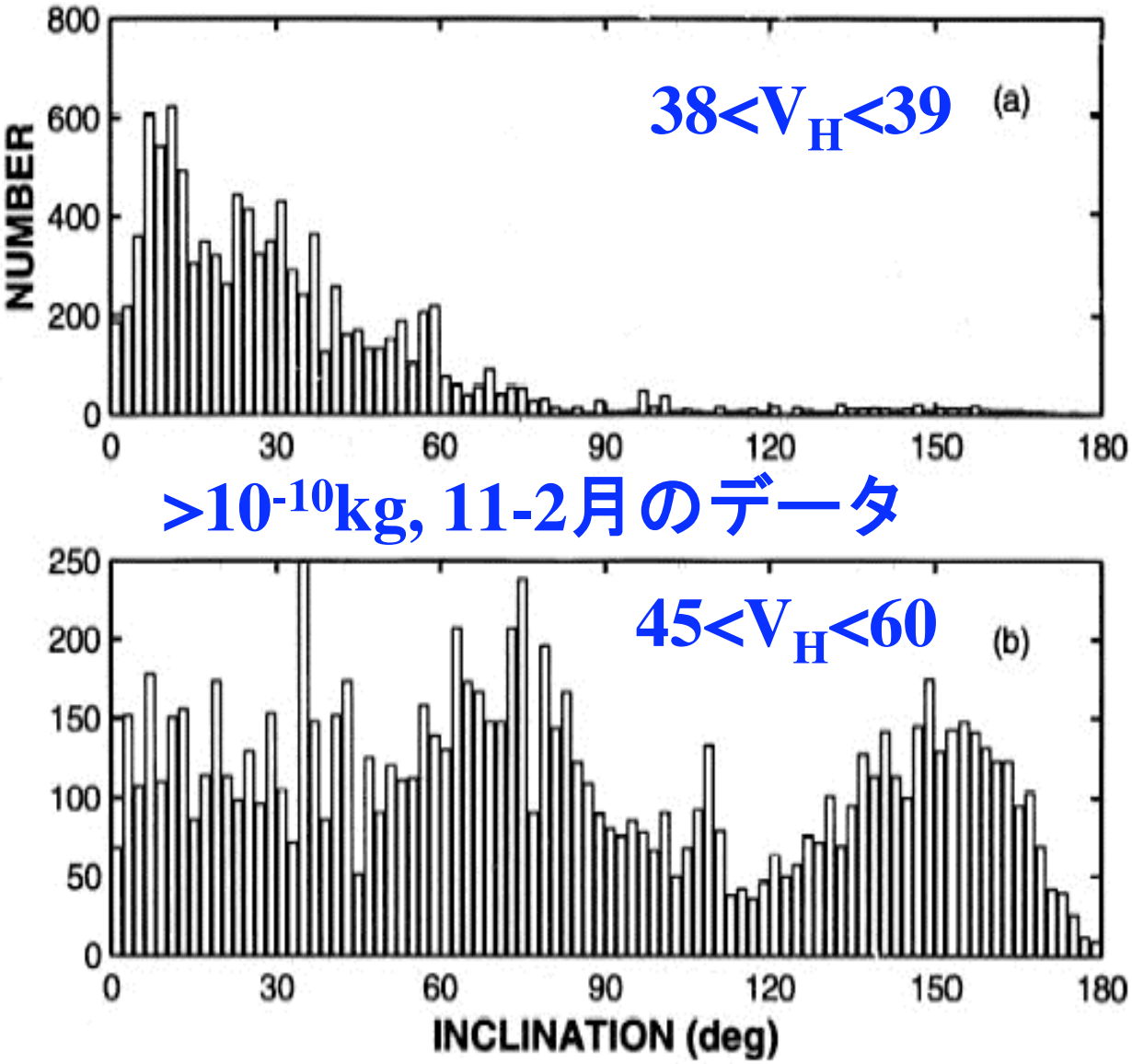

J.W. Baggaley, et al. (2000)

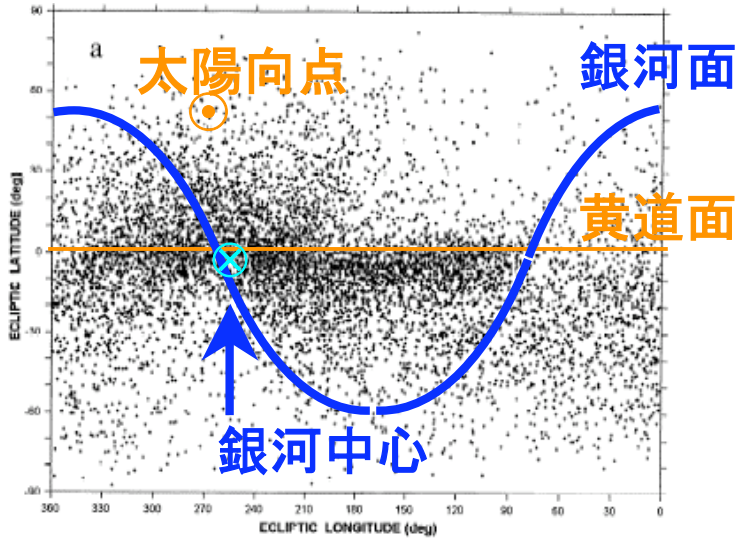

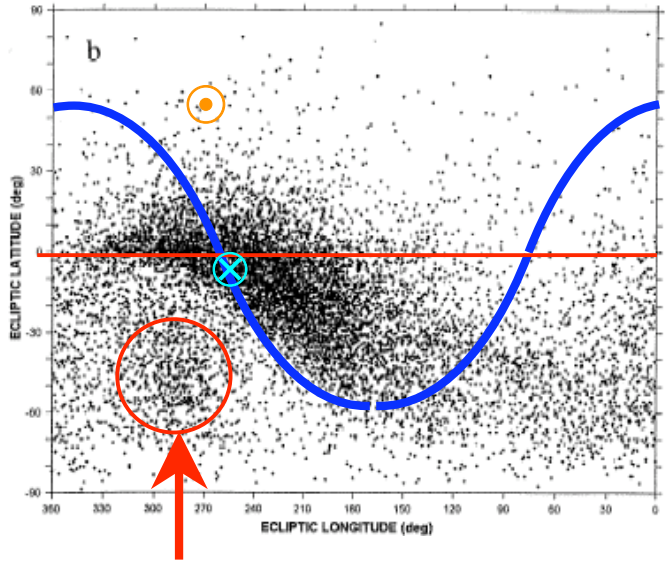

β Picの方向？

まとめ

- 探査機、レーダ、写真観測によって双曲線軌道の粒子を検出。
- I.I.-CCTV等（限界7.0等級）のステレオ観測により、0.1％が系外流星?
- I.I.-HDTV（FOV: 60°）の限界が8.0等級、対物分光システム（R~ 200）の限界が3.0等級。
- 分光観測は太陽系外の物質組成比を直接測定できる手段。
- I.I.-HDTVおよび自動検出システムによるステレオ観測ネットワークが有望。

南半球における眼視散在流星の年周変化について

泉　潔

2009,10,3　流星物理セミナー

散在流星の年周変化についてはすでに多くの研究があり、様々な文献に発表されてはいるが、眼視観測のものは全て北半球でのデータに基づくものであり、南半球での観測値から得られたものは筆者の知る限りにおいてないようである。北半球では春に少なく秋に多くなる結果がどの研究者の解析からも明確に出ており、これは主に太陽向点方向つまり黄道面に分布する流星物質が多いため、黄道面の平均的な高度の季節変化と一致しているとの見解が得られている。これが真実であるならば南半球においては逆の変化が見られるはづである。筆者は特に眼視流星からの南半球においての解析結果を探したが見つからなかった。過去において天文回報で長谷川一郎氏が南半球における散在流星の年周変化（多分電波観測）の論文を紹介されたことがあり、それによると北半球と変化が同じとのことであった。果たして南半球において、特に眼視流星の年周変化はどのようなものであろうか。筆者はこの古くて新しい問題に疑問を持ち調査を試みた。

データ解析

解析データはＩＭＯの１９９８年次のレポートを利用した。１９９８年次のデータが一番多そうだったからである。しかし、南半球における観測は少なく全てオーストラリアでの観測者からのものであり、２－３人の常連観測者が年間を通して観測している以外は流星群シャワーの時に散発的に観測している者しか見られない状況であった。１９９８年のオーストラリアでの観測データ数は２４１であった。散在流星の年周変化を見るためには日周変化の影響を除くため同一の地方時のデータを利用する必要があり、出来れば同一地点、同じ観測者のデータを解析するのが望ましい。この点を考慮し、年間を通して観測数の多かったＭＡＲＡＤ氏（ビクトリア州Ｓ３８°、１２′）ＷＯＯＪＥ氏（３１°，２３′）２氏のデータを抽出した解析も行った。この両氏のデータから更に世界時１３－１５時代（日本時間２３－０２時）のデータを抽出した。この両氏の抽出データ数は６９であった。（ＭＡＲＡＤ氏６０，ＷＯＯＪＥ氏９）　なお、観測条件は日本より抜群に良く、最微光星７．０近くのデータもざらにある。このため、日本における眼視流星（１－４等が主）とはやや異なるサンプルであることも注意したい。本来、このような解析には同一条件下で行った長期に渡る多数の個人データのみで行うのが望ましい。

結果

1　オーストラリアにおける１９９８年全データからは年周変化は認められない

2　ＭＡＲＡＤＡ、ＷＯＯＪＥ両氏の抽出データからは冬期（北半球では夏季６－８月）にやや増加が認められる。

3　北半球における年周変化（春季少なく秋ー冬に増加）はオーストラリアの眼視データからは認められない。

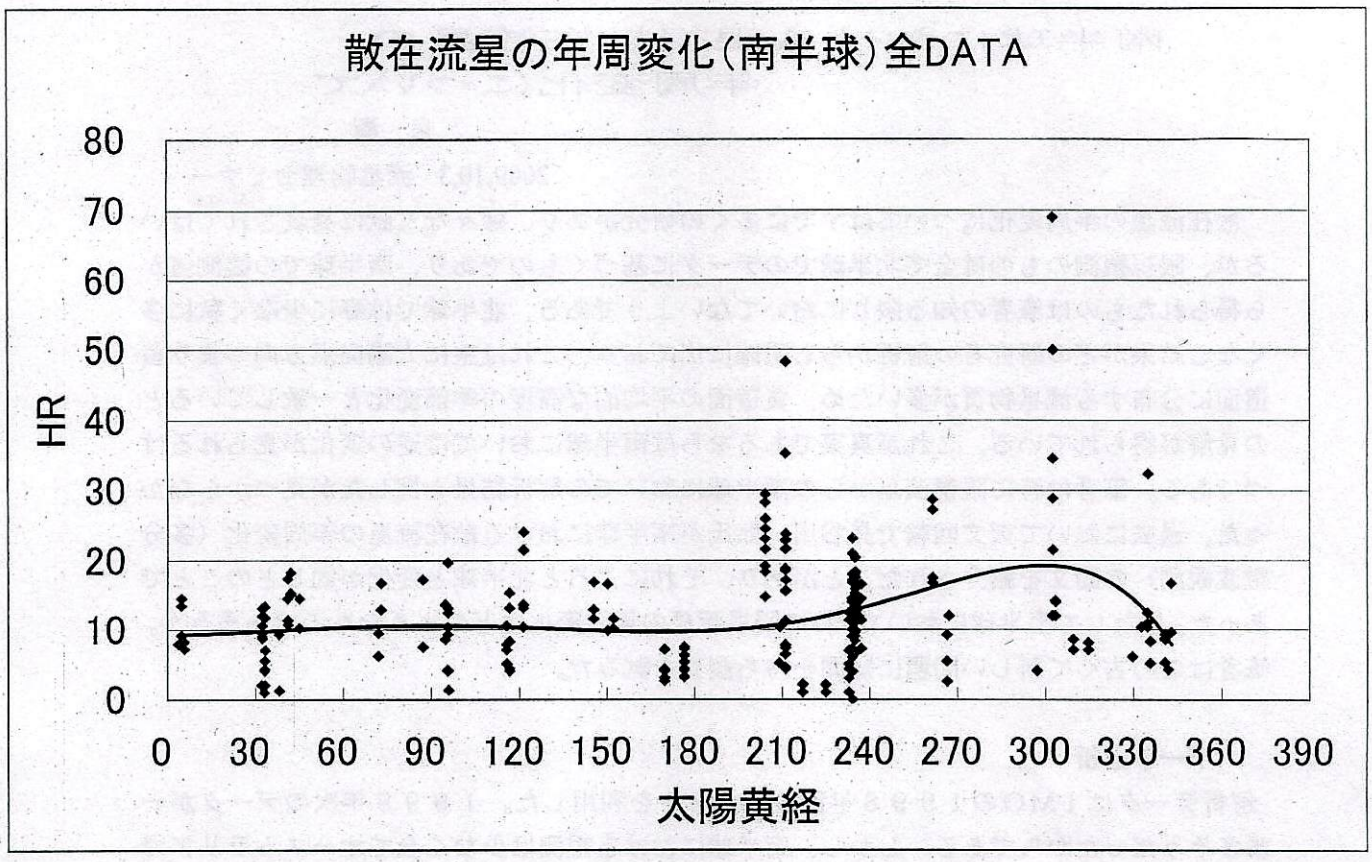
散在流星の年周変化(南半球)全DATA
HR
80
70
60
50
40
30
20
10
0
0 30 60 90 120 150 180 210 240 270 300 330 360 390
太陽黄経

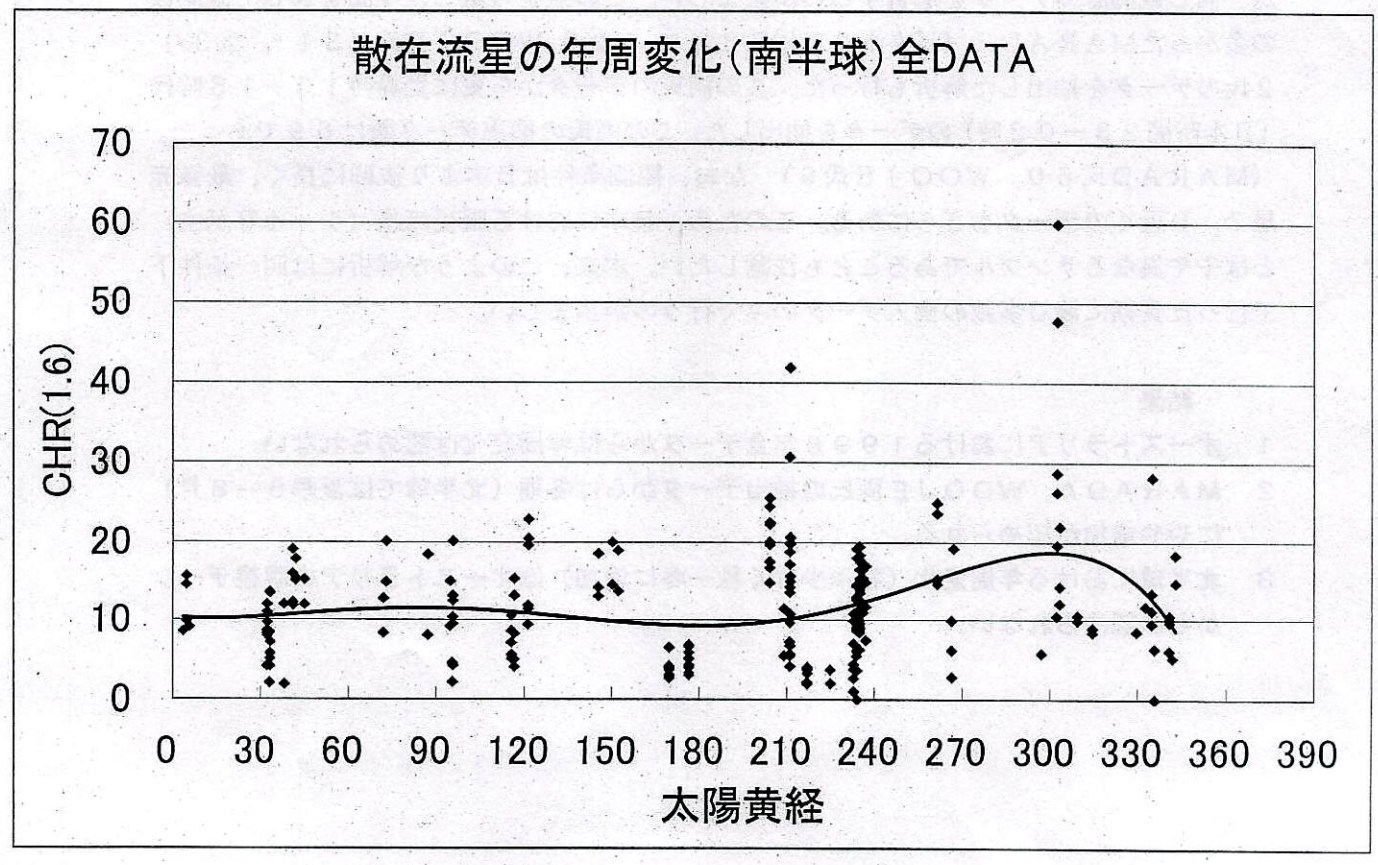
散在流星の年周変化(南半球)全DATA
CHR(1.6)
70
60
50
40
30
20
10
0
0 30 60 90 120 150 180 210 240 270 300 330 360 390
太陽黄経

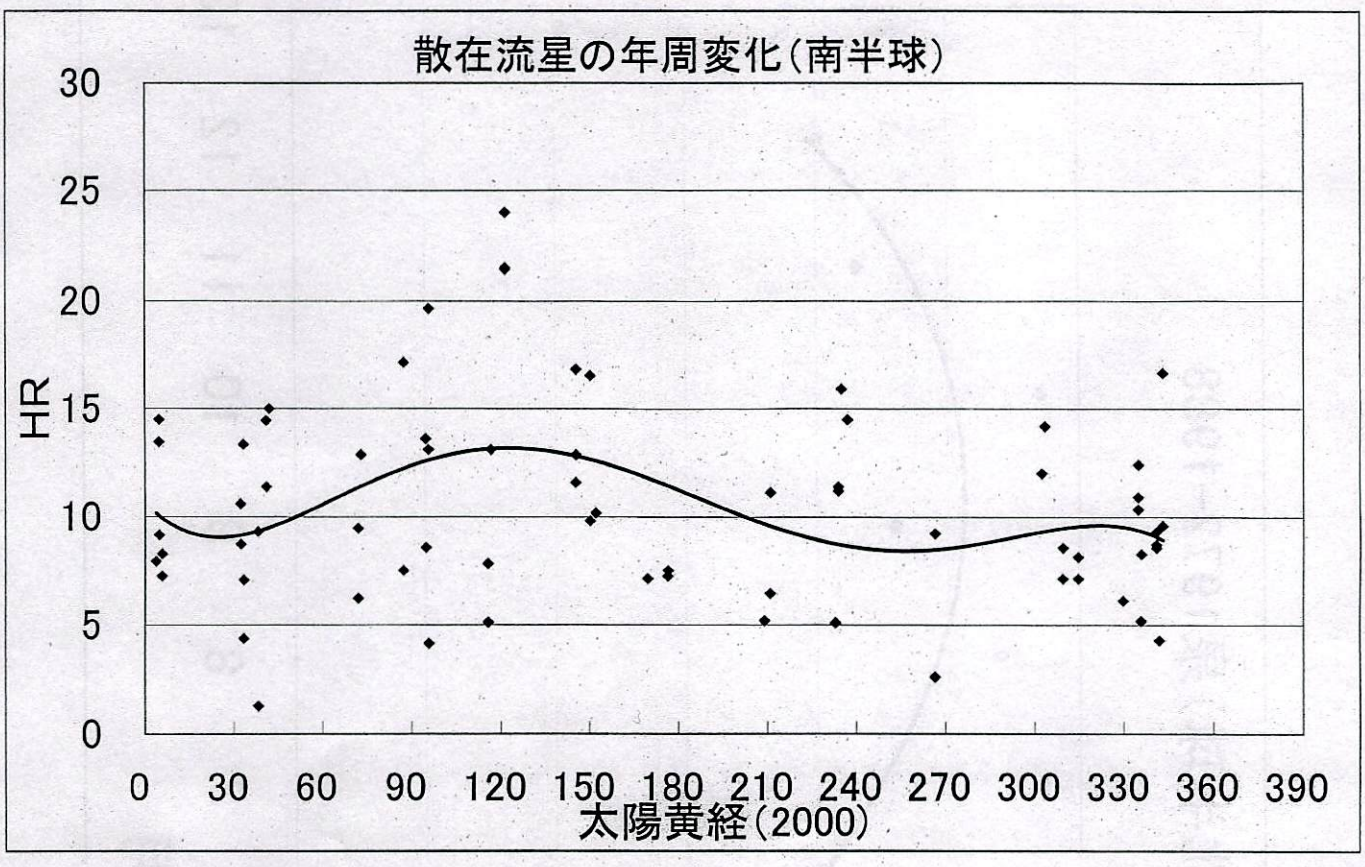
散在流星の年周変化(南半球)
HR
30
25
20
15
10
5
0
0 30 60 90 120 150 180 210 240 270 300 330 360 390
太陽黄経(2000)

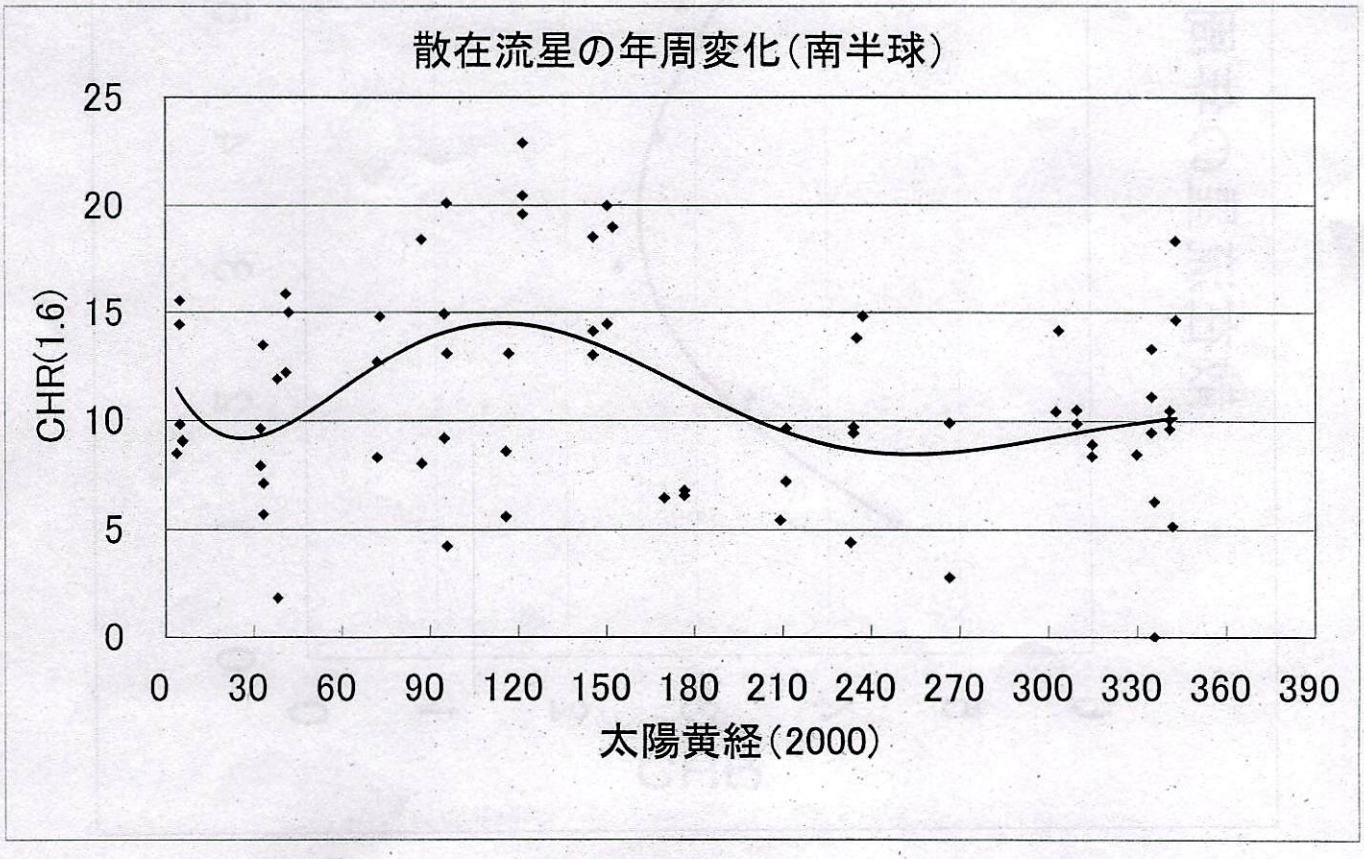
散在流星の年周変化(南半球)
CHR(1.6)
25
20
15
10
5
0
0 30 60 90 120 150 180 210 240 270 300 330 360 390
太陽黄経(2000)

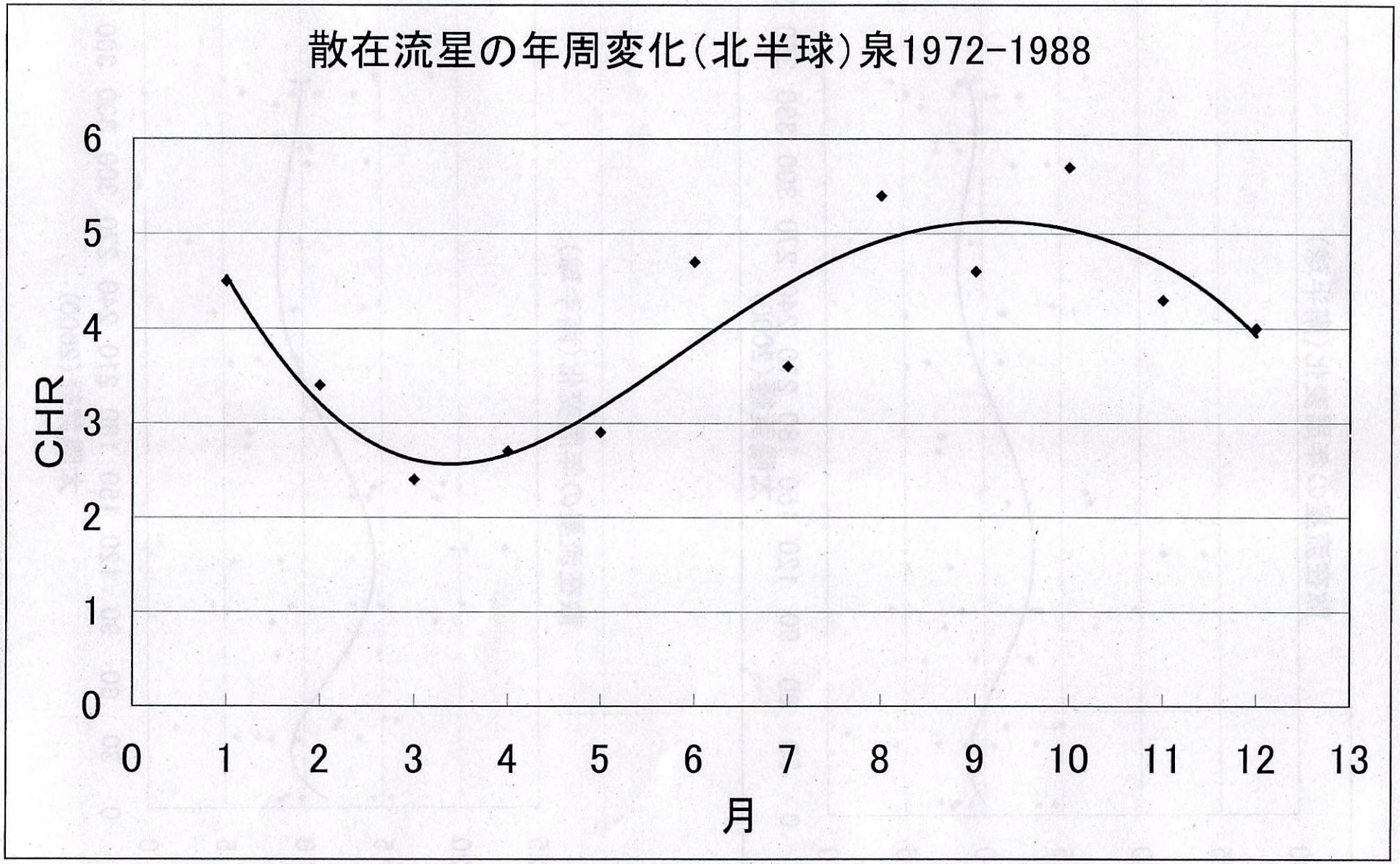
散在流星の年周変化(北半球)泉1972-1988
CHR
6
5
4
3
2
1
0
0
1
2
3
4
5
6
7
8
9
10
11
12
13
月

散在流星の年周変化についてII
Review

泉 潔

2010、2。7
流星物理セミナー

On the Annual Variation of Sporadic Meteors
IV. Theory on the Annual Variation

Tadayoshi MURAKAMI
University of Hiroshima
(Received December 9, 1950)

Abstract

The annual variation of the hourly rate of sporadic meteors as deduced from observation is expressed by a linear function of cosine of zenith distance of meteor apex. Assuming the random motion of meteoric particles and the simple proportionality of the number of meteors to the relative velocity of encounter, a simple theory has been developed as a solution of this relation. The discrepancy between theory and observation which is attributed to the irregularity of the density distribution of meteoric particles suggests some relation of these particles with the short-period comets.

1. *Introduction.*

As to the fact that the greater number of meteors are observed in the second half of the year than the first, some authors attributed it to the effect of meteoric showers which are richer in the second half of the year. The seasonal variation which exists even among sporadic meteors is admitted only in recent years. The author has shown on the basis of observation the detailed features of the annual variation of sporadic meteors, carefully excluding the effect of major and transient showers.[1]

Our reduction on the annual variation was started at first to verify our drift motion hypothesis of interstellar meteoric particles[2], but now it must be admitted that most of the meteoric particles for sporadic meteors move together with the solar system and the variation is mainly governed by the altitude of the apex of the Earth's way. When a comparison was made between the meteor rate reduced from observation and the altitude of the meteor apex, a simple relation was found between them. A theory has been developed to explain the fact. The discrepancy between theory and observation is ascribable to the irregularity of the density distribution of the meteoric particles.

2. *Dependency of Hourly Rate on the Altitude of Meteor Apex.*

The author found on examining the annual variation given in the former articles[1] that the number of meteors varies nearly as a linear function of zenith distance C of the meteor apex. This, as obvious from the diurnal discussion which will be given later, the number

---

6.36. The smoothed values (m) as deduced from this mean curve are:

Month	Jan.	Feb.	Mar.	Apr.	May	Jun.	Jul.	Aug.	Sep.	Oct.	Nov.	Dec.
(m)	5.33	4.76	3.70	3.22	4.00	5.75	8.30	9.40	9.20	8.43	7.40	6.32
Sun's long.	330°	300°	0°	30°	60°	90°	120°	150°	180°	210°	240°	270°
(m)	5.14	4.74	3.80	3.36	4.22	6.30	8.21	9.42	9.12	8.32	7.08	5.10

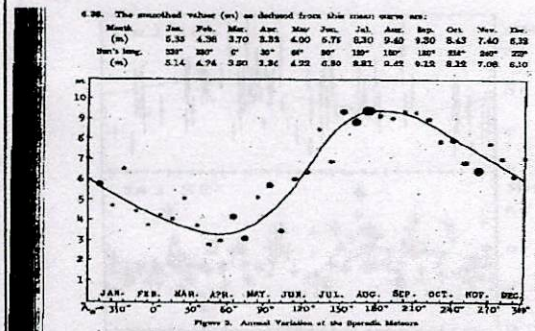

Figure 3. Annual Variation of the Sporadic Meteors

The annual variation curve of the sporadic meteors, when treated with harmonic analysis, may be developed in Fourier series, as follows:

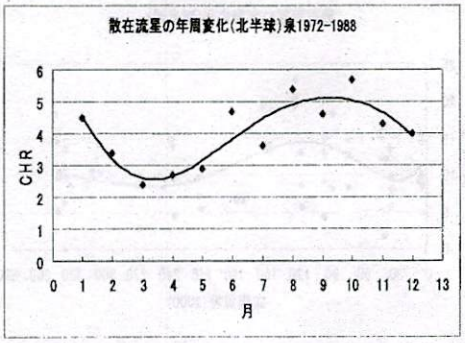

This mean curve shows roughly the probability distribution with axis at about $\delta = +23°$. This fact is easily explained when we assume that the observational directions of meteor observers are to be centered on the zenith or along the diurnal circle passing it. The shift of the axis about 6° southward may have been caused by the inclination of the observers in

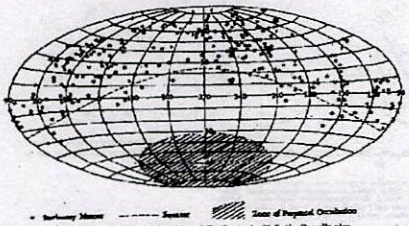

Stationary Meteor ------ Equator Zone of Perpetual Occultation

Fig. 2. Celestial Distribution of Radiants in Ecliptic Coordinates.

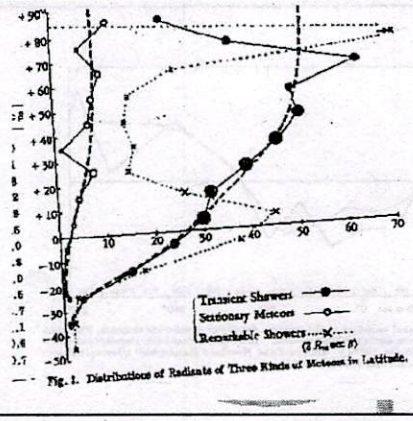

Fig. 1. Distributions of Radiants of Three Kinds of Meteors in Latitude.

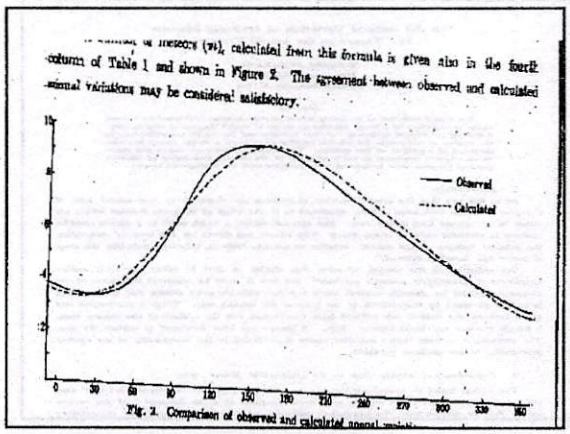

Fig. 2. Comparison of observed and calculated annual

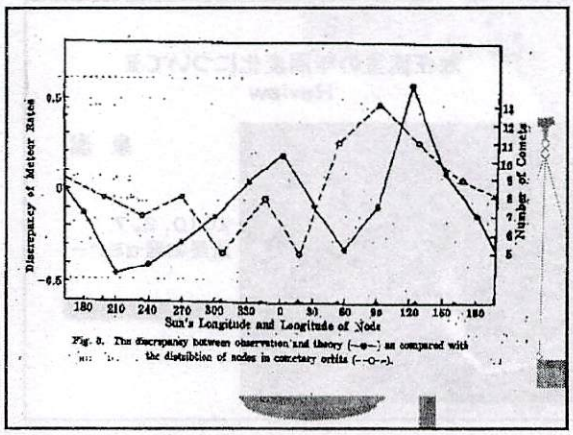

Fig. 8. The discrepancy between observation and theory (—●—) as compared with the distribution of nodes in cometary orbits (- -○- -).

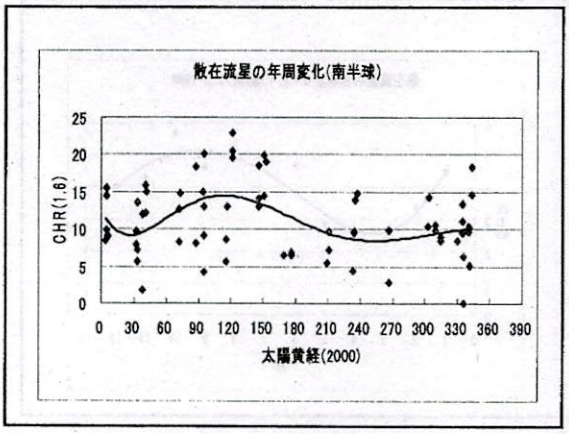

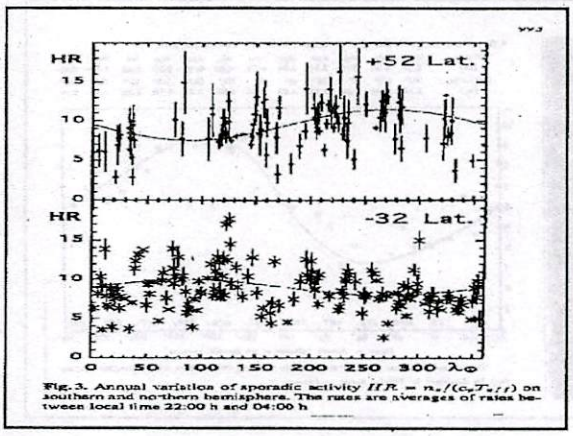

Fig. 3. Annual variation of sporadic activity $HR = n_s/(c_s T_{eff})$ on southern and northern hemisphere. The rates are averages of rates between local time 22.00 h and 04:00 h.

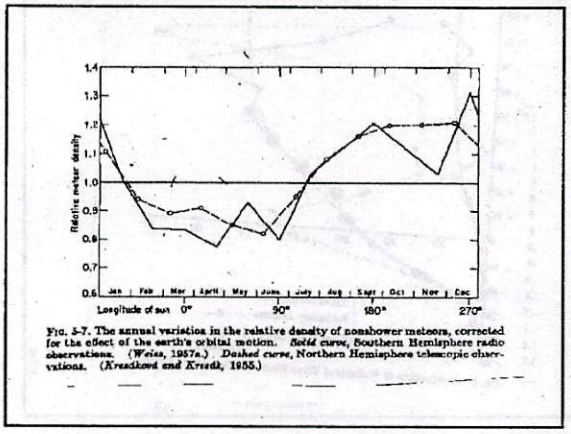

Fig. 5-7. The annual variation in the relative density of nonshower meteors, corrected for the effect of the earth's orbital motion. *Solid curve*, Southern Hemisphere radio observations. (*Weiss*, 1957a.) *Dashed curve*, Northern Hemisphere telescopic observations. (*Kresákova and Kresák*, 1955.)

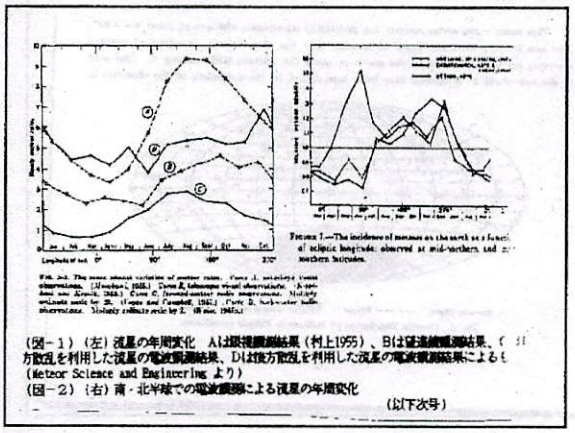

(図－1）（左）流星の年周変化　Aは[illegible]結果（村上1955）、Bは[illegible]結果、（[illegible]方散乱を利用した流星の電波観測結果、Dは後方散乱を利用した流星の電波観測結果によるも
(Meteor Science and Engineering より)
(図－2）（右）南・北半球での電波観測による流星の年周変化

(以下次号)

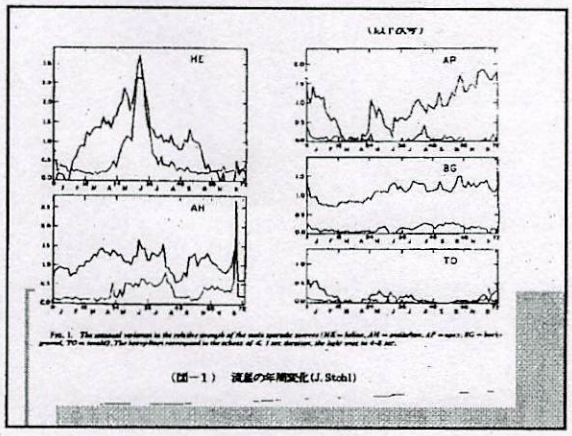

（図－１） 流星の年周変化(J. Stohl)

結論

- １ 北半球における散在流星の年周変化は年前半より後半に多くの流星出現が見られる。眼視、電波、望遠鏡共に同様の変化が見られる
- ２ 南半球における眼視流星の年周変化は認められない。電波流星では北半球と同等になっている。(北半球と南半球では年周変化のパターンが逆になるとの従来からの認識は誤りである。

考察

- １ 北半球における年周変化は真夜中の流星向点の高度の年周変化とおおむねに接近する周期彗星の交点分布の一致するが多少ずれも見られる。地球軌道傾向の影響が見られる。地球向点の高度変化だけではでは南半球は逆になるはずであるがその傾向は見られない。
- ２ 散在流星の年周変化は地球向点高度の季節変動によるものではなく、地球軌道のダスト分布そのものが後半年に多くなっていることによる
- ３ 近年はAH, H、TOな方向別の年周変化も調査されているが、特にグローバルな年周変化への寄与の大きなソースはわからない